

1991

Studies of sediments in a tidal environment

Fitzpatrick, Fiona

<http://hdl.handle.net/10026.1/513>

<http://dx.doi.org/10.24382/3659>

University of Plymouth

All content in PEARL is protected by copyright law. Author manuscripts are made available in accordance with publisher policies. Please cite only the published version using the details provided on the item record or document. In the absence of an open licence (e.g. Creative Commons), permissions for further reuse of content should be sought from the publisher or author.

STUDIES OF SEDIMENTS IN A TIDAL ENVIRONMENT

FIONA FITZPATRICK, B.Sc., M.Sc.

**A thesis submitted in partial fulfilment of the
requirements of the Council for National Academic Awards
for the degree of Doctor of Philosophy**

November 1991

**Department of Geological Sciences, Polytechnic South
West in collaboration with Plymouth Marine Laboratories.**

LIBRARY STORE

This book is to be returned on
or before the date stamped below

REFERENCE ONLY

1 - APR 2003

15 JUL 2003

STORE

13 JAN 2004

UNIVERSITY OF PLYMOUTH

PLYMOUTH LIBRARY

Tel: (01752) 232323

This book is subject to recall if required by another reader

Books may be renewed by phone

CHARGES WILL BE MADE FOR OVERDUE BOOKS

90 010 4122 6

TELEPEN



REFERENCE ONLY

UNIVERSITY OF PLYMOUTH LIBRARY SERVICES	
Item No.	900 1041226
Class No.	T 551.460833
Contl No.	X702596859

36 FIT

LIBRARY STORE

STUDIES OF SEDIMENTS IN A TIDAL ENVIRONMENT

Fiona Fitzpatrick

Abstract

Five sedimentary environments in Plymouth Sound, S.W. England, are defined by side-scan sonar surveys calibrated by direct sampling by SCUBA divers: (i) uniform mud depocentres, (ii) areas of continual sediment reworking, (iii) areas of relict sedimentation, (iv) areas of episodic deposition and, (v) clean-washed rock outcrops. Net sediment transport paths are defined using the physical properties of the sediment. Analysis of Airborne Thematic Mapper and Compact Airborne Spectrographic Imager scanner data at High and Low Water, with concurrent sampling has enabled the relationship to be established between suspended sediment concentration, percentage organics, temperature and salinity and a marked continuity between the sea bed and some surface water properties has been defined. Such techniques identify previously-unrecognized features such as tidal gyres above areas of featureless acoustic response. The anisotropy of magnetic susceptibility of diver-orientated samples, showed that the primary fabric of their sediments is controlled by modal sediment size, magnetic mineralogy and the type and intensity of the water currents. The effect of biogenic disturbances and the re-establishment of magnetic alignment under different depositional controls are significant features in the development of secondary fabric. The combination of these results has defined the history of the ancestral inlet throughout the Late Quaternary, which is shown to have been controlled by the lithology, the structure of South West England and the climatic changes experienced by the region and the English Channel. The development and characteristics of the present day hydrodynamical regime, its adaptation to the presence of the Breakwater and the response of the sea bed to this feature are identified by combining information from these techniques.

Contents

	Page
Abstract	2
List of Illustrations	7
List of Tables	9
List of Accompanying material	9
Acknowledgements	10
Authors Decleration	11
Chapter One Introduction	12
1.1 The Location of Plymouth Sound	13
1.2 The history of Plymouth Sound	13
1.3 Bathymetry	14
1.4 Tides	15
1.5 River Inflow	17
1.6 Weather	19
1.7 Temperature	19
1.8 Salinity	20
1.9 Sewage	20
1.10 The Investigation	20
Chapter Two Geology and Quaternary History of survey area	23
2.1 Introduction	23
2.2 Geological History	24
2.3 Sea level changes	32
2.3.1 Methods for identifying sea level changes	37
2.3.2 Features created by sea level changes	39
2.3.3 Critique of the evidence pertaining to sea level changes	40
2.3.4 Sea level curves and Flandrian sea level rise	43
2.3.5 Sea level rise in the English Channel	43
2.3.6 The Romano British Transgression	46
2.3.7 The South West and the collapsing forebulge	47
2.4 The PalaeoSound and evidence of sea level changes	48
2.4.1 The PalaeoTamar Valley	48
2.4.2 The PalaeoPlym	49
2.4.3 The PalaeoSound	50
2.4.4 Rock Ledges and Platforms	50

Chapter Three Side-scan sonar survey	53
3.1 Introduction	53
3.2 Navigation	53
3.3 The Echosounder	55
3.4 The Side-scan sonar	57
3.5 Sonograph processing	59
3.6 Survey results and interpretation	63
3.6.1 Featureless acoustic response	63
3.6.2 Tonal differences	65
3.6.3 Bedform dominated environments	66
3.6.4 Gravels	73
3.6.5 Rocks	77
3.6.6 Caves and Caverns	79
Chapter Four Sedimentology and sampling	80
4.1 Introduction	80
4.2 Sampling techniques	80
4.2.1 Position fixing	81
4.2.2 Diving operations	81
4.2.3 Sediment sampling	84
4.2.4 Transport and storage of samples	87
4.3 Laboratory techniques	87
4.4 Grain size and statistical analysis	95
4.5 Sediment results	100
4.5.1 Fine grained sediments	100
4.5.2 Sandy sediments	112
4.5.3 Coarse relict sediments	115
4.5.4 Rocky outcrops	118
4.5.5 Episodic deposition	126
Chapter Five Airborne remote sensing surveys	128
5.1 Introduction	128
5.2 Passive remote sensing in the marine environment	130
5.3 Instrumentation	135
5.3.1 Daedalus AADS 1268 Airborne Thematic Mapper	135
5.3.2 CASI instrument	137
5.3.3 Groundtruth survey equipment	138
5.4 The surveys	140
5.4.1 The Plymouth Sound 1989 ATM survey	142

Chapter Five cont....	
5.4.2 The Plymouth Sound 1990 ATM surveys	144
5.4.3 The Plymouth Sound 1990 CASI survey	147
5.5 Laboratory measurements	154
5.6 Image data processing	155
5.6.1 Data tapes	155
5.6.2 Image processing	155
Chapter Six Overflight results	159
6.1 Introduction	159
6.2 The <i>In situ</i> results	159
6.2.1 Secchi disc	160
6.2.2 Temperature	171
6.2.3 Salinity	174
6.3 Laboratory results	182
6.3.1 Total suspended material and total organic material	182
6.3.2 Chlorophyll- α	190
6.4 The imagery	190
6.4.1 Aerial and oblique photographs	191
6.4.2 Previous images	192
6.4.3 ATM band 11 images	198
6.4.4 ATM visible images	202
6.4.5 The CASI images	205
Chapter Seven Magnetic measurements	220
7.1 Introduction	220
7.2 Sampling	221
7.3 Susceptibility and the anisotropy of magnetic susceptibility	222
7.3.1 Uses of the anisotropy of magnetic susceptibility in unconsolidated sediments	223
7.3.2 Susceptibility and fabric results	227
7.3.3 Discussion	237
7.4 Remanence measurements	241
7.4.1 Properties of remanence	242
7.4.2 Remanence measurements	245
7.4.3 Discussion	249
7.5 Sources of magnetic carriers	251

Chapter Eight Conclusions	
8.1 Introduction	252
8.2 Present day Plymouth Sound	252
8.2.1 Present day hydrography of Plymouth Sound	252
8.2.2 Sediments in Plymouth Sound	260
8.3 The history of Plymouth Sound	266
8.4 The future of Plymouth Sound	276
8.5 Methods and Techniques	279
8.6 Future work in Plymouth Sound	283
8.7 Final Comment	283
References	285
Appendix 1 Personnel	302
Appendix 2 Sediment results	305
Appendix 3 Magnetic measurement results	336
Appendix 4 Location of all stations	339

List of Illustrations

	Page
1.2 Bathymetry of Plymouth Sound	18
2.1 The Geology of Plymouth Sound	29
2.2 Spatial extent of the Late Quaternary Ice sheets	30
2.3 Sea Level curves	33
2.4 Sea level rise in the English Channel	34
2.5 The Channel River	35
2.6 Features of sea level rise in Plymouth Sound	51
3.1 Location of side-scan survey tracks	61
3.2 The height of an object	62
3.3 Sonograph of dredge scours	67
3.4 Sonograph of the Breakwater muds	67
3.5 Sonograph of the Mountbatten muds	68
3.6 Sonograph of tonal patches	68
3.7 Sonograph of a sand sheet	69
3.8 Sonograph of sand waves	69
3.9 Sonograph of marine relict gravels	74
3.10 Sonograph of fluvial relict gravels	74
3.11 Sonograph showing cleanswept rocks	75
3.12 Location of the underwater caves	76
4.1 Location of Areas	107
4.2 Breakwater silts	107
4.3 X-ray of cores	108
4.4 Physical properties of the Breakwater silts	109
4.5 Mountbatten silts	110
4.6 Sandy sediments	120
4.7 Relict gravels	122
4.8 Rocky outcrops	123
4.9 Episodic deposition	124
5.1 Absorption of light in 10m of water	134
5.2 Spectra produced by chlorophyll- α	134
5.3 Sample charts	140
5.4 ATM 1989 flightlines and sample stations	149
5.5 ATM 1990 flightlines and sample stations	150
5.6 ATM 1990 Groundtruth campaign	150
5.7 CASI 1990 flightlines and sample stations	151
6.1 ATM 1989 L.W. Secchi disc disappearance depths	165
6.2 Secchi disc disappearance depths vs. <i>in situ</i> properties	166
6.3 ATM 1990 L.W. Secchi disc disappearance depths	167
6.4 ATM 1990 H.W. Secchi disc disappearance depths	168
6.5 CASI 1990 H.W. Secchi disc disappearance depths	169
6.6 <i>In situ</i> Temperature L.W.	179
6.7 <i>In situ</i> Temperature H.W.	180
6.8 <i>In situ</i> Salinity L.W.	181
6.9 <i>In situ</i> Salinity H.W.	184
6.10 <i>In situ</i> Laboratory results L.W.	185
6.11 <i>In situ</i> Laboratory results H.W.	187
6.12 Chlorophyll- α concentration	189
6.13 Foam lines and visible changes	193
6.14 Drake's Island upwelling	194
6.15 Daedalus AADS 1230 Hamoaze Channel	190
6.16 Daedalus AADS 1268 12.06.84	195
6.17 12.06.84 magnified image of the gyre system	195
6.18 Rame head eddy	196
6.19 ATM 1989 L.W. band 11 mosaic Plymouth Sound	197
6.20 ATM 1989 L.W. band 11 The Bridges	197

List of Illustrations cont..

6.21	ATM 1989 L.W. band 11 East Hamoaze Channel	207
6.22	ATM 1989 L.W. band 11 pseudocoloured mosaic Plymouth Sound	207
6.23	ATM 1990 L.W. band 11 mosaic Plymouth Sound	208
6.24	ATM 1990 L.W. band 11 East Hamoaze Channel	208
6.25	ATM 1990 L.W. band 11 pseudocoloured mosaic Plymouth Sound	209
6.26	ATM 1990 H.W. band 11 mosaic Plymouth Sound	209
6.27	ATM 1990 H.W. band 11 pseudocoloured mosaic Plymouth Sound	210
6.28	ATM 1989 L.W. band 2	210
6.29	ATM 1989 L.W. band 3	211
6.30	ATM 1989 L.W. band 4	211
6.31	ATM 1989 L.W. band 3 pseudocoloured East Plymouth Sound	212
6.32	ATM 1990 L.W. band 3 pseudocoloured East Plymouth Sound	212
6.33	ATM 1990 L.W. band 3 flightline 2	213
6.34	ATM 1990 H.W. band 2	213
6.35	ATM 1990 H.W. band 3	214
6.36	ATM 1990 H.W. band 4	214
6.37	ATM 1990 H.W. band 3 Plymouth Sound	215
6.38	CASI 1990 H.W. band 1	215
6.39	CASI 1990 H.W. band 2	216
6.40	CASI 1990 H.W. band 3	216
6.41	CASI 1990 H.W. band 4	217
6.42	CASI 1990 H.W. band 5	217
6.43	CASI 1990 H.W. band 6	218
6.44	CASI 1990 H.W. band 7	218
6.45	CASI 1990 H.W. band 8	219
6.46	CASI 1990 H.W. band 2 Central Hamoaze Channel	219
7.1	Orientation of the samples	225
7.2	Anisotropy of magnetic susceptibility fabrics	225
7.3	Sample stations	226
7.4	Fabric results	233
7.5	Storage and drying experiment	236
7.6	Current roses	240
7.7	Grahams' V vs. Susceptibility	240
7.8	Remanence down core	246
8.1	Development of High Water	257
8.2	Stratification of Plymouth Sound	258
8.3	Development of Low Water	259
8.4	Net sediment transport in Plymouth Sound	263
8.5	The History of sediment build-up in the Inner Breakwater	264
8.6	Plymouth Sound 20,000 B.P.	267
8.7	Plymouth Sound 9,000 - 7,000 B.P.	268
8.8	Plymouth Sound 7,000 - 6,000 B.P.	269
8.9	Planar sands in the buried channels.	270
8.10	Plymouth Sound 6,000 - 4,000 B.P.	271
8.11	Effects of sea level rise in Plymouth Sound	278

List of Tables

	Page
1.1 Devonport: observed tide amplitudes and phases.	17
1.2 1979 River inflow into Plymouth Sound.	17
2.1 Classification of the Pleistocene	31
2.2 Raised beaches throughout the Quaternary	39
2.3 Heights of marine cliffs, buried valleys and terraces	41
2.4 Postulated sea level rises	44
4.1 The Plymouth Sound sediment sieving chart	91
4.2 The relationship between ϕ and metric scales	96
4.3 Statistical parameters	98
4.4 Primary and accessory minerals	103
5.1 ATM instrument band widths	136
5.2 Modifications to the Temperature/Salinity probe	141
5.3 ATM 1989 campaign times	143
5.4 ATM 1990 campaign times	147
5.5 Sea-Wifs band widths	148
5.6 Clay spectral peaks and characteristics	148
5.7 CASI band widths, desired and actual	152
5.8 CASI 1990 campaign times	153
6.1a,b,c & d Groundtruth campaign results	161
6.2 CASI Temperature dip results	177
6.3 CASI Salinity dip results	178
7.1 Magnetic and Physical results	229
7.2 History of the storage and drying experiment	235
7.3 History of the storage and drying experiment	235
7.4 Fabric parameters observed during the storage and drying experiment	237
7.5 Remanence Results	244
7.6 Oxidation state of the cores	249
8.1 Correlation between the PalaeoTamar and the English Channel	273
8.2 Estimated contributions to sea level rise in the last 100 years	272
8.3 IPCC Buisness-as-usual estimates for 2030	279

List of Accompanying material

Figure 1.1 Location Map

- Chart 2 Plymouth Sound - Inner Breakwater
Chart 3 Plymouth Sound - Outer Breakwater


Acknowledgments

This work was carried out during the tenure of a CNAA Research Assistantship, which is gratefully acknowledged. I would like to thank Professor Don Tarling for continual encouragement throughout the project and for reading this manuscript (many times); Dr. John Reynolds has also helped me overcome many of the problems arising during the course of the study. I am greatly indebted to N.E.R.C. for both the Plymouth Sound overflights and use of the image processing facilities; in particular, for the assistance of Stuart White and Stephen Groom. In a multidisciplinary work, such as this, many people have been involved throughout the project, and without them, no data would have ever been collected. I would particularly like to thank John Vaudin for his enduring patience and many dives on "the mud"; and my colleagues and friends who made all the measurements during the groundtruth surveys: in particular Andy Revill, who ran the afternoon survey whilst I was airborne. I am indebted to the skippers of Coxside Marine Centre for many hours of ship time; and to both the Institute of Marine Studies and Plymouth Marine Laboratories for all the equipment that I have borrowed over the last three years. I would also like to thank Mr. Paul Riddy and the students of the Department of Oceanography (Southampton University) for all the side-scan sonar surveys in choppy water. I also wish to acknowledge the help of the staff and students of the Department of Geological Sciences. Finally, I would like to thank my family and friends, and especially Damian Francis for his continual support at all times


This is to certify that the work submitted for the Degree of Doctor of Philosophy under the title "Studies of sediments in a tidal inlet" is the result of original work.

All authors and works consulted are fully acknowledged. No part of this work has been accepted in substance for any other degree and is not being concurrently submitted in candidature for any other degree.

Candidate:


Fiona Fitzpatrick

Research Supervisor:


Professor D.H. Tarling

- CHAPTER ONE -

- INTRODUCTION -

The Plymouth Sound Project was initiated in 1984 by the Department of Geological Sciences at Polytechnic South West. Initially the project ran a series of high resolution seismic traverses to determine the nature of the Quaternary buried channels in Plymouth Sound (McCallum & Reynolds 1987, Reynolds 1987). In 1988 a jack-up rig provided two continuous sedimentary cores giving good correlation between sediment and seismic signature (Eddies & Reynolds 1988). The sedimentary fill of the buried channels and the progressive rise in sea level was established by analysis of the foraminiferal content of the cores. These confirmed that the ancestral inlet was a tidal river by 9,500 years B.P. (Eddles & Hart 1988). In 1989 the survey was extended to include an investigation of the actual hydrodynamics of Plymouth Sound as a tidal inlet, and to determine the form and origin of the sea bed sediments. In order to achieve this aim, it was necessary to obtain information of the lateral and vertical changes experienced by Plymouth Sound over the last 20,000 years. In doing so, six main objectives were defined:

- (i) to establish the sediment types and their spatial and temporal distribution on the sea bed, and the primary controlling factors,
- (ii) to establish the relationship between the Quaternary development of the drainage basin and present day sediments,
- (iii) to identify the paths and periodicity of sediment mobility in the inlet,
- (iv) to identify the nature of the ebb and flood tide in Plymouth Sound and attempt to understand the relationship with the pattern of sediment distribution on the sea bed,
- (v) to investigate the use and applicability of Airborne Remote Sensing in the understanding of the surface characteristics of a tidal inlet, and
- (vi) to investigate the applicability of magnetic measurements to orientated samples of unconsolidated sub tidal sediments.

1.1 The location of Plymouth Sound.

Plymouth Sound, on the border of Devon and Cornwall, is one of the largest tidal inlets on the south coast of England (Figure 1.1). The City of Plymouth lies to the north of the inlet and the Devonport Naval Dockyard is situated to the northwest of the City. The most southerly parts of the inlet are Penlee Point in the west and Andrum Point to the east. The inlet has free connection to the English Channel, but the entrance is partially blocked by an artificial east-west Breakwater. In this survey, Plymouth Sound is defined as the sea area to the north of the Breakwater in a line from Cawsand to Bovisand. The area to the south of the Breakwater, extending to a line between to Penlee Point and Andrum Point is referred to as the Outer Breakwater. Two main river systems enter Plymouth Sound. The largest is the Tamar, which lies to the northwest and is tidal to 30km upstream. It is a characteristic salt wedge estuary and is joined by the rivers Tiddy, Lynher and Tavy. The Rivers Plym and Laira join to form a well mixed estuary to the northeast of the City (all place names referred to in the text are located on Figure 1.1 in back sleeve).

1.2 The history of Plymouth Sound

The area around Plymouth has been colonized since c. 10,000 B.C. The area was inhabited by hunters and gatherers during the Mesolithic, and the lands cultivated since the Bronze Age. Since the development of tin and copper mining on Dartmoor, Sutton Harbour and Mountbatten developed as major trading posts and the Sound has been an important commercial harbour from Roman times (*Ictis* in classical literature). During the Saxon and Norman Periods the port of Plympton, on the Plym, expanded, taking trade away from the smaller port of Sutton. However, with the increased tin-streaming on Dartmoor, the estuary of the Plym began to silt-up, and ships were commonly waiting to unload at Plym mouth (Cattewater). As the waiting increased, ships began to use Sutton harbour. The first recorded use of the name "Plymouth" was in a ships ledger of 1211 and the first cargo out of the newly named port was a shipload of bacon for Portsmouth and wine for Nottingham (Gill 1966). The expansion of the Naval presence in Stonehouse began in the reign of Edward II when a fleet was assembled to sail against Gascony. At this time Plymouth was known as the "Three Cities", the towns of Stoke, Stonehouse and Sutton (Old Town) were separated by three rivers - Stonehouse Creek which extended from Mayflower Marina to Mutley, Mill

Lake which extended from Millbay to Stonehouse and Sutton Creek. The Navy expanded to Devonport throughout the Tudor Era and the land around Sutton harbour was reclaimed and the harbour fortified. Stonehouse Creek and Mill Lake were channeled underground in Victorian Times. The port of Plymouth was very successful, but was at the mercy of strong and frequent southwesterly gales, and many ships were lost at anchorage. It was not until 1796, when an East-Indianman the *Dutton* sank in the Hamoaze Channel, that the need for a breakwater became urgent. The Admiralty, fearful of having to move to Falmouth, commissioned a survey of the Sound with a view to building a breakwater. Four plans were submitted, (i) a pier out from Penlee point, that would be 1km long and 27m high - this was rejected on grounds of expense, (ii) two piers to be built from Staddon Point to Panther Rock (2km) and from Andrum Point to Shovel Rock (1.5km) - this was rejected on grounds of expense and the probability of siltation. (iii) a pier from Andrum Point to Panther Rock (2.6km) - rejected on expense and silting potential and, (iv) a solid breakwater between Panther, Shovel and St. Carlos Rocks. Two arms would be extended out at 120° at either side from the main breakwater creating a wall 1.7km long (Merratt 1980). This plan was accepted. It was estimated that it would take two million tons of stone, and cost £ 1,055,200 to build the breakwater. The first stone was dropped on 12th August 1812. By the end of 1812, 43,789 tons had been sunk and some of the rubble became visible at low water. By 1827 the wall had been constructed and the faces of the Breakwater paved with granite. It was not until 1840, and several ship wrecks, that the foundations for the lighthouses were built. The building of the Breakwater ceased in 1847, two years after the official completion date, by when a total of 3,620,444 tons of rubble had been deposited. In 1871 a concrete wavebreaker was lowered into place on the seaward side of the Breakwater. From 1928 to 1969, 430 hundred ton gabions were dropped. The top of the Breakwater is now 6.3m above L.W. Springs. The Centre Fort was built in 1860 by the Duke of Wellington on Shovel Rock, as part of the extensive Palmerstone Fort defence of Plymouth.

1.3 Bathymetry

The coastline of Plymouth Sound is steeply sloping rock, with shallower gradients occurring in the more populated areas and in the estuaries. The estuaries are characterized by extensive intertidal mud flats. There are three beaches. A sandy cove at Bovisand Bay, a granule-pebble beach

at Cawsand and a gravelly beach at Jennycliff Bay. The topography (Figure 1.2) of the inlet floor is irregular. The most remarkable feature is the deep-water Channel from Torpoint to Mallard Shoal; it has steep sides, and reaches 40m at its maximum depth. This Channel is referred to herein as the Hamoaze Channel, which acts as a blanket name and includes the navigation lanes of The Hamoaze, The Narrows, Drake Channel, Asia Pass and Smeaton's Pass. The name is derived from the Saxon "Ham-ooze" and refers to the extensive mud flats in the Lower Tamar Estuary. The body of the Sound has a sloping sea bed from an average depth of 5m in the west to 8m in the east. The area of the Inner Breakwater shallows to 6m and separates the Western Channel, which has a depth of 11-12m, from the Eastern Channel, which has a depth of 8-10m. Inside the Breakwater, these channels have a converging character; but shallow to 8m, still some 1.5km apart and lose their identity in the main part of the Sound. South of the Breakwater, the topography is characterized by two north-south rocky shoals which shallow to 5m below sea level. These are separated by sand-filled channels and extend 3.5km southward to the 30m isobath.

1.4 Tides

The amplitude and phase of tidal changes in Plymouth Sound are directly linked with the English Channel tidal distribution. In the English Channel the geostrophic (coriolis) and frictional forces are evident, causing the tidal bodies to rotate clockwise. This causes greater tidal ranges on the French coast and the co-tidal lines meet at a degenerate amphidromic point on the landward side of the Isle of Wight. In the Western English Channel, the tide has the character of a progressive wave, within which the streams are strongest in the centre (Lee & Ramster, 1976). The M_2 lunar semi-diurnal is the most significant harmonic component in the Plymouth region (Pingree 1980). The principal solar semi-diurnal component has one third of the amplitude of the M_2 tide. On spring tides, the semi-diurnal solar S_2 and the lunar tide, M_2 , are in-phase, resulting in an amplitude four times that of the out-of-phase regime. Out-of-phase neap tides have an amplitude of two thirds of that of the in-phase M_2S_2 . The residual surface-current movement in the Plymouth area of the Western English Channel throughout the year is to the west. This is predominantly due to the frequency of southwesterly winds. The bottom Atlantic-derived water correspondingly moves eastward (Lee & Ramster 1976). Initially, it was thought that

during winter the residual circulation in the English Channel was clockwise, and that it reversed in summer. This is actually due to the position of the salt tongue which lies close to the English coast in winter and closer to the French coast in summer. The migration of the salinity axis creates a density driven current system (Pingree 1980). The Ministry of Agriculture, Fisheries and Food (M.A.F.F) commissioned a series of Woodhead Sea bed Drifter drop experiments in the Western English Channel from October 1969 to January 1970 (Jones 1974). Recovery of the near-shore buoys showed the bottom-current paths to flow predominantly to the west. However, drops near the Eddystone were recaptured around Start Point, showing a trend to the east. The experiment was restricted in that drops were made in winter and the bottom-current paths may change seasonally. The circulation in Plymouth Sound is dominated by tides, of which the M_2 lunar semi-diurnal is the most significant harmonic component (Table 1.1). The mean Spring range is 4.7m, and the mean Neap range is 2.2m. The Mean High Water interval is 5 hours and 20 minutes and the age of the tide is 51 hours and 30 minutes. This means that Low Water (Spring) occurs at 13.00 hours in Devonport (George 1982). There is a permanent tidal gauge at H.M.S. Devonport. A tide gauge was placed on the Breakwater in 1941, and gave a yearly mean of 5.6m H.W (Spring Mean) and a Neap Mean H.W. of 4.8m. At Devonport, the tidal curve is slightly flattened at High Water, and sharpened at Low Water. The general maximum ebb tidal stream in Plymouth Sound is 1.2 knots (0.6 ms^{-1}). The strongest tidal streams occur in The Narrows between Wilderness and Devil's Points, and across The Bridges, where velocities are of the order of 2.8 knots (1.4 ms^{-1}). Tidal streams in the Tamar and the Lynher are quite strong: 1.6 knots under low runoff on the ebb; and 2.6 and 2.2 knots on the ebb and flood respectively (Springs). Tidal streams in the Plym are relatively weak. Typical rates of flood and ebb of the Tamar into Plymouth Sound are 0.8 ms^{-1} under low run-off conditions. Up river at Calstock, true estuarine conditions develop with a long, reduced ebb and a short, enhanced flood. With increasing freshwater discharge, the levels of Low Water and the ebb intensity are both increased.

Darwin Designation	H(cm)	K	Period
Long period			
M _f Lunar fortnightly	2.10	70.5	327h.84
Diurnal species			
O ₁ Principal lunar	5.52	344.2	25h.82
P ₁ Principal solar	2.23	95.9	24h.07
K ₁ Luni-solar	7.65	104.5	23h.93
Semidiurnal species			
N ₂ Lunar elliptic	31.64	128.8	12h.66
M ₂ Principal lunar	169.13	143.0	12h.42
S ₂ Principal solar	60.26	198.3	12h.00
K ₂ Luni-solar	17.28	196.1	11h.97
(based on Mean Spring measurements)			

Table 1.1

Devonport: observed tide amplitudes and phases.

where: K = lag of the phase of the tidal constituent behind the phase of the corresponding equilibrium constituent at the location of the tide gauge, and Period = the time required for the tidal harmonic to repeat itself in solar hours.

1.5 River Inflow

The river inflow into Plymouth Sound is strongly dependant on the regional precipitation. The Tamar inflow has a maximum of 321.56 m³s, and a minimum of 0.580 m³s. The Plym has a recorded maximum inflow of 31.01 m³s, and a minimum of 0.12 m³s. South West Water Authority have released 1979 records for the river inflows to Plymouth Sound (Table 1.2).

Gauge station Location	River	Catchment Area km ²	Average m ³ s Gauge Flow	Gauged Flow	
				Max	Min
Tiddeford	Tiddy	37.2	0.85	6.40	0.06
Pillaton	Lynher	135.5	4.25	-	-
Gunnislake	Tamar	916.9	22.42	321.56	0.58
Copewell	Tavy	205.9	6.65	-	-
Cornwood	Plym	192.0	2.18	31.01	0.12

Table 1.2

1979 River Inflow into Plymouth Sound (Hiscock & Moore 1986)

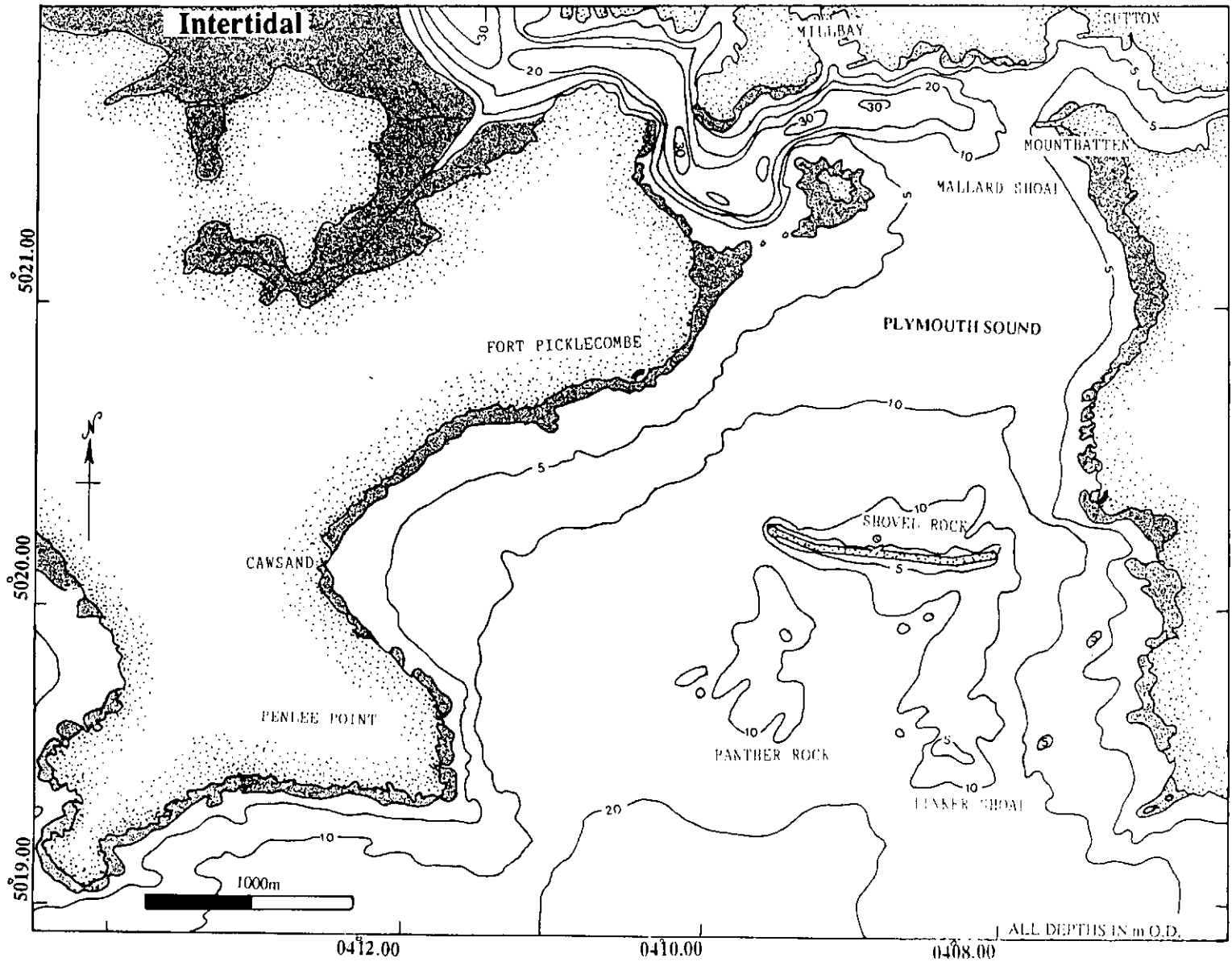


Figure 1.2 General bathymetry of Plymouth Sound.

1.6 Weather

The pressure system over southwest Britain is derived from the North Atlantic. Usually the pressure is low over Iceland and high near the Azores. In the English Channel there is an increase in pressure from north to south, creating a general air stream from a southwesterly direction. The pressure gradient is steeper in winter. During high southwesterlies, the eastern side of Plymouth Sound is affected by swell and strong wave action. The fetch at Jennycliff can be of the order of 6km, and winds of gale Force 8 can generate waves of about 1.2m height (Darbyshire & Draper, 1962). Long fetches also occur in the Lynher and Tamar. The presence of the Plymouth Breakwater offers protection to the northern shores. Storm surges on the South West coast are less frequent than in the North Sea, and are usually generated by small secondary-depression Westerlies moving over large areas of open shelf. If the surges correspond to High Water Springs, the sea level can rise an extra 2-3m. The effects of increased sea level can be exacerbated by the prevailing winds.

1.7 Temperature

The air temperature reaches a maximum at the end of July and a minimum in late February. The offshore sea temperature is monitored at the Eddystone Lighthouse and the temperatures show a seasonal increase from 8.5°C in winter to 16°C in summer (Lee & Ramster 1976). The temperature changes in Plymouth Sound lag about two weeks behind the offshore sine curve, with greater depression in winter, and elevation during summer. There is an asymmetry in Plymouth Sound, where the warming phase is shorter than the cooling phase. The Sound water surface temperatures are strongly dependent on the frequency, duration and time of dominant southwesterlies (Maddock & Swann 1977). Westerlies in Spring bring less rain than they do in Autumn. The last sea temperature monitoring of Plymouth Sound ended in 1971, the average recorded temperatures were 17°C in summer and 8.7°C in winter. Southward & Butler (1972) noted that the temperatures of the Western English Channel showed periods of definite cooling in both the air and the sea surface, from the warm 1920's to 1958, and culminating in the severe winter of 1962/63. Measurements taken in the Yealm Estuary during the cold winter of 1962/63 gave temperatures of -1.5°C (Crisp 1964). This cold winter caused a mass-mortality of much of the benthic life in the Western English Channel and associated coastal regions. Cold winters were also recorded in 1917,

1940 and 1947. Dominant warm periods also have been recorded in the 1920's and 1950's (Maddock & Swann 1977). The last warm period started in the early 1970's and is continuing today; this now appears to be a direct response to the so-called Greenhouse effect (Section 8.4).

1.8 Salinity

Data on the salinity of Plymouth Sound are sparse, but the salinity distribution in the Tamar has been monitored extensively by workers at the Plymouth Marine Laboratories (Uncles *et al.* 1983). In 1938, as part of one such experiment, the salinity at Drake's Island and the Breakwater was monitored over a year, and an average of 34.5‰ was recorded, with a minimum of 27‰ at both sites after exceptionally heavy precipitation (Hiscock & Moore 1986).

1.9 Sewage

In total there are 20 sewers discharging into Plymouth Sound. Five are located between Millbay and the Hoe and serve c. 76,610 members of the population and all are untreated. The sewers are owned by South West Water and discharge on an ebb tide. The sluice gates are old and occasionally leak (anonymous *pers.comm*). There are several outfalls in the Tamar, all of which are treated. Industrial waste is disposed through the storm drains. There are no records of any waste or sewers discharging off the Royal Naval Dockland at Devonport, which "doubtless discharges wastes into the Hamoaze although the nature of these wastes can only be speculated" (Nature Conservancy Council Report by Hiscock & Moore 1986).

1.10 The Investigation

Several investigative methods were employed at different times during the survey.

Initially, sea bed samples and observations of the character of the sea bed were made by SCUBA divers led by the author. The divers used regular SCUBA (Self Contained Underwater Breathing Apparatus) equipment with some modifications made during the study (Section 4.2.3). Diving was on a reciprocal basis in that sampling dives were scheduled if the author assisted in student training and biological sample collecting. The first samples were taken from underneath the Admiralty buoys from inflatables, but as sampling progressed and more precise position fixes were required,

the *D.V. Aquatay*, which is fitted with a Decca Navigator, was used as a diving platform. From the initial observations made on the sea bed it became apparent that the sediments in Plymouth Sound range from fine muds to cobble sized gravels with outcrops of clean-swept rocks. Diver sampling continued throughout a three year period and was supplemented in the summers of 1989 and 1990 by grab sampling (Section 4.2.3). The samples were processed according to the methods discussed in Section 4.3.

Many gravels were identified on the sea bed, which cannot be moved under any combination present day of current and wave motion. To understand the time of formation of these deposits, and those identified by the seismic surveys, an extensive literature review of sea level rises in the South West and the English Channel was undertaken (Chapter Two).

In 1989 the Sound was acoustically surveyed, using side-scan sonar (Chapter Three), to map the sediment distribution on the sea bed. The side-scan sonar was towed aft of the Polytechnic Catamaran *R.V. Catfish*, which is equipped with a Decca Navigator, Trisponder and a Hydrographic echosounder. The acoustic returns were calibrated by diver sampling and a sea bed texture chart was compiled, delineating the spatial and temporal extent of the sedimentary zones.

Traditional oceanographic techniques are often time consuming and require the repeated deployment of expensive equipment for long period of time. In order to identify the tidal streams and water bodies of Plymouth Sound, an investigation was mounted into the feasibility of using remote sensing. Plymouth Sound had already been overflown by airborne remote sensors as part of two previous campaigns (Section 6.4.2). These data were re-processed and showed several previously unidentified water bodies. In the summer of 1989 Plymouth Sound was overflown, at Low Water, by a Daedalus AADS 1268 Airborne Thematic Mapper (Section 5.4.1). Concurrent with the overflight, an extensive groundtruth collection of *in situ* data was acquired from three of the Polytechnic Vessels. The results, both airborne (Section 6.4) and ground (Sections 6.2 & 6.3), showed a marked continuity between the sea bed and the surface characteristics of the water. In 1990 the survey was repeated at High and Low Water, with a similar groundtruth collection. X-ray Diffraction analysis and processing of the 1989 groundtruth data identified distinct suspended sediment types characteristic of the different water bodies.

The suspended sediment was also found to have intrinsic spectral signatures. In 1990 a band-selectable CASI (Compact Airborne Spectrographic Imager) sensor (Section 5.4.2) was flown over Plymouth Sound, at High Water, in an attempt to delineate the different suspended sediment types. The concurrent groundtruth campaign included temperature and salinity measurements to the sea bed, in order to establish continuity between the surface and the sea bed.

The sedimentology of Plymouth Sound and the dominant directions of transport were identified during the side-scan sonar survey, with two areas being characterized by featureless acoustic response, where no current direction could be identified. In the same area, the remotely sensed imagery showed the presence of tidal gyres and the divers reported mid-water and sea bed currents. To establish the relationship between the water movement and the sea bed, orientated core samples were taken by divers and the physical and magnetic properties of the sediment were measured (Chapter Four & Chapter Seven). Sedimentological analyses of the sediment recognized a coarse shelly layer (Section 4.6.1) in the sediment at 20-25 cmbsf (centimeters below the sea floor) this was correlated to the cold winter of 1962/63 and acted as a datum (Crisp 1964).

The conclusions of the investigation are presented in Chapter Eight in three main parts (i) the present day hydrography of Plymouth Sound, (ii) the present day sedimentology and sediment transport paths, and (iii) the history of Plymouth Sound. The consequences of a global sea level rise, and the contributing factors are briefly examined. During this work several methods and techniques were put under test and modified, their performance and requirements being examined.

- CHAPTER TWO -

- GEOLOGY AND QUATERNARY HISTORY OF THE SURVEY AREA -

2.1 Introduction

In order to evaluate and quantify the different geological influences on the development of Plymouth Sound, it is necessary to examine the sedimentary and tectonic history of South West England through geological time. Two main factors must be considered - the geological history of the area and sea level changes. The geological and structural development of the Plymouth region is closely linked with that of mainland North West Europe (Section 2.2), and thus has affected the development of drainage and configuration of the region. The radical climatic changes experienced globally during the last 2.4 Ma also played a decisive role in the present coastal configuration of Plymouth Sound and the English Channel (Section 2.3.5). Currently, the Plymouth area lies in a temperate latitude and is undergoing some downwarping, directly associated with the last (Devensian) glaciation. Constant re-adjustments of the oceanographic conditions are occurring in response to the present rising sea levels. In view of these previous controls it is not surprising that there are many problems and controversies in attempting to establish the history of sea level rise in the Plymouth Area. There are several characteristic formations generally accepted to be indicative of sea level changes, for example, raised beaches, buried valleys, submarine cliffs and planation surfaces. All these features have been identified in the Plymouth Area, but their ages have been disputed. As part of this investigation, these features have been re-examined (Section 2.4) and dated as accurately as possible.

As Plymouth Sound has direct communication with the English Channel, these regions share a similar sedimentological and oceanographic history. The development of the English Channel through time is examined (Section 2.3.5) and the evidence pertaining to sea level rise is applied to the development of Plymouth Sound (Section 8.3).

2.2 Geological History

South West England is characterized mainly by Devonian and Carboniferous rocks with only a few inliers of Ordovician quartzites and Silurian limestones (Edmonds *et al.* 1969). The geology of the Plymouth area was first mapped by Ussher (1907), and has been re-mapped by House *et al.* (1977) and Chandler & McCall (1985). The structure and stratigraphy of South West England is extensively discussed by Matthews (1977) and Edmonds *et al.* (1969).

During Precambrian to Ordovician times, it is postulated that South West England formed part of an extensive landmass, known as Pretannia, surrounded by the Iapetus ocean (Cope 1987). This crystalline metasedimentary landmass forms the basement upon which the extensive Devonian sediments were deposited. At the start of the Lower Devonian, the Plymouth region formed a southerly extension of the Caledonian Continent and lay south of the equatorial belt with semi-arid climate. During the Devonian, the Siegenian transgression inundated the coastal areas and the accompanying differential subsidence of the shelf led to the development of a basin. Sediments and flash floods drained off the Caledonian highlands to the north, depositing sediments into the Armorican, or West European Geosynclinal Sea. This sea is thought to have been divided into a series of local basins (Matthews 1977). Basin subsidence was controlled by basement East-West faults and the sediments were deposited in a series of deltaic sequences which passed laterally into deep water basinal facies (Edmonds *et al.* 1969).

Throughout the Palaeozoic sedimentation in the South West was influenced by the intensifying Variscan orogeny. Initially a series of East-West trending basement faults and vertical basins developed (Pound 1983), with later superimposition of NW-SE Variscan strike-slip faulting (Selwood 1990). The Lower Devonian is represented in the Plymouth area by the Dartmouth Slates which fringe the south part of the Sound at Bovisand and Penlee Point. These slates are a continental facies (Cope 1987, Selwood 1990) and pass upwards into the Meadfoot Beds (Siegenian) and the Staddon Grit formation. Both formations are represented by a sequence of sandstones, siltstones, intraformational conglomerates and thin limestones (Evans 1983). The boundary between the two formations approximates to the Siegenian/Emsian deepening of the basin (Pound 1983). The Staddon Grit is diachronous and has a maximum thickness of 100m

(Chandler & McCall 1985) and is followed conformably by the Jennycliff Slates (Late Emsian - Early Eifelian). These sediments are composed of a series of interbedded black and grey deep water slates, with interbedded diachronous tuffs and vesicular lavas. The deposits are thought to represent the Middle Devonian transgression (Pound 1983). The Jennycliff Slates have a maximum thickness of 500m and pass upwards into the Plymstock Volcanic Member. The slates are fissile and subjected to more rapid erosion than the surrounding lithologies. The structure of the Dartmouth Slates to the Jennycliff Bay sediments was summarized by Chapman (1983). The slates are followed conformably by the Plymouth Limestone (Eifelian - Givetian). This is a massive limestone with alternations of abundant stromatoporoid colonies separated by thin calcareous muds, and "reefal" developments of abundant *in situ* fauna which pass laterally into coarse broken bioclastic coquina. The limestone is considered to have been developed on a series of East-West trending swells. The sedimentary sequence continues with the deposition of purple-grey shales of the Plympton Slate Formation (Frasnian - Late Famennian). Sediments include thin limestones, slates and diachronous ash bands.

Volcanic activity was widespread throughout the Devonian. Ash bands occur in the limestones and silts and Drake's Island is a resistant remnant of a Middle Devonian volcanic knoll. The Middle Devonian sediments are generally finer than the preceding Lower Devonian facies; this is attributed to denudation of the Caledonian high (Edmonds *et al.*: 1969) and local basin movements (Selwood 1990).

The Lower Carboniferous sediments in the Plymouth area are characteristic of a warm temperate shallowing geosynclinal sea. Lithologies include cherts, black limestones, siltstones and mudstones with interspersed volcanics. These pass upwards into the Upper Carboniferous shallow marine coal (Culm) facies composed predominantly of sandstones and shales deposited in a series of small unstable local basins, with turbidite deposition in the marginal marine zone.

The Variscan orogeny commenced at the end of the Devonian and continued to the Permian. The tectonism was polyphase and folded the Palaeozoic and Precambrian basement into a series of complex structures. The orogeny was a result of the right-lateral relative motion of a northern

plate comprising the Canadian Shield, Greenland and Europe, and a southern plate represented by the Armorican and/or the African Shield (Arthaud & Matte 1977). The lithologies of the Plymouth area were deformed into a series of first order westnorthwest-eastssoutheast fold and thrust belts following the same trend as those experienced by the Northern Plate. A series of second order North-South faults (Malvernoid) also developed. The history of local deformation is summarized in Arthaud & Matte (1977), Matthews (1977), Chapman (1983) and Gayer & Jones (1989).

The Cornubian granitic batholith was emplaced into the folded pile of Palaeozoic rocks towards the close of the orogeny (c. 295 Ma) and is presently exposed in six cupolas. The mineral veins associated with intrusion and contact metamorphism follow Northeast-Southwest trends characteristic of the Caledonian.

Throughout the Permian and Triassic the South West peninsula lay in northern low desert-belt latitudes. Initially, the area was part of a narrow graben zone caused by a late extensional phase in the Variscan tectonics (Arthaud & Matte 1977). The sediments are composed of breccia and breccio-conglomerates characteristic of flash floods washing large alluvial plains. During the Triassic non-marine marls and breccias were deposited.

During the Jurassic, much of the South West peninsula was land and formed part of the Laurasian continent. The fragmentation of the North American - Eurasian (Laurasian) plate began in the Jurassic. A marine transgression marked the start of the Cretaceous, with local block uplift causing the rivers to flow towards the west and empty into large delta-swamps. In the Lower Cretaceous the advancing sea deposited the Greensand facies in shallower water and the Gault facies in the deeper waters towards the east. The South West peninsula landmass was submerged during the Turonian. Further basinal subsidence occurred throughout Europe, in the Upper Cretaceous, and led to the deposition of the calcareous Chalk deposits. Towards the end of the Cretaceous instability began in the Alpine region.

In the Cenozoic, Eurasia was affected by the complex interplay of two major tectonic events: the continued separation of the Eurasian and North

American plates and the Alpine orogeny. In Europe, the Alpine orogeny created compressional East-West structures in response to the continent-to-continent collision between the Eurasian and North African plates. In the South West landmass, these movements were generally translated along pre-existing northwest-southeast Variscan structures. The break-up of the Eurasian and North American plates resulted in extensional features.

Uplift in the Late Palaeocene - Early Eocene raised much of the South West, in particular Dartmoor, above sea level. The granite batholith has since maintained the landmass buoyant. There are large deposits of residual fluvial gravels which accumulated during the gradual unroofing of the Dartmoor granite and by *in situ* dissolution of the Chalk. The prevailing climate was semi-arid. The Alpine uplift reached a peak during the Mid-Miocene, culminating in an inversion of the Hampshire and Channel basins, the Bristol Channel and Western Approaches basins, and updoming of the Paris Basin. In the Early Eocene, the compressional forces reactivated the major wrench faults (e.g. the Sticklepath Fault) causing large basinal downwarping, in particular the Bovey and Petrockstowe Basins. By the Late Tertiary the river systems of the South West were well established, and controlled by the Northwest-Southeast trending fault system. The sediments of the Bovey Basin were deposited by a river flowing southwards into the English Channel area. This is possibly the Palaeo-Dart.

The Lundy igneous complex was intruded on an northward extension of the Variscan Sticklepath (Northwest-Southeast) dextral wrench-fault. The Bristol Channel opened during the Alpine tectonic phase on a reactivated Variscan south-dipping thrust (Gayer & Jones 1989).

The English Channel is a funnel shaped epicontinental shelf sea with a solid rock floor extending southwest-northeast over 700km², the breadth varies from 30km in the east to 180km in the west. The Channel sea bed slopes gently southwestward from -70m O.D. in the east to -100m in the Western Approaches. The English Channel opened as a response to Alpine compression and North Atlantic extensional tectonics. The movements were translated along Variscan structural grains of a major Northeast-Southwest Palaeozoic syncline. It has been suggested that the English Channel was formed sometime during the Miocene as an

arm/aulacogen system of the North Atlantic. However, the system was deflected southeast beneath the British Isles landmass in response to the Alpine movements (Smith & Curry 1975). During the Pliocene the sea level stood at +200m O.D. (Mottershead 1977). Marine regression during the Late Tertiary cut a series of cliffs marking the strandline of pre-uplift sea levels (Edmonds *et al.* 1969). The peneplains are recognized over the coasts of the South West and Bristol area at three levels: +330m, +250m and +143m O.D. (Perkins 1972).

Miocene sediments in the Western basin of the English Channel were deformed into a series of open folds and were strongly related to the Variscan configuration of the basement blocks. An erosion surface truncates some of the folds, the surface of which is slightly warped (probably during the L. Miocene - E. Pliocene). Marine conditions prevailed in the Western Basin during the Pliocene when calcareous siltstones were deposited in a series of south to southwesterly low angle (1°) cross-sets. The presence of cross bedding is taken to indicate a high rate of sediment influx. There is evidence of basin subsidence during the Pliocene, on the same axis as the pre-Miocene basements. The geology of the Plymouth Area is summarized in Figure 2.1.

The last 2.4 Ma have been characterized by radical changes in global climate, causing continental ice to develop over some landmasses. During the glacial phases much of the free water became bound up in the ice sheets causing a decrease in global (eustatic) sea levels. During the last 100,000 years, the glacial episodes of the Quaternary were characterized by a slow accretion of ice sheets (c. 90,000 years) associated with a marine regression followed by a rapid deglacial or transgressive phase (c. 10,000 years). Due to the extensive nature of the glaciations, their deposits and erosive phases have been recognized all over Europe, and a plethora of local and regional names exist. Their correlation is complicated by differential vertical movements associated with the glacial cycles. In recent years, under the threat of rising sea levels, the bias of Quaternary research has concentrated on the extent of the ice sheets and the positions of the palaeo sea levels. The spatial extent of the ice sheets during the Late Quaternary is summarized in Figure 2.2.

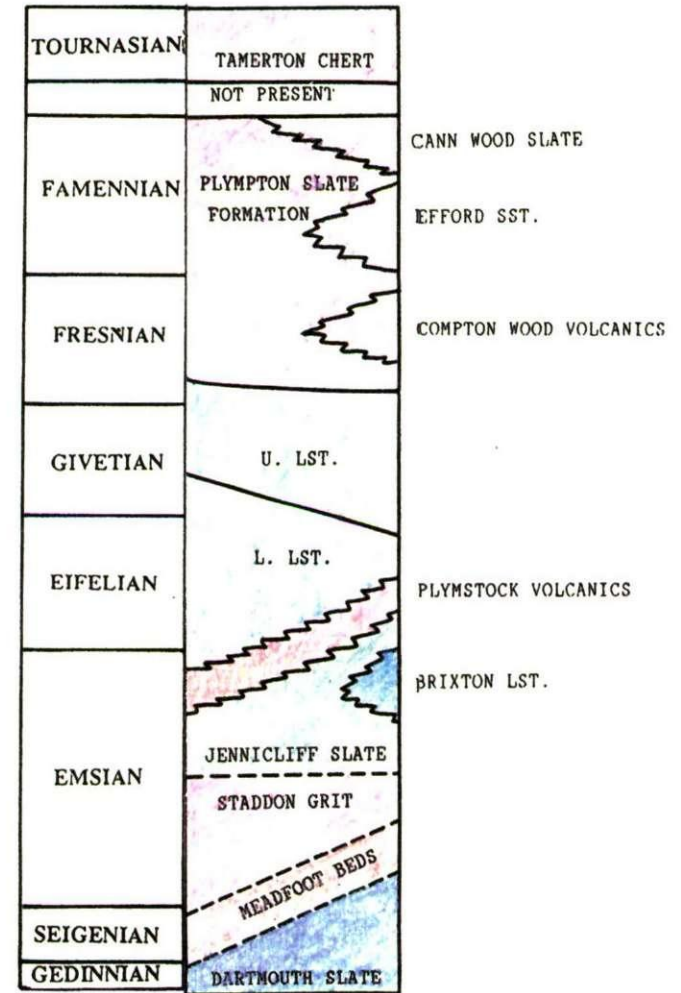
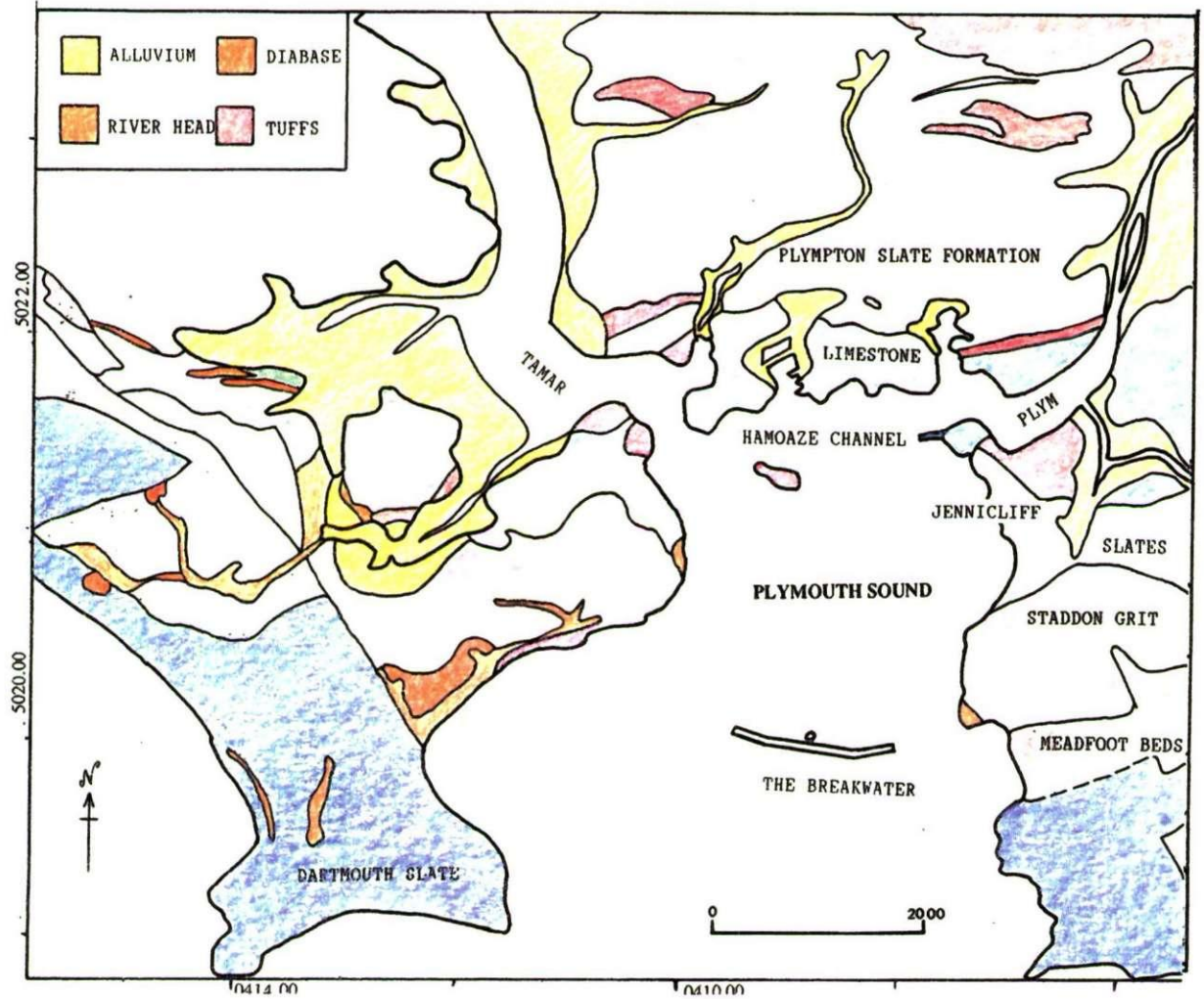


Figure 2.1 The Geology of Plymouth and environs.

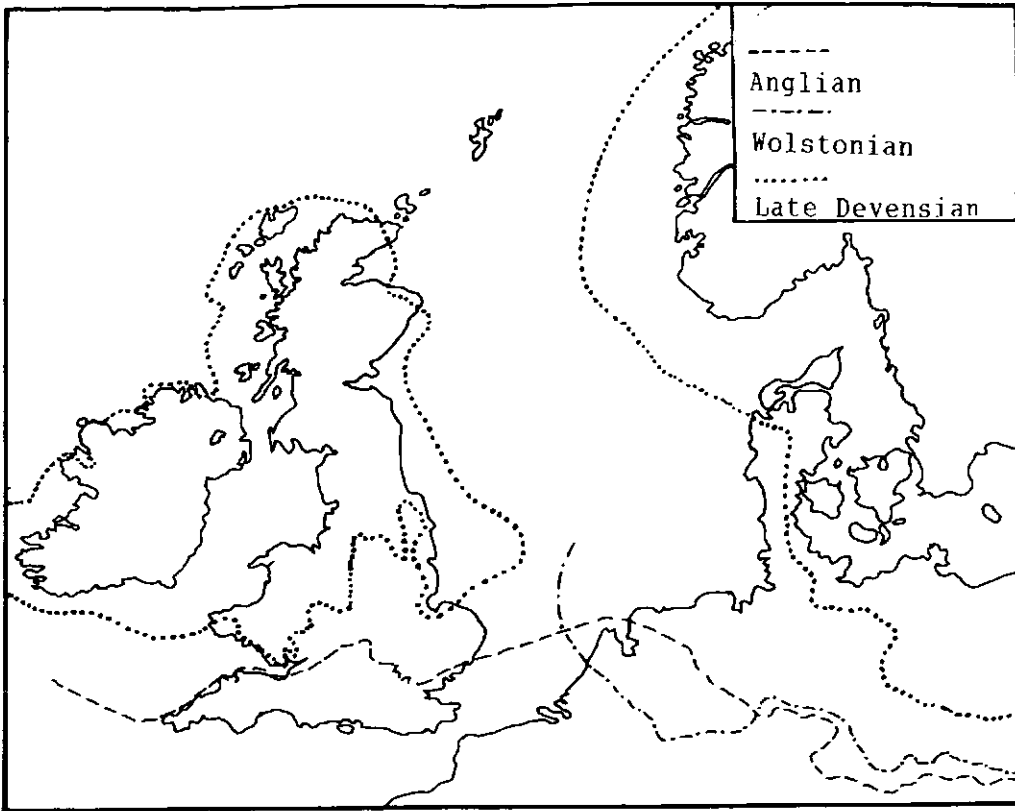


Figure 2.2 The maximum southward extent of the ice during the Late Quaternary glacial stages (Gibbard 1988).

In 1975, it became evident that a correlation of the Quaternary was necessary and the IGCP (International Geological Correlation Programme) Project 61 (1975-1982) "Sea level movements during the last deglacial hemicycle (c. 15,000 years B.P.)" was set up to collate and categorize the available information and establish a series of graphs of sea level rise. Project 61 was very successful and not only collated all the sea level curves but established a set of rules for Quaternary Research (Flemming 1982, Tooley 1985 Shennan 1989). In this thesis the British Terminology will be used (see Table 2.1)

STAGES		Prevailing	Archaeological	Years
Britain	N.W. Europe	Climate	Period	B.P
Flandrian	Holocene	Temperate	Historical	— 1,600
			Roman	— 2,000
			Iron Age	— 2,400
			Bronze Age	— 3,800
			Neolithic	— 5,000
			Mesolithic	— 10,000
L. Devensian	Weichselian	Cold	Upper Palaeolithic	— 15,000
M. Devensian			— 26,000	
E. Devensian			— 35,000	
			Middle Palaeolithic	— 70,000
Ipswichian	Eemian	Temperate	Lower Palaeolithic	— 100,000
Wolstonian	Saalian	Cold		— 200,000
Hoxnian	Holsteinian	Temperate		— ?
Anglian	Elsterian	Cold		— 2,000,000

Table 2.1

Classification of the Pleistocene (Modified from West (1988) and Culver (1979))

Glaciation in the English Channel

The evidence of glaciation in the English Channel is controversial. The main problem in proving its occurrence is that, to date, there have been only small patches of drift located on the Channel floor. However, seaward of the eroded platforms and cliffs, the sea floor has a low gradient, possibly caused by erosion by Quaternary ice. During the maximum of the Wolstonian II, the Irish Sea ice sheet is thought, by some, to have flowed around the Isles of Scilly, impinging on the Atlantic coasts of Devon and Cornwall, and extending eastward up the English Channel (Kidson 1977).

Local ice is suggested to have occurred on the Cornubian massif during the Wolstonian I (251,000 B.P. SL = -150m) and during the Wolstonian II (195,000 to 128,000 B.P. SL = -180m) (Kellaway *et al.* 1975). There is no evidence of Cornubian ice during the Devensian. Ice did, however, cover the Bay of Biscay and Central France (West 1988).

2.3 Sea Level Changes.

Sea level is the intersection of the land with the sea, but, since Roman times, it has been recognized that changes in sea level occur on different scales both spatially and temporally. Global sea level changes are defined as "eustatic". The definition of eustasy has recently been re-examined by Morner (1976) and summarized by Tooley (1985) whereby eustasy is defined as "Ocean level changes irrespective of cause, determined by climatic, earth movements and gravity".

The processes of eustatic sea level change can be summarized under two main headings although they are all interrelated and are, in most cases difficult to separate:

Temperature dependent

These processes are related to climate change.

(i) Glacio-eustasy, whereby water is trapped in continental and marine ice sheets by abstraction from the ocean basins, and is released when they melt. This process is a consequence of secular changes of climate during a glacial-deglacial cycle. All recorded glacial advances in the last 5,000 years can be related to eustatic lowering of sea level by 3-7m (Fairbridge 1961).

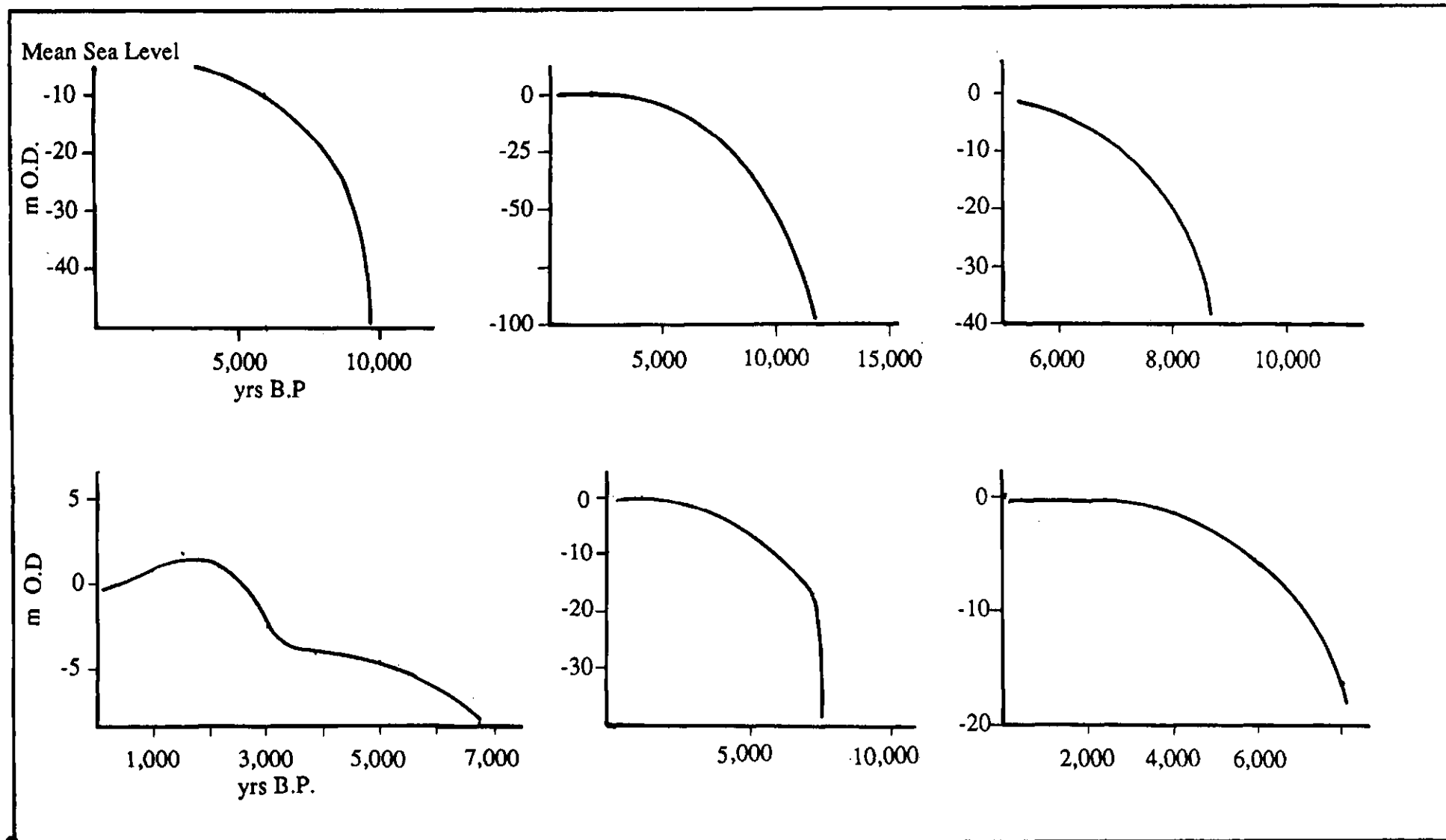


Figure 2.3 Sea Level curves for the South West (a) Clarke 1970, (b) Delibrias & Guillier 1971, (c) Hawkins 1971, (d) Delibrias & Guillier 1971, (e) Mottershead 1977, and (f) Kidson & Heyworth 1976.

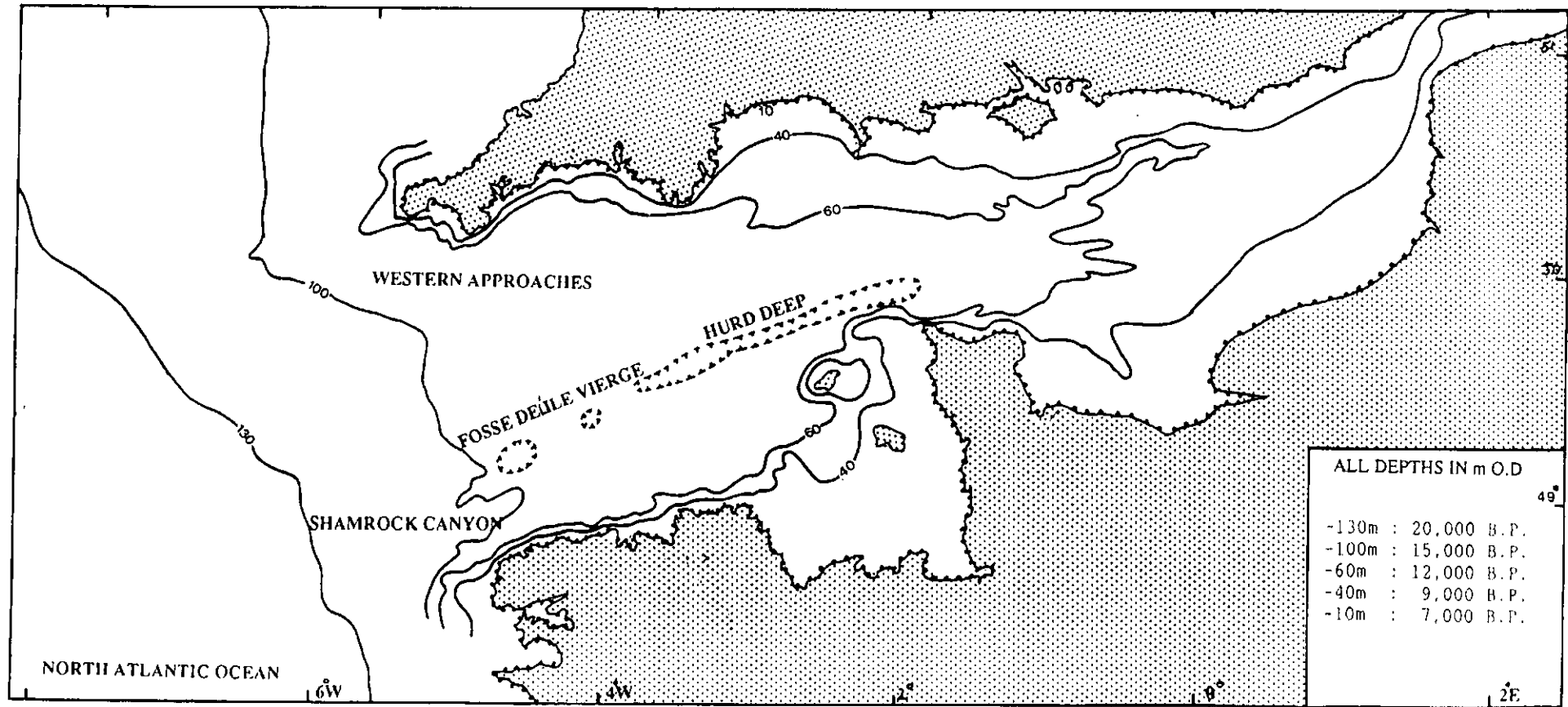


Figure 2.4 The Hurd Deep and Sea Level rise in the English Channel (Larsonneur *et al* 1982).

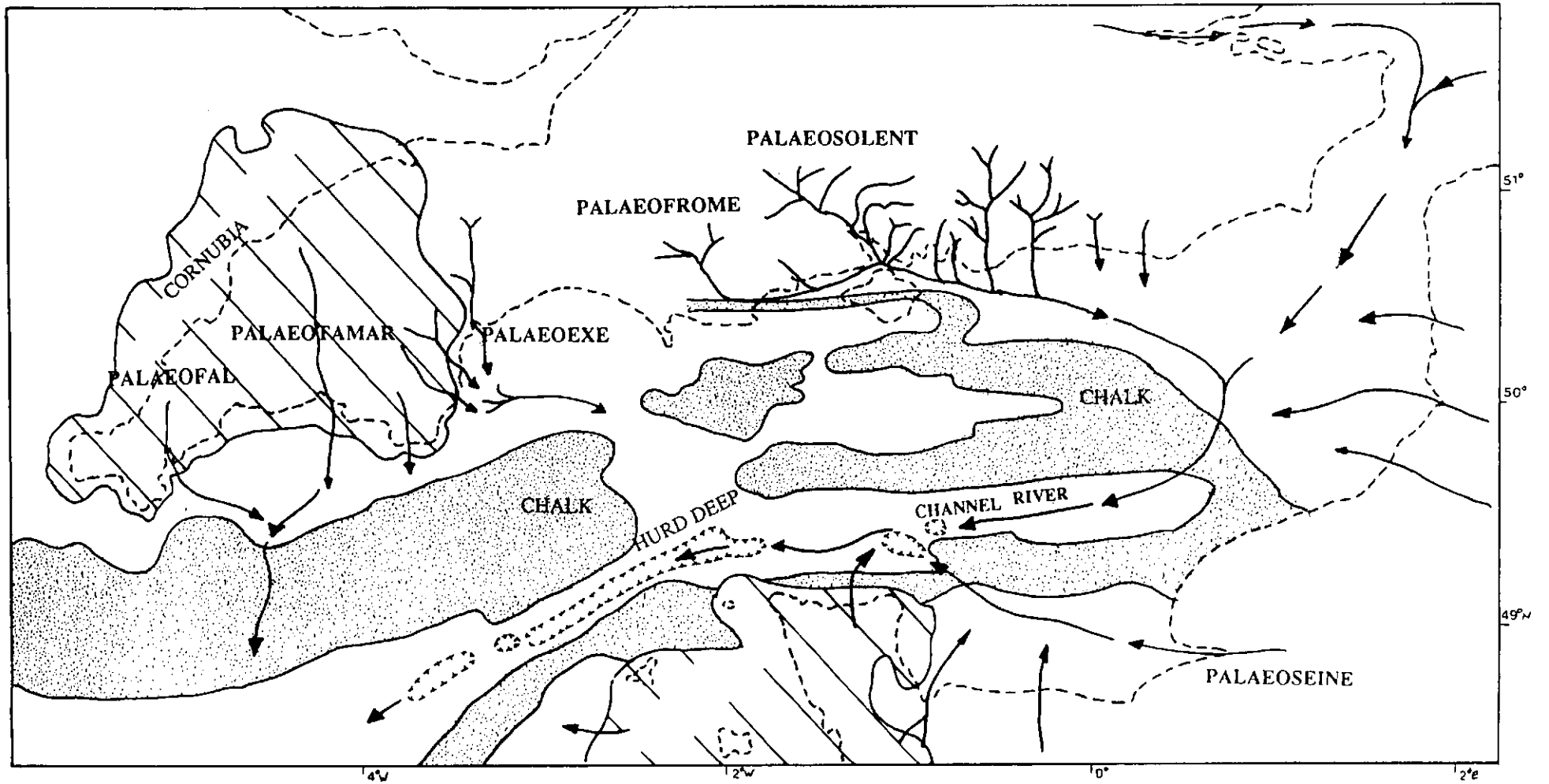


Figure 2.5 The Channel river and distributaries (Adapted from Dingwall *et al* 1975 and Gibbard 1988)

(ii) Thermal expansion of ocean water. Most models of glacial cycles assume constant sea surface temperatures. However, Fairbridge (1961) calculated that a net 1°C rise in oceanic water temperature would create a 2m sea level rise (More recent estimates are discussed in Section 8.4).

Crustal movements.

Changes in the geometry of ocean basins and associated crustal movements causing sea level changes have been described by Fairbridge (1961) as "tectono-eustasy" and have been comprehensively reviewed by Shennan (1983, 1989).

Factors influencing non-eustatic sea level changes can be divided into four categories: (i) vertical changes on coastlines caused by local isostatic movements, (ii) varying sedimentation rates, (iii) tectonic process, and (iv) anthropogenic activities. Additional small scale local changes are governed by atmospheric pressure, winds, ocean currents, geodetic changes and the density of sea water. The interrelation of all these processes is evident - local tectonic eustasy can cause local climatic changes, whereas large scale inundation or regression can result in regional or even global change in climate. There are several theories on the causes of fluctuations of climatic changes. The most plausible is the Milankovitch theory (Haq *et al.* 1987, 1988, Ruddiman & Duplessy 1985). Cold peaks on the Milankovitch radiation curve are in-phase with the cold peaks of the tropical water sea surface temperatures for the last two glacial-deglacial cycles. Milankovitch cycles occur with periodicity of 20,000, 40,000, and 100,000 years.

In response to climatic changes the global ice budget changes. Three main theories on the causes of fluctuations in the accretion and decay of ice sheets have been suggested.

(i) The Polar Front Theory was developed by Ruddiman & McIntyre (1976) whilst investigating Quaternary palynology in Scotland. They documented a periodic migration of a Polar Front which created changes in the climate on the land. An example is the relatively rapid accretion of the Scotland Ice-cap (11,000 to 10,000 years B.P.), reflected in the migration of Palaeolithic Man over North Europe.

(ii) The Decoupling of polar ice sheets (Anderson & Thomas 1991) in which rapid rise in sea level is brought about by the deterioration of terrestrial ice sheets. The increase in eustatic levels causes

decoupling of the polar ice sheets from the sea bed, resulting in rapid mass wasting and disintegration. This system produces high frequency, (10^2 to 10^3 year) but low amplitude eustatic events which can cause rapid shoreline transgressions on shallow continental gradients. This model provides a good explanation for the slow accretion of the ice sheets (90,000 years) and relatively rapid decay (10,000 years).

(iii) Much attention has been focused on the dramatic surges of mountain glaciers (Ruddiman & Duplessy 1985). These rapid advances have been attributed to ice streams "pulling" off ice sheets and caps (Hughes 1987), and surge tongues of ice slipping over proglacial surfaces (Andrews 1973). Additional theories and models are reviewed by Ruddiman & Duplessy (1985). All these models are interrelated, and, it is therefore difficult to evaluate the contribution of any individual process to the global scenario.

2.3.1 Methods for identifying sea level changes.

Sea level changes have been identified using a variety of techniques and observations.

Raised beaches and glacial material.

The oldest and most common technique is the mapping of raised beaches and the identification of glacial depository material, submerged forests (Reid 1913) and peats (Hawkins 1971) in relation to the ambient Mean High Water Mark and the intertidal zone.

Echosounder, side-scan sonar and SCUBA surveys.

In recent years, with the development of marine acoustics and SCUBA equipment, the subtidal zone can be directly investigated. The use of marine cliffs for the identification of sea level rises was first suggested by Cooper (1948) who, using an echosounder identified a cliff 4km SSW off Plymouth Breakwater known as The Ledges or Cooper's Cliff. Routine mapping of the near-shelf zone has shown continuous marine terraces and fluvial features which can be related to past sea levels. Divers were first employed to investigate marine cliffs and terraces by Fairbridge (1961) and have been widely used since (McManus 1975, Delibrias & Guillier 1971).

Seismics and buried palaeo valleys.

Continuous seismic profiling techniques have been used in rivers, inlets and shelf areas and often show the rock head to be incised some way below the present sea bed. The sediment infill usually exhibits one or more characteristic sedimentary structures. A marine regression can be identified by (i) the truncation of a boundary, (ii) onlap, (iii) basinward shift of a facies, (iv) change from marine to non-marine facies, and (v) progradation of delta lobes with incision of distributary channels.

Pollen analyses studies

Pollen in samples has been successfully used in the dating of Quaternary deposits (Oakley 1943) and estimating the ambient July temperatures. Pollen analyses of the Bay of Biscay area have been reported as showing a reliable temperature sequence (Turner & Hannon 1988).

Isotope techniques

Emiliani (1955) has published a series of carbonate temperature curves for the Late Devensian to present day whereby temperature changes can be related to sea level changes. A comprehensive review of isotope and other dating techniques is given by Catt (1988).

Radiometric methods

Both the Uranium series and ^{14}C techniques can be applied to shelly material and peat sampled in boreholes or subtidally by divers (Terasmae 1984 Catt 1988).

Amino Acids

The analysis of organic acids in shelly material is becoming more widely used. The technique and applications have been summarized by Bowen & Sykes (1988).

Tide Gauges

The use of such data has been outlined by Woodworth (1987) and the errors and problems were reviewed by Heyworth & Kidson (1982).

Archaeological information.

Submergence of dated archaeological sites can be used to establish the time of inundation (e.g. Delibrias & Guillier 1971, Hawkins 1971).

2.3.2 Features created by Sea Level changes.

The above methods are used to identify features created by possible sea level changes. These features can be described in four main groups:

Raised Beaches

Guilcher (1969), in a study of Hoxnian and Ipswichian shorelines (Table 2.2), recognized that sea level oscillated in response to glaciation. On the south coast of Britain two wave cut platforms occur with associated raised beach deposits at +35m O.D. and +20m O.D. The fauna of these sediments are Quaternary, but no precise dating has been carried out.

Marine Cliffs The use of marine cliffs in the interpretation of sea level changes has been documented by Donovan & Stride (1975) who acoustically surveyed the coastline of South West Britain, including the drowned rias of the rivers Fal, Fowey, Salcombe, Helford and Yealm extending from the intertidal zone to 8km offshore. They found the sea bed from MLWS to -20m was gently sloping and that series of marine cliffs recurred at greater depths. Marine cliff morphology is essentially constrained by four factors: (i) the original level of exposure, (ii) local tectonic warping, (iii) lithology, and (iv) the accumulation of talus at the base of the cliff. In the South West, marine cliffs were also recognized by Wood (1976) off St. Ives, and by Kelland (1975) during the Start Bay project.

Name	Cycle	Height of Beach O.D. m
Devensian	Glacial	
Ipswichian	Interglacial	+15 to +20 and +0.7m
Wolstonian	Glacial	
Hoxnian	Interglacial	+30 to +35m
Millazzian	Interglacial	+55 to +60m
Anglian	Glacial	
Sicilian	Interglacial	+80 to 100m
Gunz	Glacial	

Table 2.2

Raised Beaches throughout the Quaternary

Submerged Terraces

Submerged terraces were first described by Everard (1954), who identified several flights of terraces in Southampton Water. River cut terraces have also been identified on seismic profiles by a number of authors, as in the PalaeoSolent (Dyer 1975), the Teign and Exe (Durrance 1971, 1974).

Buried Channels

Buried channels were first described by Colenso (1832) whilst referring to tin workings in Cornwall. In 1898 Codrington described submerged valleys beneath the River Dart, Devon. Two palaeo meanders and buried channels have been identified in Start Bay; the maximum incision was to -42m and the width of the channels varied from 100 to 400m (Kelland 1975). Channels have also been recognized in the Teign (Durrance 1971), Erme and Taw-Torrige (MacFarlane 1955), the Exe (Durrance 1974) and Solent (Dyer 1975). The heights of the terraces, cliffs and buried valleys on the South West coast are summarized in Table 2.3.

2.3.3 Critique of the evidence pertaining to sea level changes.

There are many problems encountered when researching sea level changes in any one area. The problems can be summarized under five broad headings:

Seismic profiles and siliclastics.

A total of 119 global sea level changes have been postulated from the Triassic to the present day (Haq *et al.* 1977). Over 50% of these have been identified by seismic profiling and establishing coastal onlap sequences. Evans (1979) showed that exactly the same depositional sequence could be produced during both regressive and transgressive scenarios, if the major control was the abundance of mobile siliclastic material available. Evans also noted that, after a transgression, the "prograding mud-blankets extend out over the surfaces from adjacent shorelines or from other areas of...deposition". It is possible that the Plymouth Sound mud was partly formed as a response to the Flandrian transgression. Christie-Blick *et al.* (1988) added that the characteristic profiles can also be produced by a regular fluctuation in the source of the sediment supply (either marine, coastal or alluvial), or the autocyclic crustal downwarping and sediment progradation of deltas. Haq *et al.* (1988) quantified autocyclicality of deltas in relation to storm events. On static coasts, deep valleys will increase the absorption of the free marine/alluvial sediment giving a radically different profile from that of a shallow valley only a few kilometers away.

Author	Location	O.D.m	Method
Cooper 1948	Plymouth Sound	-42.0	echosounder
Clarke 1972	Torbay	-42.0	echosounder
Wood 1976	St Ives	-18.0 -26.0 -35.0 -18.0	echosounder
Durrance 1974	Exe	-3.4 -8.0 to -7.7 -11.3 -19.6	seismic
Durrance 1974	Teign	-7.8 -11.9 -20.5	seismic
Donovan & Stride 1975	S.W.Peninsula	-38.0 to -49.0 -49.0 to -58.0 -58.0 to -69.0	side-scan & echosounder
Dyer 1975	Solent	-17.0 -10.0 -20.0 -28.0 -42.0	sparker
Kelland 1975	Start Bay	-42.0 -28.0	side-scan & echosounder
Anderson 1988	Hamoaze	-14.6 -17.2 -18.8 -21.3	sparker
Eddies & Reynolds 1989	PalaeoTamar	-22.5 to -24.5 -27.5 to -32.0 -34.0 to -35.5	sparker

Table 2.3
Heights of marine cliffs, buried valleys and terraces

Tidal effects

In western Europe the continental shelves are wide, and the coasts are crenulate. This gives rise to large variations in tidal levels over relatively short distances. Variability on coasts can also be associated with large-scale fluctuations in ocean currents (Emery & Aubrey 1985). For example the Kuroshio current and the Gulf Stream have been recorded to vary in height. Such currents may also change direction, thereby affecting the availability of siliclastic material. All sea level rise estimates in the English Channel have been made assuming that the present tidal state prevailed back to 15,000 B.P. In contrast, Tooley (1985) showed that if the water level in the Bristol Channel was lowered by 20m (as at 9,500 B.P.) then the dominant M_2 semi-diurnal component would have produced a tidal range of 4.3m at the head of the estuary, compared to

15m today, and between 2.2 - 2.3m at the mouth - the increase in the M_2 tide need not be linear. Hawkins (1971) estimated that the tidal ranges in the Bristol Channel in Roman times were probably 0.9 to 1.8m less than today. The distance to the nearest point of convergence (amphidrome) of the co-tidal lines also affects the height difference between MHWS and MHWN resulting in a change in the erosive potential of the residual currents and therefore the relative height of the wave-cut platforms. The tidal difference on either coast of a basin can also be varied. Measurements are often extrapolated around a coast yet, for example, in South West England there is a difference of 2.6m in MHWS tides between the Bristol Channel and Devonport.

Stationary Datum

Many sea level rises are measured from the Perimarine zone (Tooley 1986) and cannot, in areas of differential movement, be realistically extrapolated laterally to the subtidal zone. All of the 119 post-Permian cycles are assumed to be eustatic and global, but on a local scale, the coastal onlap may be caused by differential subsidence of the continental crust. If sequential sea level changes are to be measured then the reference datum must be stationary, but it is extremely difficult to separate long-term crustal components movements from glacio-eustasy movements. This problem was identified by Fairbridge (1961) who then attempted to establish a global sea level curve, from the terraces present off the stable cratons of South Africa and West Australia. A major problem in the Plymouth area is that, until the mid 1970's, all theories described South West Britain as "periglacial" and it was not until 1975 that the "collapsing peripheral forebulge" effects were recognized (Section 2.3.7).

Local meteorological effects

Some areas are particularly susceptible to storm events and seasonal climatic/weather variations and the effects of storm surges at periods of exceptionally high tides must also be taken into account. The maximum perigee of spring tides occurs approximately every 1600 years (when the Sun is in perihelion and both Sun and Moon have 0° declination). One such tide occurred in 3,500 BC (c. 5,500 B.P.) according to Heyworth & Kidson (1982). A similar perigee tide could possibly explain the Mediaeval transgression of Fairbridge (1961).

Tectonic effects

It is possible that many of the sea level changes were rapid. For example the Alaskan earthquake of 1964 caused a global increase in sea level of 0.7mm (Bilham & Barrientos 1991).

2.3.4 Sea level curves and Flandrian sea level rise.

In response to changes in sea level a number of curves have been developed. Two schools of thought exist: the Shepard school advocates a continuous rise in sea level since 18,000 B.P. while the Fairbridge school postulates that sea level rise has been spasmodic and includes regressive, transgressive and stand-still phases. Fairbridge (1961) also recognized that most research had been done in the so-called forebulge areas, where the land masses are prone to vertical movements due to isostatic readjustments following ice loading. Sea level research is affected by the scale of specialization. Two broad time scales have evolved: (i) since 14,000 B.P. and (ii) the last 100 years, the latter being most important for future predictions. Most sea level curves show a rapid rise between 15,000 (-34m) and 7,000 B.P. (-10m) (Delibrias & Guillier 1971), with a slightly slower rise, from -10 to 0m O.D. (Greensmith & Tooley 1982), with rates similar to todays being reached 2,000 to 1,000 years ago. The results of IGCP Project 61 included three curves for the South West and North France. Several other curves exist and are presented in Figure 2.3, and Table 2.4. The melting of the Devensian ice instigated the Flandrian transgression, so called after the inundated plain of Flanders on the Atlantic coast of France. In this thesis this transgression is taken to have started during the Boreal stage, about 9,000 B.P.(after Hawkins 1971).

2.3.5 Sea Level rise in the English Channel.

During the maximum regression of the Devensian glaciation, around 20,000 B.P. the Polar front was located at about 40°N. The North Atlantic coastline then followed the -130m isobath (Delibrias & Guillier 1971, Newman & Bateman 1987) as has been confirmed recently by coral studies (Lambeck & Nakada 1991). The environment both on land and in the exposed Channel was that of moderate meltwater influx with little precipitation. Winter ice covered the North Atlantic ocean (Turner & Hannon 1988). At this time, Spain and Portugal were glaciated, but there is no evidence of ice on the South West peninsula.

Age B.P.	Global height O.D.m	Temperature °C
5,500	+6.1	
7,000	-10.0	
8,000	-21.3	
9,000	-39.6	16
10,000	-57.9	10
11,000	-76.2	
11,500		17
14,000	-128.0	9
15,000	-110.0	
16,000		
26,000	0	
70,000	-90.0	

Table 2.4

Postulated Sea Level changes and estimated palaeotemperatures (Adapted from Millman & Emery 1968, Emery & Aubrey 1985 and Fairbridge 1961).

Between 16,000 to 15,000 B.P. the continental ice sheets began to decay and, as a consequence, sea level increased to the -100m isobath. The North Atlantic was flooded by meltwater and icebergs during summer and covered in sea ice during the winter. Two marked linear deeps occur on the sea bed of the English Channel - the Hurd and the Fosse d' Ouessant, incised to 175 and 200m respectively. The Armorican and Cornubian margins of the sea are stepped in a series of submarine cliffs. Seismic profiles of a series of depressions in the English Channel show partial sediment infill (Hamilton & Smith 1972, Dingwall 1975, Smith 1989). These depressions have been divided into two forms - (i) closed and (ii) linear.

(i) Closed depressions: there are three main theories for the origin of the small closed basins. Glacial scour beneath a marginal ice-sheet has been proposed for St. Catherines Deep to the south of the Isle of Wight (Dingwall 1975). Erosion by rapid currents during phases of low sea levels has been suggested for the Cap de la Hague and the Ushant deep. Karstic weathering, dissolving isolated pits in limestone areas has been postulated for other basins.

(ii) Linear depressions: the largest of the linear deeps is the Hurd Deep (Figure 2.4) which is 200km long and 5km wide. It is slightly sinuous and parallels the structural grain of the Jurassic and Cretaceous sediments into which it is incised. There has been some controversy regarding the formation of this deep. Hamilton & Smith (1972) suggested it was formed during maximum withdrawal of the sea during the Wolstonian,

and was later enhanced by tidal scour. Kellaway *et al.* (1975) proposed it was created by glacial processes, while Dingwall (1975) proposed that a drainage system was established during the Miocene and was modified during the Quaternary - a view supported by Gibbard (1988). The Deep is now generally accepted as part of a large integrated fluvial system - the Channel River - which was a braided river during the glaciations, and drained from South England, the Dover Straits and Northwest Europe (The Seine) (Figure 2.5). Seismic profiles show that this ancestral valley continued westward to the deep off the Normandy coast, the Fosse de l'Île Vierge (Boillot 1964), and met the shelf edge at Shamrock Canyon.

By 13,000 B.P., the polar front had withdrawn to the northwest and lay parallel to the coast of Iceland. The sea temperatures in the Bay of Biscay were warmer than at present (Ruddiman & McIntyre 1976) and warm temperate conditions developed over Europe, with trees beginning to grow in Britain. By 12,000 B.P. the Western Approaches to the Channel were inundated at -60 to -50m below O.D. (Figure 2.4). Evidence of coastal bars and marine cliffs suggest a standstill at about this time (Stride 1990).

Pollen analyses for the period between 11,000 and 10,000 B.P. indicate that a re-advance of the Arctic front occurred, possibly due to the breakup of the Arctic ice sheet. At this time, sea ice covered much of the North Atlantic resulting in the continents being starved of precipitation and the development of semi-arid conditions (Turner & Hannon 1988).

The -40m isobath was reached by *c.* 9,000 B.P. when free connection was established through the Straits of Dover and the north and south basins of the North Sea were also joined. Sediments of this age show an increase in the lithoclastic content and a decrease in biogenic input (Larsonneur *et al.* 1982). This reflects the changes to the hydrography of the Channel and therefore the biotic communities. This level corresponds to Cooper's Cliff (Cooper 1948) and the Upper Cliff (Donovan & Stride 1975) in the Plymouth Sound area (Section 8.3).

The actual date of breaching of the Straits of Dover has been controversial. Smith (1989) reviewed the literature and concluded that the breach could have occurred at anytime between 150,000 and 15,000 B.P. and that there was probably a series of openings and closings through

that time. Jenkins *et al.* (1986) concluded that there was no continuity between the Pliocene foraminifera of the Channel and the impoverished faunas of the southern North Sea. There is evidence that a substantial land barrier existed during most of the Pleistocene (West 1988). This barrier was an extension of the Weald-Artois chalk ridge (Smith 1989) and was overtopped during periods of high sea level during the Quaternary. Two reasonable dates exist for the breaching of the Straits of Dover at 8,250±300 B.P. (Heyworth & Kidson 1982) and 9,000 B.P. (Larsonneur *et al.* 1971).

At 7,000 B.P. the -10m level was reached and the hydrodynamics and sediment dynamics of the present day began to be established. The sediments in the Channel thicken and young towards the west, becoming increasingly bioclastic as benthic communities developed (Carthew & Bosence 1986), with planktonic faunas probably lagging behind benthic forams (Murray 1965). The sediments have a comparatively low or diluted terrigenous component, possibly in consequence of the raising of the erosion base-level during the Flandrian transgression.

2.3.6 The Romano-British transgression

The Romano-British transgression was first proposed by Goodwin (1940) working in the Somerset Levels. He recognized sea level at about +6.4m around 5,500 B.P, which inundated land inhabited by the Romans. This high sea level has also been identified by other workers although they disagreed on the timing and height. For example Millman & Emery (1968) and Delibrias & Guillier (1971) proposed levels at +6.1m around 5,500 B.P. and +1m at 2,500 B.P. Hawkins (1971) argued that there was no evidence that sea level exceeded O.D. during the entire last deglacial, and that the Romano-British transgression is essentially a local phenomenon associated with the tilting of Eastern England. Hawkins (1979) continued to dispute the evidence for a transgression, including a critique of the lateral inconsistencies in the peat. He also presented archaeological evidence which showed that all the Roman artifacts were concentrated in tidal channels (pills). Their nature showed that the Romans only inhabited the area during the summer and the area was primarily used as a causeway. (The Somerset levels were drained during the Dark Ages).

2.3.7 South West England and the collapsing forebulge

Isostatic uplift of Scandinavia and Scotland and downwarping of South East England has created a long-term tilting effect (Morner 1980). Until recently, it was generally accepted, that as the Devensian glaciation did not cover South West England, the area was stable and suffered no vertical movement in response to glaciation. However, Newman & Bateman (1985) have since modelled variations in the Northwest European geoid for the last 14,000 years and have shown that the South West underwent downwarping until about 4,500 B.P. and is now rising.

The first reference to the downwarping of South West England by Hawkins (1971) who, during a review of the Romano-British transgression, concluded that "Doubts are raised about the stability of Newlyn". (Sea Level in the British Isles is measured from Ordnance Datum stationed at Newlyn, Cornwall). A personal communication (Thomas 1971), presented in the paper, stated that the Isles of Scilly showed a depression of 4.6 to 6.2m since Roman times - a movement bearing no apparent association with the mainland. The concept of isostatic downwarping and lateral uplift adjacent to the downwarped area was presented by Fairbridge (1961) as the peripheral forebulge model, the mechanisms of which are discussed by Shennan (1983). The idea was extended by Devoy (1987) and Peltier (1987) and developed into the "collapsing forebulge" model. This model proposes that once ice withdraws from an area and isostatic recovery commences, the uplifted peripheral areas undergo a downwarping which can continue after isostatic uplift has ceased. Flemming (1982) attempted to separate geological and eustatic parameters and, using best-fit polynomials, derived a vertical movement model of Britain. This showed South West England to be downwarping at a rate of -0.5mm a^{-1} and Scotland uplifting by 2.5mm a^{-1} . Shennan (1989) expanded Flemming's model and concluded that Scotland is undergoing curvi-linear uplift, whereas South England is experiencing a linear subsidence. In the South Bristol Channel area, during the last 8500 years, "the only clear signal is that net subsidence is apparent, in the order of $-0.24 \pm 0.19 \text{ mm a}^{-1}$ " (Shennan 1989). Extrapolation of these Bristol Channel results to the South West suggest the order of downwarp to be -0.1 to -1.4 mm a^{-1} . Analysis of tide gauge records confirm that the collapsing/relaxing forebulge model to be valid for the South West and North France (Emery & Aubrey 1985). It is now accepted that South West England is suffering downwarping in response to the collapsing forebulge effect of the Devensian glaciation maxima.

2.4 The Palaeo Plymouth Sound and evidence of sea level changes

The Plymouth Sound Project under the direction of Dr. John Reynolds was extended in 1984 to include high resolution geophysical surveys of Plymouth Sound and environs, in order to determine the existence and nature of the PalaeoTamar. The geophysical surveys ran over 100km of continuous seismic profiling lines (Eddies & Reynolds 1988) deploying a sparker source with an 8-hydrophone array. In 1988 two boreholes were drilled in Plymouth Sound. Core recovery was good and provided an excellent sedimentological correlation with the seismic records (Eddies & Reynolds 1988). Four undergraduate projects have so far been based on data acquired in Plymouth Sound (McCallum & Reynolds 1987). Two main areas were surveyed: the Tamar/Hamoaze Channel and the body of the Sound.

2.4.1 The PalaeoTamar Valley

The Tamar River flows from North Devon, across Dartmoor, into Plymouth Sound. Why the Tamar chose to flow south, rather than directly into the Bristol Channel, has been an area of controversy amongst geologists (Perkins 1972). A number of authors have noted evidence on Dartmoor of antecedent incision by the Tamar, which continued channel downcutting throughout the Alpine orogeny. The early Tertiary tilting of the Dartmoor batholith in a southerly direction led to enlarging and downcutting of the northern tributaries on the Tamar (Perkins 1972). The prevailing climate at that time was tropical and more conducive to downcutting by chemical weathering. The Tamar river is thought, on the basis of the structural grain of the South West and the fact there are no records of the occurrence fluvial material outside the immediate drainage basin, to have flowed into Plymouth Sound area since the early Tertiary.

Inglis (1878) suggested that, at some time during the Quaternary, a glacier flowed off Dartmoor in a southerly direction and that this had incised the Tamar valley and entered Plymouth Sound where it cut the deep enclosed depression of the Hamoaze Channel. Inglis also postulated that the Dartmoor glacier occurred after the deposition of the raised beach on Plymouth Hoe. This idea was supported by Worth (1898) who added that the "U" shaped configuration of Plymouth Sound was not unlike those of glaciated Welsh valleys. Codrington (1898) agreed with both authors. The first mention of the PalaeoTamar Channel was by Worth (1898) who "suspected that there was a channel connecting the deep Tamar with the English Channel, but that it was filled with sediment". He ascribed the formation of the channel to glacial action. In 1907 Ussher reviewed the

glacial history of Plymouth Sound. He attributed the depressions in bathymetry to small meltwater lakes and could not, however, be persuaded that the sinuous course of the Tamar valley could be of glacial origin. The glacial formation of the PalaeoTamar was discounted by Lattimore (1961) on the lack of evidence of glaciation in South West England.

It has been suggested (Eddies & Reynolds 1988) that the PalaeoTamar river exploited the lithological boundary between the Jennycliff Slates and the Plymouth Limestone. The two lithologies are of the same resistance to mechanical erosion due to their long burial and metamorphic history. The presence of the volcanics of Drake's Island would have prevented the river developing a course directly through The Bridges.

The Hamoaze Channel is incised to -40.0m O.D., and comparable to depths in Plymouth Sound. Eddies & Reynolds (1988) recognized 5 infilled deeps in the Hamoaze channel incised to -40 and -38m O.D. There is little evidence of sea level rise on the Devon coast of the Hamoaze but the Cornish coast does show vertical migration of the St. John's Lake creek 80m to the north east. The palaeocreek is incised to -30m O.D. A wide buried terrace occurs under the mud banks of St. John's Lake and slopes eastward from -9 to -17m O.D. Terraces have also been traced seismically on Rubble Bank at -14.6, -17.2, -18.8 and -21.3m O.D. A westward extension of the northeast-southwest thrust zone between the Plymouth Limestone and underlying Plympton Slate Formation (Chandler & McCall 1985), has also been identified in seismic section to outcrop and die out in the Hamoaze Channel to the south of Rubble Bank (Anderson 1988). It is possible that the presence of this weathered thrust zone influenced the course of the PalaeoTamar. A possible point bar sequence has been found in the Hamoaze area (Anderson 1988).

2.4.2 The PalaeoPlym

The combined estuary of the Plym and Laira is much shallower than the Tamar, due to increased sedimentation which developed as a result of tin-streaming, less tidal power and less river discharge. This shallow bathymetry and density of shipping makes it virtually impossible to survey the estuary, and as a consequence there are very few data on the extent or occurrence of buried channels in the Plym estuary. Recent boreholes sunk in Sutton Marina showed rock head at -22m O.D. beneath 10m of sediment (South West Water Company *pers.comm* 1991). The depth to rock

head underneath the Laira bridge is also -22.0m O.D (Perkins 1972). It would appear that both the Tamar and the Plym exploit the lithological weakness of the thrust zone between the Plympton slate and the Plymouth Limestone.

2.4.3 The PalaeoSound

The Central Sound area is defined as the area extending southwards from a line joining Drake's Island to Mountbatten Breakwater, following the contours of the submarine cliff at Smeaton's Pass (Section 3.6.5). The seismic surveys have shown a series buried channels, with narrow elongate deeps incised to -42m, in the eastern part of the Sound. These deeps were floored to -35.0m O.D with fluvial gravels (Eddies & Reynolds 1988) and then infilled with sediment. Extending southward from South West Winter Buoy, the Central PalaeoChannel is the most predominant and deepest. It loses its identity south of the Eastern Breakwater. Transgressing and downcutting the Central Channel fluvial gravels, are two smaller channels at -32.0m O.D. associated with terraces (Painter 1986). The seismic surveys have shown three continuous reflectors in these buried channels at -22.5 to -24.5m O.D., -27.5 to -32.0m O.D. and -34.0 to -35.5m O.D. The depths and courses of the channels are discussed by Painter (1986) and Griffin (1989).

2.4.4 Other evidence of sea level change in Plymouth Sound

Marine Cliffs

The base of Cooper's Cliff is at -42.6m and it rises sharply with a gradient of 1 in 3 to -32m O.D. Seaward of the cliff the floors are clean-swept, with only occasional sediment, sloping gently towards the Deepes of the English Channel. Cooper (1948) suggested the cliff had either been formed by a standstill in the E. Devensian or was re-excavated at that time. Cooper's Cliff was re-profiled by Murray (1965) who found a well defined vertical profile with little rubble on the upper ledge. Hawkins (1971) re-investigated the cliff using a hydrographic echosounder and traced the cliff laterally from Rame Head to the Mewstone. The top of this cliff can be compared to those identified off Northern France at depths of -37.0, -34.0 and -35m O.D (Pinot 1968, Delibrias & Guillier 1971, Guilcher 1969).

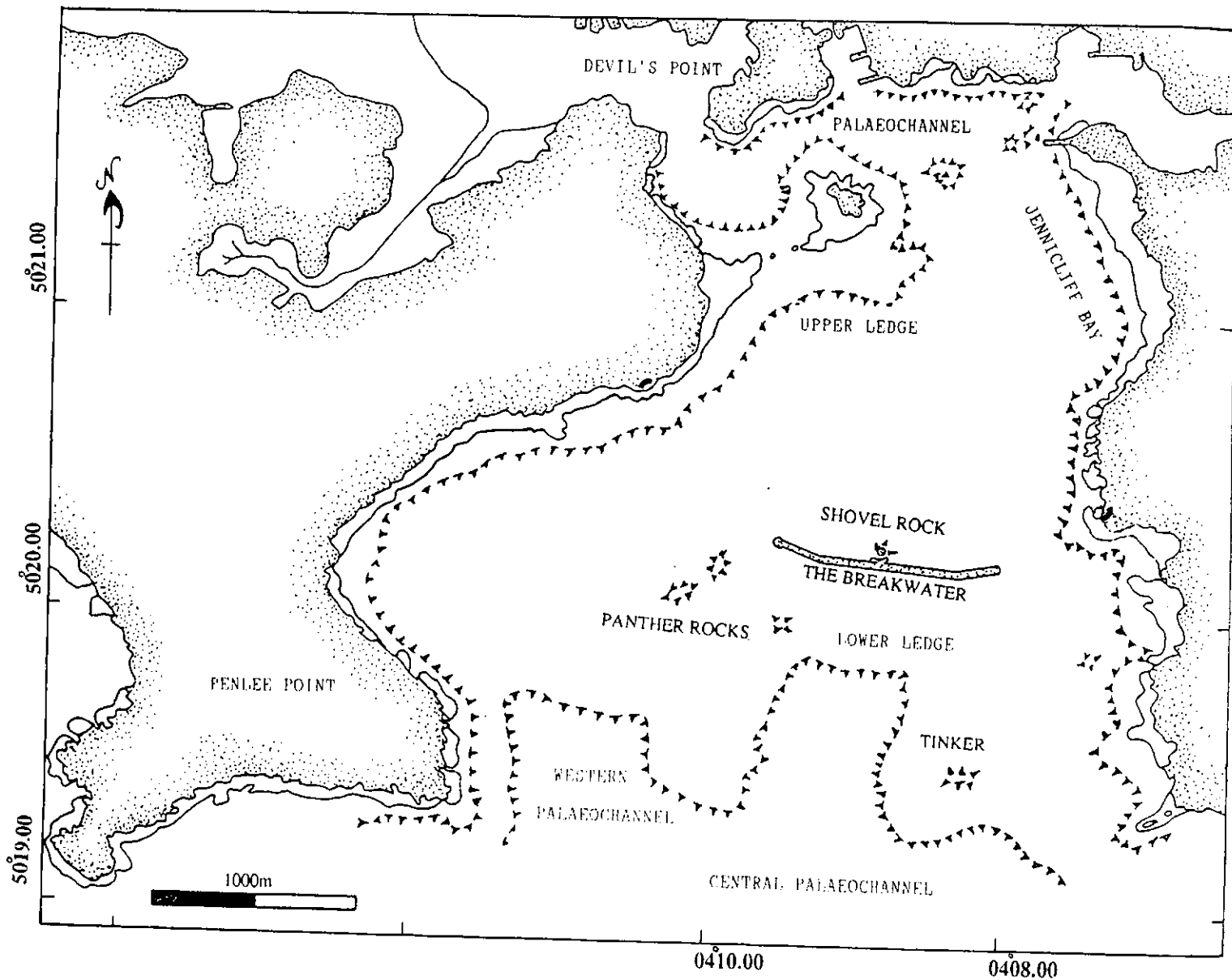


Figure 2.6 Ledges in Plymouth Sound.

The 1989 side-scan sonar survey of Plymouth Sound (Section 3.6.5) identified a number of small sheer cliffs or ledges cut into cleanswept rocks. The Ledges occur at similar depths in the rocky areas over the body of Plymouth Sound and in the Outer Breakwater area (Figure 2.6). The bases of the ledges occur at -5m (-3m to -3.5m top) in both the Inner and Outer Sound, and -15.0 to -16.0m (-13.0m top) in the Outer Sound. These ledges are named here as the Upper and Lower Ledges respectively, and are ascribed to standstills of sea level. Two continuous planation surfaces occur in association with these ledges which are characterized by little bathymetric variation and occur at -5m O.D. within the body of the Sound, and -11 to -13m O.D. outside the Breakwater. The rocky shoals in the inlet rise to -3m O.D.

Raised Beaches

In the Plymouth area, the first recognition of a raised beach was by Worth (1898) who found relict beach deposits on the limestones of Plymouth Hoe. He described these as beach breccias originating from Cawsand Bay. Masson-Phillips (1959) re-investigated this beach prior to it being covered by a retaining wall and divided the deposit into an Upper and Lower Beach. These beaches were re-named by James (1970), on the basis of their height above O.D., as the 15 and 20m Beaches. They both contain shelly fauna which give O_2 July temperatures of 3-4°C less than today (Masson-Phillips 1959). The dating of these raised beaches is still problematical and no further direct progress can be made as the deposits have either been covered or excavated.

Underwater Caves

These have been described by Roxburgh (1983, 1984, 1985), and Dart (1985). Eight caves were identified as part of the side-scan sonar survey of Plymouth Sound. Caves 1 to 7 lie at depths of -3.5 and -3.0m. O.D. off the north side of the Hamoaze Channel between Fisher's Nose and Eastern King. Cave 8 occurs 20m off Western King. Caves have also been reported by divers 20m off Devils Point.

Underwater Arches

An underwater arch was recognized by Dart (1985) at the base of the cliff at Mallard Shoal. The depth at the base of the arch is -35.0m O.D.

- CHAPTER THREE -

-SIDE-SCAN SONAR SURVEY -

3.1 Introduction

With the development, in the 1930's, of high frequency echosounders for measuring the depth to the sea floor, it became apparent that by inclining a downward looking echosounder transducer, it was possible to undertake a scan of a swathe of sea bed for wrecks, shoals and fish (D'Ollier 1979). This principle was successfully applied in the detection of submarines during World War II, using modified side-ways looking transducers. The equipment was named ASDIC (Anti [Allied] Submarine Detection Invigation Committee). In 1958 Chesterman *et al.* successfully applied the back scattering effect of 100kHz sound waves to sub-sea geological surveying, using a modified fisherman's ASDIC. The first purpose-built geological side-scan sonar (Sound Navigation And Ranging) was made commercially by Kelvin Hughes Ltd. in 1962. Since then, side-scan systems and hydroacoustics have undergone extensive development (D'Ollier 1979) - from ASDIC, to the advanced long range digital GLORIA (Geological Long Range Inclined Asdic) (Belderson *et al.* 1972) and culminating in the DOGGIE (Deep Ocean Geological and Geophysical Instrumented Explorer) (Collins 1989). Acoustic mapping of the sea floor is now used routinely in hydrographic (Hydrographic Professional Paper 24 1987), pipeline, marine geological and scientific surveys. The character and morphology of the surficial sediments on the sea floor, mapped in this way, have now been used to define, for example, current directions (Stride 1963), net sediment transport paths (Belderson & Stride 1966), sand waves (Kenyon & Stride 1970), sand ribbons (Kenyon 1970) and gravel furrows (Belderson *et al.* 1988).

The Airborne Thematic Mapper images (Section 6.4) suggested there may be continuity between the sea floor textures and the suspended sediment distributions. It was known that there is a tremendous spatial variability of sediment and type in Plymouth Sound, identified during

diving expeditions. It was therefore decided to map the sea bed using side-scan sonar, in order to link the diver observations with the actual limits of the different sediment types. Several unpublished side-scan sonar surveys of Plymouth Sound have been made by the Institute of Marine Studies (Polytechnic South West) and the Marine Biological Association. Examination of these surveys showed areas of gravels and prograding sand waves, but, they did not give complete coverage of the inlet and in some cases the bedform shape and orientation could not be determined.

On the 17th November 1989, the eastern part of Plymouth Sound was acoustically surveyed using a Waverly 3000 side-scan sonar towed aft of the Polytechnic catamaran *R.V. Catfish*. The advanced side-scan sonar system was borrowed from the Department of Oceanography, Southampton University, for the day of the survey. Unfortunately, poor weather conditions prevailed and progressively deteriorated, and this survey was aborted. The remainder of Plymouth Sound was surveyed in July 1990 from the *R.V. Squilla*, when chartered by the Department of Oceanography, University of Southampton. The unsurveyed areas were allocated to groups of students as field areas and were investigated as part of their second year assessment. The records were then kindly donated by Mr. Paul Riddy to the Plymouth Sound Project and are integrated here.

3.2 Navigation

All surveys used the following navigational systems.

Method and operation

The survey was planned to obtain 125% overlapping sonar coverage. In order to achieve this, and relatively straight survey lines, the vessel was locked onto the Decca Main Chain green lane, and steamed north and south in quarter lane intervals. The position of the ship along track during the survey was made good using the permanent Polytechnic South West Trisponder slave system. This is an electronic position fixing system and operates at frequencies of 9200 to 9500mHz. The system is based on measuring the two-way travel time of coded pulses between the shipborne Master and four shore-based Remote stations. The Del Norte 540 Master (DDMU) then converts the signal into range-range distance.

Problems and Accuracy

Repeatability of the Decca System is good and the triangulation error in the Plymouth Sound area is +/- 25m during daylight hours. The accuracy of the Trisponder system is subject to both fixed and variable errors. The fixed error is induced by the angle of cut or receiving error of the remote stations, and is described by a "circle of uncertainty": in an area of the size of Plymouth Sound and with the transducers in the positions used for this survey, the error circle has diameter of 7m. During the survey, the remote transmitters stationed at Bovisand Pier (50°77.35N/04°86.35W), Mountbatten Breakwater (53°22.01N/04°82.21W), Millbay Grain Silo (53°72.50N/04°67.40W) and Pier Cellars (49°37.72N/04°42.80W) were interrogated, and three signals were recorded at each fix point. The DDMU 540 was pre-set to abort the remote station if the incoming signal was outside the 7m uncertainty diameter; in this case another remote station was accessed. The variable errors include sky and ground wave interference on the incoming signal. Ships, either underway or at anchor, can prevent the signal reaching the Master station. Problems were encountered when ships passed close to the survey vessel and in areas of intense metal concentrations. At the start of the survey the power source on *R.V. Catfish* pulsed, causing the data logging computer to fail, so all position fixes had then to be recorded manually. The internal clock and automatic fix mark in the Thermal Linescan printer was set to bleep every 20 seconds. The sonograph observer then simply shouted "FIX". The DDMU has a freeze-screen function which was employed on the fix command, the DDMU operator could then take the three readings. It is estimated that the delay in manual recording was less than two seconds and the observers were changed every two lines to prevent boredom and fatigue errors.

Plotting and Computing Track plots

All position fixes were plotted using a Hewlett Packard position fixing programme developed by the Institute of Marine Science. The locations of the tracks are shown in Figure 3.1.

3.3 The echosounder

Model

An echosounder measures the two-way travel time of a pulse of sound, in this case 33kHz, emitted from an athwartship hull-mounted dual-purpose transducer. The sonic pulse travels through the water column and hits an

area of the sea bed. A proportion of the downwelling energy, dependent upon the character of the substrate, is reflected off the sea bed and is received by the receiving part of the transducer. The time interval between transmitting and receiving the signal is the two-way travel time. Therefore $\text{Depth} = vt/2$, where t = two way travel time and v = velocity of sound in water. The size of the acoustic footprint on the seafloor is governed by the sound beam width and the depth of water. The receiving transducer relays the received pulse to an amplifier, where it is processed and displayed as an analogue trace. A Ferrograph Atlas Deso 20 echosounder was used in conjunction with the side-scan sonar and trisponder systems. This model was preferred during the survey as it allowed rapid interactive gain change, and could be connected to the computer logging system. The Atlas Deso 20 employs a belt-driven stylus which passes over electro-sensitive ferrograph paper providing a continuous profile of the sea bed. The quality of the display can be altered by an interactive gain, which controls the sensitivity of the receiving amplifier, adjustable for variations in substrate and depth of water. The Atlas Deso 20 recording unit has four depth settings which are selected at the discretion of the operator. The position fix mark on the analogue trace was created manually by the operator on command.

Calibration

Two calibrations are required. One for the actual depth of the transducer and another for the velocity of sound in water. Both calibrations were carried out at the start and end of the survey.

(i) The draft of a vessel will vary depending on the equipment, fuel content and personnel (Appendix 1a). The transducer depth was calibrated by means of a bar check. An iron bar was lowered beneath the hull mounted transducer, dropped to 20m and then hauled up horizontally at 2m intervals. The corresponding depths were read from the paper record and plotted as errors against depth. The echosounder was then adjusted by manipulating the zero and stylus settings.

(ii) The echosounder stylus speed must also be set according to the speed of sound in water. In this case the speed of sound was measured using a MC5 Temperature/Salinity Bridge and calculated by Matthews tables of velocities. The Atlas Deso manual gives the calibration and the appropriate stylus setting for the echosounder.

Problems

Heave and roll of the ship must be taken into account. Most modern survey vessels have a Heave Compensator fitted to the echosounder, but neither the *R.V. Squilla* nor *R.V. Catfish* are equipped with the instrument. The prevailing southwesterly swell was easily identifiable on the analogue record as a sine wave with a wavelength of c. 15m superimposed on the bathymetry. During the survey the echosounder operator marked the trace where local squalls hit the vessel. Ships wakes also create heave and bubbles and, in shallow areas, silt will be stirred up in the water column, all creating false traces which must be noted. Shoals of fish can also be identified on the traces and are usually recognized by their amorphous profile. Areas of fluid mud were easily defined by comparing undulating echosounder traces with the side-scan sonar traces, whereby, a "double" depth profile will be recorded by the echosounder.

Tidal Reduction

Any measurement from the echograph must take into account the heights of the changing tidal state. This correction was completed by a process of reduction to the Lowest Astronomical Tide (L.A.T.). The tidal height was measured from the tidal curve for the day of the survey, and L.A.T. was calculated by either adding or subtracting the discrepancy from the echograph. The curve is located in the Admiralty Tide tables for the Port of Devonport (H.M.S.O 1989, 1990).

3.4 The Side-scan sonar system

The side scan sonar system operates on the same basic principles as an echosounder, with some modifications. The Waverly 3000 sonar system comprises of four main assemblies: a towfish transducer, a dual purpose tow cable (towing and transmitting), a signal processor and a thermal linescan recorder.

The Towfish

A Waverly Towfish Type 3000/T comprises a tubular streamlined hydrodynamically balanced fish with tail mounted fins. The assembly contains two transducers and transmit/receive circuits on both the port and starboard sides. The transducers convert high-voltage 100kHz pulses into high-energy acoustic pulses for transmission. Each array produces an obliquely focused beam, narrow in the horizontal plane (1.5°) and wide

vertically (50°). This creates a large acoustic lobe in the vertical plane, enabling insonification of a wide band of terrain in a direction perpendicular to the transducer axis. The pulse rate is defined by the range. During this survey a 75m range was chosen, for optimum definition and coverage. The pulse rate was 10pps and the pulse length was 100ms. As the pulse echoes off the sea bed, a proportion of the echo will be received by the transducers in the fish. The transducers convert the acoustic signals into electrical signals which are amplified within the towfish and passed to the on-board signal processor. The fins are detachable in the event of the fish striking the sea bed or an obstruction. During the November survey the towfish caught in an unmarked net, but fortunately recovery was immediate and no damage sustained. There is a problem surveying in shallow water in that the transducers will be too close to the sea surface and therefore the ship's wake and engine thereby degrading the performance of the system.

The Tow cable

The Tow cable acts as an electrical communicator between the tow fish and the signal processor, and also incorporates a strain member. The height of the towfish above the sea floor depends on the length of tow cable and the speed of the vessel. During the surveys, the fish was streamed to 30m, where no surface noise could be detected on the analogue record, and a safe height above the sea bed was maintained. It is important to account for the lay-back (cable out) whilst interpreting the sonar traces. A vessel speed of 5 knots was chosen, thus reducing compressional distortion parallel to the line of travel, whilst still complying with the time constraints of the survey.

The signal processor

The Signal Processing Unit Type 3000/S contained all the main control electronic circuits. The system control is automatic, with selectable gain and range functions. The unit microprocessor monitors the signal for range adaptive gain adjustments. The processed signals are then converted to digital form for storage, and re-converted for output to the printer.

The Thermal Linescan printer

The processed signals were output to a thermal linescan recorder, model 3700. This is a two channel programmable grey-scale graphics recorder

with a very high resolution dot matrix recorder and prints on to thermally sensitive paper. The recorder is coupled to an IEEE-488 interface for computer control of the configuration, for data input, insertion of text, or computer processing and replay of either analogue or digital data. The trigger-time, delay time and sweep-time for each channel can be altered interactively, either during the system set-up or later. The recorder has a dynamic range of 16 shades of grey, from solid black to white. It has a resolution of 9 pixels per square mm and the size of the image can be altered, allowing the recorder to be linked to another analogue system - e.g. a magnetometer. The intensity of the trace output to the recorder is usually adjusted to show a clear set of first sea bed returns and to allow signals from the periphery of the area to be clearly discerned.

3.5 Sonograph Processing

The returned signals vary in intensity and position to form an acoustic picture of the sea bed - a sonograph. When the acoustic signal hits the sea floor it is dissipated and a proportion may be lost according to the sea bed characteristics. Most of the energy is reflected back to the transducer. The vertical reflectivity of the sea floor is given as:

$$R = \frac{(Z_2 + Z_1)}{(Z_2 \times Z_1)} = \frac{(A_R)}{(A_I)} \quad (I)$$

Where A_R = Amplitude of reflected signal, A_I = Amplitude of the incident signal, Z_1 = Acoustic impedance of water = $d_1 v_1$, Z_2 = Acoustic impedance of bottom material = $d_2 v_2$, d = density and v = velocity.

The amplitude of back scattered signal is a product of the size of the back scatter elements and the angle of incidence of the beam. Reflectivity is dependant on the properties of the sea bed. For example, gravel and rock are good reflectors and the resultant tonal signal will therefore appear darker. Acoustic impedance has an inverse relationship to porosity. High porosity sediments, usually fine-grained, have low impedance and therefore low reflectivity. However, this is only a broad rule. In estuaries or transgressional tidal inlets the grain size distribution can be bi- or trimodal. Grain shape also affects porosity. Topographic features will also give different reflection intensities; for

example sand waves appear as darker traces and other large objects, including rocks and wrecks, give good reflections with an accentuated acoustic shadow.

The height of an object

The height of an object (Ht) is equal to the product of the acoustic shadow length (Ls) and the height of the fish above the sea bed (Hf), divided by the sum of the acoustic shadow length and the range distance at which it is recorded (Rs) (Figure 3.2). Thus:

$$Ht = \frac{(Ls \times Hf)}{(Ls + Rs)} \quad (II)$$

(Flemming 1976)

Distortions

(i) Slant Range

The slant range is not the same as the recorded distance over the sea floor. To determine the exact position of the object relative to the line of travel, the true range (Rt), the true distance over the ground is required, therefore by the Pythagoras theorem:

$$Rt = (Rs^2 - Hf^2)^{1/2} \quad (III)$$

(ii) Height of fish

The height of the fish above the sea bed causes a lateral distortion perpendicular to the line of travel; the higher the fish, the less the cone of insonification. In processing the data a nomogram was constructed for different heights; thus true distance could be read off the record.

(iii) Paper speed The paper speed cannot be varied as the ship's speed varies. This results in compressional distortion parallel to the line of travel. The speed of the vessel was maintained at 5 knots throughout the duration of the survey. The compression is corrected for when transferring linear displays to isometric charts. A series of distortion ellipses have been published by Flemming (1976) and are now regarded as essential in the interpretation of sonar data (Voulgaris & Collins 1991).

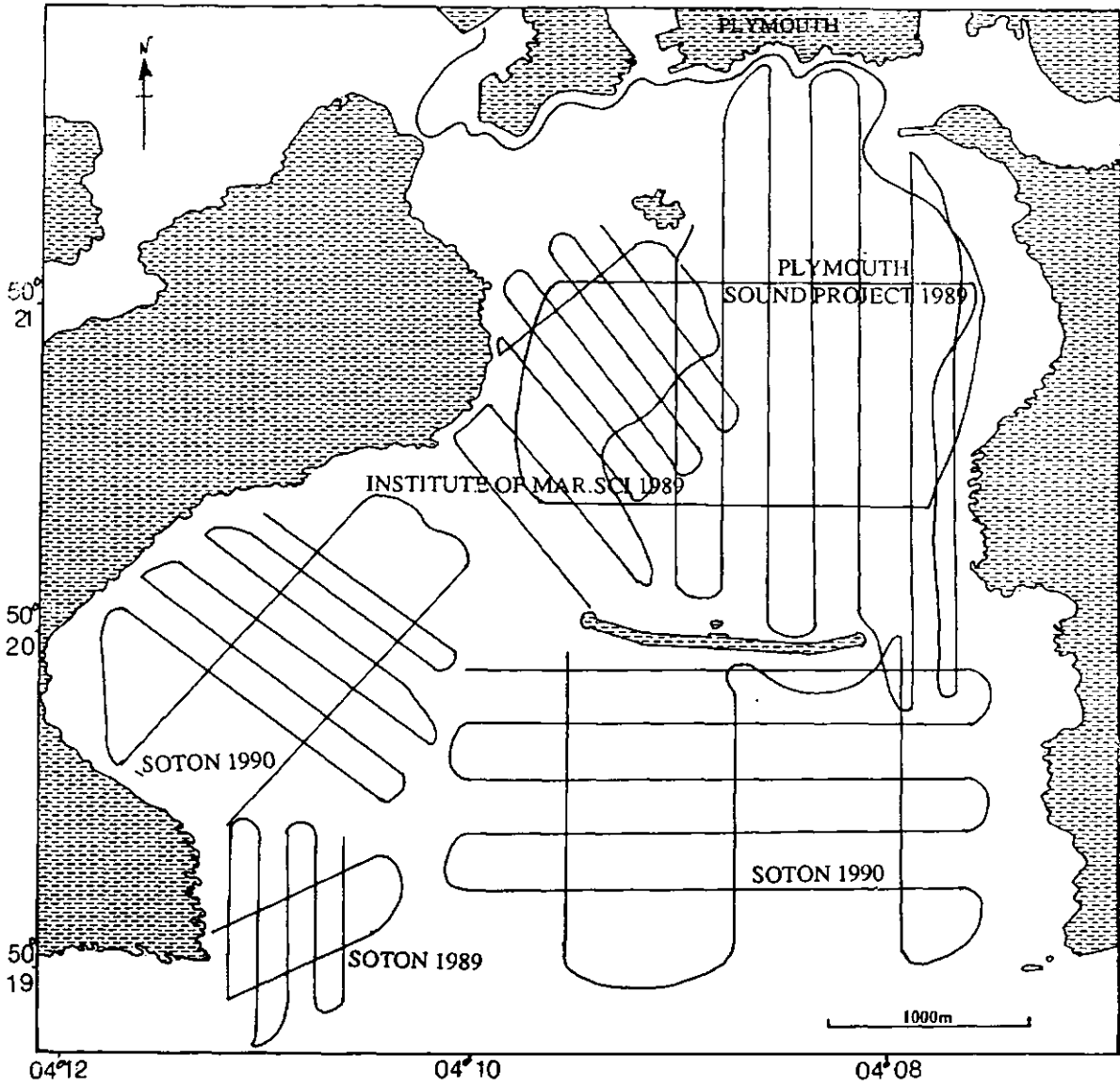


Figure 3.1 Location of side-scan sonar survey tracks in Plymouth Sound.

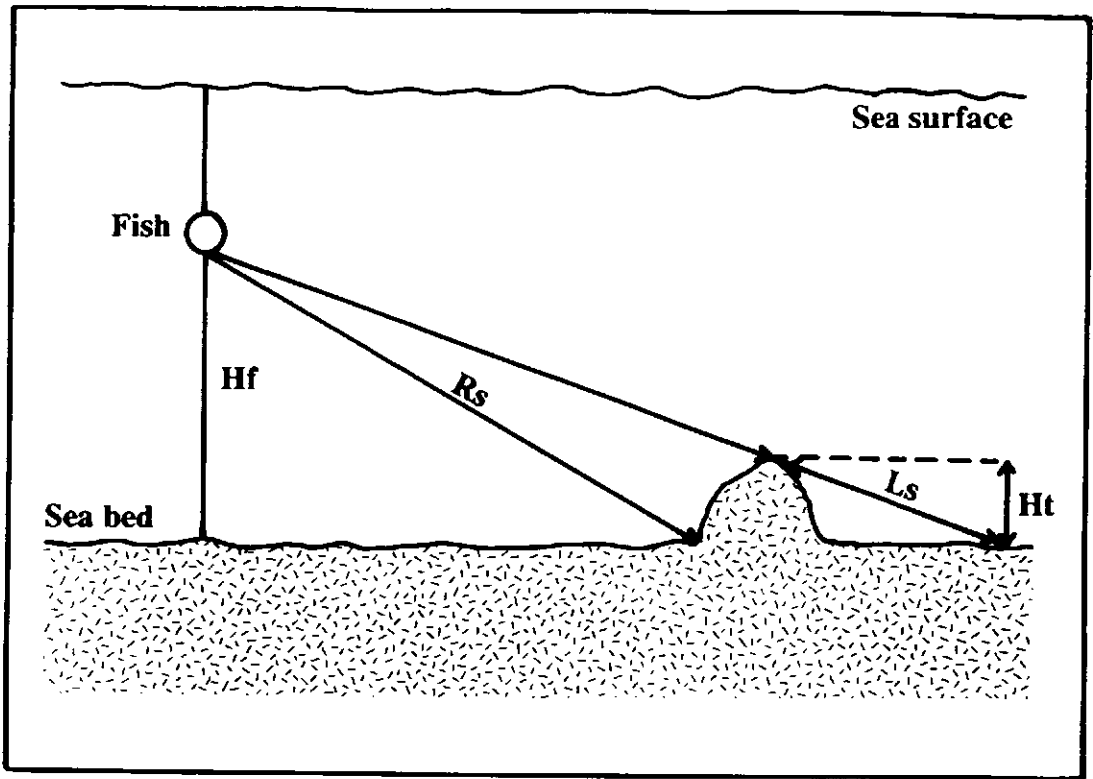


Figure 3.2 Calculation of the height of an object

(iv) Slope of the sea bed

The slope of the sea bed must also be taken into account. Whilst plotting sonograph interpretation; a sloping sea bed will create a gradient in intensity, and be confused with substrate types. This error was avoided by producing a bathymetry plot and overlaying the sonograph chart during plotting.

(v) Physical distortions

The prevailing currents and the motion of the ship can cause yawing of the fish, thereby insonifying the sea bed at a different angle to that specified by the survey. As the 1989 survey was made over the entire tidal cycle, the relative position of the fish was mapped prior to interpretation over the whole survey area. The roll of the fish had relatively little effect, being compensated by the wide beam angle in the vertical plane. The swell during the November 1989 survey caused alternate lagging and tugging on the cable giving false profiles.

(iv) Noise

Engine noise from passing vessels can create false traces on the sonograph. Whenever it occurred it was marked on the trace by the operator.

3.6 Survey Results and Interpretation

The sonograph intensity and configuration was related to the actual sea bed texture by direct diver observation and sampling. Diver sampling, by the author, in Plymouth Sound has been relatively continuous in the period from October 1988 to date (Section 4.2.2). Isometric sonograph charts have been produced in accordance with methods outlined in the Hydrographic Professional Paper 24 (1987) which combine data from all surveys (Chart 1 - North Plymouth Sound, Chart 2 - South Plymouth Sound). The sonograph patterns were used to define the textural features, bedforms and their wavelengths on the inlet floor. On the basis of their characteristic acoustic patterns the sediments can be classified into five distinct environments reflecting a progressive increase in energy.

3.6.1 Featureless acoustic response

This category includes acoustically "smooth" records, with little or no spatial variability in backscatter. Such records can be divided into two categories on their relative acoustic intensity.

Medium Intensity

These sonographs have been identified as representing sand patches with little bathymetric expression. Most of the sand sheets are broadly elongate and orientated parallel to the net sediment transport paths, but others occur transverse to the current flow (Belderson & Stride 1966). The boundaries of the sand sheets are diffuse and undulate laterally, broadly conforming to changes in bathymetry. The sands are coarse-medium and well sorted; degrading low amplitude ripples (<1cm) have been observed (Section 4.5.2). Featureless sand sheets were found primarily at:

(i) The Anchorage sand sheet (Chart 1 50°20.9N/04°09.0W), to the south of Drake's Island, is a crescentic area of fine sand orientated 030/210°. The sheet shows a net sediment movement to the east where it terminates in a zone of moribund sand waves. To the north and west the sheet is bounded by rock outcrops. The southeastern boundary is diffuse and the sand sheet is transgressed by a series of sandwaves composed of a medium sand. The sand sheet has little bathymetric expression.

(ii) Inner Cawsand Bay (Chart 2 50°20.0N/04°11.20W) sand sheet. Located to the north of the Bay, the sand sheet is uniform and acoustically smooth with no parasitic bedforms. It is thought to prograde into fine silts to the north. Historical sonographs from 1980 show the area to be periodically stripped of sand to bedrock after severe storm events.

(iii) The Western Entrance (Chart 2 50°20.0N/04°09.90W) sand sheets are fine-grained, clean-washed sand. Examination of historical sonographs show occasional closely spaced asymmetrical ripples, characteristically with low amplitude crests with a 070/250° orientation. Numerous dredge scours are evident; the last episode of dredging in the Western Entrance was October 1988 (Mouchel Ltd. *pers.com*). A side-scan survey of July 1990 clearly shows the scours (Figure 3.3, all sonographs are located on Charts 1 and 2)). The sand sheets have diffuse boundaries and transgress an area of degrading cusped sand waves to the west. The eastern boundary is more distinct and perpetuated by the Breakwater current intensification.

(iv) The Outer Breakwater (Chart 2 50°20.0N/04°09.0W) sand sheet. This is a large flat sand sheet of 1km² with no surface expression. The

boundaries are diffuse and the zone has a vaguely circular shape. The sheet tapers to a series of irregularly spaced sand ribbons in the south. To the northeast the sand progrades into fine silt and then back to sand, the boundaries of which are maintained by surrounding raised rock outcrops. Several small rocky shoals outcrop in the sand sheet.

Silt depocenters

Areas of Plymouth Sound are characterized by featureless strong acoustic responses. They have no acoustic shadows or variations in bathymetry. The sonograph response has been calibrated by diver sampling and has been identified as a fine silty mud, the surface of which is periodically covered with fluid mud. The main localities include:

(i) The Inner Breakwater silt/mud depocentre (Chart 1 50°20.10N/04°09.0W). This silt sheet has an approximate "L" shape and covers an area of 1.5Km². The area has slight change in bathymetry, in that the silt acts as a drape over the Breakwater's foundations; the St. Carlos and Shovel Shoals. The silt has accumulated in the relatively calm depositional environment provided by the Breakwater. Small circular depressions of 5m in diameter occur and appear as shadows on the sonographs. These are probably ray resting-places. The southern boundary is defined by a gradational change from silty muds to the limestone blocks and debris of the Breakwater foundations. The surrounding margins are clearly defined and controlled by bathymetry (Figure 3.4).

(ii) Mountbatten silt/mud depocentre (Chart 1 50°21.40N/04°08.00W).

This depocentre extends southward from Mountbatten Breakwater into Jennycliff Bay. Due to the density of mooring buoys in the Bay, the area remained unsurveyed and the eastern extent of the depocentre is unknown (Figure 3.5).

(iii) Several small silt patches have been mapped in Plymouth Sound (Charts 1 and 2) and include a small depression in the sea bed to the north of Duke's Rock Buoy (50°20.40N/04°08.05W) and the Outer Breakwater sand sheet.

3.6.2 Tonal Differences

Parts of the inlet floor were observed as localised areas of variable

acoustic reflectivity. The patches were characterized by discontinuous streaking, thought to represent areas of degrading ephemeral sand ribbons, or stringers. "Sand ribbon" is a descriptive term first defined by Kenyon (1970) for a longitudinal bedform, parallel to the maximum current velocity, formed in response to helical flow. The "ribbons" lack any detectable relief and have variable width and separation. Tonal patches are observed in two localities:

(i) South Drake's Island (Chart 1 50°20.19N/04°09.5W). Elongate tonal patches occur to the south of Drake's Island and have a 020/200° orientation. They have an average width of 80-100m and length of 700m. The terminal boundaries are diffuse over a distance of 50m. However, some bifurcation is present although no tapering is apparent. Drift dives made over this area showed the degrading ribbons to be transgressionary medium sand.

(ii) Cawsand Bay (Chart 2 50°19.9N/04°11.04W). The centre of Cawsand Bay has an area of coarse sand and occasional gravels, forming a circular patch of 2km². The sediment is dissected at intervals by elongated darker patches, which are neither regular nor uniform. They are 50-100m in length, with an average width of 20m, and a 030/210° orientation. They have no bathymetric expression and have not been observed by divers. During a test survey in October 1988, asymmetrical sand waves were observed transversing the area. These had wavelengths of 8m and amplitudes of 1-2m. The crests were straight with some local sinuosity. Later surveys show an absence of these sand waves so it is concluded that the tonal patches represent inactive and moribund sand wave troughs, which have the same orientation (Figure 3.6)

3.6.3 Bedform Dominated environments

Large areas of Plymouth Sound are dominated by bedforms occurring in both sand and silt, and occasionally in gravels. Sedimentary bedforms and facies are well known to demonstrate tidal current transport paths (Belderson *et al.* 1982). Sequential bedform development models, with increasing current speed, have been produced (Belderson & Stride 1966, Belderson *et al.* 1982). These models have generally been accepted, although it is recognized that variation in sand supply is the dominant factor in sequential bedform formations. The bedforms present in Plymouth Sound are described in terms of their increasing amplitude.

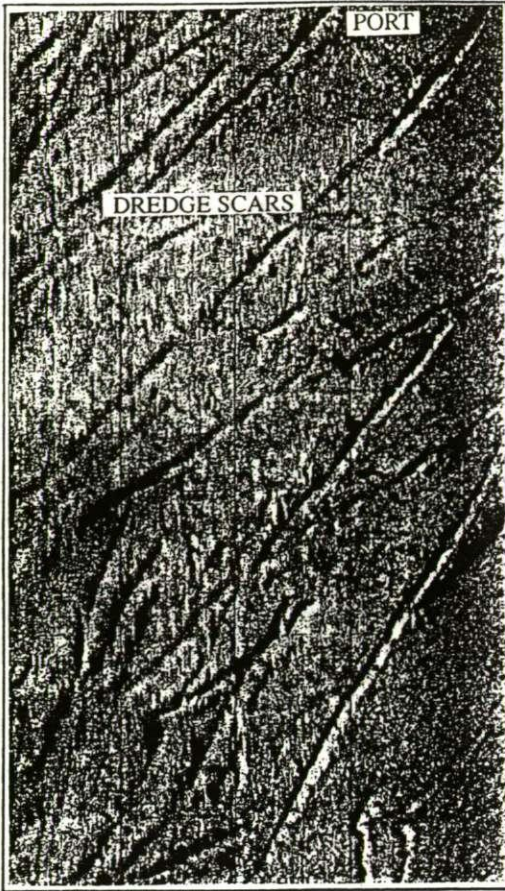
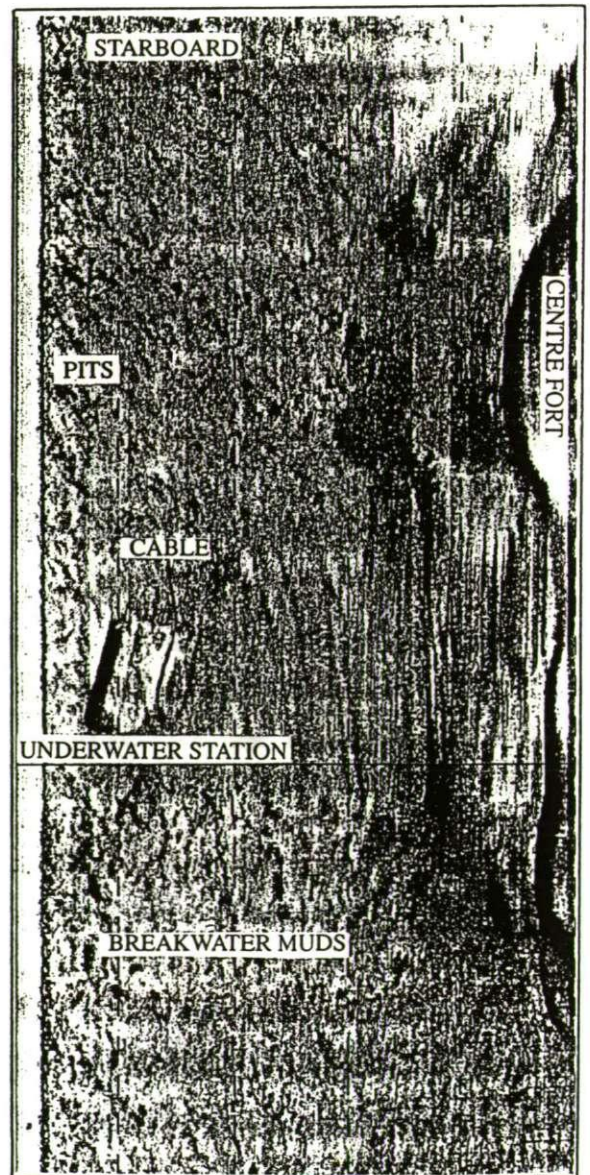


Figure 3.3 Port sonograph of dredges scours (along track scale 40m, range scale 50m).

Figure 3.4 Starboard sonograph of the Inner Breakwater Muds (along track scale 500m, range scale 100m).



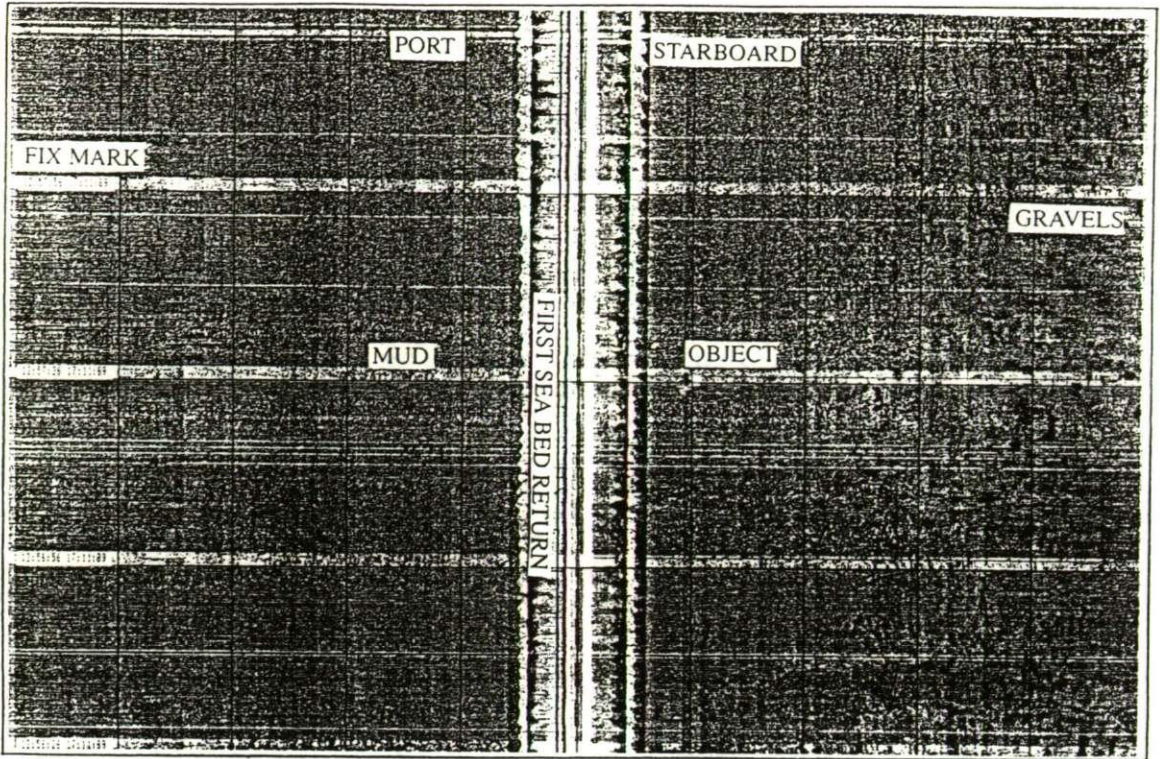


Figure 3.5 Sonograph of the Mountbatten Muds (along track scale 400m, range scale 150m).

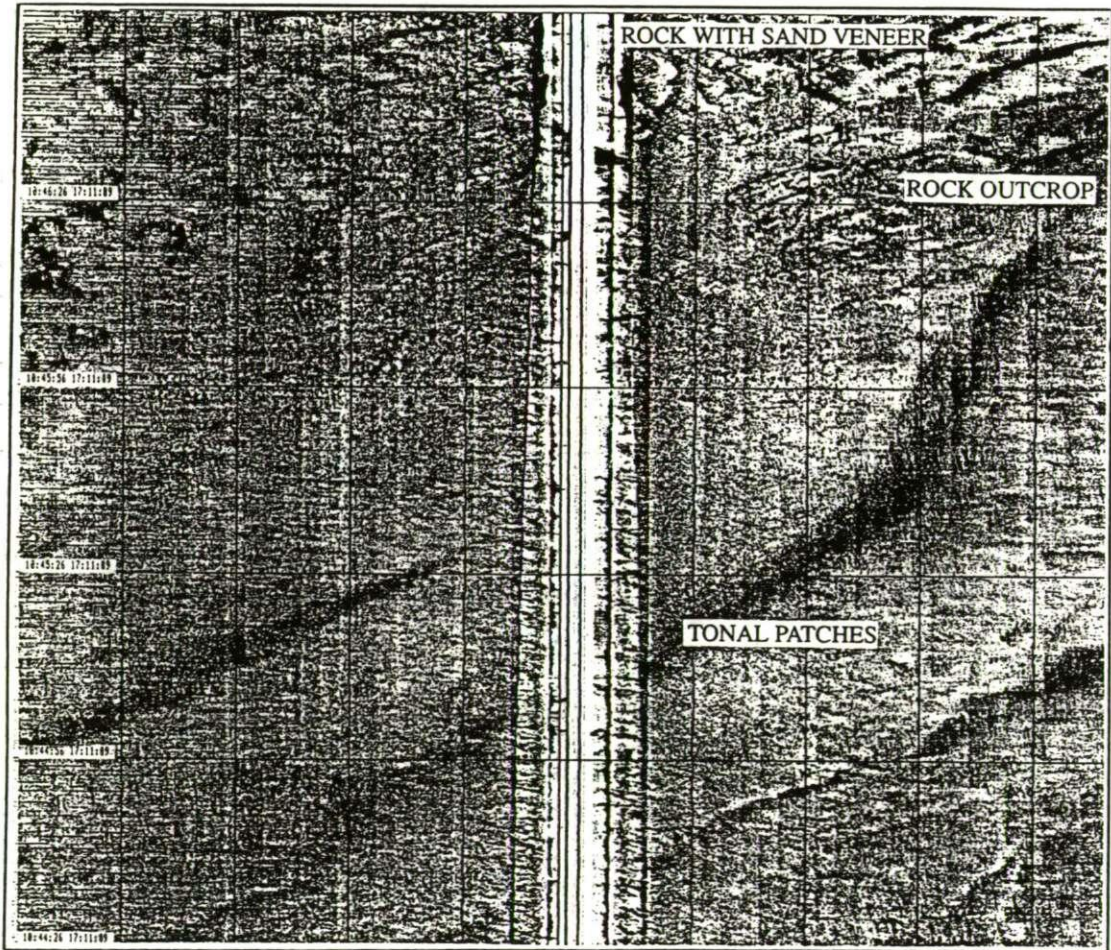


Figure 3.6 Sonograph of the tonal patches transgressing rock with sand veneer (along track scale 500m, range scale 150m).

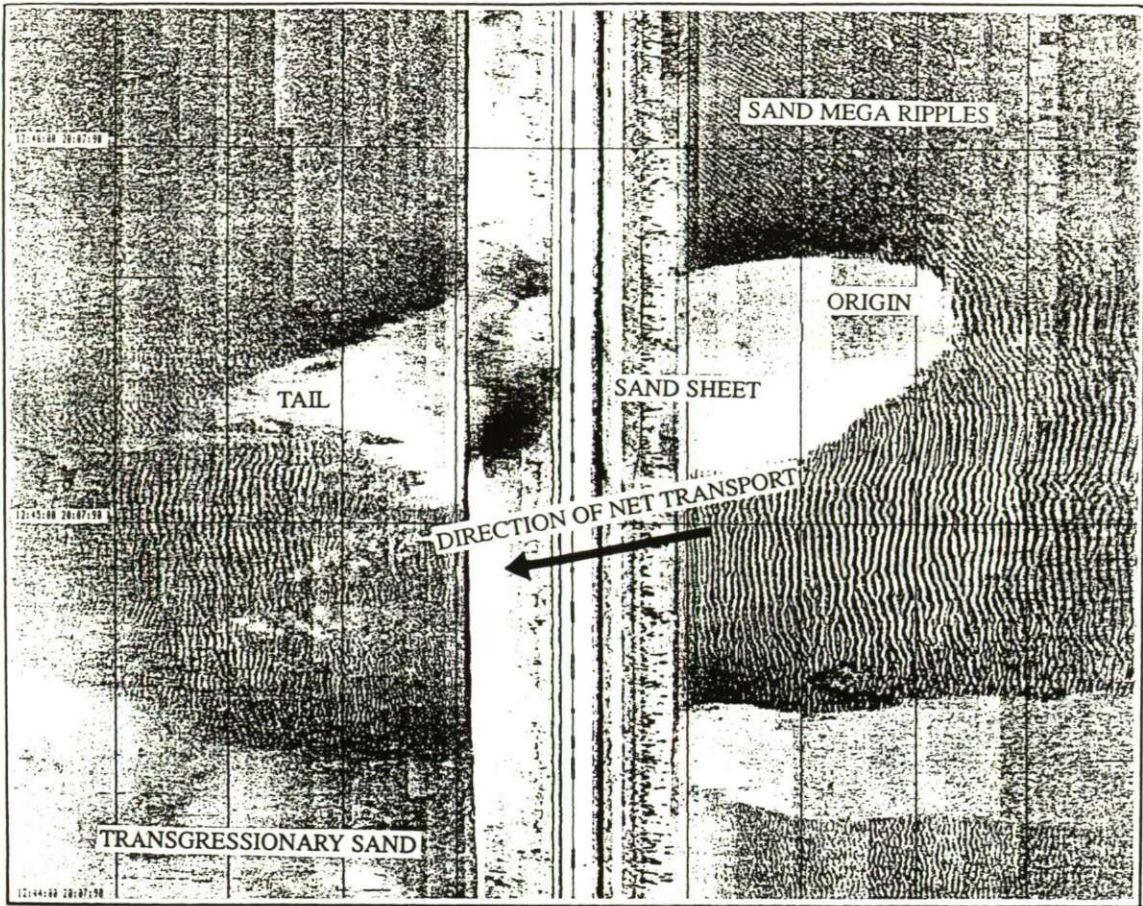


Figure 3.7 Sonograph of a typical sand sheet transgressing an area of ripples (along track scale 200m, range scale 75m).

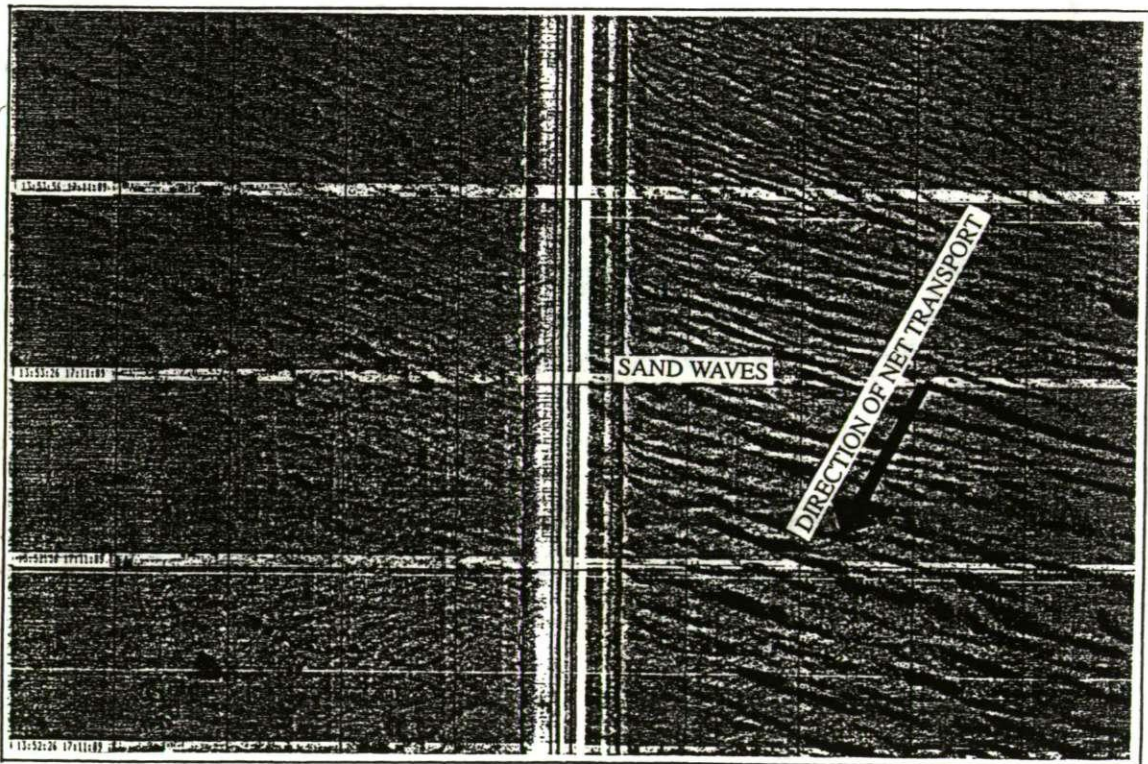


Figure 3.8 Sonograph of sand waves (along track scale 400m, range scale 75m).

Discrete sand ribbons

Sand ribbons were first located by Stride (1963) off the Eddystone Lighthouse and classified by Kenyon (1970). In Plymouth Sound they occur on the periphery of sand fields and form by a process of shedding. They generally have lengths up to 150m and are tapered in the direction of net sediment transport (Figure 3.7). The transgressing end or origin is approximately rounded and has a sharp boundary. Cusps and barbs splay off the lateral boundaries, which are usually clearly defined. The ribbons have an amplitude of 0.5m and their lateral spacing varies from 20 to 50m. Low amplitude ripples occur on the backs of the ribbons during intensification of the tidal stream. The ripples are straight crested with wavelengths of 10-15cm and are perpendicular to the direction of the tidal stream. The decrease of the wave base during prolonged winds can create asymmetric ripples. The ribbons occur in areas of the sea floor with little bathymetric expression. Discrete sand ribbons are located primarily in:

(i) The Western Entrance (Charts 1 and 2 $50^{\circ}20.1N/04^{\circ}09.70W$), where the ribbons are in a zone from Queen's Ground to the west of the Breakwater. They have lengths of 800m, an $020/200^{\circ}$ orientation and an amplitude of $<30\text{cm}$. Their lateral margins are well defined. The ribbons are spilling off from the sand field to the south, and are more clearly defined immediately after storm events. Towards the southeast the ribbons appear to transgress an area of megaripples. They show well defined tapering at the northern margins and indicating net sediment transport towards the northeast.

(ii) The Eastern Entrance (unsurveyed acoustically $50^{\circ}19.90N/04^{\circ}08.0W$) Sand ribbons exceeding 60m in length have been identified by divers in the Eastern Entrance. They transgress gravel and have distinct discrete boundaries with a north-south orientation.

Megaripples in Sand Fields

The southern part of Plymouth Sound is characterized by sand fields separated by rock outcrops. The carbonate and clastic content varies laterally (Section 4.5.2). The sand fields accumulate in areas of little bathymetric change and are often interspersed with rocky shoals or transgressed by linguoid sand sheets and longitudinal ribbons. Characteristically, the sand forms megaripples or dunes with amplitudes

of 10-50cm and wavelengths of 50-150cm dependant on the state of the tide. Generally the crests are straight during the maximum flow and develop sinuosity during tidal reversal. In areas with local disturbances the crestal sinuosity persists.

(i) Western Entrance - Penlee Point (Chart 2 50°19.80N/04°10.2W) The sand field covers an area of approximately 3km². The western and eastern boundaries are clearly defined by 1.5m raised rock ledges which mark the sides of the Western Buried PalaeoChannel (Section 2.4.4). The crests have a 120/300° orientation. There is evidence of episodic development of megaripples in the area around Queen's Ground rock (Survey - October 1988) (Figure 3.8).

(ii) Outer Breakwater (Chart 2 50°19.2N/04°09.30W). Megaripples have been observed on all surveys forming in the continuous sand field immediately south of the Breakwater. The sand field has well defined western boundary against Devonian shillets (marking the western confine of the Central PalaeoChannel - Section 2.4.4), and a more diffuse eastern boundary where sand sheets and ribbons transgress the megaripples. Well defined asymmetric megaripples are present in all surveys. The megaripples are straight crested and orientated 140/320°.

Sandwaves

Sandwaves are large amplitude (>1m) bedforms which develop transverse to flow (McCave 1971). They have been recognized on all of the surveys and are classified here into two main depositional environments:

(i) Well developed sandwaves

(i) During prolonged winds, the wave base decreases and bedforms occur in response to the oscillatory water motion. The generation of bedforms will only occur where there is enough parent material and the sea is relatively shallow. In Plymouth Sound wave dominated sandwaves commonly occur at Queen's Ground (50°20.31N/04°10.47W). These build up during southeasterly winds (direction 095°E) and have a transverse 020/200° orientation. The Sandwaves are symmetrical with sinuous crests, with amplitudes of 1m and wavelengths of 3-4m.

(i) Tidally dominated sandwaves occur in two main areas:

(A) The Anchorage (Chart 1 - 50°20.4N/04°09.0W). The sand waves are in an elongate zone from south of New Ground towards the Western Breakwater. The sandwaves are asymmetrical and parallel crested with wavelengths of 50m and amplitudes of 1m. They are orientated 050/230° and the net sediment transport is in a southeasterly direction, and in (B) the Western Entrance where sandwaves occur interspersed within a roughly triangular shaped wedge with apexes at the Western Breakwater, Fort Picklecombe and Penlee Point. They are poorly asymmetrical, straight crested with wavelengths over 8m and amplitudes greater than 1.5m. They have been observed at different states of the tide and during different seasons. The crestlines, when straight, are orientated 150-330° during the peak ebb and flood. As the flow reverses, the crests become more sinusoidal. Secondary parasitic ladderback megaripples form on the sandwaves during intensification of the ebb. These have a sinuous to cusped N-S crestlines and wavelengths of 1m.

(ii) Moribund episodic sandwaves

Episodic deposition is most common in the Anchorage (Chart 1 50°20.50N/04°08.70W) where pulses of moribund cusped sandwaves were observed on the sonographs. Two phases of deposition can be recognized; the lower phase transgresses gravels with a clearly defined linguoid boundary. The sand morphology is typified by cusped out-of-phase crestlines, with amplitudes of 1 to 1.5m. The net sediment transport is towards the East (110°). The depositional phases were separated by a period of dredging (November 1988 - Mouchel Ltd. *pers.comm.*). The upper phase is morphologically similar to the lower and the net sediment transport is towards the east (095°).

Gravel waves

Large amplitude waves have been mapped from sonographs in the gravel to the south of Winter Shoal (Chart 1 50°21.50N/04°08.50W). They are asymmetrical and straight crested, orientated 060/240°. Wavelengths are of the order of 25m, but the spacing is uneven and dependant on amplitude, varying from 50-100cm. The net sediment transport is due south. These gravel waves are thought to be relict (Section 8.3).

Gravel Furrows

Gravel furrows and ridges occur in two areas: at Melampus Buoy (Chart 1 50°21.15N/04°08.70W) and in Jennicliff Bay (Chart 1 50°21.10N/04°08.0W). The ridges are orientated due N-S and have an undulating amplitude of 2-3m, over lengths of 80-100m. They are separated by furrows 1m deep. The width:length ratio of both furrows and ridges is of the order of 1:4.

3.6.4 Gravels

The bulk of Plymouth Sound is characterized by a strong acoustic return giving the records a mottled appearance. Diver sampling and observation have shown these areas to be gravels, which can be divided into three distinct categories.

Relict Marine Gravels Identified and classified on the basis that no combination of present day sea level wave and current activity will displace the deposit. These are transgressionary and poorly sorted, exhibiting well developed bi-modality associated with cobbles and interstitial medium-fine sand. They are characteristic of a shallow, tidally dominated environment with increased deposition. Both fluvial and marine gravels are heavily colonized by sedentary epifauna, indicating prolonged stability, which are periodically covered with mobile sands. Three areas were identified by their characteristic acoustic pattern:

(i) Smeaton's Pass (Chart 1 50°21.30N/04°08.20W)

The gravel forms two elongate deposits transgressing fluvial gravels to the east and west with clearly defined boundaries. The southern margin is truncated by transgressive moribund sandwaves. The gravels probably continue underneath the sand towards the south and form an extension of the Breakwater deposit (below) (Figure 3.9)

(ii) South Jennicliff Bay (Chart 1 50°20.80N/04°07.90W) Towards Ramscliff point there is an elongate deposit of marine gravels transgressing relict fluvial gravels. The deposit has been dredged and 70cm deep scours remain which have been observed by divers. The southern margin of the gravel deposit has been transgressed by a fine sand.

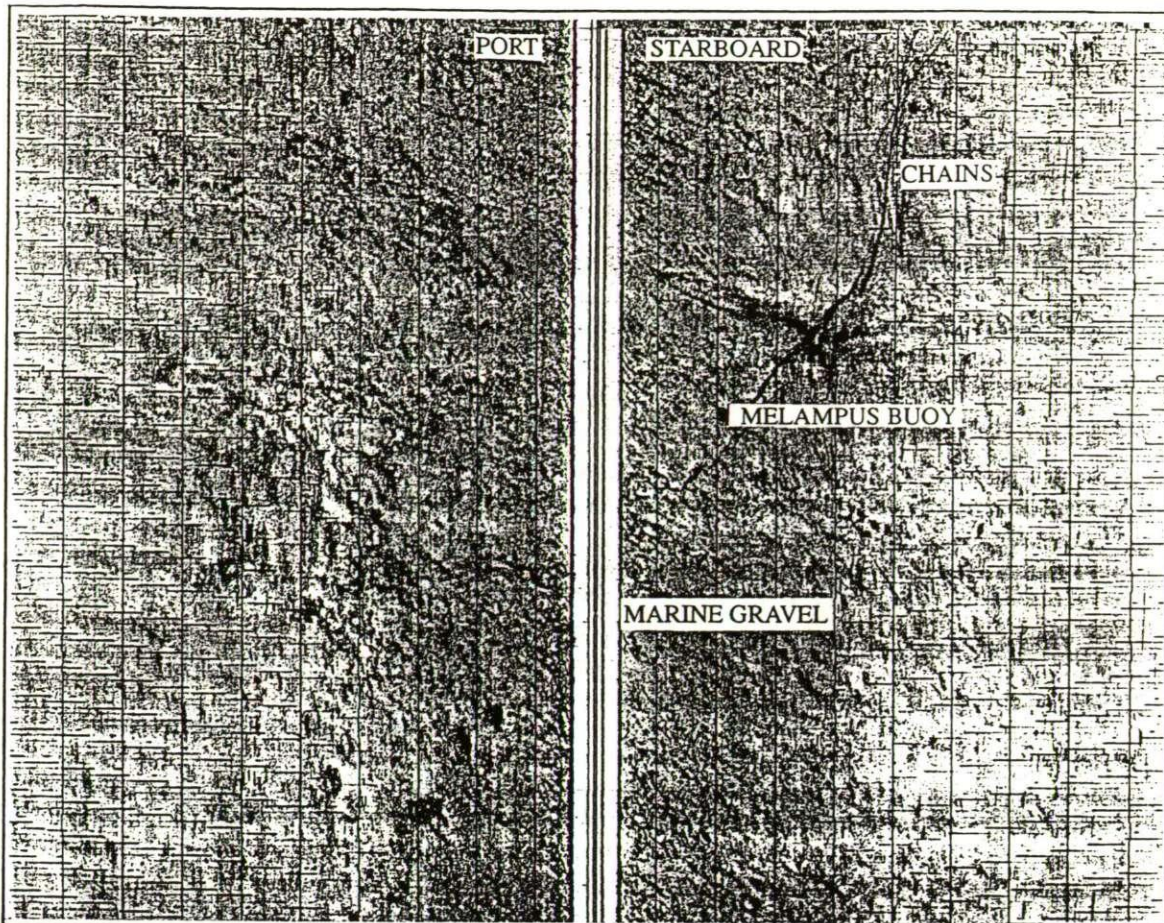


Figure 3.9 Typical sonograph of marine relict gravels and the chains of Melampus Buoy (along track scale 400m, range 150m).

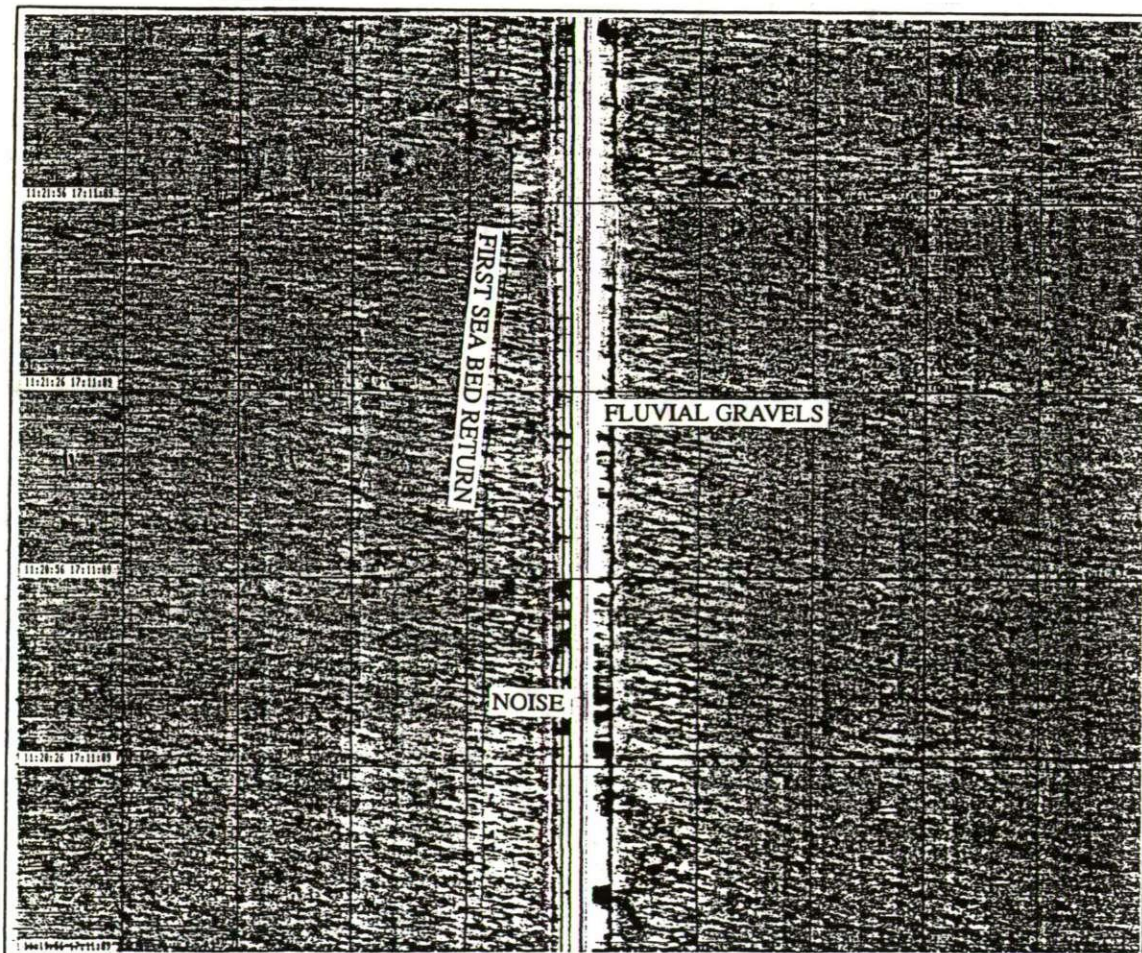


Figure 3.10 Sonograph showing fluvial relict gravels (along track scale 500m, range scale 150m).

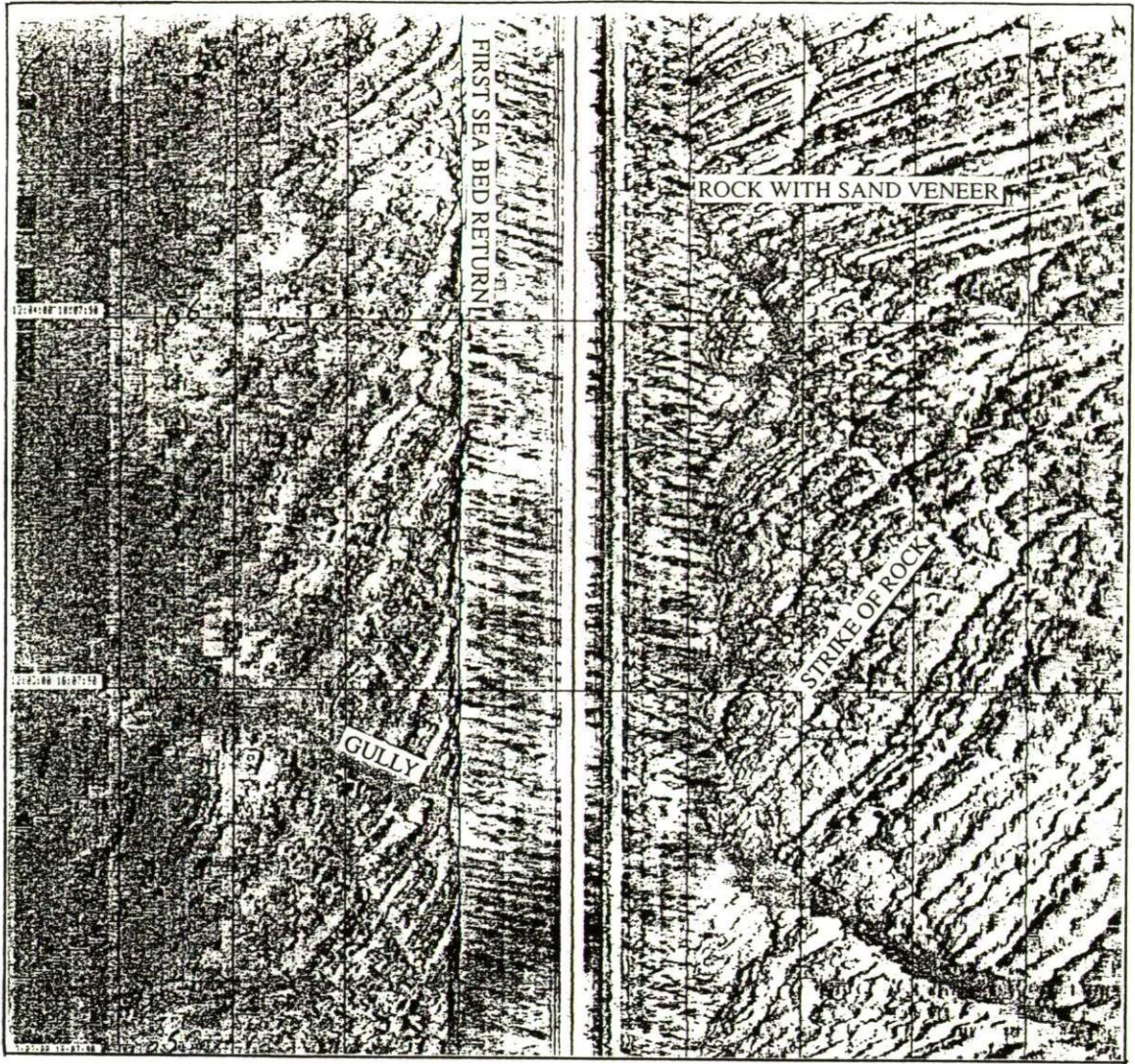


Figure 3.11 Sonograph showing cleanswept rocks with sand veneer (along track scale 600m, range scale 175m).

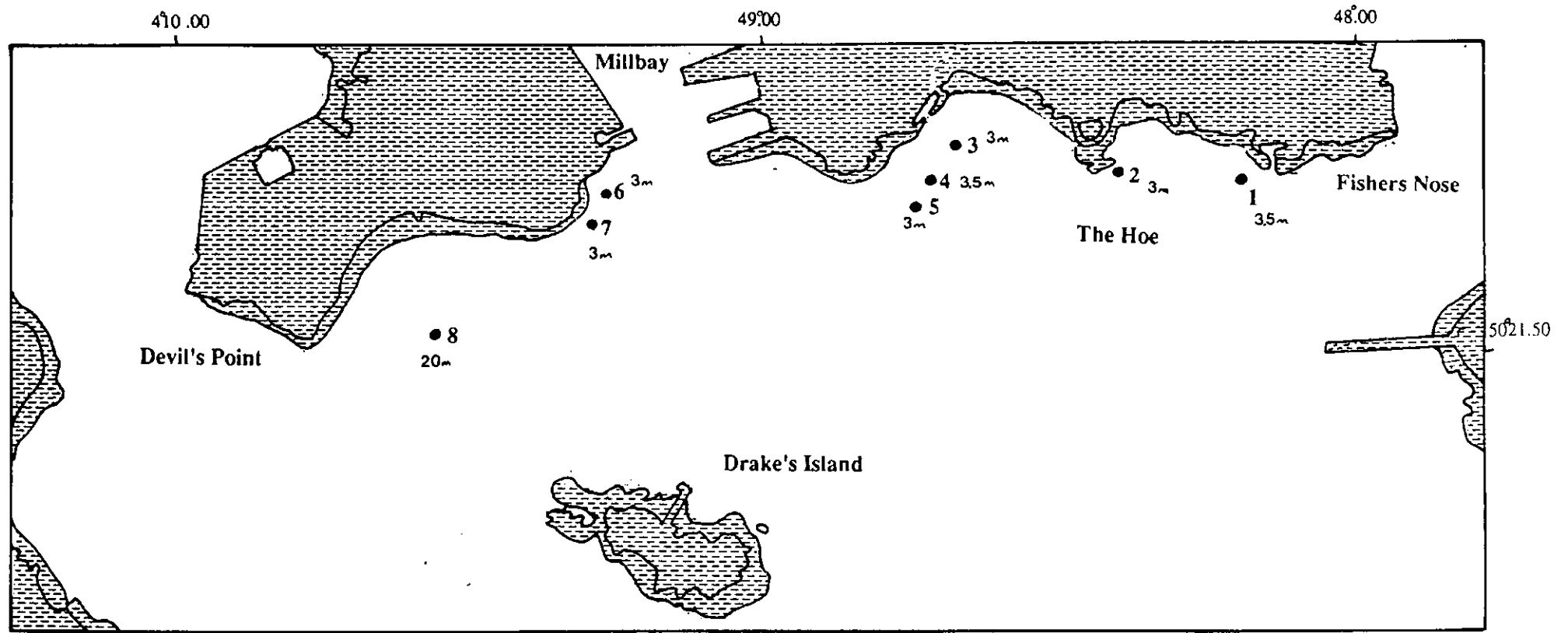


Figure 3.12 Map showing the location and depth of underwater caves off Plymouth Hoe.

(iii) Breakwater (Chart 1 50°20.45N/04°08.75W)

As already mentioned above this deposit is a possible continuation of the Smeaton's Pass deposit. The gravel forms a continuous deposit and is slightly depressed below the surrounding silts.

Relict Fluvial Gravels (Chart 1 50°21.50N/04°08.0W to 50°20.0N/04°08.0W).

These are characteristic over much of the eastern part of Plymouth Sound, and have been observed in a band from Smeaton's Pass to the Eastern Breakwater. The average width of the deposit is 700m. The sonographs have been calibrated with diver samples and observations showing the deposits to be cobble-sized and oblate, imbricated to the south (Section 4.5.3). They were deposited by the PalaeoChannel River system (Figure 3.10).

Wave dominated Gravels (coastal areas).

Beach, or wave-dominated gravels occur overlying rocks in the shallower areas adjacent to rocky shores.

3.6.5 Rocks

Areas of bedrock occur throughout Plymouth Sound. They can be classified into three categories:

Coastal and cleanswept incised rocks

Unfortunately, it is inadvisable to stream a side-scan sonar close inshore or in shallow water (<6m), so parts of Plymouth Sound remained unsurveyed. However, Band 1 of the Airborne Thematic Mapper has penetration in some areas to -4m O.D, and the nature of the near shore subtidal zone can be determined.

(i) The coastline of Plymouth Sound is generally rocky with sheer cliffs and most of the inshore sea bed is characterized by rocks. The largest rocky area links Drake's Island to the Cornish Mainland at Fort Picklecombe. The rock outcrop is generally clean-swept and rises 1m above the surrounding sediment. It is dissected by extensive strike-parallel gully systems and covers an area of 3km². The rock outcrop has little bathymetric variation, an average depth of -5m O.D with a slight ledge at 3.5m (Section 2.4.4). The outcrop has well defined boundaries, apart from the southern margin which is diffuse and grades into the sediment through a broad zone of small raised rocky shoals separated by sand.

(ii) The Hamoaze Channel (Chart 1) is incised to bedrock - to the north in the Plymouth Limestone and to the south in the Devonian Shales and the Drake's Island Volcanics. The channel has an average depth of -30m, with elongate deeps. It is -40m at its deepest point in Drake Channel and shallows abruptly to -12m at South Winter Buoy. The deeps are floored with rounded cobbles. The surface of the limestone is dissected by subaerial solution cracks. It is interesting to note the weathering is typical of freshwater/subaerial chemical weathering and not, as expected, careous saline alteration (Section 4.5.4).

(iii) Several rocky outcrops occur in the body of the Sound. These represent small remnant rocky highs of the PalaeoTamar river system. The most prominent are Mallard Shoal (Chart 1 50°21.55N/04°08.15W) and Winter Shoal (Chart 1 50°21.45N/04°08.50W) which both outcrop in Smeaton's Pass. They shallow to -3m O.D. and have steep cliffs on their eastern and western margins respectively, forming the margins of the Hamoaze Channel. Underwater caves and rock arches have been reported by divers at the base of the Mallard Shoal (Dart 1985).

(iv) Penlee Point. The cliffs around Penlee (Chart 2 50°19.0N/04°11.10W) are steeply sloping rock and continue offshore. The rocks are dissected by sandy-floored gullies, which have bell-shaped bottoms and are continually eroded by wave action. The outcrop shelves rapidly to -10m O.D. some 200m offshore and then slopes gently towards the east with little bathymetric variation. A sharp boundary at -13.5 to -14m O.D. forms the confine of the Western PalaeoChannel. The rocky area extends south eastward and terminates at the 30m contour (roughly - 46th parallel - Unpublished Marine Biological Association Survey 1965).

(v) The Knap and Panther Rocks (Chart 2 50°19.85N/04°09.80W) is an extensive rock outcrop, covering an area of >4km². The outcrop has little variation in bathymetry (Figure 3.11) with an average depth of -10 to -12m O.D. The shoals of the Panther and Knap Rocks shallow to -4 and -6m respectively. The boundaries are sharp and terminate in a 1.5 to 2m drop-off at -13m O.D.; the west and east marking the Western and Central PalaeoTamar valleys. The rocky area extends southwards to the Port Limit where it terminates in an point at (47°80.0N/04°80.0W). This marks the point where the Central and Western PalaeoChannel rivers met.

(vi) Tinker Shoal (Chart 2 50°29.15N/04°08.30W) incorporates a rocky outcrop extending from the Eastern Breakwater (St. Carlos Shoal and Shovel Rock) southwards to the Tinker Shoal where it appears to meet the coastal continuation from Andrum Point (Survey - Institute of Marine Studies, date unknown). The boundaries of the Tinker-Andrum Point rocks are clearly defined by a series of 1 to 2m drop-offs, and mark the confines of the Central and the discontinuous Eastern PalaeoChannel. The rocky area continues southwards where it meets the 30m contour (at the 46th parallel). The rocks are dissected by gullies and ridges with a 070/260° strike. Larger gullies appear to be continuations of onshore thrust zones (Chapman *et al.* 1984, Seago & Chapman 1988).

Rock with gravel veneer

The rocky headlands of Ramscliff Point and Fort Bovisand extend offshore in a zone of rocks with a thick covering of well rounded gravels and cobbles. The cobbles are typical of beach deposits.

Episodic covering

The area within Cawsand Bay was surveyed by Southampton University on the *R.V. Squilla* in July 1990, the north part of the Bay was characterized by clean-swept rocks. Re-examination of a side-scan survey run in May 1988 by the Institute of Marine Studies (unpublished M.Sc report) showed the same area to have a substantial covering of well rippled medium sand. In September 1988, while testing a Klien side-scan fish, the *R.V. Catfish* steamed over the same area, the sonographs showed a series of degrading megaripples (orientation southwest-northeast).

3.6 Caves and Caverns

Caves and caverns have a characteristic sonograph fingerprint. Roxburgh (1983,1984,1985) recognized freshwater springs discharging underneath Plymouth Hoe, and suggested possible caves or fissures in this area acting as conduits. Caves have since been investigated by divers off Millbay Docks (Dart 1985). During the November 1989 survey the side-scan was left on as the vessel returned to the mooring in an attempt to locate the caves. In total eight caves were located on the sonographs, both as freshwater discharge and shadows. Sewer outfalls were also recognized. The location and depth of the caves are shown in Figure 3.12.

- CHAPTER FOUR -

- SEDIMENTOLOGY AND SAMPLING -

4.1 Introduction

Although Plymouth Sound has been the home of the Marine Biological Association for the last 100 years and an important port since Roman times, very little work has been done on the properties of the inlet sediments. Extensive records of the in- and epi-fauna exist. However, little attention was paid to the actual size, type and spatial distribution of the host sediment. In order to identify and evaluate the type of prevailing hydrodynamic forces in an aqueous environment, studies of the size, type and degree of lithification of the sediments will give an indication of the speed of the water currents, the provenance of the currents and the rate of sedimentation. Initially, with the absence of any sea bed texture chart, reconnaissance samples were taken beneath the extensive Admiralty buoyage system in Plymouth Sound. As the survey developed and other position fixing methods became available, the sampling coverage expanded to include mid-channel sampling stations. During this, sampling, observations and measurements of the morphology of the sediment were also made by divers using slightly adapted SCUBA techniques (Section 4.2.2). The sea bed samples were used to (i) evaluate the present and past hydrodynamics of the inlet, (ii) calibrate the acoustic record (Chapter Three), and (iii) analyze the magnetic properties of the acoustically smooth depocentres (Chapter Seven). In addition to diver sampling, a comprehensive collection of sediments were obtained by grab (Section 4.2.4). The samples were analyzed in the laboratory using standard sedimentological methods to determine the modal size distribution, mineralogical and biological content, and physical properties.

4.2 Sampling techniques

Divers using SCUBA systems have made direct observations and measurements from the bed in a number of estuaries, lakes, bays and inlets, for

example: the Tay estuary (Buller & McManus 1979), Fal estuary (Farnham & Bishop 1975), Loch Tay (Duck 1985), Start Bay (Kelland & Bailley 1975), and Poole Bay (Fitzpatrick 1987). It was on the basis of the above successes, personal expertise, and the availability of diving vessels operating daily at Polytechnic South West, that diving was employed in this investigation. All diving operations had to be cleared by the Queen's Harbour Master (Port of Plymouth) prior to location on site and immersion. Once the vessel arrived at a site, the diving procedure was controlled by the visibility (both surface and sub-surface), tidal state and, most importantly, the accuracy of the location specification.

4.2.1 Position fixing

Once a location was designated as a sampling site it was plotted on a working chart and the co-ordinates read off. The sample sites were graded in order of required location precision rather than sedimentological priority. For example, side-scan sonar calibration required a sample to be taken in the area characterized by a particular type of acoustic return, for which greater precision was not required. Sediment sampling on a "pin-point" location or re-sampling for magnetic studies required a higher degree of accuracy. The sample stations were therefore graded as high- and low-accuracy. The higher-accuracy samples were obtained by diving off *D.V. Aquatay* which located a site by accessing the Decca Mainchain (Green and Purple lanes). Once on site, a marker buoy was dropped and the location was then "fixed-in" by taking hand-held compass bearings for future re-siting. Diving to collect other samples was generally made from inflatables using predetermined transit bearings taken off the working chart. Shot-lines were used by divers in high-accuracy locations, in areas of heavy shipping activity for diver safety, or if the surface/sub-surface visibility was exceptionally low. Free fall descents were made in low-accuracy locations or when a time limit was imposed by the Queen's Harbour Master. The sampling order was controlled by the availability of vessels which were designated at the discretion of the Polytechnic Coxside centre. Grab samples were also obtained by the Department of Oceanography (University of Southampton) from *R.V. Squilla* and fixed using Decca.

4.2.2 Diving Operations

All diving was carried out under the Health and Safety at Work Act (part IV) Diving Regulations. The divers participating in the survey were

qualified at least to the level of British Sub-Aqua Club Sports Diver and experienced in low visibility conditions (Appendix 1b). The Diver/Sampler was accompanied by a Buddy, who acted as an observer and carried a surface marker buoy. The surface marker buoy was also employed as a communication interface between the divers and the surface cover, by dipping the buoy beneath the surface in a series of pre-established numbered pulls. The diver employed normal SCUBA equipment with two main exceptions:

(i) A hard hat with torches attached. It was found that during winter and during plankton blooms, the incident light penetrating the water was attenuated to a minimum (Section 5.2). In order to see the sea bed it was necessary carry an underwater torch and have two hands free for sampling. Initially a beacon was carried by the Buddy diver, but this proved ineffective when sediment displaced by sampling obscured the sampler diver. The head light technique was developed by trial and error. Essentially, a hard hat was worn with two underwater torches attached at an angle, at either side, thereby illuminating the divers hands. Velcro straps were attached to the hat to facilitate deployment. During the developmental stages, it became apparent that expelled air bubbles were collecting in the hat, and holes had to be cut in the hat itself to allow the air to escape. The size of the holes were defined by the threshold at which the hat and torches remained on the divers head, and the trapped bubbles did not force the fixture to the surface. The mode of entry of the diver into the water was also modified, usually one hand holds the divers face mask and demand valve, and the other secures the weight belt. Wearing the hat it was necessary to hold it on with one hand during entry into the sea. It was found that a backward roll off the vessel allowed the air in the hat to displace more readily than a forward jump entry. There are disadvantages in head-mounted torches in that the Buddy can be temporarily blinded if eye-communication is attempted. After the sampling procedure was completed, the torches were switched off, thus signaling the exercise was complete for return to surface. During the return to surface the Buddy's torch was employed for illumination of gauges.

(ii) Extra torso weights were added to the normal requirement, usually 2-4 kg, depending on whether a dry- or wet-suit was being worn. These made the diver negatively buoyant and more stable on the sea bed. The additional weight was also used during coring to help depress the core into the sediment. When returning to the surface, the inflatable life

jacket was partially filled with air, to counteract the extra weight. In areas with high currents, ankle weights were also used to ensure non-movement of the diver on the sea bed. Once on the sea bed, the diver moved to an area of minimum disturbance and commenced sampling. Finning by either diver was kept to a minimum to prevent the fine grained sediment becoming suspended. During sampling this was often inevitable and the diver became obscured to the Buddy. Communication was maintained by touch or a buddy-line joining the divers. More commonly, the Buddy circled around the cloud of silt until it cleared sufficiently for him to observe a part of the diver or equipment. Once sampled, the sediment and sampling tools were put in a mesh diving bag whilst on the sea bed. This was secured and lifted to the surface using a buoyant ascent technique - whereby the diver inflates their drysuit or life jacket to act as a lifting bag. The sampling procedure usually took 10 minutes. If the dives exceeded 20 minutes, the surface stand-by diver was alerted for the emergency procedure to be implemented. Once at the surface the divers were picked up by the dive vessel. Anchoring of the vessel was prohibited by the diver, the surface support personnel were briefed on the urgency of relieving the divers of the weight of the bag immediately on surfacing.

Problems associated with diver sampling

- (i) Danger of exceeding the recommended decompression times with multiple descents. To prevent nitrogen saturation all diving was completed within the British Sub-Aqua Club decompression tables.
- (ii) Underwater visibility. The main causes of low visibility were suspended sediment, sewage, plankton and low incident light. Poor visibility inhibits diver communication and prevents the divers seeing any danger on the sea bed, i.e. monofilament gill nets or aggressive demersal fauna. Safe diving was therefore limited to a sampling window in the weather and tides.
- (iii) For any sampling to be carried out it is necessary for the diver to have tactile response in their hands. During winter the ambient temperature of the water (average 5°C) decreases the comfortable without-glove immersion time to c. 5 minutes.
- (iv) Logistical constraints - Regular diving was restricted to the Polytechnic term time, during the summer vacation all vessels have a re-fit. Any diving is at the discretion of the Queen's Harbour Master and prohibited around or in the vicinity of Admiralty vessels and

submarines. Unfortunately, the Port of Plymouth carries a substantial amount of naval traffic so that many planned dives were aborted.

4.2.3 Sediment sampling

The sample collecting depended directly on the type of measurement required. Observations, bags, cores and boxes were used singly and in combination during the investigation.

Observations.

Diver observations were made where samples were not required, such as in areas of bed rock, sandwaves and coarse gravels. The divers were issued with a white formica slate with an attached pop-up pencil. A metric scale was marked on the slate to aid the measurement of small-scale ripples. A waterproof measuring tape was used by pairs of divers to measure the wavelength and height of large scale features.

Bag and trowel technique

Once on the sea bed the diver would trowel some of the bed into clear 2 litre capacity pre-labelled plastic bags using a varnished builders trowel. The bag neck was twisted and excess water squeezed out and then sealed with a rubber band. The location and a description of the sea bed was recorded on a slate.

Coring

Coring techniques were essentially developed for magnetic measurements and occasionally deployed in areas where side-scan calibration required a depth control. In the experimental stages, coring tubes of varying compositions, diameters and lengths were used. After an initial testing period, plastic domestic drainpipes were chosen as a medium. The drainpipe was tested at the Plymouth Palaeomagnetism Laboratory and found to have no inherent magnetic properties. Drain pipes of 6cm inner diameter were cut into 1.5m lengths. One end was tapered on a lathe, and acted as a cutting edge. The drainpipes were cut laterally and re-taped to facilitate core removal. The core casings were painted with a fluorescent arrow prior to immersion. Once on the sea bed, the arrow was oriented to magnetic north using a diver's compass. The corer was then pressed vertically into the sediment and a rubber bung placed on the open top end. The corers were twisted sharply to shear the base from the sediment and pulled out in one continuous movement. The base of the tube

was then corked. The tubes were kept in a vertical right-way-up position as much as possible.

Problems associated and envisaged during coring

(i) The development of a bulb of reduced/increased stress below the core nose created by displacement of the sediment from the cutting edge is a common problem in coring. This generally occurs with increased depth, but did not appear to affect the Plymouth Sound cores.

(ii) The development of internal and external wall friction. This was a serious problem in the Plymouth Sound coring programme. The internal wall stress is directly related to the cohesive nature of the sediment. Different diameter core barrels were used, with and without grease. The optimum penetration of the 6cm drain pipe was found to be 50-60cm before internal friction prevented any more sediment passing into the barrel. Larger diameters penetrated deeper, but the amount of sediment sampled proved unmanageable both above and below water.

(iii) Shear failure, pressure and suction developing in the sediments parallel to the core barrel. Shearing occurred in the sediment after 70cm penetration. This was created by internal wall friction (The results of shearing were found in the magnetic measurements - Section 7.3.4).

(iv) Thinning of softer strata was not a problem as sediment in the cores was relatively uniform in firmness (see bulk density results - Section 4.5.1).

(v) Thixotropic liquefaction and textural rearrangement proved to be an almost insurmountable problem in the surface sediments. To obtain samples of the surface sediments the box technique (below) was applied directly to the sediment.

(vi) Disturbance due to the angle of entry into the sea bed was reduced by ensuring that the core barrel entered the sea bed at 90° to the surface.

(vii) Adhesion of the sample in the sub-sediment was identified as a problem early in the sampling experiments. It was found that a sharp twist sheared the core from the sea bed.

(viii) During ascent, the water pressure in the core increased, forcing the bungs open. This led to leaking of the sediment but was avoided by using maximum force to twist the bungs into the cores.

(ix) Pressure changes in the water column affecting the core and expanding the interstitial pore waters, with consequential disruption of

the sediment texture, was envisaged as a problem but, the extreme cohesive nature of the sediment meant that there were relatively few pore spaces.

Box sampling.

In addition to core samples, small specifically designed magnetic sampling boxes were used directly in sampling the surface sediment. The boxes have internal and external dimensions of 1.9 x 1.9 x 1.9cm and 2.3 x 2.3 x 2.3cm respectively and an internal volume of 6.86 cm³. The boxes are fashioned out of clear plastic and have one open end on which a lid is fitted. The basal surface of the cube has an air escape hole and an embossed arrow for orientation. During sampling the boxes were orientated on the sea bed with the arrow to magnetic north. They were pressed vertically into the sediment, and capped *in situ*. Several samples were taken from each site. This method supplemented core sampling in which the surface of the sediment was disturbed.

Grab sampling

All grab sampling was carried out from the *R.V. Squilla* by the students of Southampton University using a Shipek grab. This grab consists of two semi-cylindrical buckets which were lowered to the sea bed open-end down. Once the grab hit the sea bed it tripped a powerful spring which rotated the buckets towards each other through the surface sediment. The spring kept the buckets together during ascent. Once on the surface the grab was suspended above a collecting tray and a representative subsample obtained.

Problems associated with grab sampling

- (i) The sample is a "spot" sample and may not be representative of the overall sea bed in that area, e.g. it may collect the only boulder on a sandy floor.
- (ii) The fines are lost through the jaws during ascent and only larger particles are retained in the grab. If any bimodality existed in the sediment it can be completely destroyed.
- (iii) Any development of fabric is lost by agitation during both sampling and ascent. The depth to the anoxic layer is not usually preserved.

4.2.4 Transport and storage of samples

Once aboard the vessel the samples and cores were numbered. These numbers remained with the samples throughout the survey and aided recombination after partial analysis. The bagged trowel samples were then placed in a white reflective sealed bucket to protect them and keep them cool. The cores were strapped in a specially designed holder situated on the inner side of the vessel. The cores were topped up with water on the surface to prevent any oscillating waves forming in the core barrel and disrupting the top of the sediment. The cores were protected as much as possible from shocks and tilting on the surface. The samples were taken to the laboratory within 3 hours and stored in a walk-in refrigerator at 4°C. The bags were removed from the bucket and placed on racks and the cores suspended from hooks to ensure a vertical orientation.

4.3 Laboratory techniques

All preliminary processing was carried out within 24 hours of sampling. The samples were processed and analyzed using standard sedimentological techniques. These techniques were adapted as the investigation proceeded.

Sample preparation

(i) The trowel samples were decanted into a rimmed dish and examined visually prior to any analysis. If the sample appeared to contain >10 percent mud or silt, it was wet sieved. Before proceeding, the sample was divided equally in two - creating a wet archive which was retained in a glass jar in the refrigerator until all the analyses were completed.

(ii) The box samples were prepared immediately on return to the laboratories. They were washed free of salt, dried, and then labelled with a waterproof pen. The air escape hole was filled with grease, both the lid and the hole then being sealed with scotch tape. The boxes were then packed the right-way-up in a sealed box and maintained at 4°C until transferal to the Palaeomagnetic Laboratory.

(iii) The excess water in the core samples was siphoned and pipetted off. The core was then extracted and cut in two using plastic fish line. Initial attempts were made to stabilize the surface of the core. These included replacing the water with Analar Gelatin. The Gelatin was melted in distilled water and pipetted onto the drained surface of the sediment. The Gelatin infilled polychaete burrow holes and stabilized

the top 2-3cm thus facilitating sub-sampling. However, the Gelatin melted whilst making magnetic measurements, destroying the textural fabric (Section 7.4.3). The use of Gelatin was then restricted to impregnating samples to be X-rayed. The cores were measured and notes taken on the depth of anoxic layer, colour and faunal content. The specifically designed magnetic measuring boxes were then depressed into the core with the orientation arrow up-core and parallel to magnetic north at 5cm intervals. The core was then subsectioned for wet and dry bulk density, organic content, grain size and calcium carbonate content. One half of the core was sealed in cling film and retained as an archive until the analyses were complete.

Wet sieving technique

In order to determine the percentage of silt/clay ($<63\mu\text{m}$) in the sediment, the samples were wet sieved following the technique outlined by Buller & McManus (1979). The wet sediment was subsampled and approximately 100ml was magnetically agitated in a beaker with 500ml of Calgon solution (33g Sodium hexametaphosphate + 7g Sodium Carbonate + 1000ml distilled water) for 1 hour. The sample was then transferred to a sonic bath for 30 minutes and decanted through a $63\mu\text{m}$ metal sieve, with an attached funnel, into a collecting beaker. The residue on the sieve was washed into an evaporating dish, dried, weighed and then dry sieved. The filtrate was reduced by evaporation and then dried at 70°C in a thermostatically controlled oven for 24 hours and weighed.

Dry sieving

The predominantly sandy or clean washed sediments were placed in an open evaporating dish and washed free of salt by stirring with freshwater which was then pipetted off. The washed sample was transferred to an oven and dried at 70°C for 24 hours. Once dry, the sample was checked for the presence of mud aggregates, which were disaggregated. The sample was then split by the cone and quartering method. An average of 150g initial weight was chosen, as recommended by McManus (1965), to avoid excess loading of the sieves, especially when working with well sorted unimodal sands. The sediment was passed through a series of 26 Endicott British Standard sieves at quarter phi (ϕ) intervals ($\phi = -\log_2 d$, where d = particle diameter in mm) from -2.50 to +4.00 ϕ (i.e. $5600\text{-}63\mu\text{m}$). The sieves were placed in stacks and shaken continuously on an Ro-Tap sieve shaker for a recommended 15 minutes per stack (McManus 1965). The

fraction retained in each sieve was weighed and tabulated (Table 4.1). The sieved samples were re-combined to whole ϕ intervals for calcium carbonate analysis (below). The sieving technique gives results strongly related to the particle shape. The platy particles such as mica and shillet (local shales - Section 2.2) fragments may lie diagonally over the mesh holes whereas spherical grains of the same short axis diameter will fall through. All the captured particles in the larger sieves were checked visually to confirm that no non-spherical fragments had been mis-captured.

Particle Sizing

Samples composed of *c.* 90 percent mud or silt were measured using a Malvern Instruments Particle Sizer Model 2200 located at Plymouth Marine Laboratories, or a Micrometrics SediGraph 5000E at the Department of Geographical Sciences (Polytechnic South West). The samples were sieved through a 63 μ m sieve and the filtrate condensed by evaporation, 0.5g of which was then dispersed in Calgon Solution. The Malvern Particle Sizer operates on the principle that particles of a given size will diffract light at a given angle. A laser beam is passed through a suspension and focused on a detector. The Malvern 2000 measures the grain size distribution of sediments by employing a heuristic approach, whereby the computer makes an estimate of the size distribution and calculates the light diffraction pattern it would produce using Fraunhofer theory. The light pattern is interactively refined, to minimize the error between the actual and estimated patterns, by a least-squares regression analysis. The size distribution is produced as a histogram and a weighting in 15 bands, depending on the focal length of the lens, from 1.9 - 188 μ m (Bale *et al.* 1984). Measuring distributions using the Laser Particle Sizer is rapid - up to 30 samples can be measured in one hour. Comparison tests with other sediment size analyzers show the Malvern 2000 to perform well with unimodal sample. However the performance degrades with polymodal samples (Singer *et al.* 1987). The sedigraph operates by determining the concentration of particles remaining at decreasing sedimentation depths with time, using X-ray absorption. There is no optimum recommended sample concentration; however the radiation beam must be reduced by 40-60% once the sample is inserted. The thresholds of maximum and minimum size to be measured were set interactively before the program was run. The process is rapid, accurate and reproducible (Singer *et al.* 1987).

Dry and wet bulk density measurements

Measurements of bulk density were made on the core samples for two reasons (i) in continuation with co-operative work on bed shear stress with Plymouth Marine Laboratories (Stephens *et al.*, in press), and (ii) to identify any changes in the deposition rates over the Breakwater silts in both time and space. Bulk density measurements were carried out according to the method outlined by Delo (1988) whereby a sub-sample of sediment is homogenized and a known volume weighed. The sample is then dried at 70°C for 24 hours and re-weighed. The bulk density is given as:

$$\text{Wet Bulk Density} = \frac{\text{Mass of Wet Mud}}{\text{Volume of Wet Mud}} \quad \text{gcm}^3 \quad (\text{I})$$

Delo (1988)

The dry bulk density was also determined:

$$\text{Dry Bulk Density}(\rho) = \frac{\text{Mass of Dry Mud}}{\text{Volume of Wet Mud}} \quad \text{gcm}^3 \quad (\text{II})$$

Delo (1988)

Moisture content

The moisture content was defined using the results from the bulk density measurements. This measure is used as an index to express the degree of consolidation of the sediment. Generally, the moisture content increases as the bulk density decreases.

Moisture content is given as:

$$\text{Moisture Content} = \frac{\text{Mass of water in mud}}{\text{Mass of Dry mud}} \quad \% \quad (\text{III})$$

Delo (1988)

PLYMOUTH SOUND SEDIMENT ANALYSIS PROGRAMME Name

No	ϕ	μm	weight		Pre	Post	%	%	Went.	c. %
1	-2.50	5600		A						
2	-2.00	4000		B						
3		3350					pg			
4		2800								
5		2360								
6	-1.00	2000	C							
7		1700					vcs			
8		1400								
9		1180								
10	0.00	1000	D							
11		850					cs			
12		710								
13		600								
14	+1.00	500	E							
15		425					ms			
16		355								
17		300								
18	+2.00	250	F							
19		212					fs			
20		180								
21		150								
22	+3.00	125	G							
23		106					vfs			
24		90								
25		75								
26	+4.00	63	H							
P.										

Table 4.1

Critical Bed Shear Stress

The critical bed shear stress (τ_{cc}) for erosion of the bed composed of predominantly silt was estimated from the dry density (ρ) of the sampled sediment (Delo 1988), as a guide to the strength and compaction of the sediment, where:

$$\tau_{cc} = 0.0012 (\rho^{1.2}) \text{ N/m}^2 \quad (\text{IV})$$

Delo (1988)

The critical shear stress for unconsolidated sand and gravel, was computed using a modified Shields curve (Miller *et al.* 1977) and an extended Shields diagram (Mantz 1977).

Petrological content

The mineralogical and petrological content of the samples was identified concurrently with the biological content. Smear slides were made of the silty samples and analyzed using a petrological microscope.

Faunal content

The faunal content, both live and dead, in the samples was analyzed visually whilst the sample was decanted on a tray. The shelly material was identified using Tebble (1976) and the soft-bodied vermiform polychaeta identified by Mark Burgess (Post-graduate Biological Sciences) and Bob Foster (Marine Biological Association ret'd.).

X-Ray Diffraction Analysis

The mineralogy of the silty samples was established by the X-Ray Diffraction technique as outlined by Hardy and Tucker (1989). The sediment was subsampled and homogenized in a beaker with 25ml of Calgon solution. The beaker was placed in a sonic bath for 30 minutes, and a representative droplet was taken by pipette and dropped onto a pre-marked slide cover-slip. The slip was transferred to a hot plate and dried at 30°C for 20 minutes. The prepared slips were retained in a desiccator until measured. The sample was then analyzed using a Phillips 1710 diffractometer coupled with a PW 1712 X-Ray generator. The goniometer was set to scan from 4° to 44° 2 θ using standard Phillips software and the data output as analogue traces and d-count tables. The mineralogy was identified using the 2 θ AAPG Tables (Chad 1969). To accurately determine the composition of the clays in the <63 μm fraction a sedimentation tube was constructed to separate the sediment into

decreasing 10 μ m fractions. The tube was 50cm in length with a constricted basal exit tube (Emery tube) with an interactively operated tap. The tube operates on the principle of Stokes' Law of particle settling velocities, whereby the drag force exerted on a falling particle is proportional to the fluid viscosity, particle diameter, and the fall velocity. The equation can be restated as:

$$V_s = \frac{d^2(\rho_s - \rho)g}{18\mu} \quad (V)$$

(McManus 1989)

where V_s is the settling velocity, d is the particle diameter, ρ_s and ρ the densities of the grain and water respectively, g is the gravitational acceleration and μ is the dynamic viscosity of the fluid. The diameter and height of the tube was measured and the fall time for each 10 μ m fraction from 63 to 3 μ m was calculated for particles of clays, magnetite and haematite with specific densities of 2.5, 5.2 and 5.26kgm³ respectively. The estimated size of the dominant components was also taken into account - kaolinite (5 μ m), illite (0.1-0.3 μ m) (Hardy & Tucker 1989) and haematite (1-3 μ m) (Tarling 1983). The particles were released at a specified height in the water-filled tube, and at a pre-determined time, the sediment accumulated at the base of the tube was drawn off. The fractions were evaporated and the reduced condensate then dried onto a cover-slip and analyzed on the X-Ray diffractometer.

Magnetic separation

The magnetic separation technique, first described by Rees (1965), was used in order to determine the approximate weight percent of magnetic minerals in a sample. A magnet was suspended and covered in filter paper. The sediment was decanted onto a petri dish and weighed. The sample was then held up to the magnet and agitated gently. The magnetic particles adhered to the filter paper. The sample was then reweighed and the loss percent calculated.

Organic content

The combustible organic material content of the samples was estimated by weight loss on ignition, using a technique successfully employed by Manhein *et al.* (1972), Frankel & Pearce (1973) and Mook & Hoskin (1982). The dried samples were initially ground in a mortar and pestle. 2g of the sediment was weighed into a pre-fired porcelain crucible, placed in a

muffle furnace and combusted at 300°C for three hours. The crucibles were then removed and cooled in a desiccator. Several control samples were re-combusted at 300°C for another three hours to see if any further weight loss occurred. The amount was negligible. Once cool, the samples were re-weighed and the total organic percentage determined. The maximum temperature of 300°C was chosen in order to ensure only organic material was ignited and any inorganic hydrous minerals, such as single and mixed-layer clays, were not affected (McManus *pers.comm.*).

Calcium Carbonate content

The calcium carbonate or shelly fraction of estuarine and tidal sediments has been proven to be an accurate indication of the residual transport paths of sediment (Buller & McManus 1979). The shelly material fraction is also used as an indication of the age of a mobile sediment (Al-Dabbas & McManus 1988). The different components of the shelly material are used to ascertain the provenance of the sediment to be either wholly marine, estuarine or freshwater (Bosence 1979, Salomons & Mook 1987); this is especially of use in areas complicated by relict sedimentation (Keen 1990, Kanazawa 1990). After dry and wet sieving, the fractions retained on each sieve were recombined to whole ϕ units and subsampled. All visible shell fragments were removed and the remains treated with 10% HCl for 24 hours to digest the shelly content. After reaction had ceased, the residue was washed on a 63 μ m sieve with freshwater and transferred to the oven and dried at 70°C for 24 hours. When dry, the residue was re-weighed and the percentage of shelly material was calculated from the sample weight loss. Recombining the fractions to whole ϕ reduces the error produced by splitting and any modal size bias. Calcium carbonate concentrations of the predominantly silty samples and those composed of >90 percent mud were analyzed using a technique first suggested by Frankel & Pearce (1973) who stated that at 950°C CaCO₃ begins to ignite. The sediments were dried in an oven at 70°C. When dry, the samples were disaggregated with a mortar and pestle, desiccated and 2g weighed out into pre-fired porcelain crucibles. The samples were then transferred to a muffle furnace and combusted at 950°C for three hours. The samples were left to cool in the furnace for 24 hours and re-weighed, to determine the weight of the ashed sediment. This gives an approximate measure of the carbonate content without igniting the clay content.

X-ray of samples

In order to obtain a photomicrograph of the cores, thin longitudinal slices of Gelatin-treated core were cut from the archive set samples C27 and C28 (East Breakwater station) and sealed in cling film. A test box sample was also X-rayed in order to evaluate any mechanical distortion of the sediment caused during sub-sampling. The X-ray machine at the Department of Civil Engineering at Polytechnic South West was used. The X-ray machine is, however, designed to be used for the analysis of concrete samples, and the intensity of the source was found to be too high for sediment sampling. The intensity of the source and the length of exposure time were decided by trial and error and therefore, several photomicrographs of each core were made. This allowed different properties to be observed by varying the intensity. For example shelly material was distinct from infaunal burrows. The primary problem in X-ray analysis was cutting the unconsolidated material thin enough without causing mechanical damage (only thin slices of sediment were used in order to fit the sample in the machine). Loss of resolution was encountered when attempting to create a hardcopy from the photographic film used during the X-ray.

4.4 Grain size terminology and statistical analysis

To introduce continuity in the transformation from sieving results to statistical calculations, the standard phi (ϕ) scale was adopted as a display measure (Krumbein 1934). The relationship between ϕ and the metric scale is shown in Table 4.2. The Grain sizes are also referred to descriptively using the grain size classification suggested by Wentworth (1922) for describing the sediments in the -2.00 to +4.00 ϕ range. This scale is commonly used by sedimentologists and is regarded by most workers as a standard classification. The scale, however, does not describe the fractions outside the sand range, and it is these that are common in Plymouth Sound. To counteract this problem, the Friedman & Sanders (1978) classification was adopted for the $-2.00 < \phi > +4.00$ grain sizes. The statistical analyses and methods of presentation used in this investigation are standard.

Histogram presentation

Grain size distribution is commonly displayed as a frequency histogram; this provides a visual demonstration of the data which is easy to interpret and compare. The grain diameter is plotted on the horizontal

axis in ϕ units and the vertical axis is the weight percent in each whole ϕ fraction. The plot may be composed of several peaks (polymodal) or one single peak (unimodal) depending on the population components of the sediment. The peaks are described in terms of height and position and indicate the relative importance of the components. The weight percent of sediment residue after treatment for calcium carbonate is also presented in histogram form.

Udden-Wentworth (1922)	phi ϕ	mm	Friedman & Sanders (1978)		
Cobbles	-11.00	2048	V. large	Boulder	
	-10.00	1024	Large		
	-9.00	512	Medium		
	-8.00	256	Small		
	-7.00	128	Large		Cobbles
	-6.00	64	Small		
Pebbles	-5.00	32	V. coarse	Pebbles	
	-4.00	16	Coarse		
	-3.00	8	Medium		
	-2.00	4	Fine		
	-1.00	2	V. fine		
Granules					
V. coarse	0.00	1	V. coarse	Sand	
Coarse	+1.00	500	Coarse		
Medium	+2.00	250	Medium		
Fine	+3.00	125	Fine		
V. fine	+4.00	62	V. fine		
	+5.00	31	V. coarse		Silt
	+6.00	16	Coarse		
	+7.00	8	Medium		
	+8.00	4	Fine		
	+9.00	2	V. fine		
Clay			Clay		

Table 4.2
Relationship between ϕ and metric scales

Cumulative Frequency curve

A classic method of grain size analysis is a cumulative frequency curve. This is a probability graph, with the horizontal axis divided into quarter ϕ units and the vertical axis describing the cumulative weight percent retained in each increasingly finer sieve. The slope of the curve is used to define the different major components acting on the sediment; each straight segment identifies a different control or size distribution (sorting), inflections (modes) and the degree of asymmetry. The position and the gradient of the segments can be related to particle rolling, saltation and suspension. The statistical measurements practiced in sedimentology employ both metric and graphical measures; a review of the parameters is given by McManus (1989). In this survey it was decided to use statistical formulae based on graphical ϕ . Therefore, in addition to analysis of the actual physiographic characteristics of the curve, several ϕ percentiles can be read off the curve and are used in the statistical analysis of the sediment distribution, these are:

(i) Median (M_d) - Determined from the ϕ_{50} percentile and in this survey was confined to the description of unimodal sediments. The M_d of polymodal sediments may indeed miss the major distributions, and is therefore a redundant parameter. M_d is given as:

$$M_d = \phi_{50} \quad (\text{VI})$$

Folk (1966)

(ii) Graphical mean (M_z) - This is an accurate measure of the average grain size. M_z is calculated using percentiles taken from the tails of the spread, thereby increasing the level of confidence to 88% (Folk 1966), and is given as:

$$M_z = \frac{\phi_{84} + \phi_{50} + \phi_{16}}{3} \quad (\text{VII})$$

Folk & Ward (1957)

(iii) Inclusive Graphical Standard Deviation (Sorting - S_o) - The measures of average grain size do not evaluate the distribution about the mean. Therefore measurements of the degree of sorting or scatter are required. Sorting represents the width distribution of the sediment for which several techniques and analyses exist (McManus 1988). In this survey the Folk & Ward (1957) dimensionless parameter and definitions are used (Table 4.3). The sorting formula is extended to take in percentiles from the periphery of the distribution, thereby accommodating spread in

bimodal samples, and giving a 79% efficiency approximation of the moment (Folk 1966). The amount of sorting can be related to the degree and type of current working of the sediment and is given as:

$$S_o = \frac{\phi_{84} - \phi_{16}}{4} + \frac{\phi_{95} + \phi_5}{6.6} \quad \text{(VIII)}$$

Folk & Ward (1957)

(iv) Inclusive Graphical Skewness (SK_o) - The components of distribution in a sediment rarely form a bell-shaped curve but usually lean to either the fine or coarse end. The asymmetry or deviation from the mean is known as skewness and is geometrically independent of sorting (Dyer 1969). The graphical dimensionless parameter designed by Folk & Ward (1957) is used in this survey. The theoretical limits are +1.0 to -1.0; positive values denote a fine tail, and negative values denote a coarse tail. This measure is efficient in that it takes into account both percentiles from the centre and the tails of the distribution (McManus & Buller 1979).

$$SK_o = \frac{\phi_{16} + \phi_{84} - 2\phi_{50}}{2(\phi_{84} - \phi_{16})} + \frac{\phi_5 + \phi_{95} - 2\phi_{50}}{2(\phi_{95} - \phi_5)} \quad \text{(IX)}$$

Folk & Ward (1957)

Sorting S_o	
Very well sorted	<0.35
Well sorted	0.35 - 0.50
Moderately well sorted	0.50 - 0.70
Moderately sorted	0.70 - 1.00
Poorly sorted	1.00 - 2.00
Very poorly sorted	2.00 - 4.00
Extremely poorly sorted	>4.00
Skewness SK_o	
Very negatively skewed	<-1.0 to -0.3
Negatively skewed	-0.3 to -0.1
Symmetrical	-0.1 to +0.1
Positively skewed	+0.1 to +0.3
Very positively skewed	+0.3 to >+1.0

(all units are dimensionless)

Table 4.3
Statistical Parameters (Folk & Ward 1957)

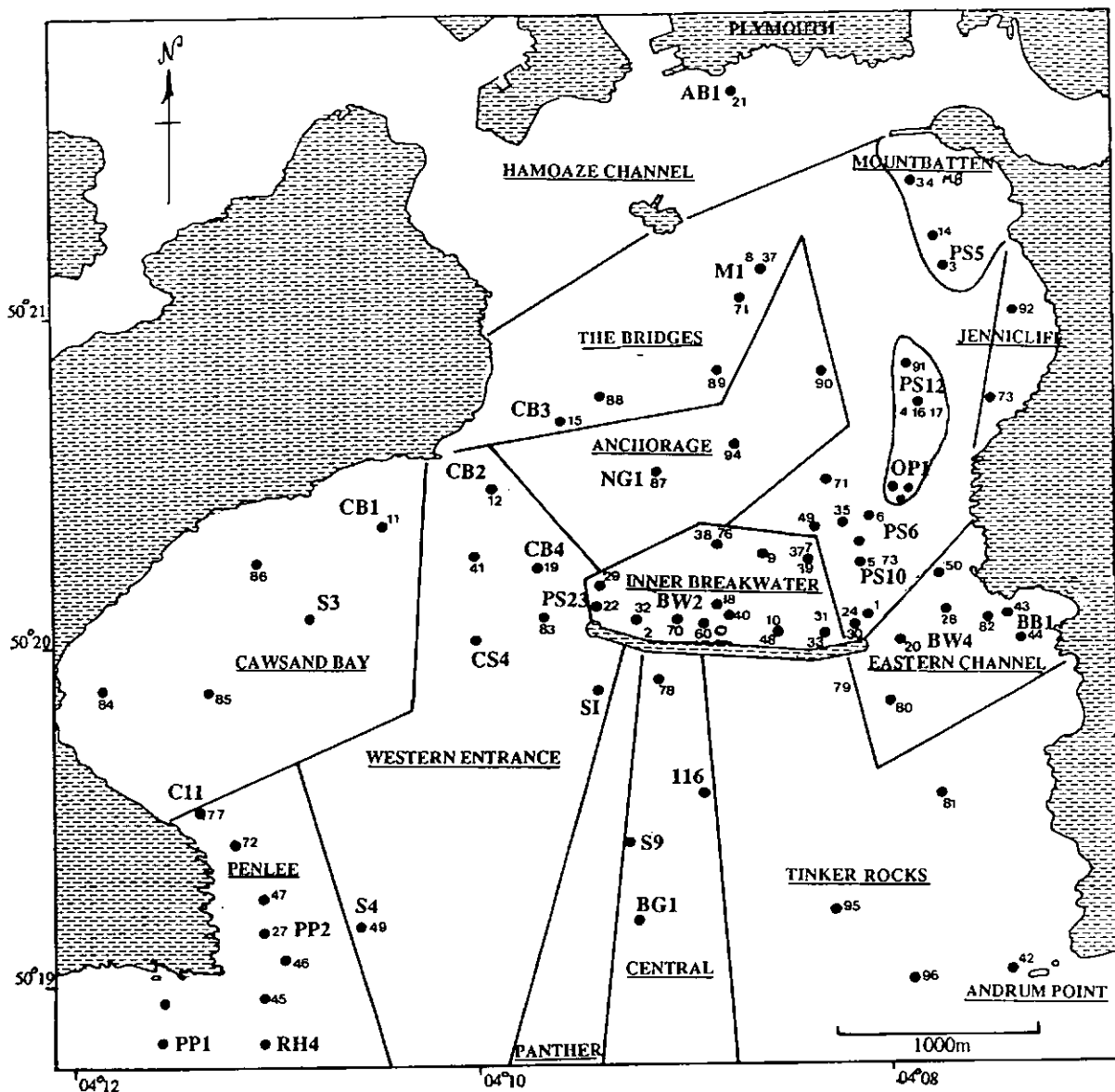


Figure 4.1 Map showing the loactions of samples and dives in Plymouth Sound and the limits of the sedimentary environments.

4.5 Sediment Results

The results of diver observations and the sedimentological analyses (Appendix 2) are presented for 14 areas (Figure 4.1). The boundaries of these areas were chosen on the basis of (i) the actual geographical location, within the confines of (ii) the sedimentary environments defined by the side-scan sonar survey (Section 3.6).

4.5.1 Fine-grained sediments

The fine grained sediments are confined to areas associated with an acoustically smooth side-scan sonar record. The sedimentology of two areas was investigated during this survey:

The Inner Breakwater

(Dive sites: 7,9,10,18,22,24,29,30,32,31,33,37,38,39,40,48,60, 70 & 76:

Samples BW1,BW2,BW24,C28,C29,C30,C31,C32,C31,C32,C33,C34,C35,C36,C37, C38,C39,C40,C41,C60,C61,C62,C63,BD1 & BD2)(Figure 4.1).

The Inner Breakwater area has been used during the last three years as a test site for the development of corers and the primary site for magnetic measurements (Chapter Seven). The boundaries of the mud depocentre were defined during the side-scan sonar survey (Section 3.6.1). The sea bed is generally smooth and featureless with the exception of (i) large circular pits of >50cm diameter and depths of 10-20cm created by rays, and (ii) smaller irregular-shaped 1-3cm deep pits created by infauna. The surface of the sediment is occasionally disturbed by locomotion traces of mobile crustacea. Anthropogenic debris (plates, ropes, iron fragments etc.) are also commonplace, especially in the areas around the Centre Fort and the mooring buoys. Currents of *c.* 0.5 knots (0.25 ms^{-1}) were recorded on the sea bed during dives. The suspended sediment concentration in this area is high (Section 6.3.1) and, consequently, the visibility from the surface to the sea bed was limited and usually within 1 to 0.5m. The surface sediments in this area are characteristically light to dark brown.

The initial samples (BW1, BW2 & BW24) were wet sieved and the $<63\mu\text{m}>$ ($<+4.00\phi>$) fractions were analyzed separately. The coarse ($>63\mu\text{m}$) fraction of the Breakwater silts (BW24) (Figure 4.2a) shows M_d and M_z values of $+0.00\phi$. It is well sorted ($S_o = 0.10$) and negatively skewed ($SK_1 = 0.50$). The $<63\mu\text{m}$ were analyzed using both Sedigraph and Laser Particle Analyzers. The Sedigraph size analyses of the surface sediments

of $<63\mu\text{m}$ gave M_z values of $+6.50\phi$ ($10\mu\text{m}$) with a poorly sorted ($S_o = 1.4$), symmetrical ($SK_o = 0.05$) distribution. A typical Sedigraph generated cumulative distribution curve shows two changes in gradient (Figure 4.2b) corresponding to an increase in particle distribution at $40\mu\text{m}$ and $4\mu\text{m}$ ($+4.50$ and $+7.75\phi$). The Malvern Laser Particle sizer results display a bimodal size distribution with peaks occurring within the $16.7-13.0\mu\text{m}$ ($+5.75$ to $+6.25\phi$) and $7.9-6.2\mu\text{m}$ ($+7.00$ to $+7.25\phi$) band widths (Figure 4.2c). A subsample from -50cm in the same core, from within the anoxic zone, was also measured and the Laser distribution showed three modal peaks within the $16.7-13.0\mu\text{m}$ ($+5.75$ to $+6.25\phi$), $7.9-6.2\mu\text{m}$ ($+7.00$ to $+7.25\phi$) and $3.8-3.0\mu\text{m}$ ($+8.00$ to $+8.25\phi$) band widths (Figure 4.2d). The third peak $3.8-3.0\mu\text{m}$ is tentatively ascribed to authigenic mineral development.

The cores samples all showed a 1-2cm thick layer of coarse sand ($M_z = 0.00\phi$) mixed with high percentages of shelly material ($>50\%$) and a dense accumulation of *Turritella communis* at -20 to -25cm . This assemblage was monospecific. The shells were whole, unworn, and had an average length of 2.5cm between 1.5 and 3cm and were scattered horizontally, on an unconformable surface, with no apparent orientation and with a density of c. 15 shells to 9cm^2 . The upper boundary of the coarse sediment layer graded upwards into fine silt over 1cm. *Turritella communis* live in the intertidal zone (e.g. The Breakwater) and graze on seaweed. Monospecific thanatocoenosis assemblages, with an associated upward coarsening in sediment size are characteristic of a change in climate, and in this case can be correlated with the cold winter of 1962/63 (Section 1.7).

The sediment showed high densities of infauna over the whole area. The population included specimens of (i) Polychaeta (*Capitella capitata*, *Scablibregma inflatum*, *Magelona alleni*, *Nephytes hombergi*, *Cerebratulus sp.*, *Caulleriella caput-esocis*) (ii) the bivalve - *Nucula turgida*, (iii) Crustaceans (*Ampelisca brevicornis*, *Ampelisca typica*, *Gonoplax rhomboides* (burrows)) and, (iv) other infauna included the burrowing anemone: *Edwardsia claparedii* and starfish *Amphiura sp.* All the polychaetes are typical of low oxic-hypoxic environments and were found in great numbers. The epifauna included fish and anemones. Shrimps and polychaete burrows were recorded to depths of -25cm . The burrows were clearly outlined on the X-radiographs taken of the cores, e.g Figure 4.3a,b,c & d (To counteract the poor reproduction resolution, line drawings have been made

of the primary features). C27 and C28 were X-rayed using different intensities of X-ray sources. C27 shows well developed laminations (Figure 4.3a), which could not be differentiated by eye, which are particularly pronounced in the top 6cm and have a spacing of c. 3mm. Shell fragments occur in discrete bands in C28. The most common shells are those of *Nucula turgida*, unbroken, and slightly worn disaggregated valves, with no visible preferred orientation. Three types of burrows can be identified (i) the vertical traces of the nereiid *Capitella capitata*, (ii) larger infilled burrow of the common shrimp *Ampelisca brevicornis* and, (iii) backfilled faecal traces of *Nephytes hombergi*. The X-rayed box sample showed well defined laminations which were slightly deflected upwards against the friction of emplacement.

The mineralogy of the surface sediments from the Eastern and Western End of the Breakwater was identified using X-ray diffraction techniques (Table 4.4). To identify the mineralogies characteristic of the different size peaks, the sediment was separated into decreasing size fractions from 63 μ m in a sedimentation tube. A smear was also taken of the whole sample.

The results showed similar minerals present at both sites. The surface smear sample contained the same mixed-layer kaolinite, illite and montmorillonite, pure chlorites, primary and accessory minerals, with the exception of pyrite, which was only recognized at the West Breakwater site. The 63-37 μ m fraction included the same minerals, with the exception of the occurrence of mixed-layer illites, and absence of diopside in the East Breakwater site. Neither biotite nor mixed-layer montmorillonite were present in the >37 μ m fractions. Some minerals were absent in sample sizes of >8 μ m, which contained chlorite, kaolinite, illite, muscovite, plagioclase and diopside. It is interesting that only Na-feldspars were identified in the sediments. (Unfortunately, due to the time constraints on using the X-ray Diffractometer, not all samples were processed).

Dried subsamples were taken from five cores and an attempt was made to separate the magnetic fraction. There was less than 1% variation down core. The experiment was then aborted on the grounds that the magnet was not strong enough.

Site and size	Primary Minerals									Accessory Minerals		
	1	2	3	4	5	6	7	8	9			
East Breakwater												
>63 μ m	*	#	#	#	*	*	*	*	*		Ru	Di St
63-37 μ m	#	#	#	#	*	*	*	*	*		Ru	St
31-15 μ m	#	*	*	*	*	*		*	*		Di	St
8-4 μ m	*	*		*		*					Di	
West Breakwater												
>63 μ m	*	#	#	#	*	*	*	*	*		Ru	Di Py Ap
63-37 μ m	#	#	#	*	*	*	*	*	*		Ru	St Di
15-9 μ m	#	*		*	*	*		*	*		St	Di
8-4 μ m	#	*		*	*	*					Di	

* pure
mixed-layer clays

Primary minerals

1 - chlorite $(Mg,Fe)(Al,Si)O_{10}(OH)_8$
2 - kaolinite $Al_2Si_2O_5(OH)_4$
3 - montmorillonite $(Ca,Na)_{0.65}(Al,Mg,Fe)_{4-6}(Si,Al)_8O_{10}(OH).H_2O$
4 - illite $(K,Na,H_3O)_{1-2}Al_4(Si_{7-6}Al_{1-2})O_{20}(OH)_4$
5 - plagioclase $(Na,Ca)_2AlSi_3O_8$
6 - muscovite $KAl_2(Si_3Al)O_{10}(OH)_2$
7 - biotite $K_2(Mg,Fe^{2+})_{6-8}Al_{0-1}(Si_{6-5}Al_{2-3})O_{20}(OH,F)_4$
8 - goethite $Fe_2O_3.H_2O$
9 - haematite Fe_{23}

Accessory minerals

St - staurolite $(Mg,Fe^{2+})_2AlFe^{3+}_9O_6[SiO_4]_4(O.OH)_2$
Di - diopside $CuSiO_2(OH)_2$
Ru - rutile TiO_2
Py - pyrite FeO_2
Ap - apatite $Ca_5(PO_4)_3(F,OH,Cl)$

Table 4.4

Primary and accessory minerals present in the Breakwater sediments and their general chemical composition. Quartz, calcite and halite are present in all samples.

The depth to the anoxic layer varied between sites (Table 7.6). The cores were subsampled at 5cm intervals and bulk density (wet and dry), moisture content (M), organic content (O_2), calcium carbonate content ($CaCO$) and critical shear stress (τ_{cc}) were measured (Table 7.1a-d). The

results and site locations are presented in presented in Figure 4.4 and discussed in site order.

(i) East Breakwater

The wet bulk density increased irregularly with depth down core by 11% between 1.5 and 1.7gcm³. The profile showed an initial increase between the surface and -5cm of 6% and a decrease of 6% at -10cm. This was followed by a sharp increase from 1.5 to 1.75gcm³ at -15cm. The dry bulk density showed a similar profile, with an overall 8% increase with depth. The moisture content of the samples varied with depth, showing an initial drop between 0.40% at 0cm and 0.35% at -5cm, followed by an increase to 0.39% at -10cm. It then decreased at -20cm and -25cm to 0.37%, with a marked increase to 0.41% at -30cm. The total organic material (TOM) and calcium carbonate content (CaCO₃) both showed down core variation in concentration. The surface sediments had a TOM content of 3% and a CaCO₃ content of 12%. The TOM content increased at -5cm to 4.5% and the CaCO₃ content showed a decrease to 10%. There was a marked decrease of TOM at -20cm and an increase of CaCO₃ to 2% and 12% respectively. The critical shear stress values showed a general increase with depth between 3.10 and 3.56N/m². There was a sharp decrease of critical shear stress at -10cm of c. 3%..

(ii) West Breakwater

The wet bulk density results showed an increase down core by 8% between 1.6 and 1.75gcm³, with a sharp decrease at -25cm to 1.6gcm³. The dry bulk density measurements showed a similar down core increase, with the exception of C34 which decreased from 2.3 to 2.0gcm³ at -25cm. The moisture content generally decreased down core and had surface values of c. 0.45%, except for C34 which showed a rapid decrease to 0.27% at -25cm. The TOM content of C32 showed little down core variation, with a 1% decrease at -5 and -25cm, and an increase of 1% at -15cm. The CaCO₃ content of the surface samples was c. 12% , with a 1% decrease at -15cm. C331 showed stable TOM and CaCO₃ down core contents, with a 1% decrease at -20 and -15cm. The TOM content of the surface of C34 was low (3%) and decreased down core. There was a sharp 8% increase at -5cm. The CaCO₃ content profile of the cores showed surface values of 13%, followed by a sharp decrease at -5cm to 7%. The CaCO₃ content stabilized to 11-12% with depth. The critical shear stress show a general increase with depth, with the exception of (i) cores C33 and C34, which exhibited a

decrease in critical shear stress between the surface and -5cm of 1.8 and 2.0% respectively, and (ii) cores C32 and C34 which showed a decrease at -25cm of 7.5 and 23.2% respectively.

(iii) West Breakwater 2

The wet bulk densities showed a general down core increase, with the exception of C38 and C39, which had high surface values (1.7 and 2.8gcm^3) that decreased at -5cm to 1.5 and 1.6gcm^3 respectively. Cores C36 and C38 showed two 0.01gcm^3 decreases at -25 and -14cm. The dry bulk densities also showed a general increase down core, with surface values ranging between 2.2 to 2.5gcm^3 . C36 showed a down core increase in dry bulk density of 0.2gcm^3 and a decrease of 0.01gcm^3 at -25cm. C38 and C39 showed more varied profiles with decreases at -10cm, of 0.2 and 0.1gcm^2 respectively. The moisture content in all four cores decreased down core. C35 and C36 had high surface values of 0.47 and 1.48% whereas C38 and C39 had low surface values 0.38 and 0.36% . C36 and C39 showed an increase in moisture content at -25cm of 0.5 and 0.4% . C39 showed a marked decrease between -10 and -20cm. The cores showed an overall increase in TOM and CaCO_3 when compared to those of East Breakwater and West Breakwater 1. The TOM content generally decreased with depth, although C36 and C38, increased by 0.1% at -25cm and -20cm respectively. C38 and C39 had low surface values of TOM between 0.8 and 1.2% , C39 also had a 0.9% decrease-at -25cm. The CaCO_3 values of the four cores showed, with the exception of C36, high surface contents (17 to 23%). The critical shear stress of C35 increased with depth from *c.* 3.10N/m^2 at -5cm to *c.* 3.40N/m^2 at -15cm. C36 showed a surface value of 3.12N/m^2 , and a marked increase to 3.36N/m^2 at -5cm, the critical shear stress reached a peak (*c.* 3.56N/m^2) at -16cm and decreased thereafter with depth. C38 and C39 showed relatively high surface values of 3.43 and 3.60N/m^2 , respectively. C38 had a peak increase in critical shear stress at -10cm to *c.* 3.38N/m^2 and then, decreased linearly down core to 2.95N/m^2 . C39 exhibited a decrease from -2cm to -10cm of 0.25N/m^2 , followed by an increase at -20cm of *c.* 0.36N/m^2 and a second sharp decrease to 3.26N/m^2 at -25cm.

(iv) Centre Fort

The wet bulk densities showed a decrease with depth, with the exception of C41 in which down core values increased from the surface to -15cm (1.6gcm^3), followed by a decrease to -30cm (1.5gcm^3). The dry bulk

density showed a similar profile with a general increase with depth and a marked 8% decrease at -30cm. The moisture content of C40 and C41 decreased linearly with depth from -5cm to -20cm and -25cm respectively, where a 0.04% increase occurred. The TOM content C40 showed a low surface value of c. 0.4% which decreased down core with two separate increases at -5cm (1.2%) and -30cm (3.0%). The TOM profile of C41 showed a linear decrease with depth to -20cm, and a 0.4% increase at -25cm. C40 had high surface values of CaCO_3 content (25%) which decreased down core to 16% at -5cm, and remained constant to -30cm, where they decreased to 12%. The CaCO_3 content of C41 was constant down core (12-13%). The surface critical shear stresses were high (3.55N/m^2) in C40, with two sharp decreases at -10cm and -15cm of 0.20 and 0.26N/m^2 respectively. The critical shear stress values in C41 showed low values of 2.99N/m^2 at the surface which increased with depth to 3.35N/m^2 at -15cm, after which they decreased linearly to -30cm (3.07N/m^2).

(v) Charlie Buoy

The wet bulk density of the cores at Charlie Buoy site showed two slightly different profiles - C60 demonstrated a decrease between 0 and -15cm (20%), whereas C61 showed a 30% increase between the same depths. Both cores showed a down core decrease in wet bulk density from -20cm. The dry bulk density of C60 showed a high surface value (2.5gcm^3), whereas C61 showed low values (1.9gcm^3). The dry bulk densities were stable down core, with a slight increase (0.2gcm^3) at -20cm. C60 showed a rapid increase in moisture content of 0.30% between the surface and -5cm. The moisture content then decreased with depth to -25cm where it showed an increase of 0.1% at -30cm. The moisture content of C61 showed a linear decrease with depth from the surface to -25cm (56%) and a marked increase at -35cm to 0.63%. The TOM measurements showed the cores to have high surface values (5.0 & 7.3%) which generally decreased down core. C60 showed a peak increase at -10cm to 6.4%, and C61 showed a peak increase at -20cm to 10.0%. The CaCO_3 values of C60 were relatively constant between the surface and 5cm (12%), and were followed by an increase to 16% at -10cm and a decrease back to 12/13% at -25cm. Core C61 showed relatively constant CaCO_3 results of c. 12% with a marked increase at -25cm to 20%. Both cores showed similar critical shear stress values with a marked c. 11% increase at -20cm.

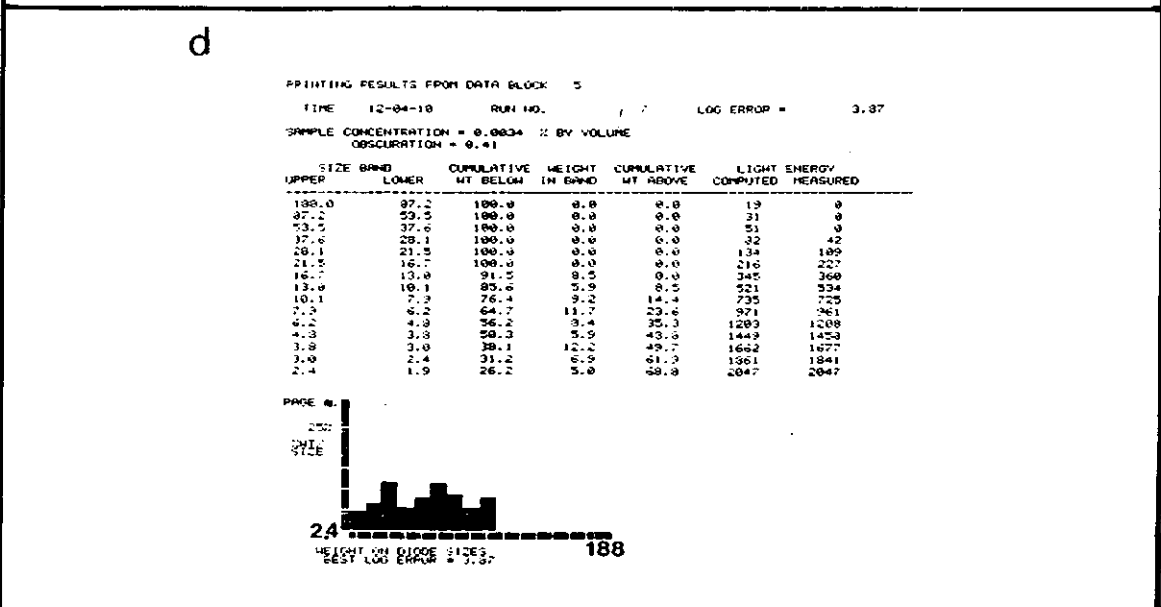
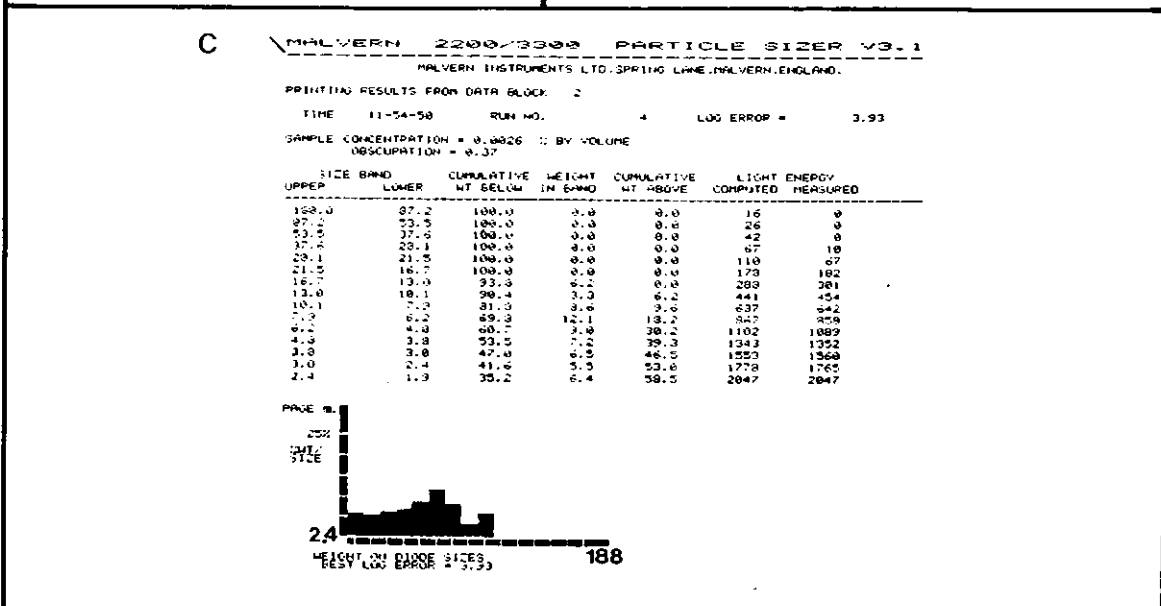
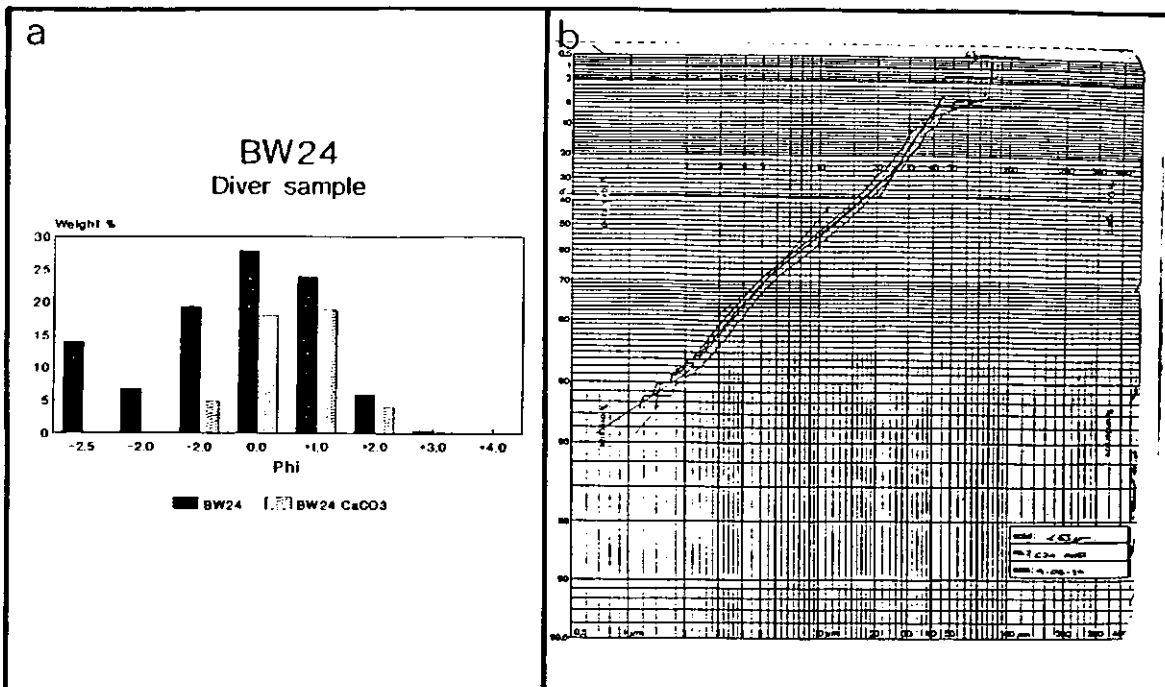


Figure 4.2 The Breakwater Muds (a) Frequency histogram BW24, (b) Sedigraph profile - surface mud, (c) Malvern Particle sizer profile surface mud, and (d) Malvern Particle sizer profile -50cm depth.

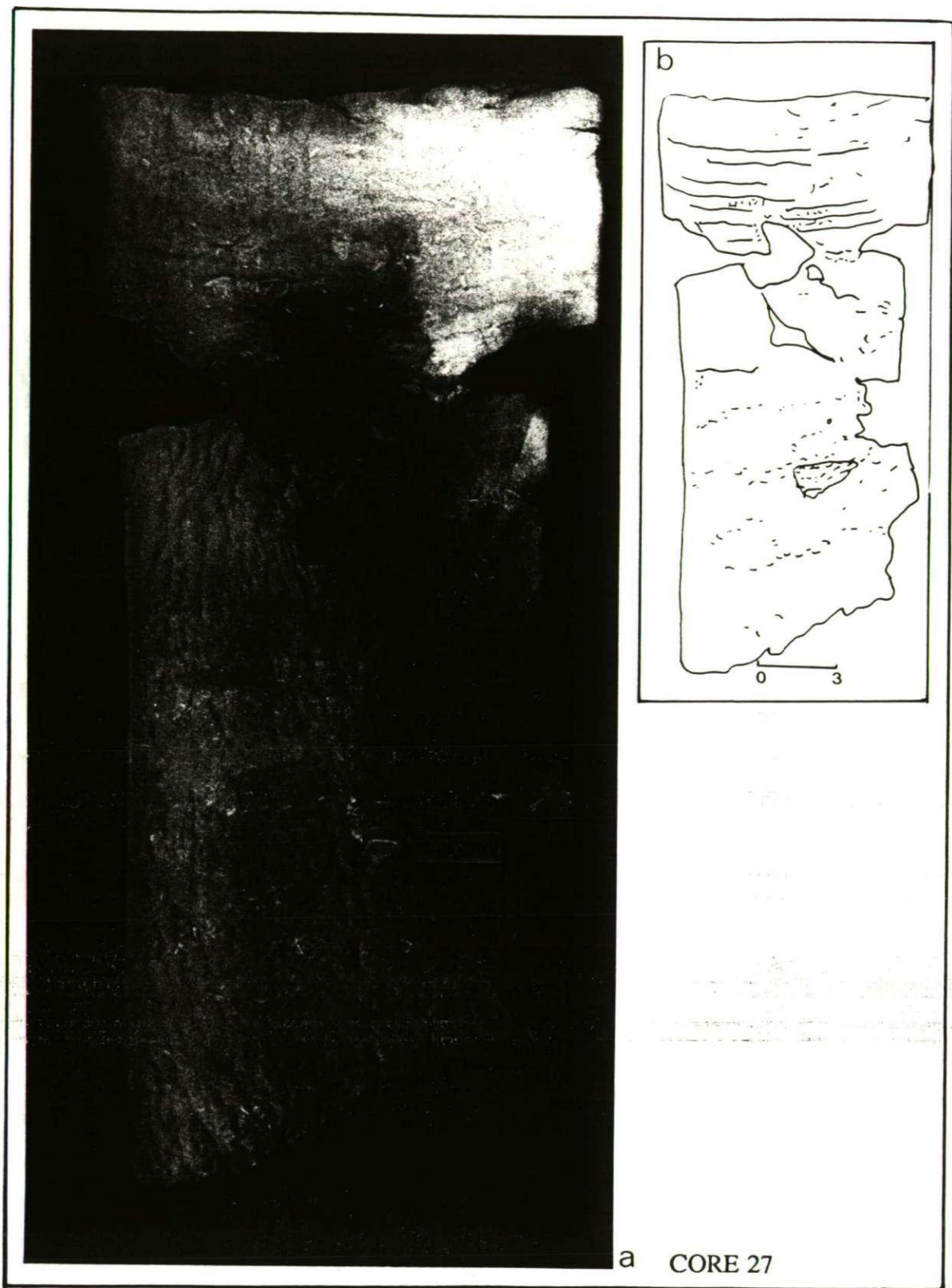


Figure 4.3 X-radiograph of the Breakwater Muds Core 27 (a) photograph of X-ray, and (b) line drawing.

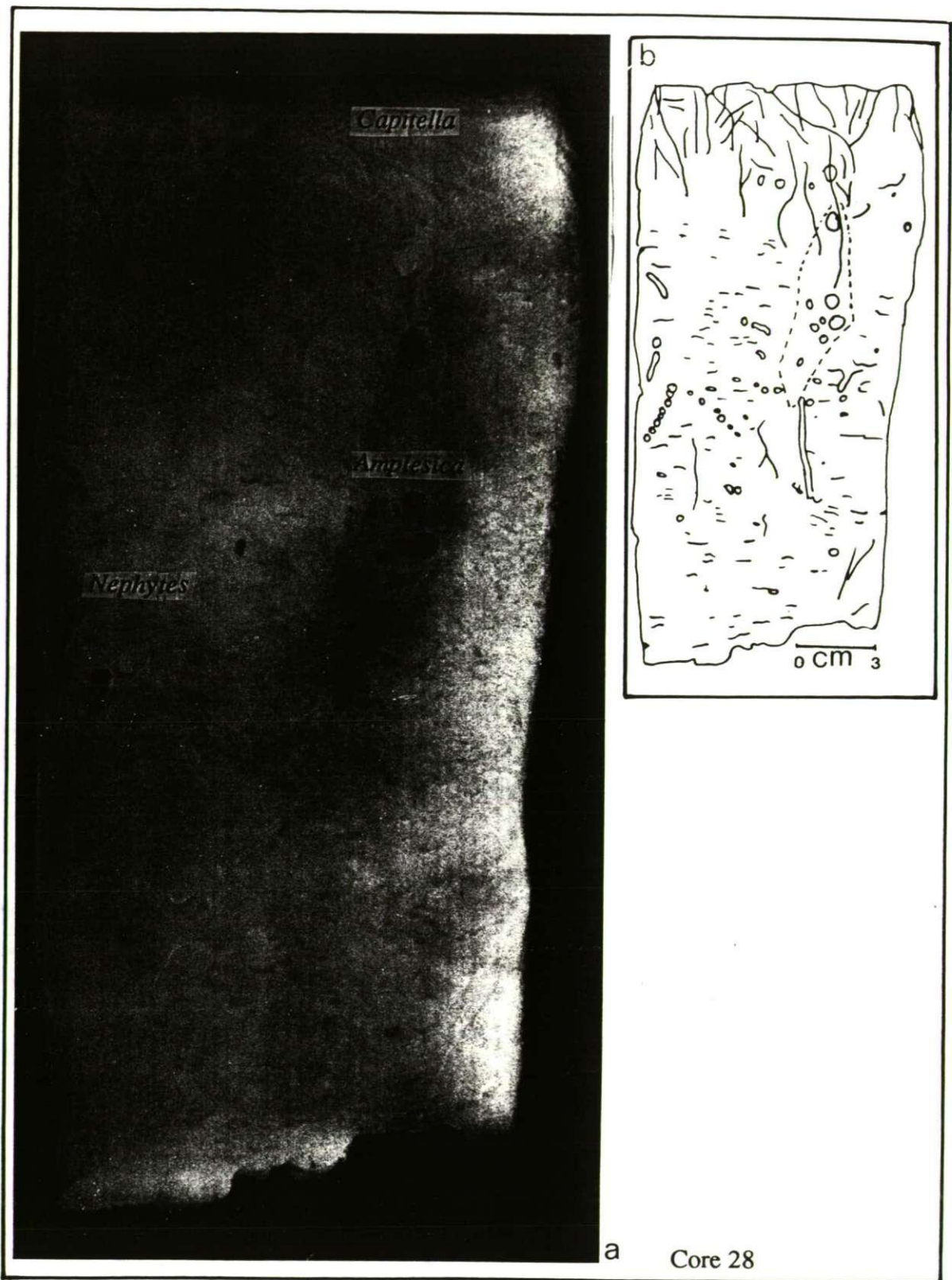


Figure 4.3 cont.. X-radiograph of the Breakwater Mud Core 28 (a) photograph of X-ray, and (b) line drawing.

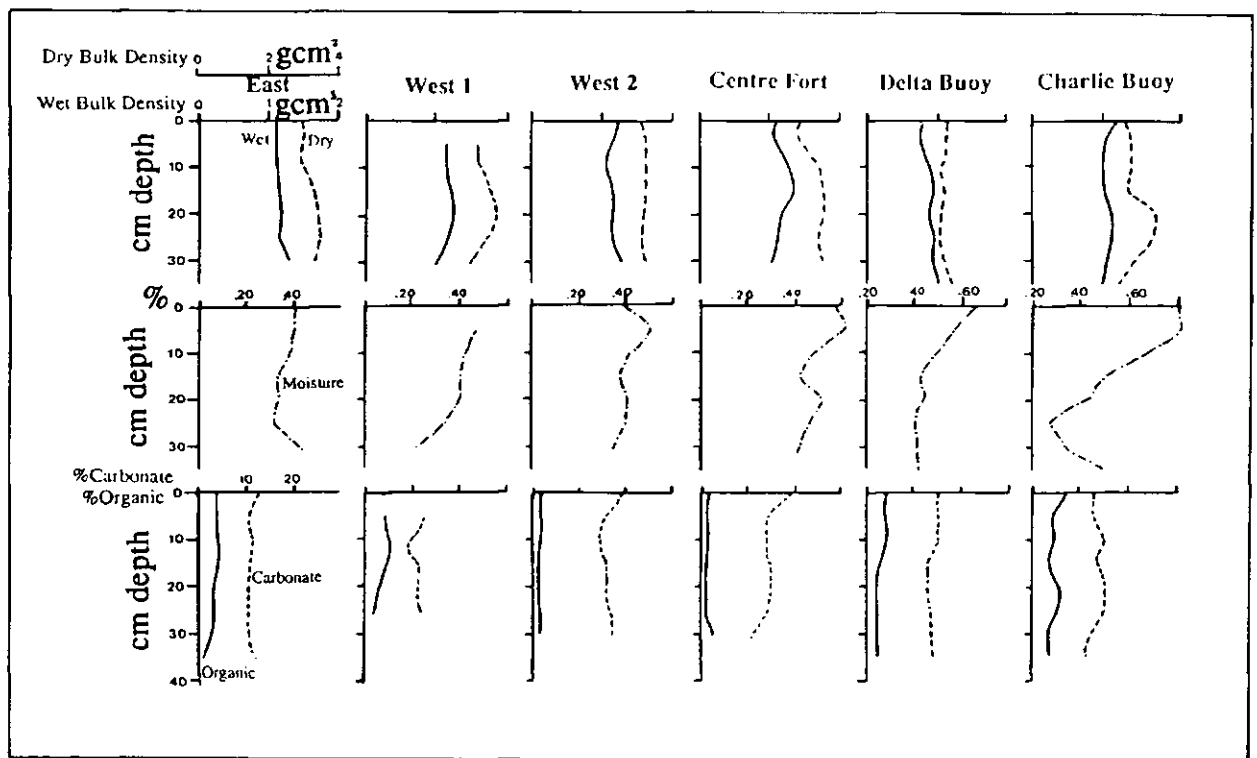
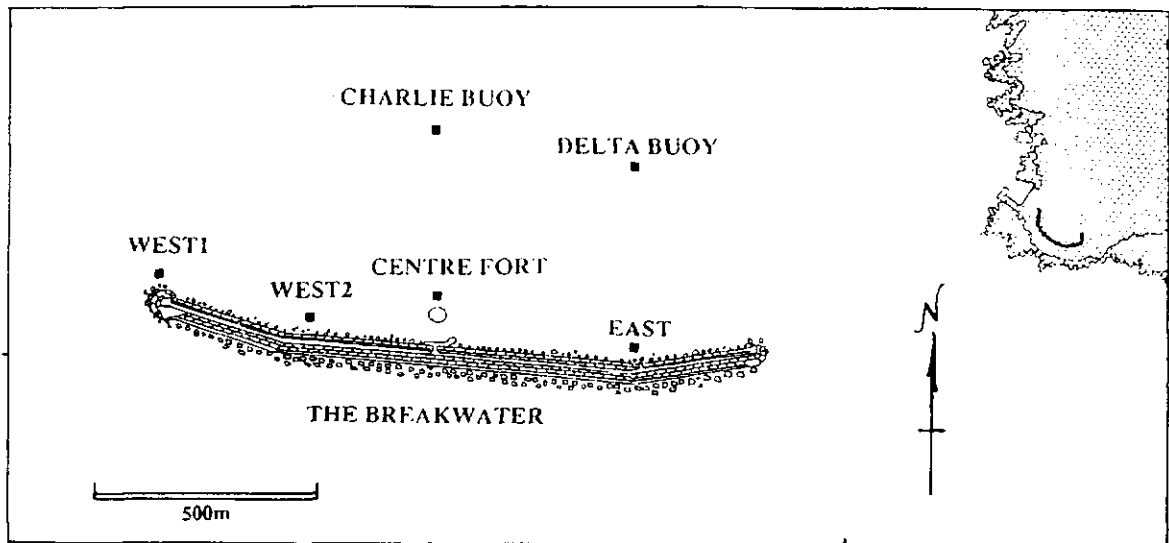


Figure 4.4 Location of the Inner Breakwater sites and the averaged physical property results of each site.

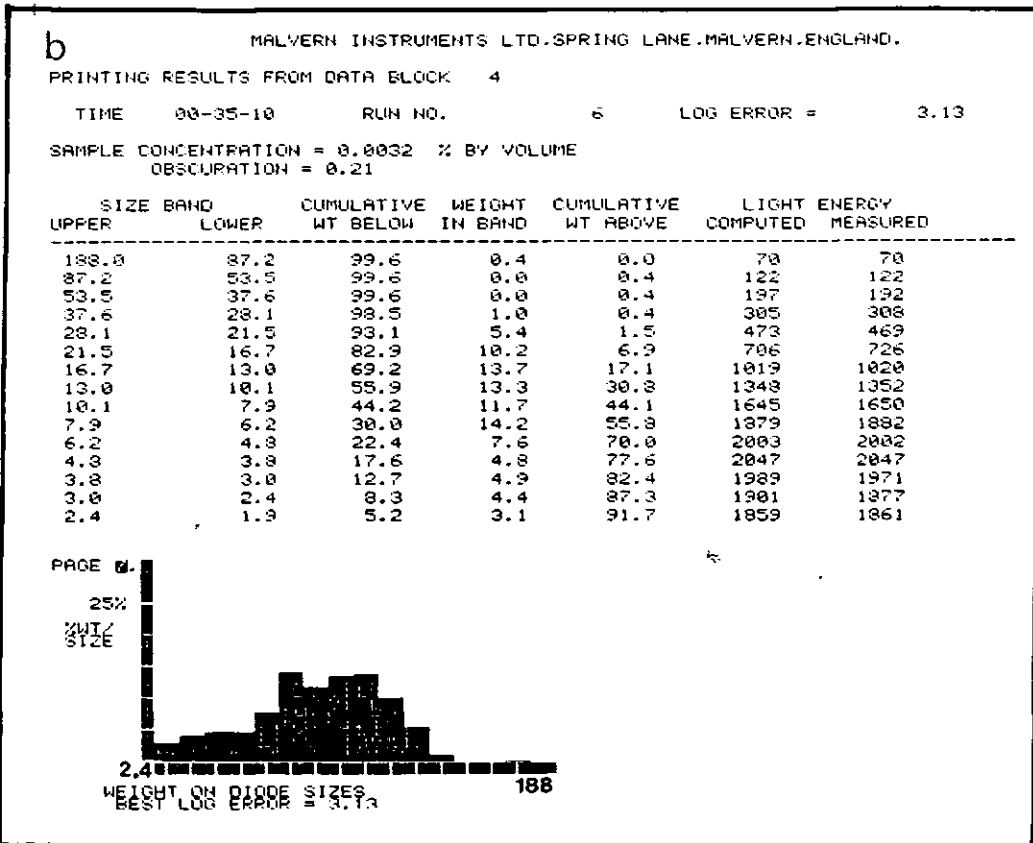
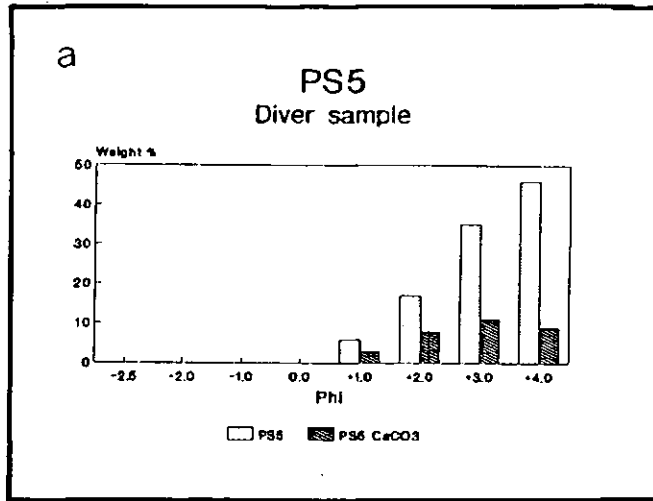


Figure 4.5 Mountbatten Muds (a) frequency histogram of the coarse fraction and, (b) Malvern Particle sizer profile.

(vi) Delta Buoy

The wet bulk density of the cores taken at Delta Buoy both showed a slight down core increase between 1.1gcm^3 at the surface, to 1.3gcm^3 at -35cm . The dry bulk density showed low surface values of 1.9gcm^3 and a stable profile from -5cm to -35cm of $c. 2.0\text{gcm}^3$. The moisture content decreased down core from surface values of 0.76% and 0.59% to 0.52% at -30cm . The TOM content of the surface sediments were high (3.6 and 3.3%) and both C62 and C63 showed a marked decrease in TOM of $c. 1\%$ at -15 and -20cm . C63 showed an increase in TOM of 1% at -20cm . The CaCO_3 content of the cores generally remained constant with depth - C62 showed a 1% increase at -5cm , and C63 has a 1% increase at -5 and -20cm . The critical shear stress values of C62 showed a high surface value 2.68N/m^2 and a decrease to 2.42N/m^2 at -5cm , with two high peaks at -10cm and -20cm of 2.92 and 2.82N/m^2 respectively. Core C63 showed two maximum critical shear stress values at -15cm and -30cm of 2.95N/m^2 . The box samples BD1 and BD2 showed high wet bulk density and dry bulk density values of 1.8gcm^3 and $c. 2.4\text{gcm}^3$. The moisture content in the samples varied between 0.18 and 0.47% and the critical shear stress values were high - 3.09 and 3.71N/m^2 .

The Mountbatten depocentre (Dives: 3,14 & 34; Samples PS5, MB1,2,3,& 4). The mud depocentre is located south of Mountbatten Breakwater and extends $c. 1\text{km}$ southward into Jennicliff Bay. The eastern confines of the sediment body were defined during the side-scan sonar survey (Section 3.6.1). The sea bed in this area is generally brown in colour and composed dominantly of silts. Due to the predominance of these fine unconsolidated silts on the sea bed, suspended material was frequently created during finning and as a consequence, the visibility was less than 50cm . No epifauna was visible on the sea bed, however, anthropogenic debris was commonplace. The anoxic zone was located at -2 to -3cm depth in the sediment, there appeared to be no hypoxic layer. Dives underneath Dunstone Rock Buoy showed pits of 20cm depth and diameters of $40\text{-}50\text{cm}$ to occur with a regular quadratic spacing of 1m . These pits were not present at either of the other sample sites or identified on the side-scan sonar record. It is assumed, therefore, that they are confined to the south of the Mountbatten depocentre. The bag-sampled sediment (PS5) was initially wet sieved and the $<63\mu\text{m}>$ fractions were processed separately. The $>63\mu\text{m}$ fraction was dry sieved and the distribution had M_d and M_z values of $+3.50\phi$ and $+3.25\phi$, in a poorly sorted ($S_o = 1.05$) and

very negatively skewed ($SK = -0.43$) profile. The sediment was mostly composed of quartz and mica, with less than 12% calcium carbonate (Figure 4.5a). The fine fraction ($<63\mu\text{m}$) was analyzed on the Laser Particle Sizer and results showed a unimodal, moderately well sorted distribution with a broad peak between 21.5 and $7.2\mu\text{m}$ ($+5.50$ to $+7.00\phi$) (Figure 4.5b).

The sediment therefore has a size distribution between 710 and $1.9\mu\text{m}$ ($+0.50$ and $+9.00\phi$). The infaunal community (present only at Dunstone Rock Buoy) supported the same species as the Breakwater depocentre (above), with two additional bivalves - *Corbula gibbosa* and *Mya truncata*. The chain of Dunstone Rock Buoy was heavily colonized by an opulent community of Mussels (*Mytilus edulis*). These are sessile filtre feeders and characteristically live in waters with high nutrient levels.

4.5.2 Sandy sediments

(i) The Anchorage (Dives:15,87,90 & 94; Samples: CB3 & NG1)

The Anchorage (Figure 4.1) contains large-scale sedimentary features which are discussed in Section 3.6.3. At the time of sampling station CB3, megaripples were present on the sea bed, with a height of *c.* 15cm and wavelength of 70cm. These were parallel crested and orientated perpendicular to the flooding current at $050/230^\circ$ and were typically unimodal coarse sands with a distribution which showed M_d and M_z values of $+0.25$ and $+0.08\phi$, in a moderately well sorted ($S_o = 0.75$) and negatively skewed ($SK_1 = -0.36$) distribution (Figure 4.6a). The larger fractions $>-2.50\phi$, were composed of shells of *Venus sp.* which were disaggregated and unworn. The calcium carbonate content in the sand fraction was generally high (*c.* 90-33%) and decreased with grain size. The critical shear stress values were calculated for the modal peak of the clastic and carbonate fraction of the sediment and gave values of 4.0 and 7.0N/m^2 respectively. Sample NG1 was taken from directly underneath New Ground Buoy one hour before Low Water (Neaps). A current of 0.8 knots was flowing in a southwest direction. Ripples were present on the sea bed, the crests were sinuous and orientated $130/310^\circ$. The ripples had a maximum amplitude of 10cm and a wavelength of 50cm. The sediment was dry sieved and showed a unimodal distribution with a well developed peak at $+0.00$ and $+1.00\phi$. The M_d and M_z were located at $+0.75\phi$ and $+0.66\phi$, the distribution was poorly sorted ($S_o = 1.00$) and positively skewed ($SK_1 = 0.09$) (Figure 4.6b). The sediment contained an overall high shelly (*c.* 80%) content with recognizable fragments of the bivalve *Scrobicularia sp.*

in the $>-1.00\phi$ fractions. The critical shear stress values for the clastic and carbonate fractions were 7.0 and 4.0N/m^2 .

(ii) The Western Entrance

(Dive sites 12,19,41,49,83; Samples CB2,CB4 CS4,S4 & PS23)

The area of the Western Entrance is defined in Figure 4.1, and the large-scale features are discussed in Section 3.6.3. Sample CB2 was acquired on a flooding tide in 2m horizontal visibility, ripples were present and had a height of 20cm and wavelength of 60cm. The crests were parallel and orientated $110/290^\circ$. The ripples were slightly asymmetrical, and moving in a northeastward direction, perpendicular to the prevailing current. Although substantial swell was present on the surface, there was no indication of oscillatory swell motion on the sea bed. After sampling, the divers allowed themselves to drift with the current for 600m. Several small rocky outcrops ($<2\text{m}$ length) were observed with a sparse covering of opportunistic species of red algae and starfish. No encrusting microorganisms were present indicating episodic covering of the rocks by sand. The sediment sample showed a clean washed coarse sand with M_d and M_z values of -0.75ϕ and -0.91ϕ , the profile showed a unimodal distribution which was well sorted ($S_o = 0.41$) and very negatively skewed ($SK_1 = -0.30$). The calcium carbonate content showed an average value of 64% which varies between a minimum of 23% in the fine pebble fraction, and 85% in the coarse sand fraction (Figure 4.6c). The fine pebbles were composed shales derived from the Staddon Grits (Section 2.2). The sample contained no living fauna. Sample CB4 was taken during a time of very low underwater visibility. Unfortunately the diver and buddy became separated and the dive had to be aborted before any morphological measurement of the configuration of the sand could be made. The sediment was clean washed with M_d and M_z diameters of $+0.25\phi$ and -0.33ϕ respectively. The sediment was moderately well sorted ($S_o = 0.87$) and symmetrical ($SK_1 = -0.01$). A medium sized pebble composed of purple shale, was present and gave the histogram (Figure 4.6d) a slight bimodality. The whole ϕ fractions were all composed of c. 50% calcium carbonate and recognizable shell fragments included the bivalves - *Spisula sp. Alba abra*, *Cardium sp.* and *Venus sp.* The highest percentage of shelly material occurred in the very coarse sand fraction. The calculated critical shear stresses required to move the clastic and carbonate fraction were 4.0 and 7.0N/m^2 . The grab sample CS4, showed a clean washed sediment with M_d and M_z diameters of -1.50 and -0.66ϕ

respectively. The distribution profile was very well sorted ($S_o = -0.10$) and symmetrical ($SK_1 = 0.00$). The sediment was predominantly composed of well-rounded particles of quartz and shales, with low percentages of calcium carbonate present in the granule (8%) fraction increasing to 40% in the coarse sand fraction (Figure 4.6e). The critical shear stresses of the clastic and carbonate fractions were 15.0 and 4.0N/m². Grab sample S4 showed a bimodal distribution with a prominent peak at -2.50 ϕ and a second less well defined peak at +1.00 ϕ . The sample profile gave M_d and M_z mean particle diameters of -1.25 and -0.25 ϕ . The sediment distribution was very well sorted ($S_o = 0.27$) and very positively skewed ($SK_1 = 1.00$). The overall shelly content was high with a maximum of 75% in the very coarse sand fraction (Figure 4.6f). The critical shear stresses for the clastic and carbonate fraction are >20.0 and 7.0N/m² respectively. The >-2.50 ϕ fraction of the sample was composed entirely of whole live bivalves *Glycimeris glycimeris*, which typically live in shelly sands. Sample PS23 was acquired 100m due west of the Western End of the Breakwater, the sediment distribution was unimodal with a peak at +1.00 ϕ . The profile showed M_d and M_z values of +0.50 and +0.33 ϕ , in a poorly sorted ($S_o = 1.70$) negatively skewed ($SK_1 = -0.11$) distribution. The sediments had a high shelly content and showed a unimodal peak at 0.00 ϕ of 80% (Figure 4.6g). The critical shear stress for the clastic and carbonate content was 4.0 and 7.0N/m².

(iii) Central PalaeoChannel (Dive 78; Samples 116,S9 & BG1)

The confines of the Central PalaeoChannel (2.4) were identified during the side-scan sonar survey (Section 3.6.5). The sediments in the northernmost part of the area were observed on drift-dive 78 and shown to form a series of sand sheets. Grab sample 116, was obtained from the north part of the area, and showed a unimodal distribution with a peak at +4.00 ϕ . The profile gave M_d and M_z values of +1.50 ϕ in a moderately sorted ($S_o = 0.72$), very positively skewed ($SK_1 = 0.52$) distribution. The shelly content of the sediment showed unimodal distribution with a maximum of c. 50% at +3.00 ϕ (Figure 4.6h). The critical shear stress for the clastic component was 0.02N/m², and 7.0N/m² for the carbonate fraction. The grab sample S9 was taken 500m southwest of 116. The sample was dry sieved and the sediment profile showed a pronounced bimodality with a peaks at -2.50 and +4.00 ϕ . The -2.50 ϕ peak was formed by oblate granules of shales and oyster fragments. The remainder of the sample gave M_d and M_z values of -1.75 and +0.41 ϕ , in a poorly sorted ($S_o = 1.20$)

symmetrical ($SK_1 = -0.03$) profile. The -2.00 to $+2.00\phi$ fractions contained little (c. 25%) shelly material, and the $+3.00\phi$ fraction was composed of a maximum 40% calcium carbonate (Figure 4.6i). The critical shear stress required to initiate movement was calculated as $>20.0N/m^2$ for the clastic content and $0.02N/m^2$ for the dominant carbonate fraction. Grab sample BG1 showed a well defined unimodal distribution with a peak at -1.00ϕ . The profile showed M_d and M_z values of -1.50ϕ , in a very well sorted ($S_o = 0.13$), very negatively skewed profile ($SK_1 = -1.50$). The sample contained $<1\%$ of shelly material was composed entirely of well rounded shale particles, which had a critical shear stress of $15.0N/m^2$ (Figure 4.6j).

(iv) Bovisand Bay (Dives: 43,44 & 82 Samples: BB1)The sea bed sloped gently westward with a sandy bottom surrounded by kelp-covered rocks. The sediment was clean-washed and unimodal with a peak at $+2.00\phi$. Dry sieving showed M_d and M_z values of $+1.50\phi$. The sediment was poorly sorted ($S_o = 0.50$) and symmetrical ($SK_1 = 0.07$). The shelly content was moderate and averaged c. 50% over the distribution (Figure 4.6k). The critical shear stress for the dominant clastic mode was calculated as $1.4N/m^2$, and $4.0N/m^2$ for the dominant carbonate fraction. The sediment also had a high pottery content.

4.5.3 Coarse relict sediments

The relict sediments are defined as those which cannot be moved under any combination of present day wave and tidal forces. These are common on the bed of Plymouth Sound and are related to the change of depositional forces during the Flandrian transgression (Section 2.3.4). The gravels are divided into three classes, on the basis of their acoustic response and sediment characteristics.

Relict Marine Gravels

(i) Smeaton's Pass and South Jennycliff Bay (Dives: 4,16,17,41,91,92 & 93: Samples M1, PS12, OP1, BM1,BM2 & BM3).

The location and extent of these deposits is given in Section 3.6.4. They have been observed on many drift dives, and appear to be transgressionary overlying relict fluvial gravels. Marine gravels were characteristically bimodal, and composed of cobbles and interstitial medium to fine sands. Diver sample M1 was taken from the interstices of small boulders. The distribution showed a unimodal profile with a peak

at $+3.00\phi$, the M_d and M_z values were calculated as $+1.75\phi$ and $+1.58\phi$, in a poorly sorted ($S_o = 1.46$) very negatively skewed ($SK_1 = -0.26$) distribution. The shelly content was negligible over the distribution, with the exception of -1.00ϕ fraction, where it formed 45% of the sediment, the shells were identified as consisting almost entirely of *Tellina sp* (Figure 4.7a). The critical shear stress required to initiate movement of the dominant non-cohesive clastic mode was 0.6N/m^2 and 7.0N/m^2 for the carbonate mode. Grab sample OP1 was taken from the area to the south of Jennicliff Bay. The sample was unimodal with a peak at $+2.00\phi$ which corresponds to a critical shear stress of 1.4N/m^2 , and gave M_d and M_z values of $+1.00\phi$, in a poorly sorted ($S_o = 1.20$) and positively skewed distribution ($SK_1 = 0.16$). The shelly content varied from a minimum of c. 15% in the tails of the distribution, to a maximum of c. 80% at 0.00ϕ , which required a critical shear stress of 7.0N/m^2 to initiate movement (Figure 4.7b). The sediment sample from the sea bed under Foxtrot Buoy, PS11, was also taken from the interstices between boulders. The sample was initially wet sieved and divided into $<63\mu\text{m}>$ fractions. The $>63\mu\text{m}$ fraction showed a unimodal distribution with a peak at $+3.00\phi$. The distribution curve gave M_d and M_z values of -2.50 and -2.25ϕ in a poorly sorted ($S_o = 1.09$), and negatively skewed ($SK_1 = -0.30$) profile. The shelly content showed a unimodal distribution with a peak percentage (82%) at 0.00ϕ , which requires a critical shear stress of 7.0N/m^2 (Figure 4.7c). The $<63\mu\text{m}>$ fraction was analyzed on the Laser Particle sizer and showed a positively skewed unimodal distribution with a peak in the $16.7\text{-}13.0\mu\text{m}$ band ($+5.75$ to $+6.50\phi$) (Figure 4.7d). The surface box samples BM1, BM2 and BM3 were taken underneath Melampus buoy from a silty surface deposit and the results are presented in Table 7.1d. The physical measurements showed wet bulk densities of c. 2.0gcm^3 and dry bulk densities of c. 2.5gcm^3 . The samples had a moisture content of 0.17-0.21%, and high TOM concentrations of c. 10%. The calcium carbonate content showed values of 14%, and the calculated critical shear stress gave values of c. 3.30N/m^2 .

(ii) The Eastern Entrance (Dive sites: 20,80 Sample BW4)

The area (Figure 4.1) was not surveyed by side-scan sonar due to the bad weather on the day of the survey (Section 3.6). Observations by divers identified the sediments on the substrate to be bimodal and composed of gravels covered by transgressionary sand ribbons and sheets. The gravel was predominantly composed of shales and whole worn shells. The shale

clasts were derived from the Staddon Grit Formation and were sub-angular to rounded ranging in size from very large boulders to granules. The shells were dominantly large (average length *c.* 10cm), disaggregated valves of *Ostrea sp.*, *Arctica islandica* and *Callista chione*. A type example of the substrate (Sample BW4) was taken from the western end of the Eastern Channel, the sample showed bimodality with a pronounced peak at -2.50ϕ which was composed of large rounded clasts of shales. The second peak occurred at $+1.00\phi$, and formed more of a positively skewed ($SK_1 = 1.70$) spread between -2.00 and $+4.00\phi$. The shelly content varied between a minimum of 33% in the very fine sand fraction, and a maximum of 80% which was located in the very coarse sand fraction (Figure 4.7e). The calculated critical shear stress for the clastic content was $>20.0N/m^2$ and $4.0N/m^2$ for the carbonate content. The transgressionary sands occurred as ribbons and sheets and were clean washed, fine-medium grained and had a high shelly content (*c.* 60%). The estimated critical shear stress for these sands was $1.4N/m^2$.

Fluvial Gravels

(i) Eastern Plymouth Sound (Dives:5,6,23,35,71,73,74 Samples PS10 & PS6)

The relict fluvial gravels present in Plymouth Sound were observed on a number of dives, due to the abundant fauna present, the site was much frequented by biologists, and therefore used as a collecting site. The gravels were characteristically cobble-sized, oblate and imbricated to the south. They have positively skewed distributions and were generally relatively well sorted, indicating a lag deposit (McLaren & Bowles 1985) deposited by the PalaeoTamar river system (Section 2.4.1). The relict fluvial gravels have been recognized in a band extending from Smeaton's Pass to the Eastern Breakwater. Diver sample PS6 was from the interstices of cobbles. The sample showed a large percentage of the sediment to be $>-2.50\phi$, which was mostly composed of oblate granules of shales. The -2.00 to $+4.00\phi$ fractions showed a uniform distribution of sediment, with M_d and M_z values of -0.75 and $+0.58\phi$, in a poorly sorted ($S_o = 1.10$) positively skewed ($SK_1 = 1.00$) profile. The shelly content of the sediment was high and varied between a maximum of 92% at -1.00ϕ to 42% at $+4.00\phi$ (Figure 4.7f). The estimated critical shear stress for the clastic content was $7.0N/m^2$, and $15.0N/m^2$ for the carbonate content. Sediment sample PS10 was taken from the sea bed beneath Duke Rock Buoy from between the interstices of a small cobble deposit. The sample again, showed a high proportion of the sediment to be $>-2.50\phi$. The

<-2.50 ϕ sediments showed a unimodal distribution with a broad peak at 0.00 and +1.00 ϕ . The distribution profile showed M_d and M_z values of 0.00 and +0.08 ϕ in a poorly sorted ($S_o = 1.60$) and positively skewed profile ($SK_1 = 0.52$). The >-2.50 ϕ fraction was composed of oblate quartz fragments and shelly debris dominated by *Arctica islandica* and *Pecten maximus*. The shelly content of the <-2.50 ϕ fraction showed a unimodal distribution with high percentages (80%) occurring at +1.00 ϕ (Figure 4.7g). The critical shear stresses for the >-2.50 ϕ fractions was 15.0N/m².

Relict Beach Gravels (Dives 92, 93)

These gravels occur in the shallow areas adjacent to the rocky shores. The gravels are characteristically clean-washed, well rounded and trimodal with peaks at cobble, granule and medium sand sizes. They show no imbrication and may be covered by epigenetic transgressional sands.

The relict gravels all supported a high diversity in- and epifauna communities. Both the clasts and the shells had a dense covering of epibionts including algae, serpulids and bryozoans. The fauna included (i) polychaeta (*Chaetozone setosa*, *Caulleriella sp.*, *Lumbrinereis sp.*, *Magelonia filiformis*, *Mellinna palmata*, *Notomastus latericeus* and *Tharyx sp.*), (ii) Crustaceans (*Ampelisca brevicornis* and crabs), (iii) bivalve (*Abra alba*, *Lucinoma borealis*, *Mya truncata (juv)*). *Spisula elliptica*, *Venus striata* and *Pecten maximus*) and, (iv) sea weeds and grazing gastropods. No live *Ostrea sp.*, *Arctica islandica* nor *Callista chione* were found.

4.5.4 Rocky outcrops

(i) Hamoaze Channel (Dive 21; Sample AB1)

The Hamoaze Channel is incised to bedrock and has an average depth of -30m (Section 3.6.5). Sample AB1 (Ash Buoy) was taken four hours before High Water (Springs) in a 2 knot current. It is undesirable to dive in the Hamoaze Channel on an ebbing tide as the sluice gates of the sewers are open. Over the last 3 years, several dives were planned in the Hamoaze Channel, but each time, permission was denied by the Queen's Harbour Master. The substrate under Ash Buoy was clean swept of sediment and the Plymouth Limestone showed sub-aerial weathering with careous hollows and elongate solution cracks. The rocks were colonized by a dense covering of beadlet anemones and an almost monospecific population

of brittle stars (*Amphiura filiformis*), which are both opportunistic species. The lack of any other animals is attributed to the high currents, exacerbated by the poor water quality. Sample AB1 was taken from a solution hollow, and dry sieved. The sample showed a bimodal distribution with peaks at -2.50 and -1.00ϕ . The distribution profile showed M_d and M_z diameters of -1.50 and -0.25ϕ , in a moderately well sorted ($S_o = 0.52$), negatively skewed profile. The $>-2.50\phi$ fraction was composed of large sub angular clasts of the Plymouth Limestone. The estimated critical shear stress for AB1 was $15.0N/m^2$. The shelly content of the granule fraction (Figure 4.8a) was high and consisted mostly of fragments of *Mytilus edulis*, which inhabit the chains of the mooring and navigation buoys in the Hamoaze Channel. An X-ray diffraction profile of the silt fraction of AB1 showed high concentrations mixed-layer chlorite, pure kaolinite and illite, with accessory calcite, goethite, rutile, diopside and apatite.

(ii) Panther and Tinker Shoal to Andrum Point (Dives: 42,78,79,95 & 96: Sample S1)

The limits of the Knap and Panther rocks and Tinker shoals (Section 3.6.5) have been identified during the side-scan sonar surveys. The rocks are generally clean-swept of sediment and have dense kelp communities in the shallower waters ($>-8m$). The rocks outcrop as a series of ridges with occasional sand-filled gullies. The gullies are periodically filled with a clean-washed sand which has a moderate shelly content (c. 50%). The rocks are also scattered with pottery, dumped during the late 19th and early 20th century. The grab sample S1 was taken adjacent to Panther Knoll Buoy. (Prior to obtaining S1, the grab bounced twice in the same area). The sample was predominantly composed of angular shale fragments which were covered in serpulids which formed a peak at $>-2.50\phi$ in Figure 4.8b. The sediment profile gave M_d and M_z values of -1.75 and $+0.41$, in a distribution that was poorly sorted ($S_o = 1.20$) and very negatively skewed ($SK_1 = -0.60$). The shelly content of the sample showed an increase with diminishing size - from 14% at -1.00ϕ to 64% at $+2.00\phi$. The critical shear stresses required to initiate movement were $15.0N/m^2$ for the clastic component and $1.4N/m^2$ for the carbonate content. The sample is thought to be a veneer over rocks.

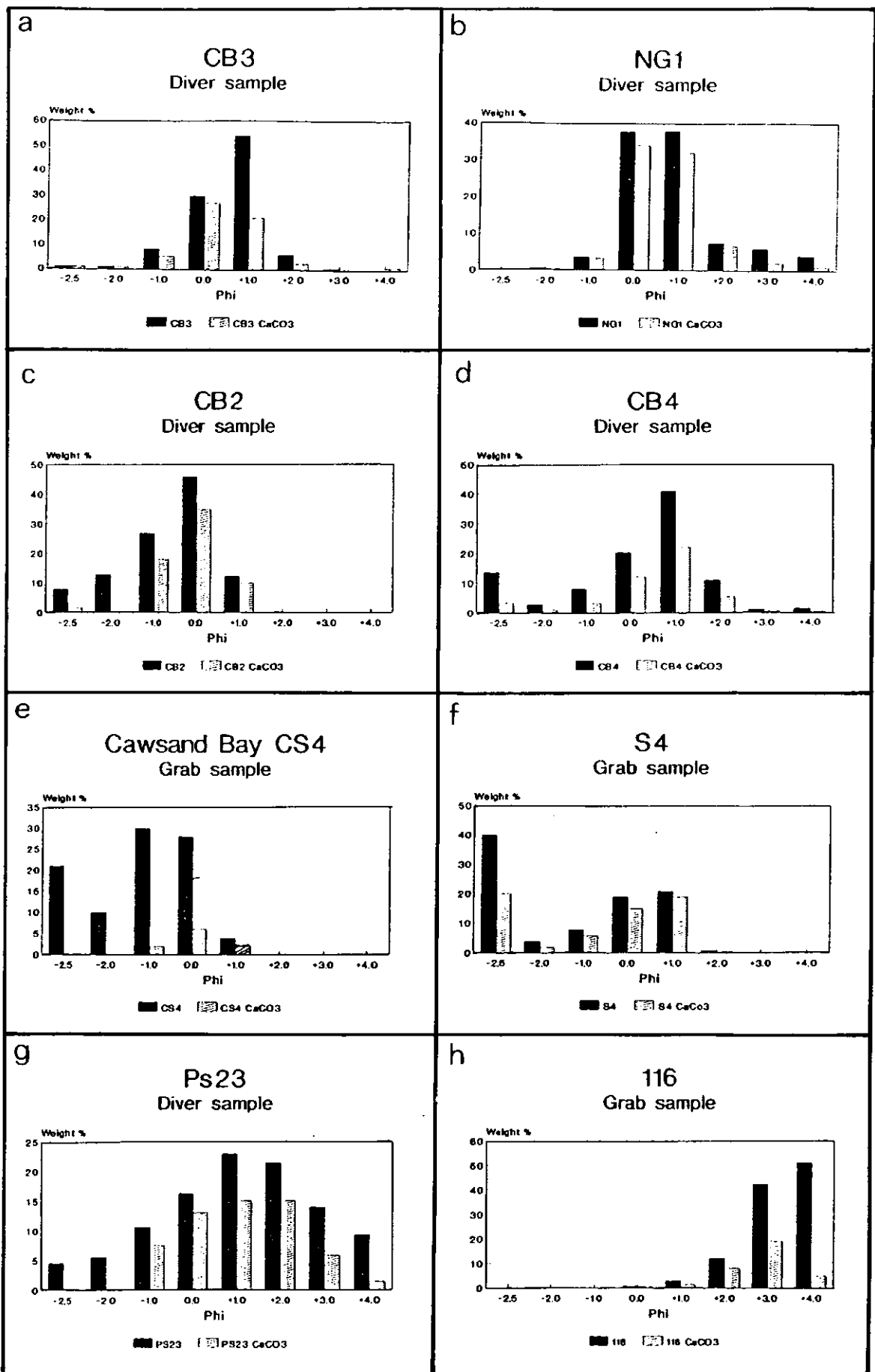


Figure 4.6 The Sandy sediments frequency histograms of (a) CB3, (b) NG1, (c) CB2, (d) CB4, (e) CS4, (f) S4, (g) PS23, and (h) 116.

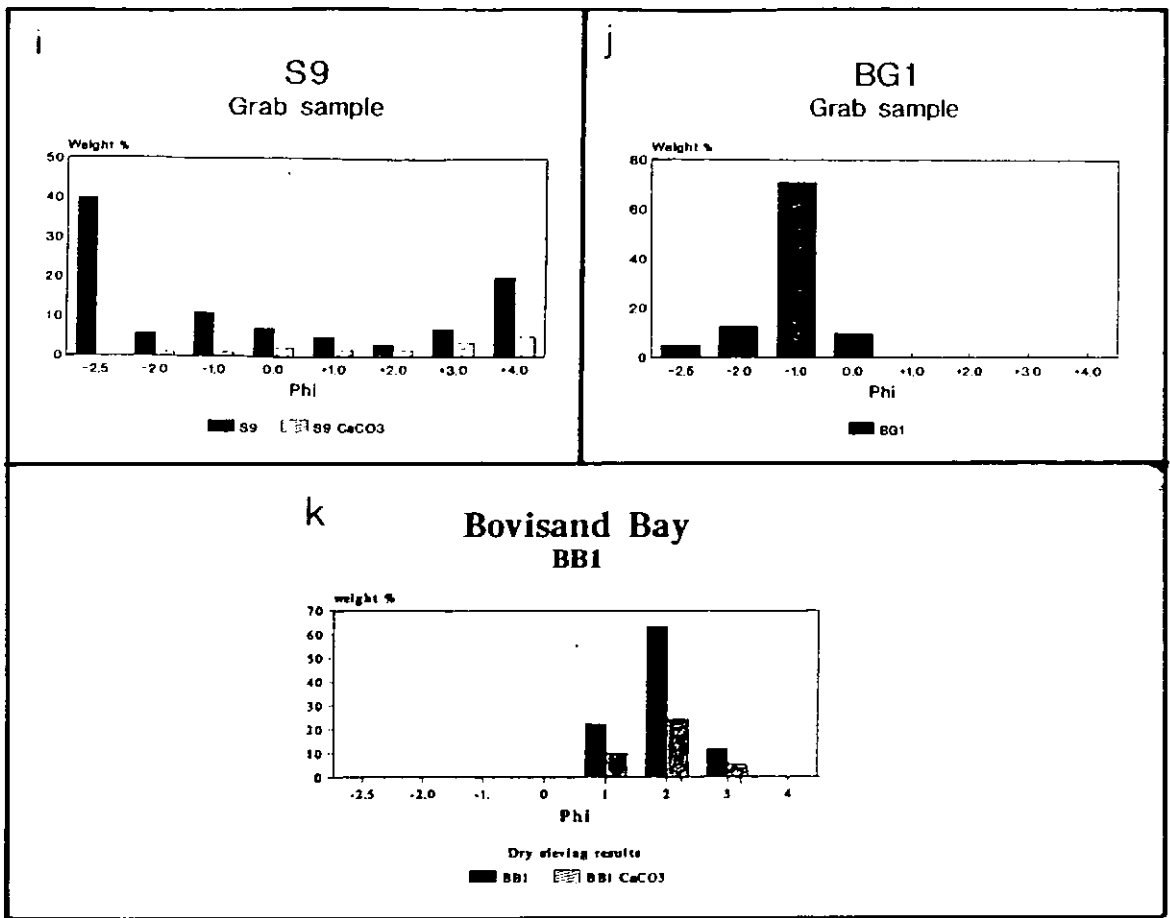


Figure 4.6 cont..The Sandy sediments frequency histograms of (i) S9, (j) BG1, and (k) BB1.

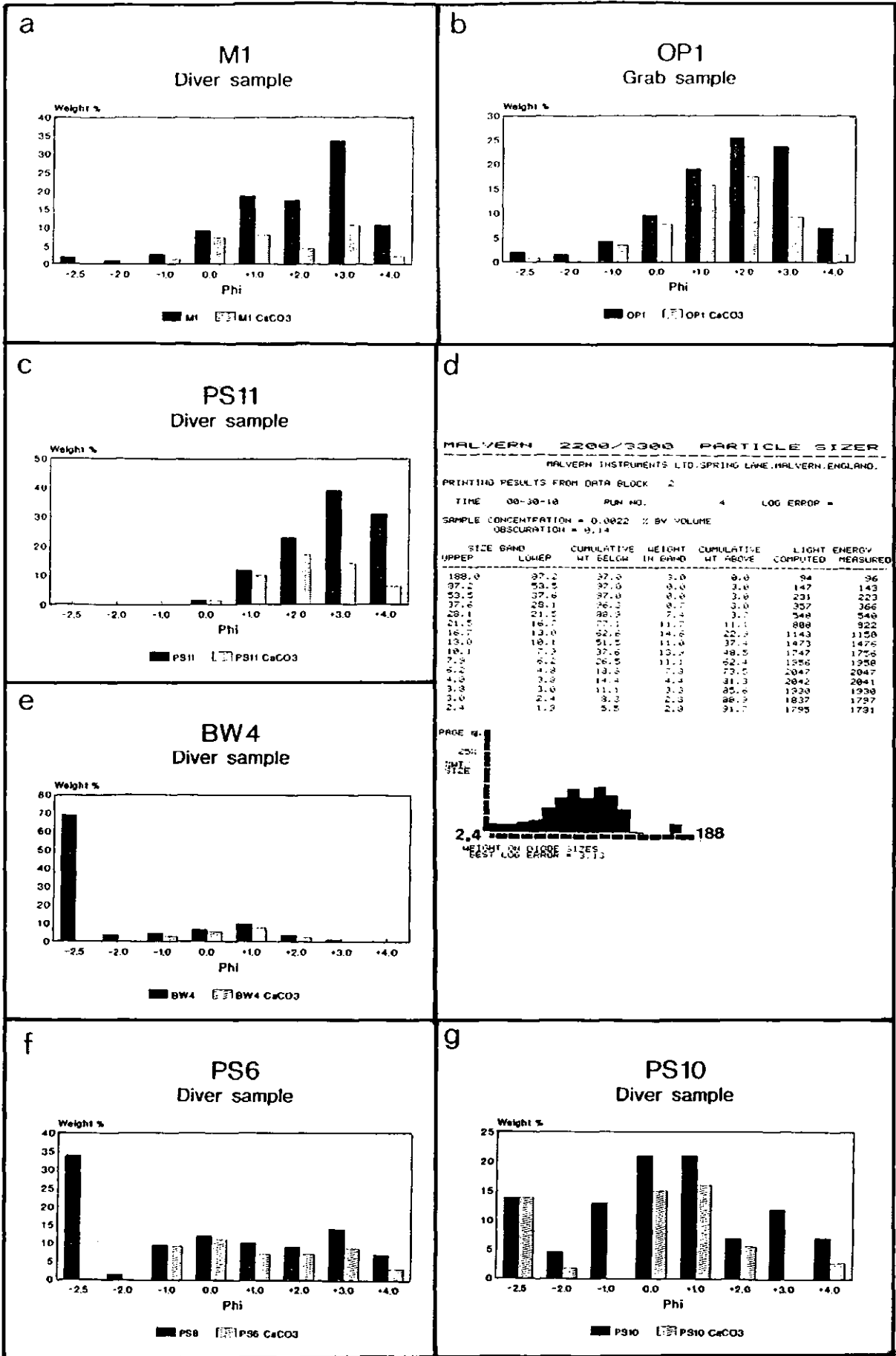


Figure 4.7 The Relict gravels frequency histograms of (a) M1, (b) OP1, (c) PS11, (d) Malvern Particle sizer profile of the fine fractions of Ps11, (e) BW4, (f) PS6, and (g) PS10.

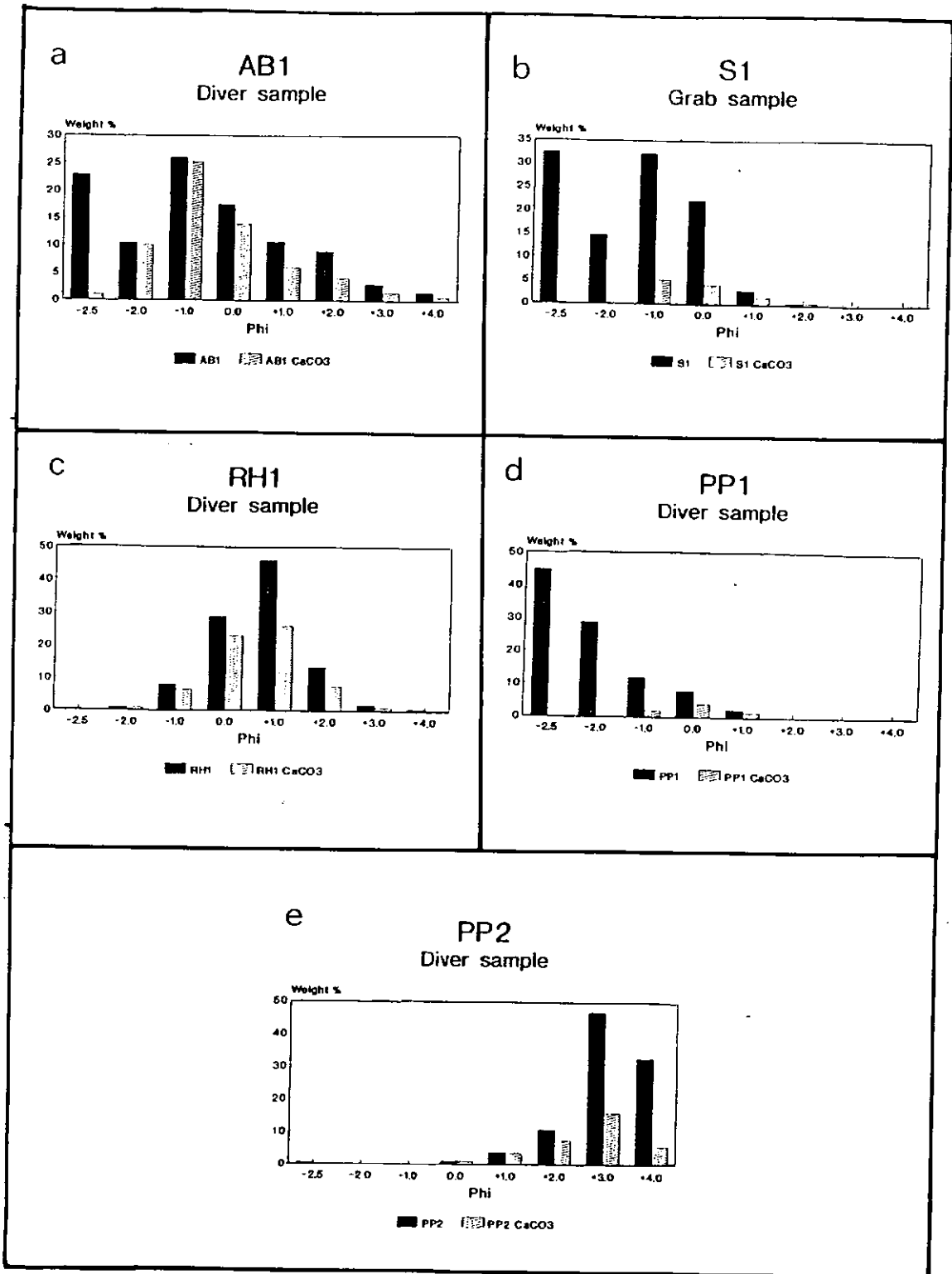


Figure 4.8 The Rocky sediments frequency histograms (a) AB1, (b) S1, (c) RH1, (d) PP1, and (e) PP2.

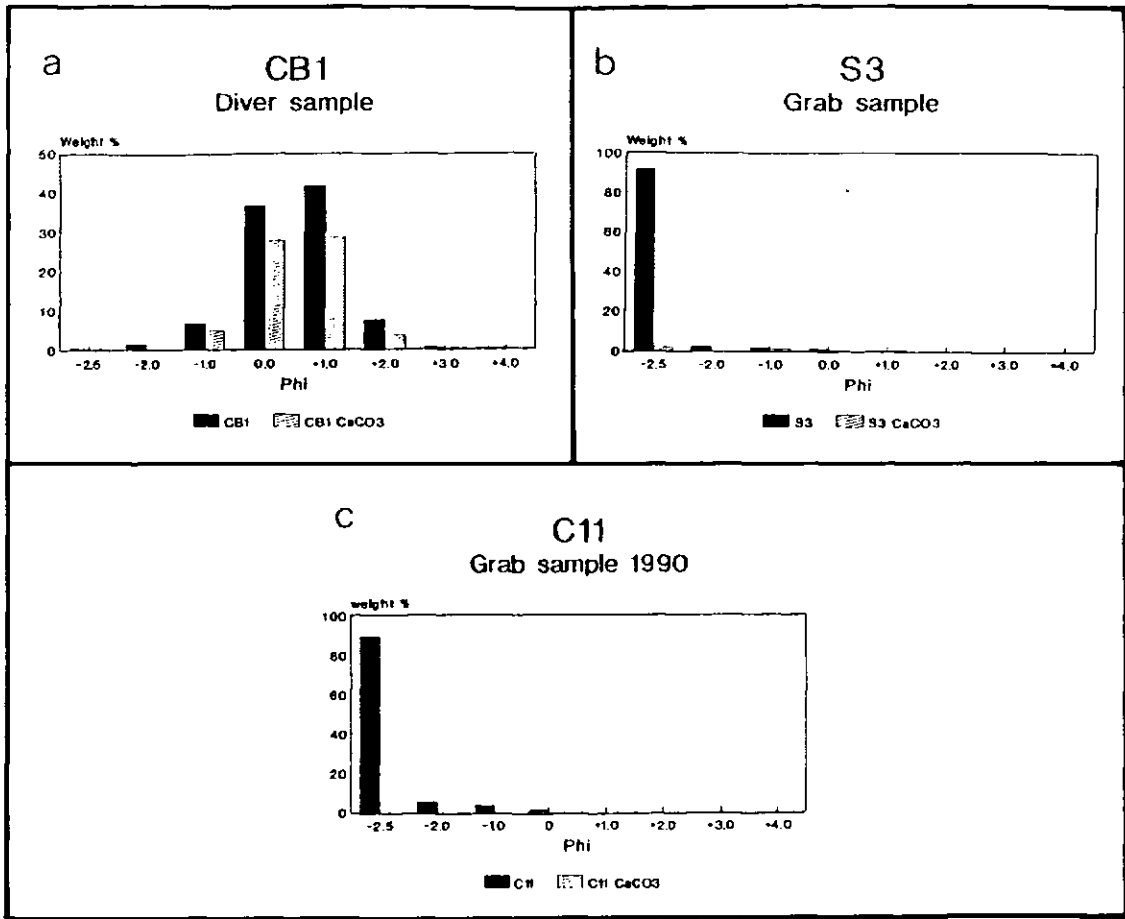


Figure 4.9 Episodic deposition frequency histograms (a) CB1, (b) S3, and (c) C11.

ITEM ON HOLD

Studies of sediments in a
tidal environment / by
Fiona Fitzpatrick.
Fitzpatrick, Fiona.
Thesis 551.46083336 FIT



29/10/2009
PLYMOUTH COUNTER

(iii) The Bridges (Dives: 88 & 89)

The area of The Bridges is defined in Section 3.6.5. The rocks are clean swept of sediment and have a covering of bladderwrack in the intertidal zone. The sub tidal zone is characterized by a diverse well established epifauna including hydroids, sponges, anemones and bryozoans which encrust the rocks in a distinctive grey-green felt-like coating of microorganisms.

(iv) Penlee Point (Dive sites 27, 45, 46, 47 & 72 Samples: PP1, PP2 & RH4). This area was used as a training ground for novice divers, and has been dived extensively during the period of the survey. The rocky outcrops (Section 3.6.5) are clean washed and have a dense covering of kelp and encrusting microorganisms. The rocks are dissected by gullies, 50m long and c. 10m wide. The gullies trend east-west following the main structural grain of the rocks (Section 2.2). The samples were taken from the sandy floor of the gullies. Dive sample RH4 was 500m south of Penlee Point, the sands showed decaying sinuous ripples, with an amplitude of 3cm and a wavelength of 25cm. The sediment showed a unimodal distribution with M_d and M_z sizes of +1.50 and +1.30 ϕ , respectively. The profile was moderately well sorted ($S_o = 0.91$) and positively skewed ($SK_1 = 0.26$). The shelly content in the sediment was high c.90% (Figure 4.8c). The estimated critical shear stress for the clastic fraction was 1.4N/m² and 7.0N/m² for the carbonate fraction. Sample PP1 was from a site to the west of RH4, at a depth of 10m, from clean washed sands. The sands were unimodal and had M_d and M_z values of -2.50 and -1.30 ϕ . The distribution was well sorted ($S_o = 0.3$) and very negatively skewed ($SK_1 = -1.00$). The >2.50 ϕ fraction was composed of oblate clasts derived from the Staddon Grit Formation. The sample contained no shelly material in the >-2.00 fraction. The -2.00 to +2.00 ϕ fraction, however, showed an increase in carbonate material from 19 to 72%, corresponding to a critical shear stress of 1.4N/m² (Figure 4.8d). Dive sample PP2 was taken from a site to the east of Penlee Point from a depth of 18m. The sample showed a unimodal distribution with M_d and M_z of +2.75 and +2.66 ϕ , in a moderately sorted ($S_o = 0.72$) and positively skewed ($SK_1 = 0.23$) profile. The shelly content varied from a maximum of 90% in the >+1.00 ϕ fraction to a minimum of 17% in the +4.00 ϕ fraction (Figure 4.8e). The coarse fractions contained shells of *Ostrea edulis* and oblate rounded shale clasts. The estimated critical shear stress required to initiate

grain movement from an unconsolidated bed were 0.6 and 7.0N/m², for the clastic and carbonate content respectively.

4.5.5 Episodic deposition

Some sites in Plymouth Sound have been dived many times during this survey. Areas of episodic deposition of sands have been observed.

(i) Cawsand Bay (Dive sites: 11,84,85 & 86; Sample S3,CB1 & C11).

The substrate of the area (Figure 4.1) of the northern part of the Bay (Section 3.6.3) is characterized by rocks which are periodically covered by clean-washed medium sands (Section 3.6.5). Sample CB1 was from the Inner Cawsand Bay sand sheet (Section 3.6.2). At the time of sampling, there was a heavy southeasterly swell which penetrated to the sea bed (8m). The visibility on the sea bed was poor (maximum 3m), but an area of a 20m radius was covered and the sea bed appeared to have a uniform covering of sand. Curvilinear ripples were present, formed by the substantial swell, with an amplitude of 12cm and a wavelength of 50cm. The crests were orientated 060/240° perpendicular to the incident swell and showed some bifurcation. The troughs of the ripples had large (average c. 9cm) worn disarticulated valves of *Arctica islandica* and rounded clasts of coal. Coal is particularly common in Plymouth Sound and was derived from the power station at Millbay and from the steam ships. The sample was dry sieved and showed a unimodal distribution with a modal peak at +1.00φ and M₂ and M₄ diameters of 0.00φ. The profile was moderately sorted (S₀ = 0.79) and very positively skewed (SK₁ = 0.50). The shelly content was high, between 50 and 100% with the highest percentage occurring in the +4.00φ fraction (Figure 4.9a). The critical shear stresses for the clastic and carbonate fractions are 4.0 and 0.02N/m² respectively. Observational dives 84 and 85 recorded fine clean-washed sand transgressing rounded gravels. The gravel clasts were poorly sorted and sizes ranged between small boulders and granules. Grab sample S3 showed a distinct bimodality, with a predominance of medium-fine pebbles composed almost entirely of shale clasts and a secondary population of very coarse to medium sands. The gravels had a critical shear stress of >20.0N/m². The clasts were sub-rounded with a dense population of serpulids. The sands had a high shelly content (>80%) which appeared to infill the interstices with a critical shear stress of 4.0N/m² (Figure 4.9b). Live fauna included: echinoderms (*Amphiura filiformis* *Echinocyamus pusillus*); polychaeta (*Magelonia*

alleni, *Magelonia filiformis*, *Nephytes hombergi*, *Scablibregma inflatum*, *Scoloplos armiger*); crustacea (*Ampelisca brevicornis*) and crabs;; bivalves: *Abra alba*, *Corbula gibba*, *Cultellus pellocidus*, *Nucula turgida*, *Spisula elliptica*, *Venus striata*. Grab sample C11, was a good example of the gravel deposit, where over 90% of the sample was $>2.50\phi$ and composed of oblate shale clasts, with no shelly material at all (Figure 4.9c).

- CHAPTER FIVE -

- REMOTE SENSING SURVEYS -

5.1 Introduction

Remote Sensing is defined as the acquisition of information about an object from measurements taken at a distance away from it. In a marine environment remote sensing is primarily concerned with spatial measurement of electromagnetic radiation. When electromagnetic radiation interacts with matter it is modified and can be reflected, absorbed or transmitted, resulting in different patterns on the sea surface. In recent years the use of remotely sensed data from space and airborne platforms has provided an additional source of information for coastal investigations, e.g: Landsat (Barua 1990, Collins & Pattiaratchi 1984), Airborne Thematic Mapper (ATM) (Anderson & Callinson 1987, Anderson 1989, Purdie & Garcia 1988, Rimmer *et al.* 1986), Coastal Zone Colour Scanner (CZCS) (Simpson & Brown 1987, Holligan *et al.* 1989), National Oceanographic and Atmospheric Administration (NOAA) (Johnsson 1986) and Advanced Very High Resolution Radiometer (AVHRR) (Holligan *et al.* 1989) to name but a few examples. A comprehensive review of remote sensing in shallow marine environments is given by Cracknell (1989).

The Plymouth Sound area has been overflown by a N.E.R.C. aircraft with passive scanners on board during three previous surveys. The Hamoaze Channel was overflown on July 4th 1983 (oceanographic time of overpass 1 hour before L.W. Neaps) with a Daedalus AADS 1230 Thermal Infrared Line Scanner in a successful attempt to identify cold freshwater plumes issuing from the Plymouth Limestone (Roxburgh 1983, 1985). On the 12th June 1984, Plymouth Sound was included in part of a Trans-Manche experiment, when the Daedalus AADS 1268 Airborne Thematic Mapper line was accidentally left on at the end of a Roscoff to Plymouth flight (oceanographic time of overpass was 3 hours before H.W. Springs, Groom *in prep.* 1991). The area around Rame Head was also imaged on a second Trans-Manche ATM flight on 19th June 1984 (oceanographic time of overpass

1 hour after H.W.)(Anderson & Callinson 1987).

In order to evaluate the possible use of passive remote sensing in the present study, the previous ATM data were reprocessed at the N.E.R.C. Image processing facility at Polytechnic South West. The images were geometrically corrected and enhanced, and showed a series of well-defined tidal fronts and gyre systems in the inlet; in both the visible and infrared wavebands. As no ground truth data sets existed to derive a correlation or calibration for these images, the overflights described below, were planned to coincide with the maximum physical differentiation of the water features.

On the basis of the structures identified during image reprocessing, a collaborative proposal was put to N.E.R.C. for the Sound area to be overflown by the Daedalus AADS 1268. The proposal was submitted under the convenorship of Dr. Ruth Weaver (Geographical Sciences) and included areas suggested by individual scientists from the Departments of Environmental, Geological and Geographical Sciences (all Polytechnic South West) and Plymouth Marine Laboratories. The areas of interest were geographically separate and the marine overflights included four main areas: Plymouth Sound (Chief Scientist: Fiona Fitzpatrick), Whitsand Bay and the Exe Estuary (Chief Scientist: Ruth Weaver) and the Tamar (Chief Scientist: Reg Uncles and Keith Dyer). The proposal was granted and Plymouth Sound was included in the 1989 South West England Airborne campaign. The convenorship of the planning committee was then passed over to the author. During the planning meetings it was decided to standardize all methods and combine equipment and facilities. The actual planning of each flightline and execution of ground surveys, in the different areas was entirely the responsibility of the Chief Scientist. In Plymouth Sound, extensive concurrent measurements and water samples were acquired from several vessels (Section 5.4.1). The water samples were processed at the Polytechnic and Plymouth Marine Laboratories.

The 1989 survey was very successful. It was, however, essentially a "look-see" operation and was limited in that it was carried out on an ebb tide and no *in situ* optical properties were measured. Initial analysis of the thermal and visible bands of the Airborne Thematic Mapper (ATM) images (Fitzpatrick 1990a, 1990b) showed an unexpected and significant continuity between the sea bed sediment distributions and the tidal

fronts in Plymouth Sound (Section 8.2.1). To ascertain the total effect of the tidal current on the sea bed, it was decided to apply for a second set of ATM (See Section 5.4) overflights. During discussions with colleagues from the Institute of Marine Sciences, it was realized that a possible overflight held areas of mutual interest. The final proposal to N.E.R.C. for a repeat survey was submitted in December 1989 by Fiona Fitzpatrick (Chief Scientist), Gerald Moore (Atmospheric corrections) and Derek Pilgrim (Marine Optics). On the basis of the success of the 1989 campaign and rapid publication of the results, N.E.R.C. awarded the 1990 proposal an "A" grading, and agreed that the aircraft should return to fly over the area in two separate overflights at different states of the tide. The overflights and the ground truth collection were again the responsibility of the individual scientist (Section 5.4). In 1990, a Compact Airborne Spectrographic Imager (CASI) instrument (Section 5.3.2), which allows greater spectral resolution than the ATM, was made available by N.E.R.C. and flown over the Sound on 15th June 1990 with all the *in situ* measurements taken under the direction of the Chief Scientist. Unfortunately, the CASI images were not made available for processing until 20th June 1991, and therefore only preliminary processing has been carried out. The airborne image data tapes were processed on the N.E.R.C. I²S facility based at the Polytechnic (Section 5.6).

5.2 Passive remote sensing of the marine environment

The passive spectral scanners used in remote sensing of the marine environment measure the interaction between intrinsic water properties and electromagnetic radiation. The types of response - reflection, transmission and absorption can be examined in relation to the various water properties. Emissivity and fluorescence of marine waters is also described.

Reflection

Two forms of reflection of energy can be identified, (i) *Specular reflection* is where the angle of reflection is equal to the angle of incidence. This is optimized for a smooth sea surface in the the visible and near visible wavelengths. The reflectance from turbid waters is generally restricted to the top few mm of the water column. (ii) *Diffuse reflection* occurs where reflected energy is scattered and broken randomly from a rough surface. Specular reflection can be used to measure the degree and pattern of surface roughness, from which the wind speed or

speed of a vessel can be evaluated. In marine remote sensing, it is the pattern and the wavelengths of the diffuse reflection which are the most informative. In the visible part of the electromagnetic spectrum (400 - 700nm), the amount of energy reflected, in different wavelengths (R_λ), is intrinsic to the material in suspension. The size and peakedness of the reflectance curve depends on the individual spectral components of the total suspended sediment concentration. Suspended sediment is generally a good reflector in the 600 to 700nm range. The presence of suspended sediment plays an important role in determining the extent of the mixing of water bodies, for example, river plumes (Barua 1990, Congxian *et al.* 1991), estuary mixing zones (Cracknell *et al.* 1982, Collins & Pattiaratchi 1984), tidal fronts (Holligan *et al.* 1989), and flow regimes (Amos & Alfondi 1979, Bohme *et al.* 1986, Jonsson 1986, Simpson & Brown 1987). Early work on the correlation of suspended material and spectral signature in macrotidal environments gave poor results (Buller *et al.* 1975, Evans & Collins 1975), due to errors in the correlation induced by size and particle spatial sorting differences. Comprehensive reviews of suspended sediment types and models of the total volume reflectance of different types (Sathyendranath & Morel 1983, Novo *et al.* 1989, Albanakas 1990) have since been developed. The relationship between the strength of the spectral signature (R_λ) and the suspended sediment concentration (SSC) is still subject to debate. However, in turbid coastal waters, the relationship between SSC and R_λ is now generally considered to be log (SSC) linear with (R_λ) in the visible wavelengths (450-700nm, i.e. ATM 1-5) and linear between 700 and 1050nm wavelengths (Novo *et al.* 1989, Chen *et al.* 1990). The SSC- R_λ relationship can be summarized to be complicated by the following:

- (i) The range of SSC types present,
- (ii) The vertical and horizontal particle size distribution,
- (iii) The particle shape,
- (iv) The particle mineralogy,
- (v) The presence of algal and organic components, and
- (vi) The geometry of measurement, i.e. sensor zenith angle.

The SSC reflectance is also dependent on the orientation, colour and temporal stability of the incident light. The sea state also plays an important role in reflectance. If the suspended particulate matter is highly coloured, for example, by kaolinite which is common in Plymouth Sound, the strength of the colour can be correlated linearly with the amount of sediment (Robinson 1985, Boxall *pers.comm.* 1990). With the

development and increase in the spectral resolution of airborne sensors, it is accepted that the distribution of suspended sediment can be accurately used in the interpretation of macrotidal regimes, at least at a parochial level, only if a sound knowledge of the suspended sediment type, shape, size and reflectance has been acquired. This therefore inhibits the practical use of sensor images and makes it imperative to have groundtruth to calibrate the images.

Another important application for reflectance studies is the development of foam-lines on the sea surface. These are formed of residual material, mostly from dead phyto- and zoo-plankton, which accumulate in relatively thin lines, or bands, in areas dominated by water body mixing (Peltzer & Griffin 1988). Tidal fronts are often delineated by such lines, the lateral perseverance mimics the mixing zone and the width depends on both the amount of decaying matter and the age of the front. The foam lines are especially well developed immediately after plankton blooms.

Reflectance from the sea bed, allowing a classification of sea bed material is another important application for passive remote sensing; however, if the volume of suspended material is high, then the sea bed reflectance signature ($E_{u\lambda}$) may be masked by surface effects (Spitzer & Dirks 1986, Topliss *et al.* 1990).

Transmission

The transmission of electromagnetic radiation through water is essentially limited to the visible spectrum, and is greatest in the blue and green wavelengths. The light absorption by 10m of pure water as a function of wavelength, is controlled by the turbidity of water (Figure 5.1). The use of transmission is partially limited in turbid environments such as Plymouth Sound.

Absorption and Emissivity

Some materials do not reflect electromagnetic radiation and the incident spectral wavelengths are selectively absorbed at the surface and during transmission. The incident energy is often re-emitted as heat, the amount of which is governed by the temperature and emissivity spectra of the media. The peak emissivity of water is in the thermal infrared region of the electromagnetic spectrum, allowing sea surface temperatures to be measured with a high degree of accuracy (+/- 0.5°C). The radiation

from the sea surface is composed of two components: emitted radiation (emissivity) and reflected radiation (reflected atmospheric and reflected solar). The radiation in the 800 to 1300nm window (water temperature signal) is effectively self-emitted and is a function of view angle and wavelength. On a clear day the radiance reaching a scanner in this band from sky radiation is only 1% (Anderson & Callinson 1987). The presence of clouds or haze (Relative Humidity) creates strong absorption. Reflected solar radiation by the sea in the infrared bands is therefore negligible and can be ignored. Thus, infrared images can be analyzed without applying any atmospheric correction as the energy measured by the sensor is almost entirely emitted from the sea surface (Anderson & Callinson 1987).

Fluorescence

Another type of emission is fluorescence, which occurs when absorbed energy is re-emitted at a longer wavelength without being converted to thermal energy. This property is especially useful in the detection and identification of the green pigment - chlorophyll- α , algal types and pollutants. Water changes from visible blue to visible green as the concentration of phytoplankton and therefore chlorophyll increases. Phytoplankton have different absorbing and scattering elements according to species and age of the population. The spectra produced are shown in Figure 5.2. (Morel 1980). In areas of mixed water bodies, such as Plymouth Sound, the presence of chlorophyll and its degradation products can be used to identify the origin of the water, whether marine or estuarine, and thereby allow delineation of the boundaries of the intrinsic water masses.

Much work has been done on identifying the presence of chlorophyll- α and the degradation products (phaeopigment α) in fresh (George & Hewitt 1989, George 1990) and salt water (Fisher & Schlussel 1990, Holligan *et al.* 1989, Lopez-Garcia & Casselles 1990). It has been found that the best spectral band for chlorophyll- α quantification is 450-690nm. Unfortunately, this overlies the carotene fluorescence peak at 520nm, and also coincides with a signature from dissolved organic matter, living plankton and non-living scattering suspended sediment. Nevertheless, Højerslev (1982) concluded that it is possible to establish a radiance algorithm between chlorophyll and spectra, although the relationship will be site-specific.

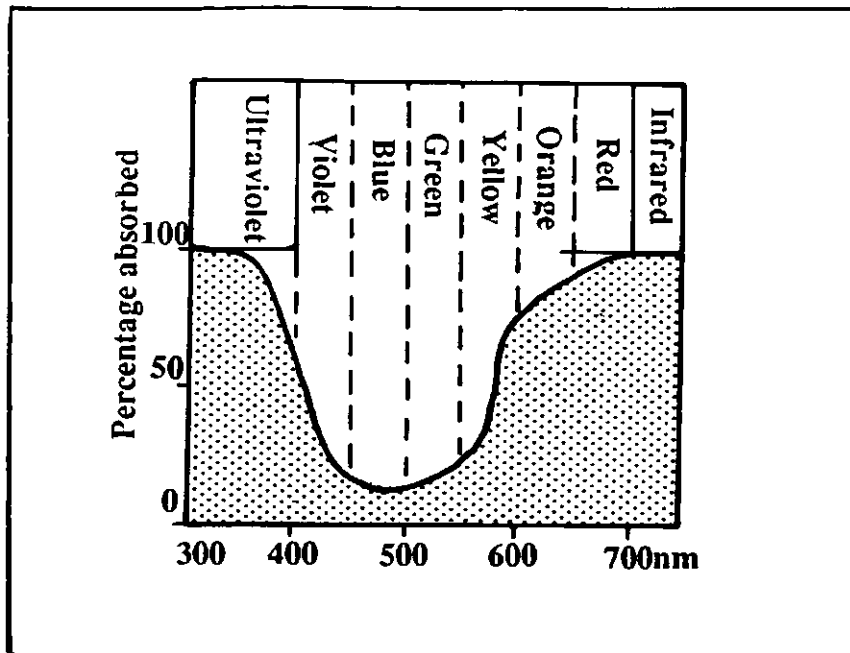


Figure 5.1 Light absorption by 10m of pure water as a function of wavelength (Robinson 1985)

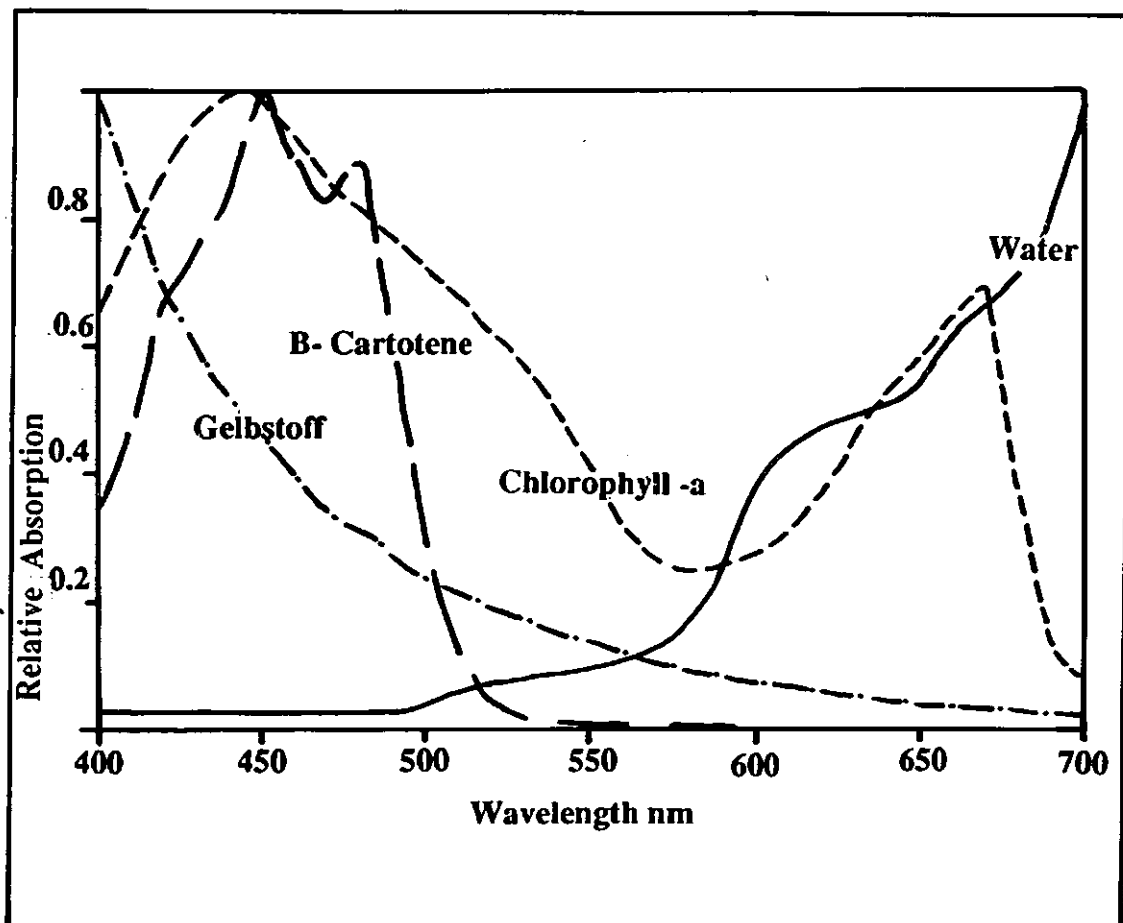


Figure 5.2 Relative absorption spectra of pure water, chlorophyll- α , β -carotene and Gelbstoff (Pilgrim 1988).

The remote sensing of chlorophyll- α has been successful in recent years with the development of selectable band spectrometers (e.g. Compact Airborne Spectrographic Imager (CASI)(Boxall & Reilly 1989) and Fluorescence Line Imager (FLI), (Boxall & Matthews 1990). The wavebands in these instruments are interactively set to pick out the chlorophyll fluorescence line maximum at 685nm (Gower and Borstad 1990), thereby allowing chlorophyll to be separated from yellow substance and other constituents (Fisher & Schlussel 1990). The wavebands selected during the Plymouth Sound CASI campaign (Section 5.4.3), were designed to differentiate the chlorophyll peak from suspended sediment and organic products.

5.3 Instrumentation

During the airborne campaigns two passive scanners were deployed - the N.E.R.C. Airborne Thematic Mapper (ATM) and a Compact Airborne Spectrographic Instrument (CASI) on hire from Europe. The scanners have different spectral bands and specifications. The ATM was employed during the 1989 and 1990 overflights, and the CASI in a separate overflight in 1990. The scanners were deployed aboard the N.E.R.C. Piper Navajo Chieftain aircraft, which is fitted with a Racal RNAV-2 navigation management system with Decca Mk.32. The fuselage has been modified to accommodate two camera mounts and a survey hole. During the Plymouth Sound surveys a Heerbrugg Wild RC-8 Aerial camera was also deployed, in which it is interesting to note the optical width of the photograph approximates the swathe width of the scanner (2km).

5.3.1 The Daedalus AADS 1268 Airborne Thematic Mapper

The ATM was initially developed for testing and simulating the five band Multi Spectral Scanner (MSS) carried by LANDSAT 1 to 3, and the seven-band Thematic Mapper (TM) on LANDSAT 4 and 5. Cooperation between NASA and Daedalus Enterprises Inc. has since lead to the development of the Daedalus AADS 1268 Airborne Thematic Mapper which collects and records electromagnetic radiation from an airborne platform. The ATM system is composed of a scan head, a spectrometer, a digitizer, an operator console, a thermal reference source system and a magnetic tape recording system (Cook *et al.* 1989). It is a linescan system which can record digital image data in 11 channels (spectral bands) and channel 12 at half gain, ranging over the electromagnetic spectrum from visible blue to thermal infrared (Table 5.1). Five channels are in the visible, three

in the near infrared, two in the short wave infrared and one in the thermal infrared. This provides spectral data similar to Landsat MSS, Landsat TM, the French SPOT-HRV and other Earth Observing Satellites.

Spectral Characteristics of the Airborne Thematic Mapper			
Band Edges (nm)			
Daedalus ATM AADS 1268		LANDSAT TM	
Channel 1	420 - 450	Channel 1	450 - 520
Channel 2	450 - 520	Channel 2	530 - 600
Channel 3	520 - 600	Channel 3	630 - 690
Channel 4	605 - 625	Channel 4	760 - 900
Channel 5	630 - 690	Channel 5	1550 - 1750
Channel 6	695 - 750	Channel 7	2080 - 2350
Channel 7	760 - 900	Channel 6	1040 - 1250
Channel 8	910 - 1050		
Channel 9	1550 - 1750		
Channel 10	2080 - 2350		
Channel 11	850 - 1300		

Instantaneous Field of View (IFOV) 2.5m rad
 2.5m at 1,000m Above Ground Level
 5.0m at 2,000m Above Ground Level
 Digitized FOV.....85.92°
 Swathwidth (for a 74° total Field of View)
 1.5km at 1,000 Above Ground level
 3.0km at 2,000 Above Ground level
 Scan rate.....12.5,25,50 scan/sec⁻¹
 Gimble Roll Correction...+/- 15°

Table 5.1

Instrument characteristics and band widths of the Daedalus AADS 1268 and Landsat TM (after Cook *et al.* 1989).

The sea surface signals are received by opto-mechanical scan mirror in the scanner head, which successively exposes the detecting elements at a pre-set speed of scans/sec. The detecting elements, the Charge Coupled Device (CCD), are cooled by liquid nitrogen. As the aircraft progresses, successive strips of the ground surface are covered, producing an image of the surface of interest. The digitization results in a 10,000 bit per inch packing density on High Density Digital Tape. This cannot be read directly and is transferred to Computer Compatible Tape (CCT) at the N.E.R.C. Computing facilities (Cook *et al.* 1989). The radiometric calibration of the Daedalus AADS 1268 ATM is performed by Global Earth Sciences Ltd., before and after each N.E.R.C. campaign, the data set

closest to the date of flight is used in processing.

A variety of corrections are required and must be taken into account when processing the images. These are undertaken by N.E.R.C. and comprise:-

(i) "S" bend correction

The image suffers a geometric distortion/compression at the edges to counteract this, the Daedalus AADS 1268 carries an optional "S" bend correction, which is applied during digitization. The "S" bend correction was applied during the Plymouth Sound campaigns as the data were required to be geographically accurate, the correction is usually left out of data acquired for algorithm developments.

(ii) Roll Correction

The image is built up by a line scanning system as a continuous swath of ground by scanning from -37 to $+37^\circ$ about a vertical axis. The vertical gyro assembly measures the roll of the aircraft, and enables the digitizer to record imagery only when the scanner is imaging between these limits.

(iii) Pitch and Yaw

Variation in aircraft altitude will cause geometric distortions on the recorded image. Pitch and yaw cannot be corrected by the electronics of the system but are eliminated during data processing.

Resolution is dependant on the Instantaneous Field Of View (IFOV) which is defined as the angular width of the sensor, i.e. the physical limit of scanner resolution. With the Daedalus AADS 1268 the system resolution element is 2.5 rad. The AADS 1268 resamples every 2.093 mrad over the total Field of View (FOV) giving 716 pixels. The signal in each detector is recorded as a series of digital numbers (DN) from 0 to 255 (Grey-scale); each number depending on the amount of radiation reaching the individual pixel. Therefore, as for all scanners the ground resolution is at its best at nadir and decreases towards the edge of a scene by a factor of (approximately) 2. In both overflights the scanner was flown at 2000m and the nadir ground resolution gave a pixel size of 4.186m and a physical across track resolution of 5m.

5.3.2 CASI Instrument

The CASI instrument (Compact Airborne Spectrographic Imager) was

developed by ITRES Research Ltd., Canada, as a multispectral "pushbroom" sensor, i.e, that it detects an entire row of images at one instant with a two dimensional Charge Coupled Device. This device allows a longer dwell time per pixel and thus has a higher spatial and spectral sensitivity compared to rotating scanners such as the ATM. The band widths are all programmable and allow spectral resolution of up to 1.8nm from 450 to 950nm. The CASI instrument has been used successfully in both the marine environment (Boxall & Matthews 1990, Pettersson 1990) and over land sites (Rollin 1990). The instrument consists of a sensor head, instrument control unit, monitor and keyboard. The sensor head is installed on an aircraft pointing downwards so lines across the flight path are imaged onto the spectrograph slit as the aircraft moves forward. Light emerging from the slit is collimated, dispersed by the reflection grating and is then focused onto the Charge Coupled Device (CCD). This device is orientated to obtain 578 pixels across the flight path. To achieve manageable data sets, the instrument operates in two separate modes:

- (i) Multispectral Imaging mode which provides maximum spatial resolution (578 pixels) for a limited number of programmable non-overlapping spectral band widths.
- (ii) Multispectrometer mode in which full spectra are collected by the CCD from a limited number and spacing of programmable look directions - in effect the chosen arrays act as individual spectrometers (Babey & Anger 1989). The data are written directly onto 8mm Video Tape in a high density digital format. The tapes are then copied onto VAX compatible tapes for use on an I²S system.

5.3.3 Groundtruth Survey Equipment

Constraints on planning a groundtruth survey are many. The main problem in the planning of all the surveys was the availability of vessels at the time of the overflight. In any investigation in which concurrent measurements are required over a large area, the instruments and techniques employed must be balanced against the actual time it takes to make the measurement, the availability of vessels and the number of stations. It was decided in advance to take as many measurements as possible from different stations. The vessels supplied by the Polytechnic for the overflights varied in number and speed. All the *in situ* measurements were made using standard oceanographic techniques, which were chosen on the basis that they are all relatively rapid and not

too complicated. The vessels were designated different areas and sampling stations on the basis of their speed. The survey personnel consisted of friends, fellow postgraduates and members of staff. The volunteer survey personnel were briefed on measurement procedures prior to the survey, fortunately, most of the crew volunteered for all the surveys (Appendix 1c).

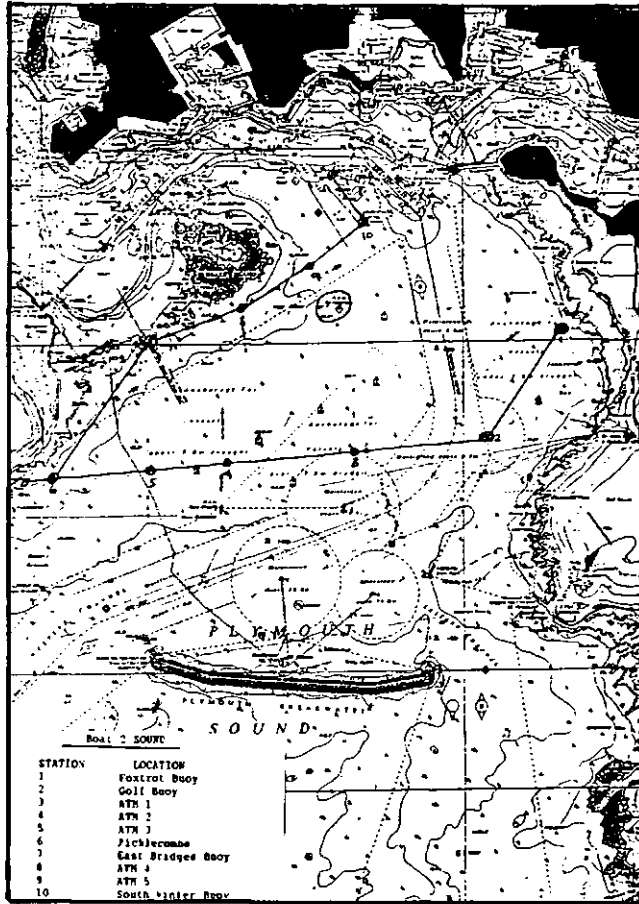
Secchi disc

The Secchi disc is one of the most widely used instruments in oceanographic and limnological work. The first Secchi disc was a dinner plate caught in a net observed by a Captain Bernard (1786-1853). The principle of disappearance depths was then expanded by Commander Cialdi of the Papal Navy in 1865, when he commissioned Professor Secchi to carry out scientific observations using discs of different colours. Secchi established the disappearance depth of the disc as a measure of transparency of the water. Today, discs are characteristically 30-40cm in diameter and matt white, they are deployed from the sunny-side of a vessel and monitored through a glass-bottomed looking bucket. The depth at which the disc is observed to disappear on descent and re-appear on ascent is measured and averaged, this gives the Secchi disc disappearance depth, Z_{sd} . The relationships between Z_{sd} and downwelling light (Poole and Aitkens 1929, Tyler 1968), algal biomass per unit chlorophyll- α (Lorenzen *et al.* 1980, Megard & Berman 1989), and gravimetric particle concentration (Pilgrim 1988) have been established. In a tidal environment, such as Plymouth Sound in which the suspended material component is characterized by several different species of minerals and clays, it was envisaged that Secchi disc measurements could possibly be used to define the geographical limits of the different components.

Temperature/Salinity

Temperature and salinity were measured using M.C.5 Salinity/Temperature Bridges (I.O.S. Approved). These were borrowed from N.E.R.C. R.V. *Barry*, and calibrated prior to all the surveys. A 1kg weight was attached to the cable, above the thermistor head, to ensure vertical sinking of the probe into the water column. During the CASI ground truth campaign T/S dips were made at each station. The probe cable was marked with coloured insulating tape prior to the survey thereby eliminating the need for measuring depth (Table 5.2).

a



b

SOUND							
STATION	LOCATION	TIME	LOTUS	BEAM	T ₀	TRACON	REMARKS
1	FOXROAT	0844 ↓ 0850	PS 32 PS 33	2.75m 3.00	14.00	< 20	
2	GOLF	0852 ↓ 0900	PS 32 PS 33	3.90 3.80	13.60	< 1	
3	ATM 1	0914 ↓ 0918	PS 25 PS 31	4.00 3.69	11.30	33.90	HEIGHT 220°M PS 040° RANGE 272°
4	ATM 2	0921 ↓ 0925	PS 44 PS 37	4.15 3.65	13.40	34.05	HEIGHT 150°M DTM 257° PS 047°
5	ATM 3	0922 ↓ 0931	PS 38 PS 40	4.25 3.90	13.20	34.25	HEIGHT 150° RANGE 189° PS 050°
6	PICHLER-COMBE	0933 ↓ 0937	PS 34 PS 26	5.35 5.60	13.40	33.90	HEIGHT 131°M DTM 065° SHM 092°
7	EAST BRIDGES BUOY	0940 ↓ 0944	PS 27 PS 45	4.20 3.80	13.40	33.25	
8	ATM 4	0946 ↓ 0950	PS 28 PS 46	4.5 4.3	13.40	33.50	HEIGHT 160° SHM 115° PS 068°
9	ATM 5	0951 ↓ 0955	PS 35 PS 41	3.6 3.55	13.40	33.00	HEIGHT 162° SHM 120° PS 068°
10	SOUTH WINTER BUOY	0957 ↓ 10.00	PS 42 PS 29	2.98 3.20	14.00	33.10	

Figure 5.3 Groundtruth collection (a) map and (b) chart.

Water Bottles

Water samples on the surveys were collected in 1 litre sterilized and pre-labelled sample bottles. At each site 2 litres were acquired. During the CASI groundtruth campaign, additional 500ml bottles were used to collect water for spectral analysis. Once filled the bottles were stored in opaque plastic boxes and covered by a black bin-liner to inhibit plankton blooming.

Depth Markings for Temperature Salinity probes	
<u>Depth</u>	<u>Markings</u>
0m	- -
1m	- 1 blue
2m	- 2 blue
5m	- 5 blue
10m	- 2 blue 1 red
20m	- 3 blue 2 red

Table 5.2

The Temperature/Salinity probe markings

Recording Charts

All vessels were supplied with a map (Figure 5.5a) of the sample sequence and locations. A pre-prepared sampling chart (Figure 5.5b) was also provided, the chart was drawn on waterproof paper and attached to a clipboard. Pop-up pencils were tied to the clipboard.

Other Equipment

Biooptical Equipment was also deployed during the 1990 surveys, the instruments include a 4π Quantum Scalar Irradiance meter, SeaTech Beam Transmissometer, Hydrooptics Beam Transmissometer, WS Ocean Systems Irradiance meter, Hand Held Spectral irradiance meter and a D and A Optical Backscatter meter, the results are held by Dr. D. A. Pilgrim.

During all the surveys, the vessels maintained radio contact using portable VHF Marine Radios. A personal communication channel was designated by H.M. Queen's Harbour Master on the day-of-the-flights prior to the vessels leaving port. Contact between the aircraft and *D.V. Aquatay* was made by single channel VHF radio. All vessels were given packets of chocolate biscuits to sustain the groundtruth crew for the duration of the survey. On the 1990 ATM campaign the crew were picked up by *D.V. Aquatay* and taken to the Half-way House at Cawsand for lunch.

5.4 The Surveys

Three surveys were flown; one in 1989 (ATM) and two in 1990 (ATM and CASI). The 1989 ATM overflight was coincident with Low Water and the 1990 CASI flown at High Water. The 1990 ATM survey was flown at both High and Low Water on the same day. All groundtruth measurements were simultaneous with the overflights.

5.4.1 The Plymouth Sound 1989 ATM survey

The Plymouth Sound part of the proposal had three main objectives:

- (i) to determine the form and origin of estuarine sediments in Plymouth Sound,
- (ii) to develop methods for determining the depositional conditions of the sediments from geophysical studies, thereby allowing the prediction of depositional properties from a reduced number of samples and,
- (iii) to examine the detailed relationship between suspended sediments concentration and spectral response.

The proposal was awarded grade C and was planned to fly in July 1989 (N.E.R.C. Site 89/6 Total cost allocated £ 5,418).

Logistics

The logistical constraints on planning of an airborne survey are many. The most important is to avoid other air and sea traffic. Once clearance was obtained to fly over H.M. Restricted Airspace, the planning of the airborne part of the survey proceeded. The choice of day-of-the-flight was planned to coincide with a maximum spring tide in order to optimize the contrast between estuarine waters and tidal water. During Springs the mud flats of the Plym and St. Johns Lake are totally covered by sea water and so a high degree of mud sequestration occurs, thus increasing the total suspended sediment concentration and hence the temperature. The survey was also planned to avoid the plankton blooms expected in June and August (Hiscock & Moore 1986) as such a bloom would obscure and confuse the interpretation of the suspended sediment results, as the plankton increases the organic content of the water and thereby accelerates flocculation. The overflight was also planned as close as possible to slack water as taking measurements from a constantly moving body of water is difficult and the ground results, obtained at different times, cannot be related to the overflight images which are almost instantaneous. The week of July 17th to 21st 1989 was suggested as a possible window.

Sun-glint

The flightlines were planned to fly North-South to avoid sunglint created by the summer angle of incidence of the Sun in the Northern Hemisphere.

Geometric correction control

North-South flightlines also should allow the capture of a continuous coastal section on one side of the image, and sufficient marine landmarks in order to orientate the data for geometric correction. As with all airborne systems, sinuosity created by pitch and yaw is only definable where an area of coast is imaged in a scan line.

The survey

On the 17th of July 1989, the Plymouth Sound area was overflown by the N.E.R.C. Piper Navajo Chieftain deploying the Daedalus AADS 1268 and Wild RC-8 Aerial camera. The area was scanned in three paths (see Figure 5.4) between 11.49 and 11.59 (BST) at a ground speed of 160 knots and a height of 2000m. At 716 pixels per scan line, this is equal to a nominal spatial resolution of 4m. Low water at H.M.S Devonport was expected at 11.45 hours and, due to the excellent weather conditions during the week leading up to the survey, the timing of maximum low water (1.6m O.D.) was accurate. The maximum surface current speed was 0.2 knot at The Bridges. The surface of the Sound was still. The weather conditions on the 17th July at 12.00 hours were good, with slight South Westerly winds. (0.1 Knot). The air temperature was 19.5°C and the Relative Humidity 77%. The precipitation a week leading up to the overflight was negligible and outflow from the Tamar and Plym was low.

Sea-truth measurements were collected at 35 stations from four vessels. These comprised two inflatables, the Marine Biological Association Research vessel *R.V. Squilla* and the Polytechnic South West Diving support vessel *D.V. Aquatay*. Unfortunately radio contact was lost between the ground survey and the aircraft, which was delayed for 1 hour. The sea based survey started on schedule at 10.30 hours as previously planned. The *in situ* samples were taken from 10.30 to 12.05 BST, i.e. 5.00 hours to 6.35 hours after High Water (Table 5.3). The samples positions were designated in advance, making maximum use of the existing Admiralty buoyage system. Correction for the buoys' deviation on an ebb tide was made from the buoy movement ellipses from H.M. Port Surveyor's offices. In the navigation channels fixes were taken by hand-held

compass bearings and checked using the Racal-Decca system on *D.V. Aquatay* (Green and Purple mainchain lanes). It had been planned to drop cement-based buoys into Plymouth Sound to act as marked sample stations but, although permission had been granted by the Port Surveyor, the Polytechnic refused access to vessels for the drop of the buoys during weekend days.

1989 ATM Survey			
Overflight Run	Time BST	Direction magnetic	Tidal state minutes after L.W.
1	11.49	N	7
2	11.54	S	12
3	11.59	N	17
Vessel		Sampling time BST	
Inflatable 1		10.30 - 12.05	
Inflatable 2		10.28 - 11.47	
<i>R.V. Squilla</i>		11.30 - 12.30	
<i>D.V. Aquatay</i>		10.27 - 12.00	

Table 5.3
1989 Survey

At each of the 35 sites 2 litres of sea water were acquired, temperature/salinity were measured 10cm below the air/water interface and Secchi disc disappearance depths (Z_{sd}) taken. The water samples were immediately covered by sheets of black plastic to inhibit plankton blooming and transferred to a 4°C refrigerator within an hour of completion of the sampling.

5.4.2 The 1990 ATM Overflights

The proposal incorporated several new investigative methods, which were grouped under three main topics of research:

(i) to expand work into the tidal hydrodynamics at Low and High Water; in particular to determine the suspended sediment type and distribution combining X-ray diffraction analyses with spectral response.

(ii) to calibrate state-of-the-art ocean optical equipment with remotely sensed oceanography in an inlet, thus enabling future suspended sediment and hydrodynamics to be established by relatively few samples. The optical equipment deployed should allow vertical measurements of the changing depositions to be related to flocculation in an attempt to develop a model of upwelling radiance on a vertical profile.

(iii) to further develop the atmospheric correction algorithms, initially developed for the North Sea with low suspended sediment concentration ($<10\text{mg l}^{-1}$) compared to the turbid waters of the lower Tamar ($>100\text{mg l}^{-1}$) (Moore & Dyer, *unpublished paper*).

The proposed survey ideally required two overflights as close to slack water as practical. One at Low Water and the other at High Water. The weather in the Plymouth region is most stable in July. The weeks of July 9-13th and 23-27th were suggested as they had both slack waters during daylight hours. The overflights did not have to be on the same day. The proposal was accepted by N.E.R.C. and received an "A" grading (Site Number 90/25) and flight-time for both the ATM and CASI overflights was allocated in March 1990. The actual day for the overflights were confirmed in early June (CASI) and early July (ATM).

The 1990 ATM survey

The Plymouth Sound area was planned to be overflown by the N.E.R.C. aircraft deploying the ATM Daedalus 1268 and Wild RC-8 camera on 11th July 1990. The survey went ahead without any cancellations. The vessels were booked from the Coxside Marine centre (Polytechnic South West) in advance and equipment loaded the afternoon before the overflights. The five vessels were designated to specific areas and temporary names were pasted on their hulls to avoid confusion in the morning. Final confirmation of the departure of the aircraft from Oxford was made by telephone at 05.45 hours BST. The survey crew arrived by minibus and Land Rover from the Polytechnic at 07.00 hours. The vessels left Coxside Marine Centre moorings by 07.30 hours and sampling was underway by 08.00 hours. The groundtruth party returned from Cawsand at 13.00 hours and left moorings by 13.30 hours. Groundtruth sampling was underway by 13.55 hours (Figure 5.5). On the morning overflight, the aircraft overflew Plymouth Sound in three Easterly paths (Figure 5.6). The afternoon flights were flown in three overpasses, run 1 flew due south over the Tamar and to Cawsand Bay. The flight path was changed in-flight to avoid sunglint and the other two runs flew due north (Figure 5.6). Both sorties flew at a height of 2000m. Sampling times are shown in Table 5.4.

Site positions were designated in advance, again making maximum use of the Admiralty buoyage system. In unmarked channels, position fixes were taken using a hand-held yachtsman's compass. Samples were acquired at each station by the same methods employed during the 1989 overflight.

Unfortunately the Temperature/Salinity Bridge on one of the vessels failed, so a replacement was obtained for the afternoon sortie. *D.V. Aquatay* steamed between Melampus and Dunstone Rock Buoy alternately, sampling at each site and recording measurements of K (downwelling irradiance). All vessels maintained radio contact and radio communication was also made between the N.E.R.C. aircraft and *D.V. Aquatay* prior to each run. Many thanks are due here to Stuart White and John Cook of N.E.R.C. for allowing the author in the aircraft during the afternoon overflights.

Vessel & Area	Sample times BST		Site Numbers
	Morning	Afternoon	
Hamoaze Dory	08.50-09.49	14.00-14.43	11
Sound Inflatable	08.44-10.02	14.00-14.59	11
Breakwater R.V.Bass	08.57-10.16	14.00-15.03	11
Panther Dory	08.55-09.35	13.55-14.48	7
<i>D.V. Aquatay</i>	09.00-10.00	14.00-15.00	6
Aircraft flightlines	Direction Magnetic °		Time BST
1	120		09.12
2	120		09.18
3	120		09.26
4	180		14.25
5	0		14.32
6	0		14.39

Table 5.4
ATM 1990 overflights times

Problems encountered and envisaged with the two overflights

(i) Different orientation in Sun's reflection

The overflights were planned to avoid sunglint. Analysis of the 1989 (N-S-N) overflight showed that although the angle of the sun had been taken into account, substantial sunglint was present on one of the images. The 1990 morning survey was therefore planned to fly in three easterly directions in an experimental attempt to minimize sunglint. It should be noted this was very successful and largely due to the experience of Mr. John Cook (Navigator). The afternoon airborne survey changed flight plan in-flight to avoid sunglint. It was concluded that the only reasonable method of sunglint avoidance, is to check the site prior to commencing the airborne survey and, where practical, modify the

flightlines.

(ii) The development of clouds or haze was envisaged during the planning stages as being a problem. On the day of the overflight there was no wind and the Relative Humidity maintained a steady 60% causing no problems.

(iii) Different sea states in the same region could be a potential problem, small wind-driven waves can often interfere with the spectral signature for suspended material. Fortunately no wind waves developed in the Plymouth Area during the day.

5.4.3 The Plymouth Sound 1990 CASI survey

An application for a CASI overflight was included in the ATM 1990 proposal. The CASI instrument was only rented by N.E.R.C. during the week of 11-15th July and no suggestions of days were given in the proposal. A request was made that the overflight should be as close as possible to slack water at either state of the tide. The wave bands selected for the CASI overflight imaging mode were chosen with one general, and two specific objectives:

(i) Simulation of *Sea-Wifs* sensor.

The *Sea-Wifs* (Sea-Viewing Wide-Field Sensor) sensor is being developed by NASA at the moment as the successor to CZCS (Coastal Zone Colour Scanner, Holligan *et al.* 1989). *Sea-Wifs* was due to be carried on Landsat 7 and scheduled for launch in Autumn 1993; the date of launch has now been deferred until late 1993. The sensor is primarily designed for marine work with the onus on commercial and research aspects of remotely sensed imagery. The band widths chosen for *Sea-Wifs* optimize the bio-optical algorithms for productivity estimates and provide moderate resolution global maps of pigments and primary productivity (Eosat/Nasa 1987). The choice of *Sea-Wifs* compatible bands for the 1990 CASI spatial mode was hoped to give a preview of the *Sea-Wifs* spectral images; and possibly allow a preliminary start on the required chlorophyll algorithms (Table 5.5)

(ii) The kaolinite spectral signature.

The spectral bands of the ATM are broad and do not allow differentiation of aluminium silicates (clay minerals) from dissolved material (Gelbstoff) derived from river run-off. It was desired to obtain the exact shape of the waveband curves throughout the body of Plymouth Sound.

The 1989 *in situ* sampling showed a variation in the spatial distribution of clays and organics, differentiating areas of mixed estuarine waters from truly tidal waters. Sub-bottom sampling and XRD analysis of the sea bed sediments (Section 4.2.3 & 4.3) in the Sound and Tamar showed the clay minerals to be represented by kaolinite, illite, montmorillonite and chlorite with mixed layer montmorillonite and kaolinite (Table 5.6)(Stephens *et al.*, *in press*).

Sea-Wifs NASA sensor		
	Band widths (nm)	Purpose
1	433-453	Low Chlorophyll
2	490-510	Other pigments
3	555-575	Baseline Chlorophyll
4	655-675	Subsurface scattering
5	745-785	Atmospheric correction
6	843-887	Atmospheric correction
n.b. The Thermal bands, originally proposed have now been dropped due to the excessive cost.		

Table 5.5
Sea-Wifs sensor band widths

(iii) The chlorophyll- α fluorescence band.

The presence of chlorophyll mixed environments is an accurate indication of the presence or dilution of dominantly marine water (Section 5.2).

Clay mineral compositions	
Chlorite	$(\text{Mg, Fe}) (\text{Al, Si}) \text{O}_{10} (\text{OH})$
Montmorillonite	$(\text{Ca, Na})_{0.65} (\text{Al, Mg, Fe})_{4-6} (\text{Si, Al})_8 \text{O}_{10} (\text{OH}) \cdot \text{H}_2\text{O}$
Kaolinite	$(\text{Al}_2 \text{Si}_2 \text{O}_5 (\text{OH}))_4$
Illite	$(\text{K, Na, H}_3\text{O})_{3-4} \text{Al}_4 (\text{Si}_{7-6} \text{Al}_{1-2}) \text{O}_{20} (\text{OH})_4$
Spectral Peaks (nm)	
Chlorite	700, 900 (mixed layer) and 1100
Montmorillonite	700 and 1400
Kaolinite	500 and 1400
Illite	estimated at c.550

Table 5.6
Characteristics of the common clay minerals, after Hunt & Salisbury 1970, Novo *et al.* 1989

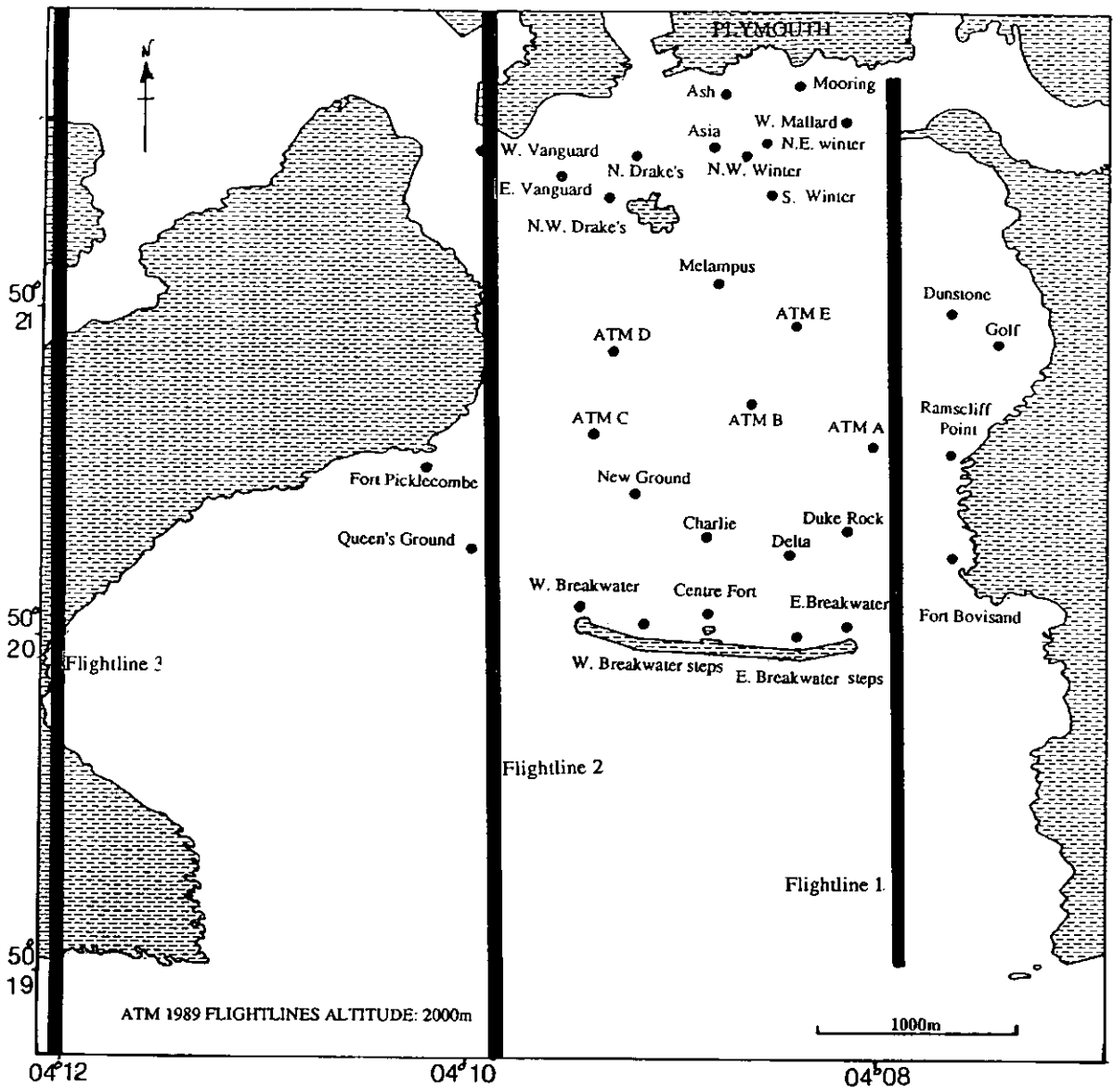


Figure 5.4 1989 ATM groundtruth sample stations and flightlines.



Figure 5.5 1990 Groundtruth collection fleet, from right to left- Breakwater Dory, Panther, Sound, Hamoaze Dory and D.V. Aquatay (centre).

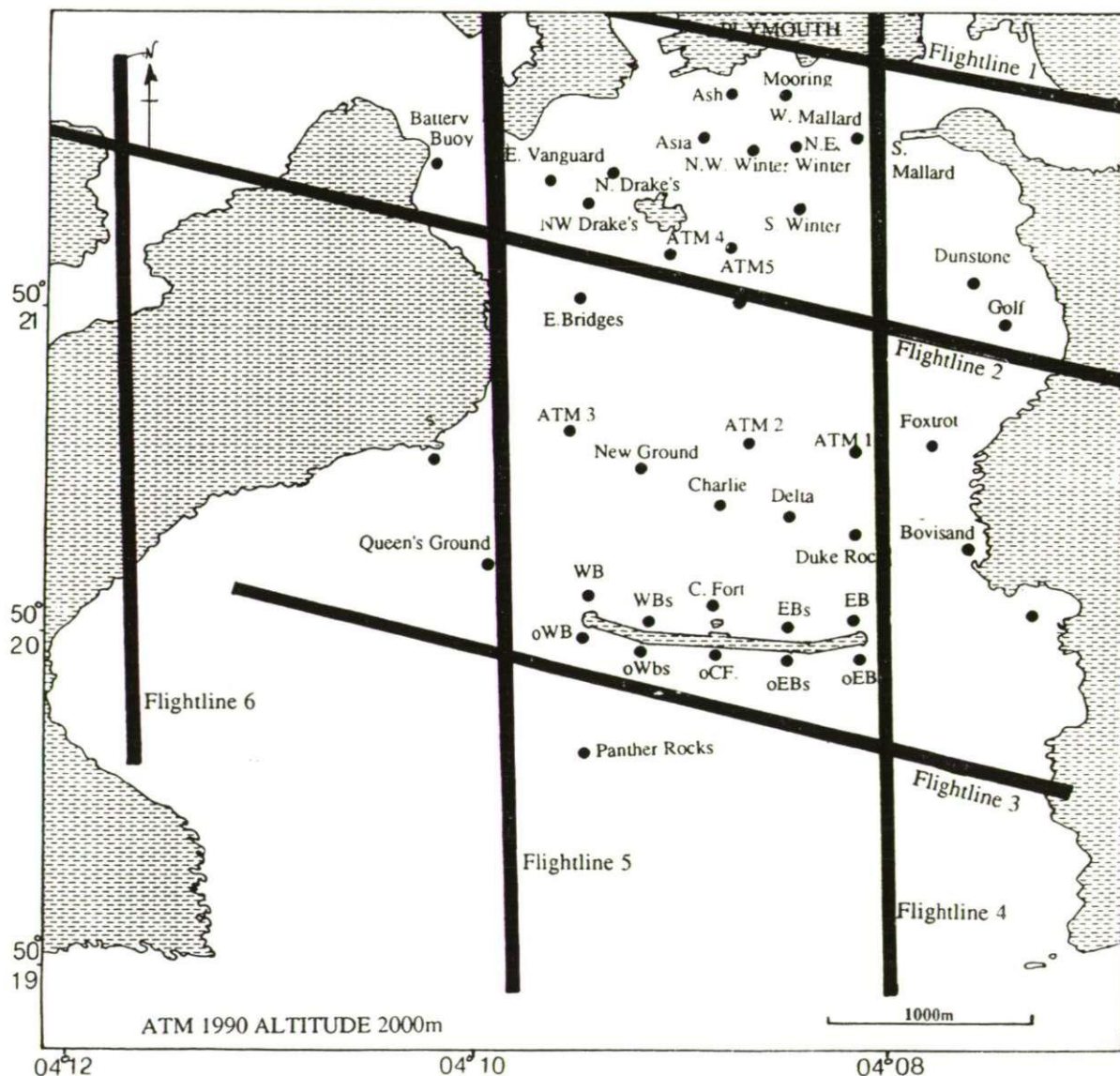


Figure 5.6 1990 ATM groundtruth stations and flightlines (WB=West Breakwater, WBs=West Breakwater steps, EBs=East Breakwater steps, EB=East Breakwater, oWB=Outer West Breakwater, oWBs=Outer West Breakwater steps, oCF=Outer Centre Fort, oEBs=Outer East Breakwater steps and oEB=Outer East Breakwater).

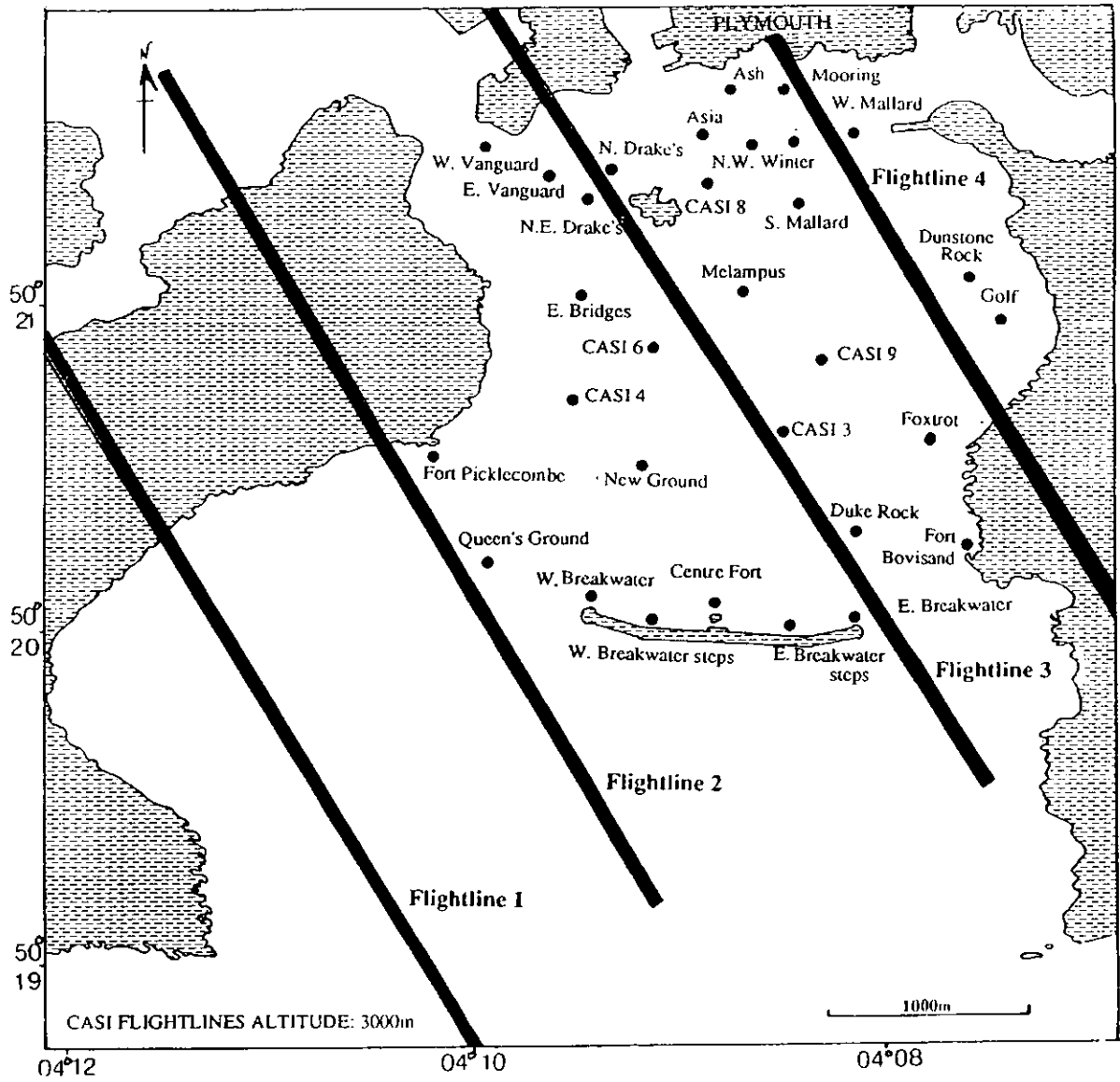


Figure 5.7 1990 CASI groundtruth sample stations and flightlines

Unfortunately, the desired bands were not selected prior to the overflight; this appears to have been due to some misunderstanding between the operator and the N.E.R.C. staff. The actual bands used during the Plymouth campaign were those previously selected for an overflight over a freshwater lake, and not really suitable for a turbid marine environment.

Desired Band settings and simulation	
1.	450 - 453 CZCS(1) and Seawifs(1)
2.	490 - 510 Seawifs(2)
3.	510 - 530 CZCS(2)
4.	540 - 560 CZCS(2)
5.	560 - 575 ATM(3) and Seawifs(3)
6.	655 - 675 Seawifs(4)
7.	677 - 687 Chlorophyll fluorescence peak
8.	705 - 725 Atmospheric/Chlorophyll fluorescence ratio
9.	745 - 759 Seawifs (5-a)
10.	770 - 785 Seawifs (5-b)
11.	843 - 887 Seawifs (5-a)
Actual bands selected by Operator	
1.	436 - 473
2.	540 - 551
3.	586 - 595
4.	634 - 642
5.	661 - 670
6.	679 - 686
7.	709 - 715
8.	746 - 765
Swath FOV 15-60°	
Spatial Resolution 578 pixels	
Spectral Resolution 288 pixels	
Line Rate Up to 100 lines/second	

Table 5.7
CASI selected band widths, desired and actual

The CASI overflight was planned by N.E.R.C. on the 12th of June but the cloud level (1000m) was so low, the overflight was cancelled at 06.00 hours with 1 hour notice. Low cloud also prevented an overflight on the 13th and 14th. On the 14th, all the vessels were in the water awaiting the go-ahead, before the aircraft radio-ed to cancel.

The Survey

Plymouth Sound was overflown (finally) by the CASI instrument and the Wild RC-8 aerial camera on the morning of 15th June 1990. The area was

imaged in six over-passes; three in spatial mode and three in spectral mode (Figure 5.7) at a height of 3000m. The Weather Report at 05.00 hours from the Longroom (H.M. Queen's Harbour Master) gave a forecast for a Northerly wind of 2-3 knots, and a maximum temperature of 16°C. The visibility was good, up to 8km, and the sea-state smooth. High Water slack (Neaps) was expected at 11.01 hours BST. The Ground Survey crew were briefed prior to the overflights. Due to the delay in the flight day, the people staffing the vessels changed as the week went on, so that several re-briefings and recruitments were required. The crew were contacted by telephone at 07.30 hours and were mini-bussed to Coxside Marine centre at 08.30 hours. Firstly, permission to survey was obtained from H.M. Queen's Harbour Master, prior to leaving the Marina. The survey vessels left Coxside Marina at 09.30 and sampling was underway by 09.51 hours (Table 5.8). Samples were taken from three vessels at 31 stations 10m south of the Admiralty buoys in Plymouth Sound. At each site 2 litres of sea water were acquired in standard plastic bottles. Additional 500ml bottles were filled for spectral analysis. Secchi disc disappearance depths were recorded. Temperature and salinity were measured at depth intervals of 0, 1, 2, 5, 10 and 20m (or sea bed). Mid-channel fixes were made using a hand-held compass. Optical *in situ* measurements were taken from *D.V. Aquatay*, which moved from Dunstone Rock Buoy to Melampus Buoy continually throughout the sampling period. At the end of the ground survey, the vessels returned to *D.V. Aquatay* to unload samples. Sea traffic on the day of the CASI flight was relatively heavy; two frigates, the Brittany ferry and a container ship left the port through the Western Entrance during the sampling period. Problems were also encountered by the inflatable operating in the Hamoaze Channel when it strayed too close to an incoming Hunter-Killer submarine. The inflatable was intercepted by the water police but was released in time to complete the sampling on schedule.

Vessels & Areas	Sampling Times BST	Number of stations
<i>Sound Dory</i>	09.51-11.18	9
<i>Breakwater Inflatable</i>	10.00-12.06	10
<i>Hamoaze Inflatable</i>	10.05-11.50	12
<i>D.V. Aquatay</i>	10.00-11.45	6

Table 5.8

The CASI overflight ground sampling times, unfortunately no times are available for the overflights due to computer error aboard the aircraft.

5.5 Laboratory Measurements.

The processing of the survey results can be divided into two categories. The groundtruth (wet) data and tape (dry) airborne images.

Suspended sediment concentration

The water samples, from all the groundtruth campaigns, were filtered separately through 0.45µm Endicott nucelpore filter papers using a standard 1 litre Millepore filtration system. The papers were dried for two hours at 30°C and then removed to a desiccator to cool. The filtrate volume was measured and the end result corrected for 1 litre (mg l⁻¹). The filter papers were reweighed and the suspended sediment concentration measured. The papers were then transferred to a muffle furnace. In order to measure the total organic material (TOM), the modified combustion technique (Meade *et al.* 1975) was used in which the furnace was heated to 300°C for 4 hours and left to cool. (Usually, the filtrate is combusted at 500°C but this can drive off water in the clay lattice and give a reduced filtrate weight (McManus *pers.comm.*)). The filtered residue was then measured to give the total organic matter (TOM). The salinity of each sample from the 1990 (ATM) morning overflight was measured in the laboratory owing to probe failure.

Chlorophyll-α concentration

The chlorophyll-α (mg l⁻³) of the seawater samples was quantified by first filtering the sample through 0.45µm ultra-cellulose Endicott filter paper at the Polytechnic Geography laboratory. The filter papers were pre-weighed, labelled, and the filtrate frozen at -10°C prior to transfer to Plymouth Marine Laboratories. Chlorophyll-α was measured at the North Sea Project Laboratory (Plymouth Marine Laboratory). The classic spectrophotometric (Volt-meter) technique of Strickland and Parsons (1968) was employed; chlorophyll-α was extracted in a 1:1 solution of 10 percent acetone and dimethyl-sulphoxide. The results were corrected for the degradation of chlorophyll-α (phaeopigment-α) by acidification.

Chlorophyll-α (mg l⁻³) = 0.08955 (Rb-Ra) x dilution factor

Phaeopigment (mg l⁻³) = 0.08955 {(1.7 x Ra)-Rb} x dilution factor

where, 0.08955 = slope (Ra-Rb) vs. volts (measured from spinach assay)

Rb = fluorescence before acid

Ra = fluorescence after acid

dilution factor (ml) = $\frac{\text{Volume of extract}}{\text{Sample Volume}}$

5.6 Image data processing

The airborne images are dispatched to the Chief Scientist by N.E.R.C., usually within a few months of the overflights. All tape processing was carried out in Plymouth.

5.6.1 Data Tapes

The ATM data were recorded on High Density Computer Tape (HDCT). The HDCT's were transcribed at N.E.R.C. Computer services to Computer Compatible Tapes (CCT's), using a packing density of 1600 bits per inch (bpi). The data were digitally recorded on the tape standard band interleaved by line (BIL) format (Hunting Geology and Geophysical Ltd. 1985). The CCT's were then dispatched to the principle investigator for the respective ATM campaign. The tapes arrived in Plymouth 3 months after the overflights. The CASI tapes arrived in Plymouth on 12.04.91 but the software that allowed the tapes to be read by the I²S system did not arrive until 20.06.91. So far only preliminary processing has been carried out on the images.

5.6.2 Image Processing

Digital data from the Daedalus scanner were analyzed at the N.E.R.C. Image Processing Unit at Polytechnic South West. The image analysis unit is the International Imaging System (I²S) Model 75 and is controlled by a VAX VMS Model 700. The Model 75 is a general purpose image array processor, which has additional computational components in which interactive or recursive programs can be carried out in near real time (I²S Users Manual). The images are displayed in extracted 512 x 512 pixel sections. Interpretation and spatial measurements of the images are made from hard copies taken by a Honeywell Matrix Camera 8000 which is attached to the I²S on 35mm Kodachrome 100 ASA slide positives. The colour bands are exposed separately to the film.

Atmospheric corrections

(i) Visual Bands

The 1989 data were calibrated and processed using a modified CZCS atmospheric algorithm by Moore & Dyer (*unpublished paper*). The broad spectral bands of the ATM do not differentiate between the clays present in Plymouth Sound, and therefore the application of a correction did not enhance the data at all. It was decided that, for the purpose of this

investigation, atmospheric corrections for the visible bands was unnecessary.

(ii) Thermal bands

Both the 1989 and 1990 ATM surveys were flown over short periods of time, and the Relative Humidity was stable. After extensive discussions with Graeme Ferrier (Ferrier & Anderson 1990) and Simon Boxall (Southampton), it was decided that any atmospheric corrections to the thermal band would be expensive and time consuming and were not justified by the potential advantages.

Geometric correction of data

Images recorded from an airborne platform generally incorporate geometric distortion. This is produced by the curvature of the Earth, the non-uniformity of scanner motion and the non-linearity of the scanner mirror. The ATM is flown on a relatively stable platform and the images are small scale. The main requirement of geometric correction programs is that they are capable of rotating, rescaling and changing the offset of the data. Two corrections were applied to the images:

(i) *Cpwarp*. The I²S Model 75 software includes a *cpwarp* warping package in which a transformation is computed between an image and a map. The program collects a set of interactively collected Ground Control Points (GCPs) from a digitized chart of Plymouth Sound and corresponding pixels on the image. The transformation is determined by a least squares best fit of bivariate Legendre polynomials (I²S program manual). The least squares model assumes the map GCPs are picked accurately and reflect the geometric properties of the map space.

(ii) *Delaunay Triangles*. The Delaunay triangulation algorithm (McCullagh & Ross 1980) was incorporated into the I²S software in 1990 and successfully applied to the 1990 images. The triangulation is based on the Thiessen polygon method, which is a geographical method of isothrithmic mapping whereby an area of influence is defined at any point in an areal context. The process matches picked data points with their neighbours by rotating them in a clockwise direction. The Delaunay correction operates by drawing triangles between the GCP's in both the map and image space. The image triangles are then resampled, by vector geometry to match the triangles in the map. The correction induces no residual error and has proved more accurate than the best-fit warp (Deveraux *et al.* 1990).

There were, however problems in both geometric correction methods. The warps can only be applied to the edge of the image with reliable CGPs can be derived from known headlands or buoys. The Plymouth Sound images have reliable headland CGP's on one edge, but unmarked navigation channels on the other. Removal of geometric distortions was essentially by trial and error, with much use made of visual comparisons with the aerial photographs. All data were warped to the British National Grid using Chart 1722, The chart was digitised into the map space on the VAX. An average of 50 CGPs were chosen per-image, the number increasing locally especially in areas of high distortion.

Image enhancement

Enhancement methods are applied to an image after geometric corrections have been made. These have been designed to aid the extraction and interpretation of data by emphasis on features or by colouring. The ATM pixel data has 0 to 255 levels of intensity (Digital Numbers) and manipulation of the levels of intensity can visually enhance data by two standard methods:

(i) **Contrast enhancement:** This is a process of accentuating the relative intensity of the image elements and is accomplished by manipulation of the quantitative distribution of Digital Numbers (DN) values across the image - the DN histogram. Contrast enhancement can be implemented in a number of ways depending on the requirements of the task, in this case two programs were used:

(i) *Scale.* This program performs a linear intensity stretch on an image, between the desired maximum and minimum clip levels. It transforms DN below the minimum black and the values above the maximum to white. All other DN values are assigned proportionally throughout the range (0-255) (I²S Users manual). It is possible to select different ranges to allow the desired contrast and apply that scaling to the entire output image. When the input image has three bands, scaling is applied to each colour separately. The results can be displayed as a colour image or in monochrome.

(ii) *Tracker Linear Mapper (TLM).* This interactively manipulates a positive or negative linear intensity transformation of the input image. The slope and cut-off points can be chosen when viewing the image. This is especially useful when applied to visible band composite images.

(ii) Colour enhancement (single band and multispectral images)

The human eye can only differentiate 20 to 30 shades of grey, but can discriminate between hundreds of colours. The implementation of colour can thus increase the amount of perceived information. This is especially useful when processing single band images. Three band composite images (red, green and blue) can be loaded into the I²S in different combinations. A near real colour composite can be achieved by filing the image as band 4, band 3, and band 2 as red, blue and green respectively. The images were enhanced using a I²S program *Pseudocolour*, which generates a colour map. The algorithm uses hue, saturation and lightness to define colour, such that a particular colour is defined for each pixel intensity. This enhancement is of particular use in the visible bands where "real" colours can be enhanced.

Density slicing

It is possible to simplify the quantity of information by reducing the number of available digital levels. High contrast images can be produced by assigning a dark colour to one level and no colour to another. This method can be used, for example to separate land from sea. This was achieved using *Level slice*, which is a program that interactively colours a range of pixel values on a single band image and is used to enhance features by eliminating unwanted pixels. For example, in order to eliminate the land signatures from an image, a band was used in which the radiances between the land and water are greatest. The histogram will show two distinct shapes; this allows the user to define a threshold by which they can be separated. The pixel radiances above and below the threshold are assigned a different colour.

Image Classification

An image can be divided into distinct classes, whereby pixels with the same spectral properties are grouped into the same class. This is usually completed by statistical or geometric methods. The separation of the classes is most successful where the contrasts of the targets are the most extreme and was implemented by accessing *Key classes* - which adds a grey scale intensity key to an image. Initially the pixel DN is calibrated to the *in situ* property. The pixel classes are chosen and classnames assigned. The image can then be coloured by *pseudocolour* to clarify the information.

- CHAPTER SIX -

- OVERFLIGHT RESULTS -

6.1 Introduction

During the four overflight campaigns (Section 5.4), a total of 14 flightlines were flown and concurrent water properties were measured at each groundtruth station. In this chapter, the results of each campaign are presented separately as the groundtruth (*in situ* measurements) and airborne (images).

6.2 The *In situ* results

The groundtruth survey measurements were obtained using the methods and laboratory processes outlined in Section 5.3.3. The groundtruth results are presented in two sections (i) *in situ* measurements including Secchi disc disappearance depths (Z_{sd}), Temperature/Salinity, and (ii) laboratory processing of water samples taken at each site, giving measurements of Total Suspended Material (TSM) and Total Organic Material (TOM). During the CASI campaign, in addition to the above measurements, Temperature/Salinity profiles were obtained to a depth of 20m (or the sea bed), and an estimation of chlorophyll- α was derived from water samples in the laboratory. The data acquired at Low and High Water is discussed separately, i.e. Low Water: ATM 1989 & 1990, High Water ATM 1990 & CASI 1990.

Initial examination of the salinity data showed the recorded results to be higher than expected. There is no known reason for this as the Temperature/Salinity Bridges were calibrated prior to each survey against three separate known saline solutions. Discussion with scientists, at the Plymouth Marine Laboratories, have confirmed that similar high salinities have been previously measured in Plymouth Sound and the average recorded salinity is 34.5‰ (Hiscock & Moore 1986). As the samples were taken on an excessively hot day it was concluded that the results were real and there is no reason why their values should not be considered reliable in a relative sense.

Measurements were made at each station during all four overflights. The *in situ* groundtruth data are presented in a series of hand-contoured maps and tables (Table 6.1, 6.2 & 6.3).

6.2.1 Secchi Disc

The Secchi disc disappearance depths (Z_{sd}) results are presented as contour plots, and, to evaluate the relationship between Z_{sd} and different bodies of water in Plymouth Sound, in histogram form (Z_{sd} vs. Frequency).

Low Water Scenario: 1989:

The 1989 ATM frequency histogram (Figure 6.1a) shows a trimodal distribution, with modal peaks occurring at $-2.5m_{sd}$, $-4m_{sd}$ and $-9m_{sd}$. The peaks at $-2.5m_{sd}$ and $-9m_{sd}$ show a regular distribution around the mean, whereas, the $4m$ peak is positively skewed. The contour plot (Figure 6.1b) showed that, during the overflight, the northern coast of the Hamoaze area was characterized by Z_{sd} measurements of *c.* $-2m$. The South Hamoaze was separated by a well defined boundary and had average Z_{sd} depths of $-4m$ to $-5m$. This area extended southeastward into the Sound to the south of Jennicliff Bay. Measurements made in the western part of the Sound showed increasing Z_{sd} from $-4m$ at The Bridges to $-6m$ at the Inner Breakwater. The Eastern and Western Entrances showed Z_{sd} maximae of -8 and $-7m$ respectively. The 1989 Z_{sd} measurements are also plotted in histogram form against Total Suspended Material (TSM) (Figure 6.2a), Total Organic Material (TOM)(Figure 6.2b), Temperature/Salinity (Figure 6.2c & 6.2d). The Z_{sd} vs. TSM histogram (Figure 6.2a) exhibits a scattered distribution, with well defined peaks at -4.5 and $-6.5m_{sd}$ and less well defined distributions at $-3m_{sd}$ and $-9m_{sd}$. A similar distribution is established in Figure 6.2b (Z_{sd} vs TOM), in which the $-4.5m_{sd}$ peak appears to correspond with low values of TSM and a high percentage of TOM. The skewed distribution at $-6m_{sd}$ is characterized by low TSM and 50% TOM. No correlation is apparent between Z_{sd} vs Temperature (Figure 6.2c) or Z_{sd} vs Salinity (Figure 6.2d). In an attempt to establish the nature of the suspended sediment populations, Z_{sd} was plotted against values of TSM composed of $<40\%$ TOM (Figure 6.2e). Two populations of suspended sediment were observed, linear regression curves and the correlation coefficient (r) were also calculated - (i)A, which is present in the Eastern and Western Entrances ($r = -0.40$), and, (ii) B, which is confined to the Hamoaze Channel ($r = -0.22$).

ATM 1989 LOW WATER						
Location site	Time	T	S	Z _{sd}	TSM	TOM
	B.S.T	°C	‰	m	mg l ⁻¹	%
West Vanguard	10.28	17.8	32.75	3.3	67	23
East Vanguard	10.36	17.6	32.92	4.6	74	55
N.W.Drake	10.43	17.4	32.92	4.4	18	40
N. Drake	10.50	17.6	32.91	4.12	26	54
Asia Knoll	10.58	17.25	33.00	4.55	20	25
Ash Buoy	11.05	17.7	32.83	2.6	18	66
Mooring	11.11	17.8	32.86	2.7	15	87
W.Mallard	11.17	18.0	32.59	1.9	81	28
S.Mallard	11.28	17.8	32.84	2.6	34	65
N.E.Winter	11.34	17.6	33.00	4.0	26	72
N.W.Winter	11.39	17.4	32.98	4.15	24	46
S.Winter	11.47	17.5	32.96	4.36	17	12
Dunstone	10.27	17.0	33.50	4.7	24	10
Golf	10.43	13.5	34.00	5.8	24	10
Ramscliff	10.53	17.5	34.00	6.7	20	11
A	11.04	17.0	33.50	4.8	58	80
B	11.11	17.0	34.00	6.4	22	14
C	11.22	18.0	33.00	4.0	13	40
D	11.29	17.0	34.00	5.0	44	26
Melampus	11.37	17.0	34.00	6.5	43	48
E	12.05	17.9	33.60	4.9	93	38
Bovisand	10.30	17.0	33.50	7.25	52	27
Duke Rock	10.37	17.5	33.40	8.75	67	35
E.Breakwater	10.42	17.5	33.35	9.15	44	38
E.Break. steps	10.46	17.5	33.40	6.95	27	50
C.Fort	10.51	17.0	33.25	6.25	11	20
W.Break. steps	10.55	16.75	33.25	7.25	58	96
W.Breakwater	11.18	17.5	33.25	9.75	60	100
Queen's Ground	11.24	17.0	33.10	6.10	46	54
F.Picklecombe	11.31	18.0	33.30	>4.55	72	23
New Ground	11.38	17.5	32.90	5.25	36	91
Charlie	11.43	17.5	33.15	5.75	60	36
Delta	11.05	17.5	33.30	5.95	16	0
Squilla 1	11.30	-	-	-	68	6
Squilla 2	12.00	-	-	-	20	15
Squilla 3	12.30	-	-	-	18	6

Table 6.1a

Legend to Tables

T = Temperature in °C

S = Salinity in ‰

Z_{sd} = Secchi disc disappearance depths in m

TSM = Total Suspended Material in mg l⁻¹

TOM = Total Organic Material in weight %

Chl = Chlorophyll-α in mg l⁻³

ATM 1990 HIGH WATER						
Location site	Time	T	S	Z _{sd}	TSM	TOM
	B.S.T	°C	‰	m		
Battery	08.50	13.8	36.50	4.77	32	6
W.Vanguard	08.57	13.5	37.00	4.90	36	63
E.Vanguard	09.02	13.6	37.00	5.10	33	60
N.W.Drake	09.07	13.6	35.00	4.92	93	55
N.Drake	09.10	13.6	35.00	4.75	90	45
Asia	09.17	13.6	37.00	5.50	31	22
Ash	09.23	13.6	37.00	4.80	40	37
Mooring	09.28	14.2	36.00	4.22	50	60
W.Mallard	09.33	13.95	35.50	3.87	63	47
S.Mallard	09.39	13.8	36.00	4.72	77	36
N.E.Winter	09.44	14.2	36.50	4.42	67	28
Foxtrot	08.44	14.0	36.50	3.95	44	0
Golf Buoy	08.52	13.6	36.00	4.85	93	70
ATM 1	09.14	13.9	36.00	4.85	72	18
ATM 2	09.21	13.4	37.50	4.90	73	37
ATM 3	09.27	13.2	36.50	5.07	101	78
Picklecombe	09.33	13.4	36.50	6.37	95	35
E.Bridges	09.40	13.4	36.00	5.00	91	19
ATM 4	09.46	13.4	37.00	5.4	95	22
ATM 5	09.51	13.4	36.00	4.57	93	14
S.Winter	09.57	14.0	35.50	4.09	108	30
N.W.Winter	10.02	14.0	36.00	4.55	99	16
Bovisand	08.57	13.5	35.50	>5.0	101	50
Duke Rock	09.05	13.5	37.00	5.22	69	30
Delta	09.13	13.5	38.00	5.15	100	20
Charlie	09.18	13.6	36.50	5.37	86	50
New Ground	09.25	13.45	34.50	5.02	69	27
Queen's Ground	09.33	13.5	36.00	5.70	65	61
W. Breakwater	09.44	13.6	36.50	4.80	102	41
W.Break.steps	09.51	13.7	38.00	4.75	96	22
C.Fort	09.58	13.7	37.00	4.85	52	38
E.Break.steps	10.03	13.6	38.00	4.75	70	21
E.Breakwater	10.13	13.6	36.00	4.45	85	48
Bovisand Bay	08.55	#	37.00	7.20	107	26
o.E.Breakwater	09.06	#	38.00	7.90	101	32
o.E.Break.step	09.14	#	37.50	9.05	85	16
o.C.Fort	09.19	#	38.00	9.75	26	50
o.W.Break.step	09.24	#	38.00	8.65	50	32
Panther	09.28	#	38.00	7.15	66	49
o.W.Breakwater	09.33	#	37.00	8.40	51	24
Melampus	09.15			*	94	32
Dunstone Rock	09.26			4.80	78	16

Table 6.1b

probe failure

* measurement not made

ATM 1990 LOW WATER						
Location site	Time	T	S	Z _{sd}	TSM	TOM
	B.S.T	°C	‰	m		‰
Battery Buoy	14.00	15.0	35.00	2.45	122	37
W.Vanguard	14.04	15.1	33.50	2.25	130	22
E.Vanguard	14.08	14.8	35.00	2.47	89	30
N.W.Drake	14.12	14.4	34.50	2.80	39	60
N.Drake	14.16	14.6	35.00	2.45	45	30
Asia	14.12	14.6	35.00	3.05	50	84
Ash	14.24	14.4	34.50	2.85	46	45
Mooring	14.28	15.2	35.00	2.55	52	50
W.Mallard	14.34	14.6	34.50	3.17	55	85
S.Mallard	14.37	14.6	34.00	3.17	88	30
N.E.Winter	14.41	14.4	35.00	2.85	68	45
Foxtrot	14.00	15.0	36.50	3.52	104	17
Golf	14.07	14.5	35.00	3.67	109	34
ATM 1	14.13	14.5	35.00	3.80	130	27
ATM 2	14.20	14.5	37.00	2.92	102	13
ATM 3	14.25	14.6	34.00	3.15	105	20
Picklecombe	14.31	15.0	35.50	3.81	109	26
E.Bridges	14.37	15.2	33.00	2.15	140	24
ATM 4	14.42	15.0	35.00	3.77	135	16
ATM 5	14.48	15.0	35.50	3.45	105	38
S.Winter	14.52	14.4	35.50	2.92	40	60
N.W.Winter	14.57	14.6	35.00	2.70	114	35
Bovisand	14.00	14.5	37.00	>5.0	101	41
Duke Rock	14.07	14.4	36.00	3.75	103	44
Delta	14.12	15.1	36.00	3.45	57	21
Charlie	14.19	14.6	35.50	3.30	97	45
New Ground	14.26	14.3	36.00	3.35	91	30
Queen's Ground	14.33	14.9	35.50	3.85	97	15
W.Breakwater	14.41	14.6	35.00	3.57	79	50
W.Break.steps	14.45	14.7	37.00	3.42	49	47
C.Fort	14.49	14.7	37.00	4.25	93	30
E.Break.steps	14.57	14.6	35.50	4.02	53	50
E.Breakwater	15.01	14.4	35.00	3.85	48	40
Bovisand Bay	13.55	19.6	35.00	5.35	48	40
o.E.Breakwater	14.11	15.0	36.00	5.10	86	30
o.E.Break.step	14.18	15.3	37.00	7.55	31	30
o.C.Fort	14.25	15.2	36.00	7.80	82	47
o.W.Break.step	14.30	15.1	35.50	7.15	92	40
Panther	14.37	15.0	37.00	6.85	45	24
o.W.Breakwater	14.43	15.1	35.00	6.50	87	62
Dunstone Rock					78	26
Melampus					93	33
Dunstone Rock					96	37
Melampus					97	30
Midway					80	36

Table 6.1c

CASI HIGH WATER							
Location site	Time B.S.T	T °C	S ‰	Z _{sd} m	TSM mg l ⁻¹	TOM %	Chl mg l ⁻³
West Vanguard	10.05	13.6	34.80	6.2	58	30	7.66
East Vanguard	10.16	13.6	34.75	6.2	65	100	10.89
N.W.Drake	10.22	13.9	34.65	6.0	71	100	7.18
N.Drake	10.30	13.9	34.65	5.9	59	100	8.35
Asia Knoll	10.43	14.0	34.71	6.6	75	100	7.68
Ash	10.53	14.0	34.64	6.1	55	100	7.68
Mooring	11.04	14.2	34.66	6.3	19	5	7.49
W.Mallard	11.10	14.1	34.30	7.1	82	30	6.15
S.Mallard	11.19	14.1	34.54	7.2	56	100	9.08
N.E.Winter	11.28	13.8	34.80	7.6	59	16	6.23
N.W.Winter	11.35	13.8	34.86	7.2	71	100	7.27
S.Winter	11.43	14.3	34.66	7.4	90	40	7.44
Golf	09.51	13.8	35.00	5.3	59	54	8.13
Foxtrot	10.03	14.4	34.20	4.6	54	100	8.82
CASI 3	10.14	*	*	7.6	52	100	7.31
CASI 4	10.26	14.8	35.00	7.4	43	100	8.67
CASI 5	10.35	14.6	35.65	6.5	62	30	6.26
CASI 6	10.45	14.4	36.00	8.4	57	100	6.84
CASI 7	10.52	14.2	34.50	6.2	41	100	11.00
CASI 8	11.00	14.2	34.90	>5.	67	16	10.03
CASI 9	11.13	15.4	36.00	6.4	59	15	10.55
Melampus	10.05	13.7	35.20	8.6	75	100	5.59
Dunstone	10.19	13.9	34.50	6.0	70	95	12.49
Melampus	10.42	13.8	34.70	8.9	61	100	7.85
Dunstone	11.00	13.9	34.60	5.7	88	100	11.87
Melampus	11.33	13.9	34.70	7.7	73	100	-
Dunstone	11.45	14.2	34.70	6.2	56	100	15.39
Bovisand	10.00	13.3	36.05	7.8	46	100	10.40
Duke Rock	10.15	13.5	33.00	5.4	52	100	9.25
E.Breakwater	10.30	13.7	36.00	6.9	89	100	9.06
E.Break.steps	10.43	13.5	36.35	6.9	41	100	5.37
C.Fort	10.55	13.4	36.50	7.4	56	60	12.30
W.Break.steps	11.07	13.4	35.95	7.2	73	100	12.28
W.Breakwater	11.16	13.7	35.95	6.9	76	100	9.56
Queen's Ground	11.29	13.8	36.50	9.2	41	100	7.14
Picklecombe	11.40	13.9	36.50	8.8	59	100	4.53
New Ground	11.58	13.6	36.50	7.5	85	67	4.92

Table 6.1d

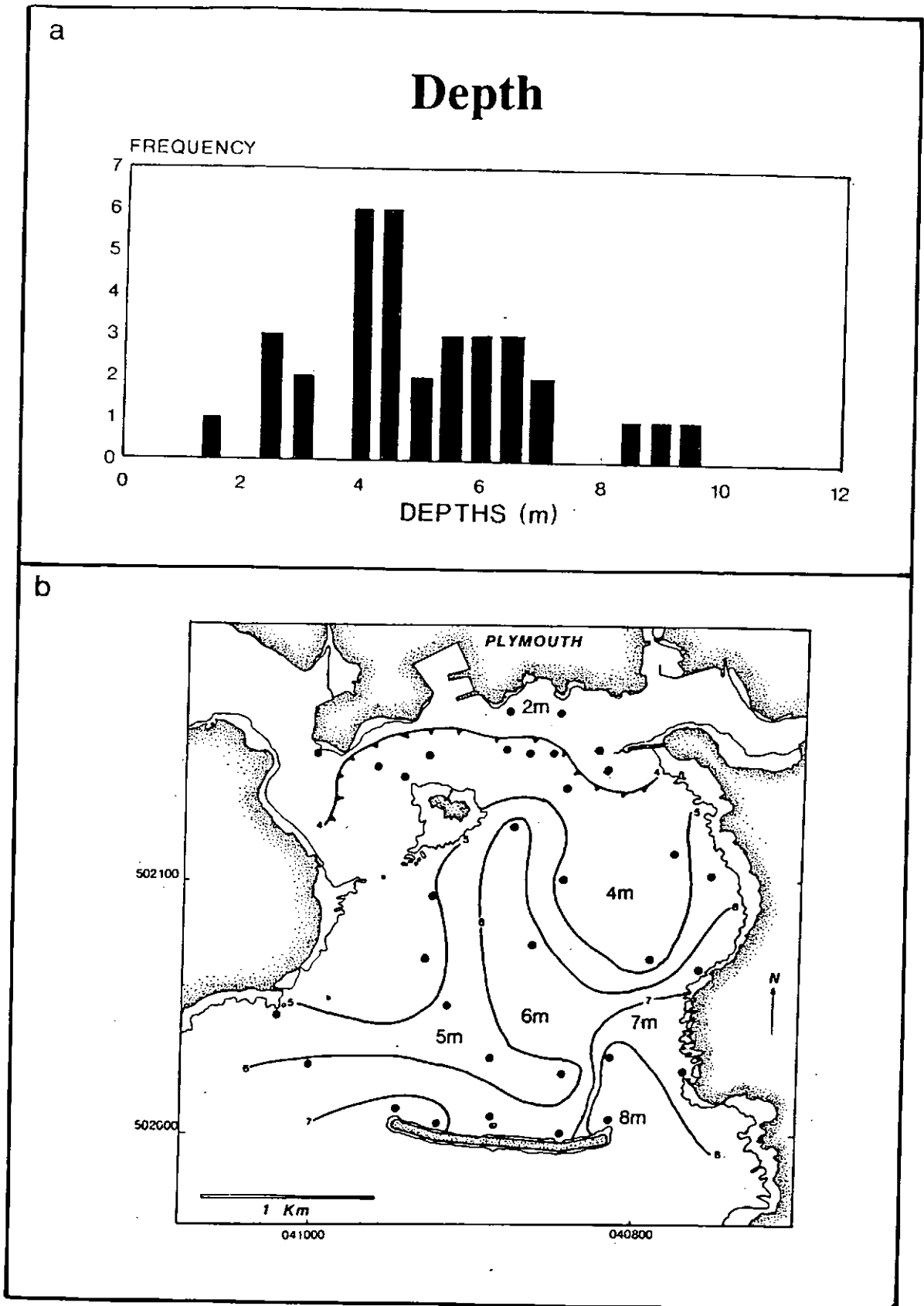


Figure 6.1 ATM 1989 Low Water Secchi disc disappearance depths (a) frequency histogram and (b) spatial distribution.

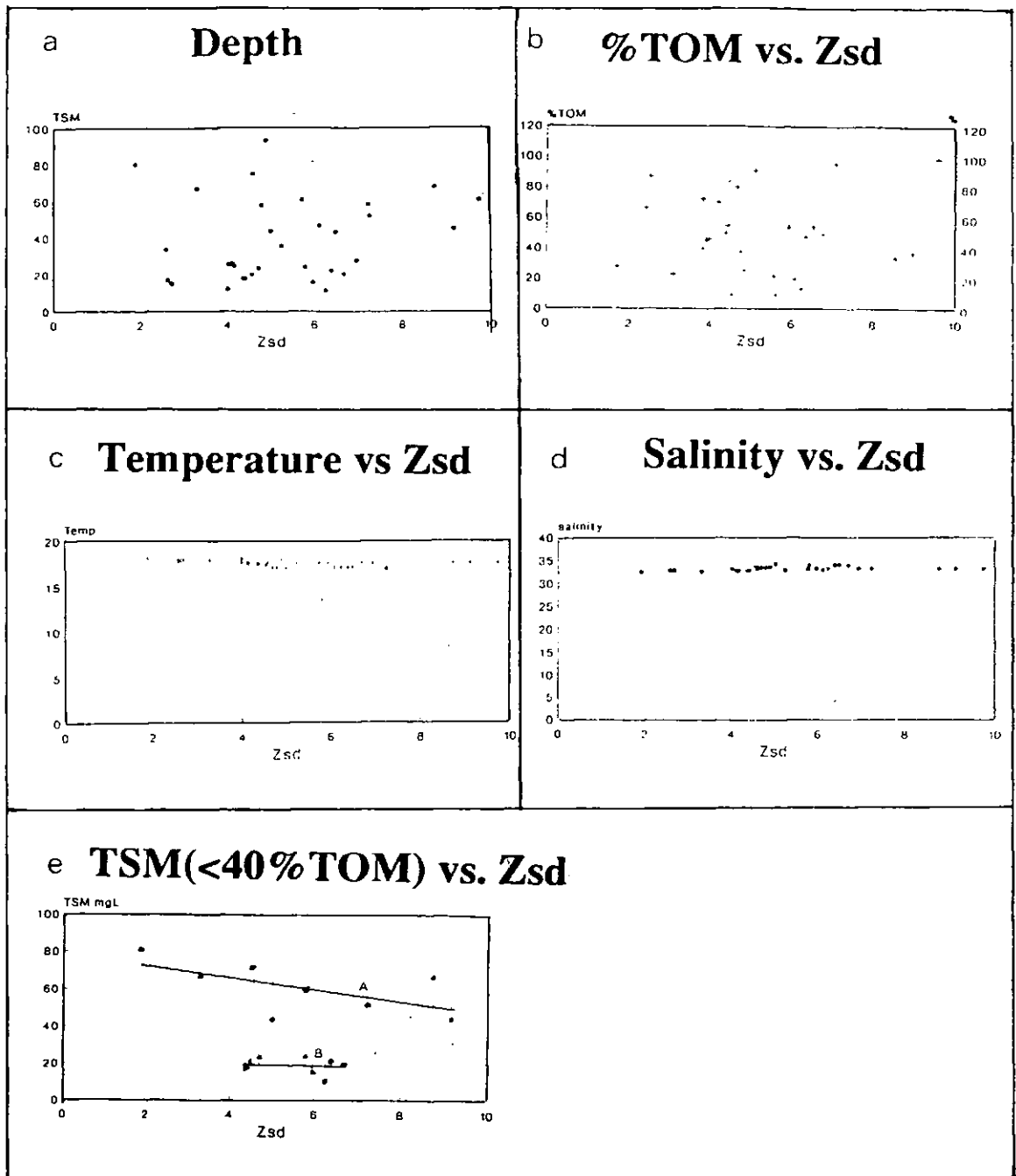


Figure 6.2 Secchi disc disappearance depths vs. *in situ* properties (a) TSM vs. Z_{sd} , (b) %TOM vs. Z_{sd} , (c) Temperature vs. Z_{sd} , (d) Salinity vs. Z_{sd} , and (e) TSM(<40%TOM) vs. Z_{sd} , with populations A and B.

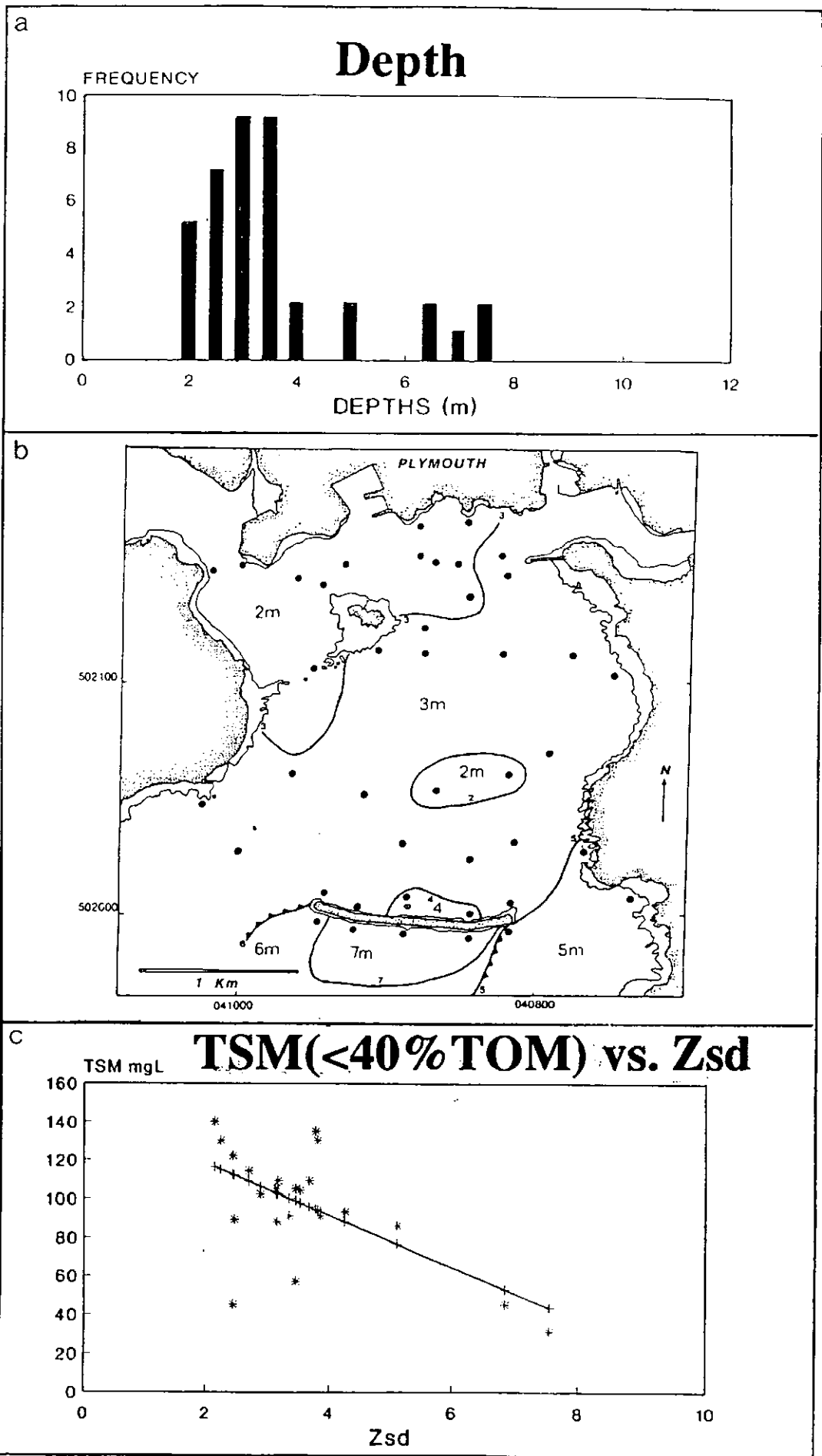


Figure 6.3 ATM 1990 Low Water Secchi disc disappearance depths (a) frequency histogram, (b) spatial distribution, and (c) TSM(<40% TOM) vs. Z_{sd} .

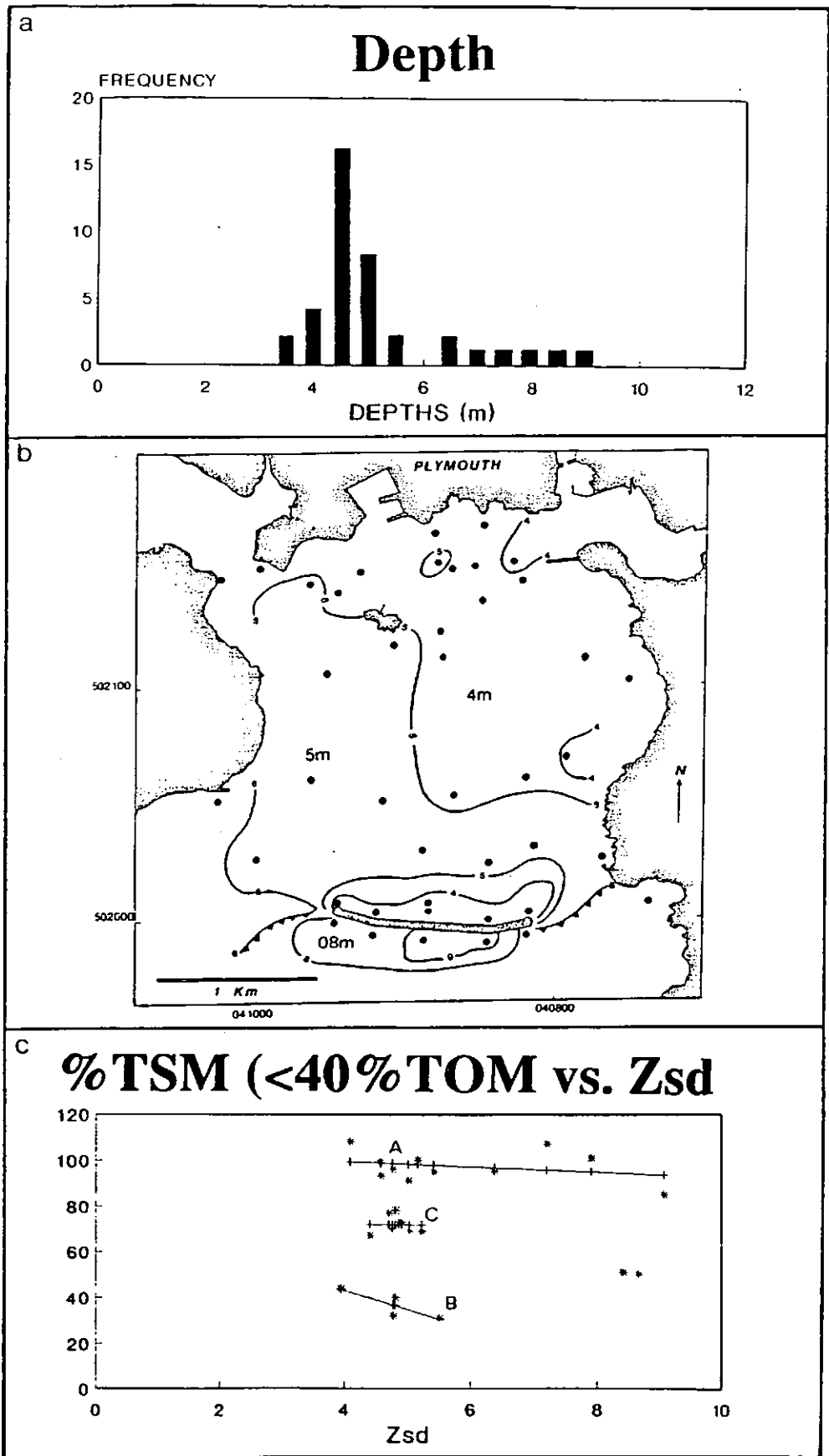


Figure 6.4 ATM 1990 High Water Secchi disc disappearance depths (a) frequency histogram, (b) spatial distribution, and (c) TSM (<40% TOM) vs. Z_{sd} , with populations A, B and C (the two isolated readings were derived from the Outer Breakwater).

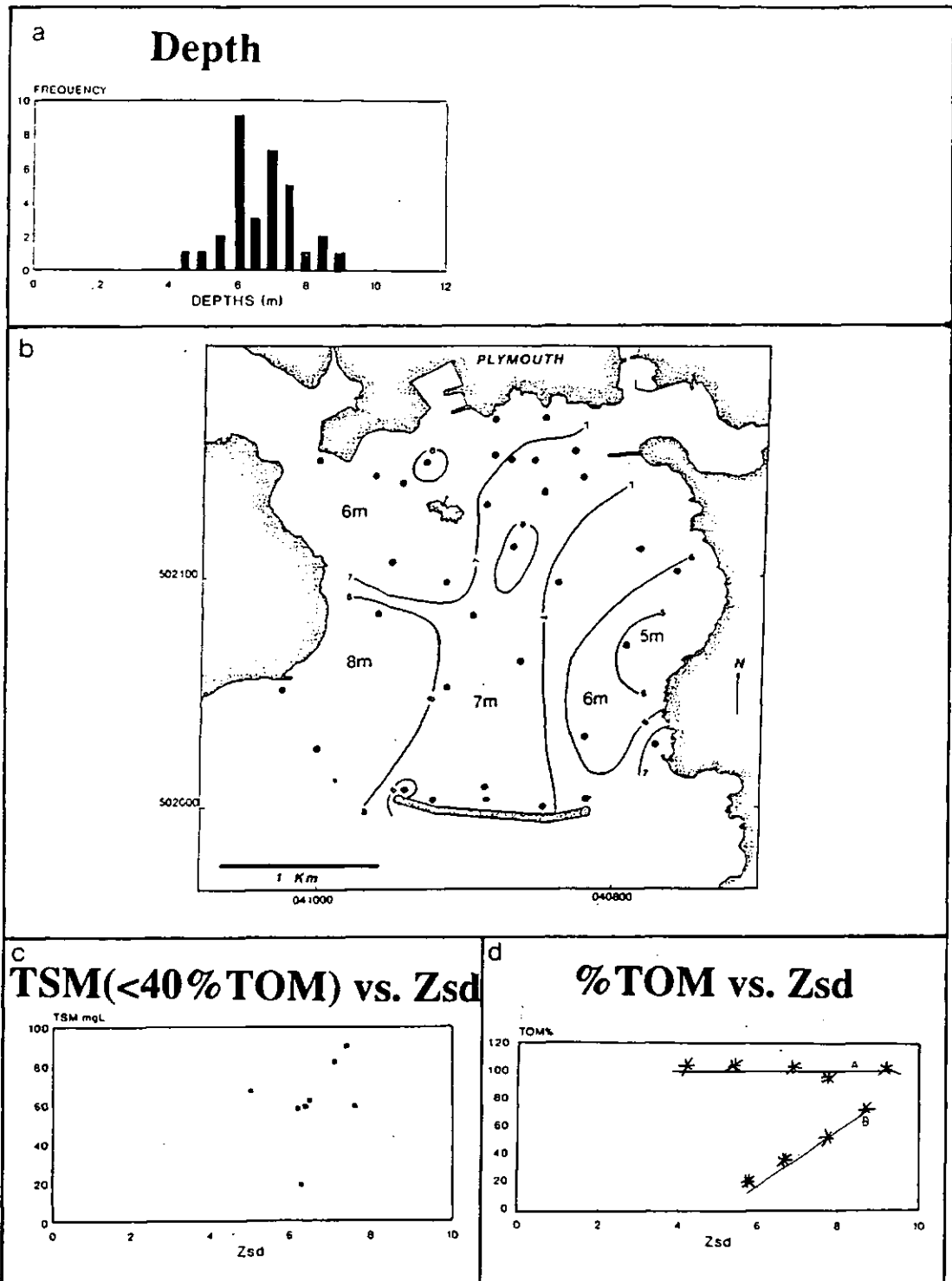


Figure 6.5 CASI 1990 High Water Secchi disc disappearance depths (a) Frequency histogram, (b) spatial distribution, (c) TSM(<40% TOM) vs. Z_{sd} and (d) TSM (<40% TOM) vs. Z_{sd}, with populations A and B.

Low Water Scenario 1990:

The 1990 Low Water ATM Z_{sd} vs. Frequency plot (Figure 6.3a) shows a pronounced bimodality with a prominent peak at $-3m_{sd}$ and less well defined peak at $-7m_{sd}$. The contour map (Figure 6.3b) illustrates the Hamoaze channel to have had Z_{sd} measurements of $-2m$ in the west and $-3m$ in the east. The Z_{sd} increased southward from the Plym, with a marked turbid "spot" in the centre of the Sound. The Inner Breakwater had a Z_{sd} of $-4m$. There were marked changes at either side of the Breakwater, with a difference from -3 to $-6m_{sd}$ in the Western Entrance compared to -5 and $-6m_{sd}$ in the Eastern Entrance. There was also a decrease in Z_{sd} measurements immediately adjacent to the coast. If the histogram and spatial distributions are compared, it is possible to correlate the modal distribution peaks against geographical areas, i.e. the $-3m_{sd}$ modal peak is formed from measurements taken from the body of the Sound and the $-7m_{sd}$ peak is formed from measurements made in the Outer Breakwater. Z_{sd} vs. TSM(<40% TOM) (Figure 6.3c) illustrates the presence of one dominant sediment type which has a linear relationship with Z_{sd} ($r = -0.47$).

High Water scenario 1990:

The 1990 ATM Z_{sd} vs. Frequency plot (Figure 6.4a) shows low bimodality with a symmetrical peak at $-4.5m_{sd}$ and a spread, rather than a peak from $-6m$ to $-9m_{sd}$. Geographically, the $-4.5m$ peak can be correlated with the turbid plume of the Plym estuary which can be traced westwards (Figure 6.4b) into the Hamoaze Channel. The Z_{sd} measurements made in Plymouth Sound were generally uniform and between -4 to $-5m_{sd}$. The Z_{sd} depths increased towards the south west. The Inner Breakwater measurements gave depths between -4.45 to $-4.85m_{sd}$. There were sharp contrasts in Z_{sd} between the Sound and the Outer Breakwater area with a rapid increase in depth to $-9m$ in the Panther Zone. Z_{sd} vs. TSM(<40% TOM) (Figure 6.4c) illustrates the possible presence of three populations of suspended material: (i) A, which describes a linear relationship ($r = -0.20$), (ii) B, which shows an inverse linear relationship ($r = -0.88$), and (iii) C, which is more of a cluster with $Z_{sd} = c. 5m$ and $TSM = c. 70mg l^{-1}$.

CASI High Water (neaps) Z_{sd} vs. Frequency plot (Figure 6.5a) show a uni-modal distribution at $-6m_{sd}$. The spatial plot (Figure 6.5b) shows the Hamoaze Channel to have been divided into two depths, with $-6m_{sd}$ in the northwest and $-7m_{sd}$ in the southeast. The turbid plume of the Plym ($-6m_{sd}$) is observed to have been deflected towards the northwest by the

last stages of the flooding tide. It must be noted that at most sample stations, a slight flood current was observed. The presence of moving water was also identified in the multiple measurements made at Dunstone Rock and Melampus Buoy (Table 6.4). The body of the Sound showed Z_{sd} of -5m in the east at Jennycliff Bay to -8m at Fort Picklecombe in the west. A "more-transparent" stream was observed to dissect the surface of the Sound in a line from the Western Entrance, northeastward to the Hamoaze Channel. The centre of the Inner Breakwater had Z_{sd} depths of -7.0 to -7.4m_{sd} with a slight decrease at either end of the Breakwater to -6.9m_{sd}. Z_{sd} vs. TSM(<40% TOM) (Figure 6.5c) shows a scatter of points, with no apparent correlation ($r = 0.15$), however most water samples taken during the CASI campaign averaged 100%. In an attempt to clarify the relationship between Z_{sd} and TSM, Z_{sd} was plotted against %TOM (6.5d). This graph shows two distinct populations: (i) A with a poor correlation of $r = 0.21$, and (ii), B which has a well defined linear relationship where $r = 0.67$.

6.2.2 Temperature

The *in situ* groundtruth surface temperature measurements for all the campaigns are presented in Figures 6.6 & 6.7 and Table 6.1. The CASI Temperature dip profiles are presented in Table 6.2.

Low Water Scenario 1989:

The 1989 ATM ground campaign demonstrated that the surface of the Sound had an average surface water temperature of 17.5°C with a minimum of 13.5°C and a maximum at 18°C (Table 6.1). The contour map (Figure 6.6a) shows the Hamoaze Channel area to have been characterized by a surface temperature of 17.6°C, with a 0.2°C decrease in temperature in the centre of the Channel. The body of Plymouth Sound had a surface temperature of 17.0°C, and was dissected by a warm stream (>18°C) which extended from Mountbatten Breakwater towards the Western Entrance in a southwesterly direction. Temperatures of 17.5°C were identified in Jennycliff Bay. Measurements made at Golf Buoy were of the order of 13.5°C, slightly cooler than the surrounding waters. The Inner Breakwater area showed a decrease in temperature from 17.5° to 16.7°C between the Eastern and Western End.

Low Water Scenario 1990

The 1990 ATM Low Water *in situ* temperature measurements showed a slightly different spatial pattern (Figure 6.6b). The average temperature of the surface of the Sound was *c.* 14.5°C. The surface waters of the Hamoaze channel were fortunately not disrupted during sampling and showed a cooler stream of <14.5°C issuing from Millbay Docks. A warm plume emitting from the Plym estuary was clearly defined with a temperature signature of >15°C. The surface of the Hamoaze Channel appeared to cool eastward from 15.1°C in the Narrows Passage to 14.4°C at Mountbatten Breakwater. The surface of the Sound exhibited a westward increase in surface temperature between 14°C at Jennicliff Bay and 15°C at Fort Picklecombe. The Inner Breakwater measurements displayed an increase in temperature from 14.6° and 14.4°C at the Western and Eastern End respectively, to 14.7°C at the Centre Fort. Results identified a temperature difference of 0.5°C between the Inner and Outer Breakwater sampling sites.

High Water Scenario 1990:

The ATM 1990 High Water *in situ* temperature measurements (Figure 6.7a, Table 6.1) showed the surface of the Sound to have had an average temperature of *c.* 13.6° and lie between 13.2° and 14.2°C. A difference of 0.3°C was recorded between the Cornish coast (13.8°C) and the Devon coast (13.5°) in The Narrows. The Hamoaze Channel exhibited an 0.8°C eastward increase in temperature between Drake's Island and Mountbatten Breakwater. The surface outflow from the Plym was marked by a 14°C plume of water, warmer than the surrounding Hamoaze Channel. The body of the Sound displayed a decrease in temperature between the east and west. There was a warm "spot" around the area of Foxtrot Buoy, 0.5°C higher than the surrounding waters. The Inner Breakwater sample stations revealed a very small increase in temperature (0.1°C) between the Eastern and Western End.

The temperature data acquired during the CASI overflight are presented in Figure 6.7b and Table 6.1. The measurements were made close to maximum slack water (Section 5.4.3). The Temperature Salinity probe failed at site CASI 3, and was replaced. At each station temperature/salinity dips were made at each station, to the sea bed or a maximum depth of -20m (Table 6.2). The average temperature over the surface of the Sound was *c.* 14.0°C, and ranged between 13.4 and 15.4°C. The Lower Tamar was

defined by surface temperatures of 13.6 to 13.9°C in a plume which extended towards the southeast into the Hamoaze Channel. The Western Hamoaze Channel exhibited an increase from 13.6°C at West Vanguard Buoy to 14.2°C at the Mooring Buoy. There was an area of cooler water (13.8°C) at sample stations in the Winter Passage. The surface temperatures in the body of the Sound showed a increase of 0.8°C between the eastern and western coasts. Measurements made at CASI 9 showed warmer temperatures (15.4°C) than the surrounding water. The Inner Breakwater sites revealed a 0.3°C increase in temperature between the Eastern End and the Centre Fort. The temperature profiles obtained during the groundtruth campaign generally displayed a temperature decrease with depth, often in a series of steps or thermoclines. Temperature dip measurements made in the Hamoaze Channel showed a decrease with depth at all stations, with the exception of West Vanguard Buoy which had an increase with depth (i.e. inversion) of 0.2°C between -5 and -10m. Measurements at East Vanguard exhibited a constant temperature between the surface and -20m, where the temperature then decreased from 13.6° to 13.5°C. The temperature signatures at North West Drake's, North Drake's, Asia, South Winter and Mooring stations showed a rapid change in temperature between *c.* 14.0°C and 13.6°C, at varying depths, and a second rapid decrease in temperature between 13.6° and 13.4°C at depths of -10 to -20m. West and South Mallard stations had a surface water temperature of 14.1°C which decreased to *c.* 13.6°C between -1 and -2m, and a second rapid 0.2°C decrease in temperature at -10 to -20m. The water column in the area of North East Winter and North West Winter Buoys showed a uniform temperature of *c.* 13.7°C to -10 to -20m where the temperature dropped to 13.6°C. The temperature in the body of the Sound were generally 0.7°C cooler than in the Hamoaze Channel. The temperature profile at Melampus Buoy illustrated a uniform temperature decrease with depth from 13.7°C on the surface to 13.2°C at -20m. The temperature measurements from Dunstone Rock and Foxtrot Buoy gave warm surface signatures of 13.9°C and 14.4°C, respectively, with a decrease at -2m to 13.6°C and 13.7°C at 2m depth, and a second decrease at -5m to 13.4°C and 13.3°C. Temperature profiles at Golf Buoy displayed a rapid decrease of 0.3°C between the surface and -1m, and a second decrease of 0.2°C at 2m, the temperature then remained stable until -10m where a 0.3°C inversion was recorded. The temperature profile at CASI 4 showed an increase between the surface and -1m of 0.2°C, temperatures, which then dropped 1° to 14.0°C at -2m and decreased uniformly with depth to

-20m where an inversion was recorded and water temperature increased to 13.8°C. The temperature profile at CASI 5 showed a rapid decrease in temperature from 14.6 to 14.1°C from the surface to 1m, and then decreased with depth to 13.6°C at -20m. The sample station CASI 6 had a warm surface signature of 14.4°C followed by a rapid decrease at -1m of c. 0.5°C. The profiles at CASI 7 and CASI 8 identified a temperature decrease of 0.2°C between the surface and -1 to -2m. Sample station CASI 9 had a high surface temperature of 15.4°C with a marked 1°C decrease at -1m, and a second decrease of 0.3°C at -2 to -5m. The temperature profiles at Queen's Ground Buoy and Fort Picklecombe both showed a marked decrease between the surface and -1m, followed by a uniform decrease with depth to c. 12.8°C. The profile at New Ground Buoy showed a difference of -0.1°C between the surface and -1m, and a temperature inversion at -2m to 13.6°C. Measurements at East Breakwater, East Breakwater steps and West Breakwater stations indicated a rapid decrease in temperature between the surface and 1m, the temperature signature then decreased with depth. Sample stations at Centre Fort and West Breakwater steps showed a decrease between the surface and 1m of 1-2°C.

6.2.3 Salinity

The *in situ* salinity results for the four groundtruth campaigns are presented as a series of contour maps (Figures 6.8-9) and in Table 6.1. The Salinity profiles acquired during the CASI groundtruth campaign are recorded in Table 6.3.

Low Water Scenario 1989:

The 1989 ATM Low Water salinity contour plot (Figure 6.8a) shows a tri-partite distribution of salinity. The Hamoze Channel was characterized by salinities of 32.80-32.90‰, with the exception of Asia Knoll which had a salinity of 33.00‰. The body of the Sound had salinity between 33.50 and 34.00‰ with two "salty" patches that had salinities of >34.00‰, one to the south of Melampus and a second in Jennicliff Bay. A decrease in salinity to 32.90‰ was observed at New Ground Buoy. The Inner Breakwater showed a decrease in salinity from 33.35‰ at the Eastern End to 33.25‰ at the Western End.

Low Water Scenario 1990:

The 1990 ATM Low Water distribution of surface salinity (Figure 6.8b) displayed an overall greater variation in salinity than in 1989. The

Western Hamoaze Channel appeared to have been divided into three east-west orientated surface bodies, with salinities of $<35\text{‰}$ in the north and south, separated by salinities of 35.00 to 35.50‰ in the centre of the channel. Measurements at West Mallard and South Mallard Buoys recorded salinities of $<35\text{‰}$. Sample stations ATM 5 and South Winter Buoy showed a salinity increase of 0.50‰ compared to the surrounding area. The body of the Sound showed salinities to generally increase southward from 35.00‰ in the north, to a maximum of 37.00‰ at the Inner Breakwater. Several exceptions to this pattern were identified - an increase in salinity to 37.00‰ at ATM 2, and a decrease to 35.00‰ at Charlie Buoy and ATM 1. A sharp boundary occurred at the eastern end of the Breakwater between salinities of 35.00‰ and 37.00‰. Salinities recorded at the Western End of the Breakwater appeared to increase southward over 1km distance between 35.00‰ and 37.00‰.

High Water Scenario 1990:

The 1990 ATM High Water salinity measurements are presented in Figure 6.9a. The Western Hamoaze channel showed a surface variation between 36.50‰, at Battery Buoy, to 37.00‰ at West Vanguard, Asia Knoll and Ash Buoy. There was a marked drop to 35.00‰ at North West Drake's and North Drake's Buoys. The salinities in the Eastern Hamoaze Channel changed from 36.50‰ northeast of Drake's Island to $<36.00\text{‰}$ at West Mallard and South Winter Buoys. The body of the Sound showed a southward increase in salinity from 36.00‰ in the north, to $>38.00\text{‰}$ at the Inner Breakwater. There were two exceptions to this pattern - a decrease in salinity at New Ground Buoy to 34.00‰ and increase at ATM 4 to 37.00‰. A salinity of 36.50‰ was recorded at the Western Entrance compared to 37.00‰ in the Eastern Entrance.

The CASI 1990 High Water salinity measurements (Figure 6.9b) showed that the Hamoaze Channel and the area immediately south of The Bridges had surface salinities of $<35.00\text{‰}$. The body of the Sound showed a southward increase of surface salinity. The maximum surface salinities were at Queen's Ground, Fort Picklecombe and New Ground. The salinity data profiles are presented in Table 6.3. The profile measured in the Hamoaze Channel indicated that the salinity generally increased with depth in a series of marked steps or pycnoclines. Measurements at West Vanguard Buoy showed a constant salinity of 34.80‰ with a decrease or

inversion at -5m of the order of 0.20‰ . Salinity at East Vanguard Buoy showed an increase of 0.02‰ at -2m followed by a second increase of 0.10‰ at -20m. Sample stations at North West Drake's Buoy, North Drakes's Buoy, Asia Knoll, Ash Buoy and Mooring Buoy demonstrated a marked increase in salinity of *c.* $+0.20\text{‰}$ between -2 and -5m, and a second increase of *c.* $+0.40\text{‰}$ between -10 and -20m. A salinity inversion of -0.03‰ occurred at -1m at North Drake's Buoy. Salinity profiles at West and South Mallard Buoys show 15 percent lower surface salinities than the surrounding water, with similar salinity/depth structures to the above stations. The profile at South Winter Buoy showed an irregular increase in salinity with depth. The salinity profile at Melampus Buoy identified an inversion of -0.10‰ at -1m and a second inversion of -0.10‰ at -2m. Measurements at Dunstone Rock Buoy also defined a -0.10‰ inversion at -1m, followed by a marked pycnocline of $+0.25\text{‰}$ between -2 and -5m. The salinity profile recorded at Golf Buoy detected a marked inversion between 34.80‰ and 34.20‰ at -5m. At Foxtrot Buoy, the salinities decreased with depth with two marked pycnoclines present at -5m and -10m. A salinity inversion was also recorded between -10m and the sea bed. The salinity profile at CASI 4 indicated an increase with depth from 35.00 to 34.40‰ and a marked $+0.90\text{‰}$ change between -2 and -5m. Profiles at stations CASI 5, CASI 6, CASI 7 and CASI 8 demonstrated high surface salinities with a marked inversion between -2 and -5m to salinities of $<20.00\text{‰}$. A similar profile was observed at sample station CASI 9 where an inversion was measured at -5m. Salinity profiles at Queen's Ground Buoy, Fort Picklecombe and New Ground Buoy revealed an increase in salinity with depth, with an inversion of -0.05‰ occurring at -14m at Queen's Ground Buoy. At Fort Bovisand there was a similar profile with an inversion of -0.05‰ close to the sea bed. The salinities recorded at Duke Rock Buoy were all in the order of 33.00‰ which is unrealistic, and so it is assumed that this measurement is an operator error and will therefore be ignored in the interpretation. Profiles acquired at West Breakwater and West Breakwater steps showed the salinity to increase sharply at -2m between 36.50 to 36.65‰ and then increased with depth. Measurements at Centre Fort, East Breakwater steps and East Breakwater demonstrated salinity to increase with depth in a series of pycnoclines at *c.* -1m, -2m and -10m.

Location	-0m	-1m	-2m	-5m	-10m	-20m
HAMOAZE						
W.Vanguard	13.6	13.6	13.6	13.6	13.8	13.8 (15m)
E.Vanguard	13.6	13.6	13.6	13.6	13.6	13.5
N.W.Drake	13.9	13.8	13.7	13.7	13.6	13.6
N.Drake	13.9	13.9	13.9	13.8	13.6	13.4 (13m)
Asia Knoll	14.0	14.0	13.8	13.6	13.6	13.6
Ash	14.0	13.8	13.8	13.6	13.4	13.4
Mooring	14.2	14.1	14.0	13.6	13.6	13.6 (15m)
W.Mallard	14.1	14.0	13.7	13.6	13.6	13.6
S.Mallard	14.1	14.0	13.6	13.6	13.4	13.4
N.E.Winter	13.8	13.7	13.7	13.7	13.6	13.4
N.W.Winter	13.8	13.8	13.8	13.8	13.8	13.6 (18m)
S.Winter	14.3	14.0	14.0	13.7	13.6	13.5 (17m)
SOUND						
Melampus	13.7	13.6	13.6	13.4	13.2	
Dunstone	13.9	13.9	13.6	13.4	13.3	
Golf	13.8	13.5	13.3	13.3	13.6	(btm)
Foxtrot	14.4	13.8	13.7	13.3	13.2	13.2 (15m)
CASI 4	14.8	15.0	14.0	13.8	13.7	13.8 (btm)
CASI 5	14.6	14.1	14.0	13.9	13.6	13.6
CASI 6	14.4	13.9	13.7	13.6	13.2	13.4
CASI 7	14.2	14.0	14.0	13.8	(btm)	
CASI 8	14.2	14.2	14.0	13.9	(btm)	
CASI 9	15.4	14.4	14.1	13.8	13.6	13.6
Fort Bovisand	13.3	13.3	13.1	13.0	13.1	(btm)
Duke Rock	13.5	13.3	13.3	13.0	12.9	12.9 (15m)
Queen's Ground	13.8	13.1	13.1	13.0	12.9	12.8 (14m)
Picklecombe	13.9	13.6	13.0	12.9	12.9	(8m)
New Ground	13.6	13.5	13.6	13.4	13.3	13.1 (15m)
BREAKWATER						
E.Breakwater	13.7	13.2	13.1	13.0	12.9	12.9 (15m)
E.Break.steps	13.5	13.3	13.1	13.1	13.0	12.9 (12m)
Centre Fort	13.4	13.3	13.0	13.0	12.9	12.9 (19m)
W.Break.steps	13.4	13.2	13.1	13.0	13.0	13.0 (17m)
W.Breakwater	13.8	13.2	13.1	13.0	13.0	12.8 (17m)

Table 6.2
Temperature Dips CASI campaign

location	0m	-1m	-2m	-5m	-10m	-20m
W.Vanguard	34.80	34.80	34.80	34.60	34.80	34.80 (15m)
E.Vanguard	34.76	34.76	34.78	34.78	34.80	34.90
N.W.Drake	34.65	34.68	34.72	34.72	34.79	34.84
N.Drake	34.65	34.62	34.60	34.68	34.86	34.96 (13m)
Asia Knoll	34.71	34.71	34.74	34.90	34.94	35.00
Ash	34.64	34.71	34.70	34.85	34.94	34.94
Mooring	34.66	34.65	34.70	34.88	34.86	34.94 (15m)
W.Mallard	34.30	34.65	34.80	34.85	34.94	34.96
S.Mallard	34.54	34.58	34.89	34.89	34.94	35.05
N.E.Winter	34.80	34.84	34.84	34.86	34.95	35.01
N.W.Winter	34.86	34.84	34.84	34.82	34.85	35.04 (18m)
S.Winter	34.66	34.72	34.76	34.85	34.95	35.00 (17m)
SOUND						
Melampus	35.20	35.10	35.00	35.00	35.00	
Dunstone	34.50	34.40	34.50	34.75	34.75	
Golf	35.00	35.40	34.80	34.20	34.80	(btm)
Foxtrot	34.20	34.40	34.40	34.60	34.45	34.45 (15m)
CASI 4	35.00	35.00	35.10	34.20	34.20	34.40 (btm)
CASI 5	35.65	34.40	28.00	25.10	<20.0	<20.0
CASI 6	36.00	34.30	<20.0	<20.0	<20.0	<20.0
CASI 7	34.50	34.40	<20.0	<20.0	(btm)	
CASI 8	34.90	34.80	34.60	19.40	(btm)	
CASI 9	36.00	35.50	35.60	<20.0	<20.0	<20.0
Fort Bovisand	36.05	36.05	36.15	36.25	36.20	(btm)
Duke Rock	33.00	33.05	33.10	33.40	33.50	33.60 (btm)
Queen's Ground	36.50	36.55	36.65	36.70	36.70	36.65 (14m)
Picklecombe	36.50	36.55	36.65	36.70	36.70	(8m)
New Ground	36.50	36.55	36.50	36.55	36.55	36.70 (15m)
BREAKWATER						
E.Breakwater	36.00	36.00	36.15	36.25	36.35	36.45 (15m)
E.Break.steps	36.35	36.35	36.40	36.45	36.50	36.55 (12m)
Break. Fort	36.50	36.45	36.50	36.55	36.60	36.65 (19m)
W.Break.steps	35.95	35.95	36.50	36.55	36.55	36.55 (17m)
W.Breakwater	35.95	36.10	36.65	36.60	36.65	36.80 (17m)

Table 6.3

Salinity Dips CASI campaign

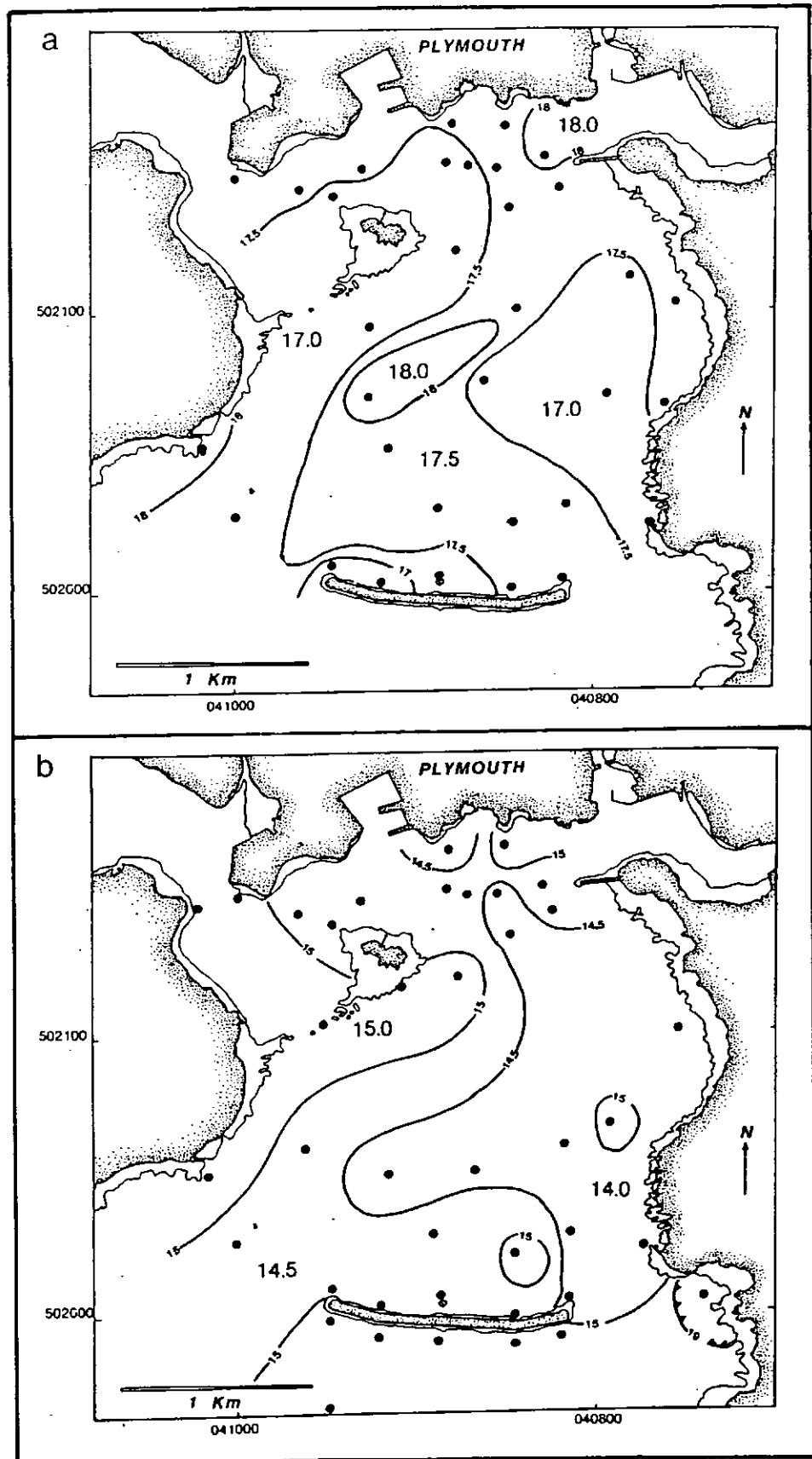


Figure 6.6 Spatial distributions of *in situ* Temperature Low Water (a) 1989 ATM and (b) 1990 ATM.

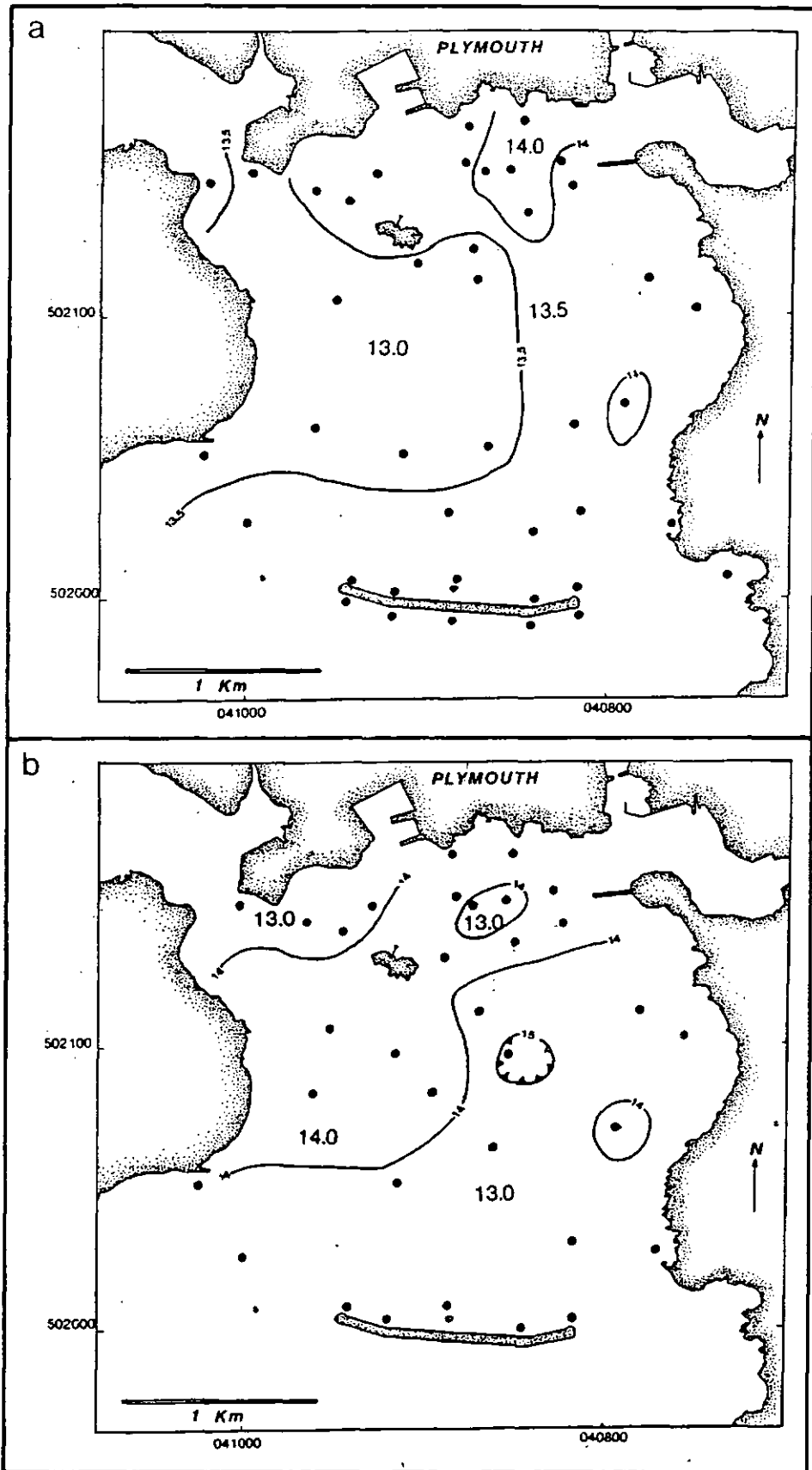


Figure 6.7 Spatial distributions of *in situ* Temperature High Water (a) 1990 ATM and (b) 1990 CASI (The chevrons indicate the direction of rapid increases in temperature).

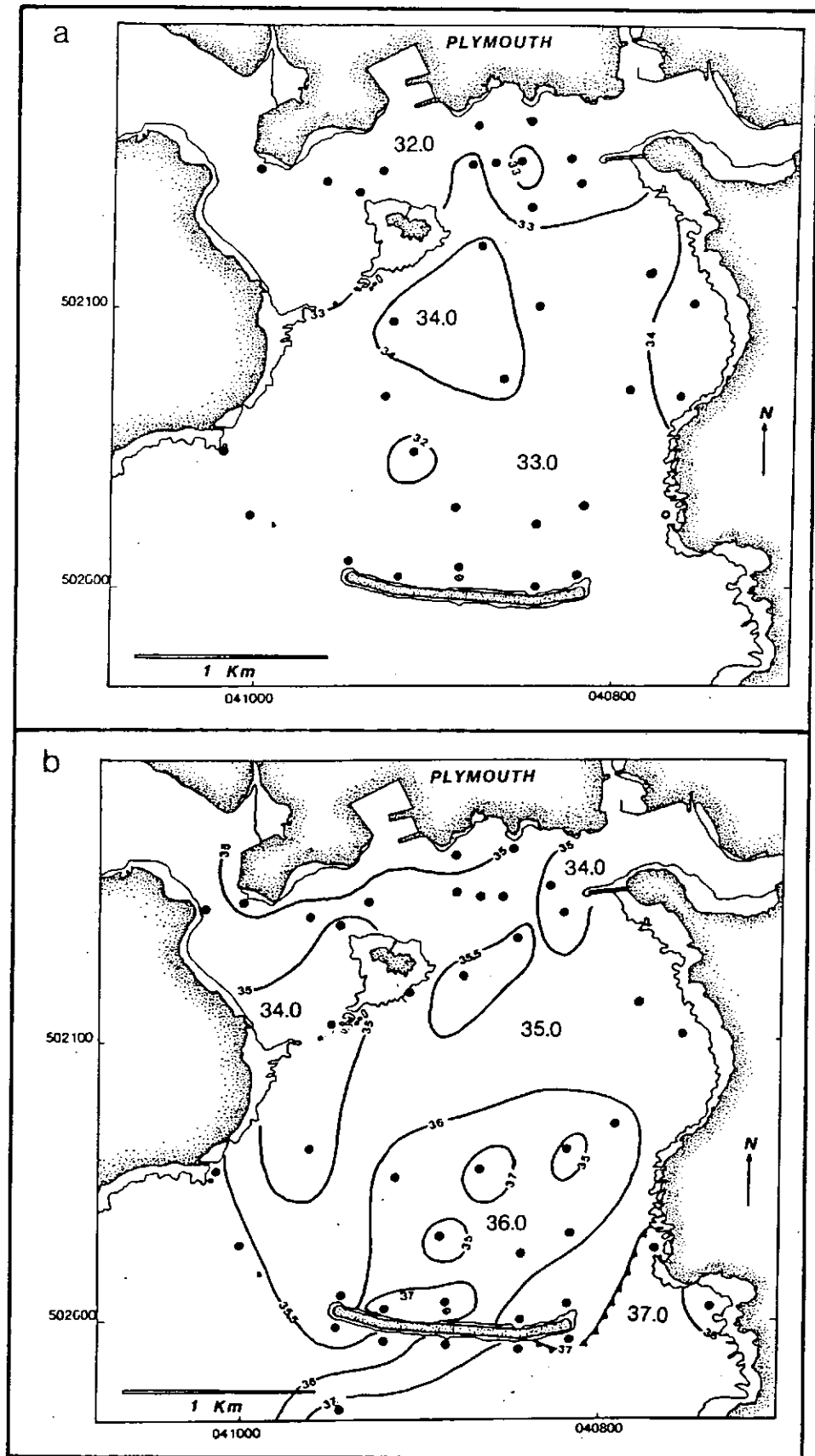


Figure 6.8 Spatial distributions of *in situ* Salinity Low Water (a) 1989 ATM and (b) 1990 ATM (The chevrons indicate the direction of rapid increases in salinity).

6.3 Laboratory results

6.3.1 Total Suspended Material and Total Organic Material

Evaluation of the Total Suspended Material (TSM) and Total Organic Material (TOM) for each of the water samples was obtained using the methods outlined in Section 5.5. The results are presented in Table 6.1 and as contour plots in Figures 6.10 & 6.11.

Low Water Scenario 1989:

The ATM 1989 measurements of TSM are mapped in Figure 6.10a. The highest concentrations ($>100\text{mg l}^{-1}$) were in the Plym estuary and around Plymouth Hoe. The lowest values ($<10\text{mg l}^{-1}$) were at Centre Fort. The Central Hamoaze Channel had values of $40\text{-}60\text{mg l}^{-1}$ with an increase in TSM towards the west and east. The body of the Sound had an average TSM value of $30\text{-}60\text{mg l}^{-1}$, increasing to 80mg l^{-1} in the area immediately adjacent to the western coast. Samples from Jennicliff Bay had TSM concentrations of $20\text{-}40\text{mg l}^{-1}$. The Inner Breakwater area showed low concentrations at Centre Fort (11mg l^{-1}) increasing westwards (60mg l^{-1}) and eastwards (44mg l^{-1}). Figure 6.10b shows the TOM percentage distribution of the waters in Plymouth Sound during the 1989 overflight. The highest concentrations were in the Hamoaze Channel, in which the sampling crew reported large recognizable particulates directly derived from the sewers. A sharp increase in TOM of 28% to $>50\%$ was observed between West Mallard Buoy and the surrounding waters. The body of the Sound showed an average TOM of 30-50%, which decreased towards the coasts and increased to $>80\%$ at Ramscliff Point. The Western Inner Breakwater exhibited high percentages of TOM with a decrease towards Centre Fort and the Eastern End. The East and Western Entrances showed TOM values of 30-50%.

Low Water Scenario 1990:

The 1990 ATM Low Water overflight concentrations of TSM are presented in Figure 6.10c. The highest concentrations were at station ATM 4 (135mg l^{-1}) and the lowest in the Outer Breakwater area. The Lower Tamar Estuary, and the area to the south of The Bridges, had TSM concentrations of $>130\text{mg l}^{-1}$ decreasing rapidly to $<50\text{mg l}^{-1}$ in the Central Hamoaze Channel. The Eastern Hamoaze Channel was characterized by TSM concentrations of *c.* 50mg l^{-1} and the body of the Sound by $90\text{-}130\text{mg l}^{-1}$ increasing southward to the centre of the Inner Breakwater and an isolated sample taken from ATM 1. Water samples from the Eastern Entrance showed low concentrations of TSM (*c.* 40mg l^{-1}) whereas the

Western Entrance was characterized by high concentrations ($>90\text{mg l}^{-1}$). The distribution of TOM percent measured from water samples is presented in Figure 2.10d. The highest percentages were in the Hamoaze Channel at Asia Knoll (84%), and the lowest percentage at ATM 1 (13%). The Hamoaze Channel displayed an eastward increase towards the Plym estuary. In the body of the Sound, the TOM percentages decreased southward towards the centre and increased towards the Inner Breakwater. The Inner Breakwater showed TOM values of 30% at the Centre Fort and an increase to 50% at the West Breakwater and East Breakwater steps. The percentages of TOM present in the Outer Breakwater sites showed a noticeable 50% increase between the Eastern and Western End.

High Water Scenario 1990:

The 1990 ATM High Water TSM concentrations are mapped in Figure 6.11a. The highest value occurred at ATM 3 (109mg l^{-1}) and the lowest value at Outer Centre Fort (26mg l^{-1}). The centre of the Hamoaze Channel had high ($<90\text{mg l}^{-1}$) concentrations, with two areas of low TSM concentrations - the Lower Tamar Estuary and the area to the south of The Hoe. The northeast part of the Sound was dominated by a continuation of the high Hamoaze concentrations, whereas the Jennycliff Bay water samples had low concentrations ($40\text{-}50\text{mg l}^{-1}$). The southern part of the Sound was dominated by $60\text{-}80\text{mg l}^{-1}$ concentrations with an increase towards the Eastern Entrance. The water samples from Inner Breakwater area showed a series of isolated high concentrations at Charlie Buoy, Delta Buoy, West Breakwater and West Breakwater steps, and a decrease in concentration at the Centre Fort. Samples at the Outer Breakwater sites showed the concentration of TSM to increase eastwards, from 26mg l^{-1} at the Outer Centre Fort to 101mg l^{-1} at the East Breakwater site.

The TOM percentage measured from the 1990 ATM water samples (Figure 6.11b) showed the Hamoaze Channel to be divided into two broad north-south trending zones: 50-70% concentrations in the west, and slightly lower concentrations in the east (30-50%), with isolated samples bearing high percentages of TOM. The body of the Sound was also divided in two, with 10-30% TOM in the northern area, and 50-70% in the south and Inner Breakwater area. There were also high percentages of TOM present in Jennycliff Bay (70%) and at station ATM 3 (78%). The percentages of TOM measured in the Inner Breakwater showed an increase between the Eastern and Western End.

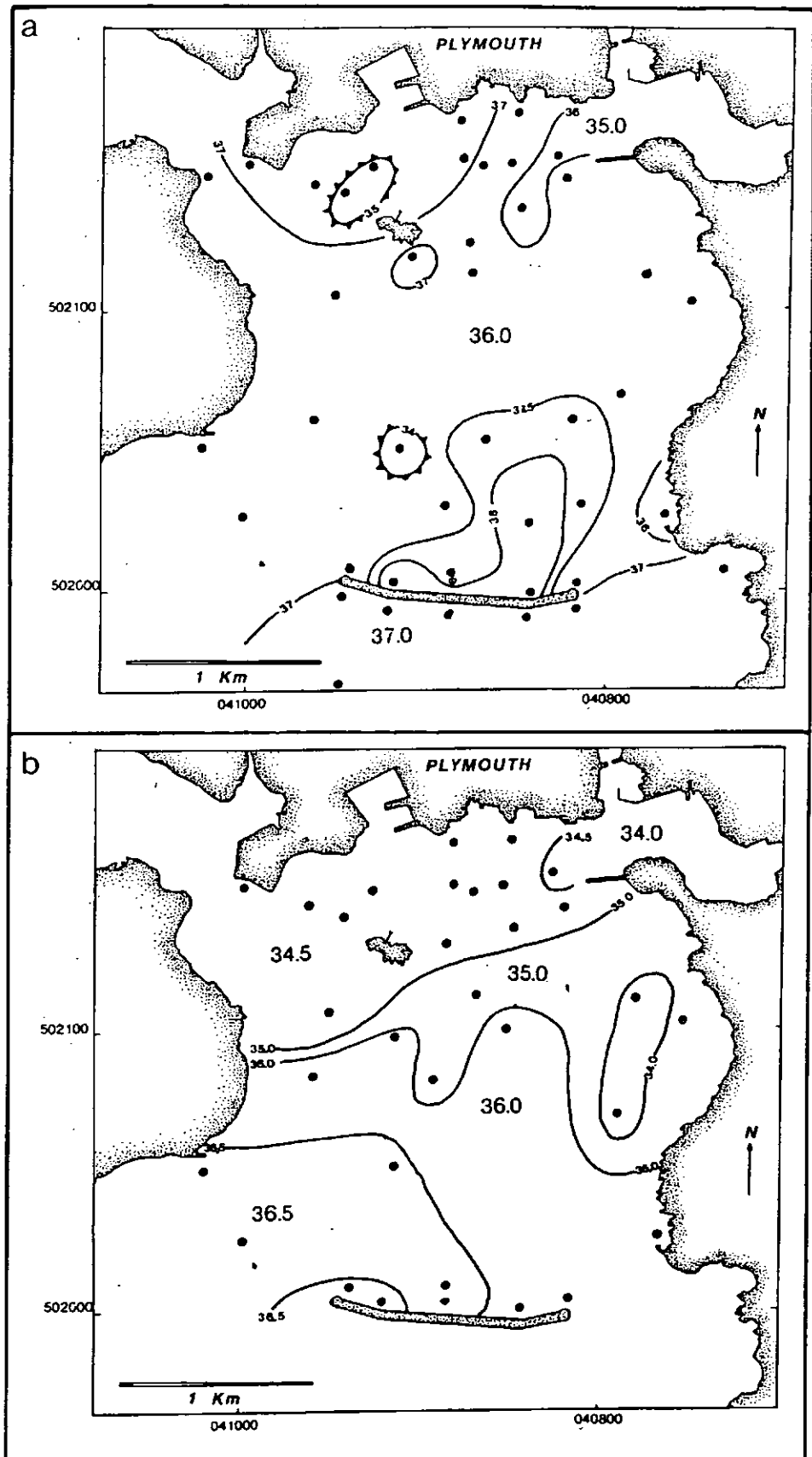


Figure 6.9 Spatial distributions of *in situ* Salinity High Water (a) 1990 ATM and (b) 1990 CASI (The chevrons indicate the direction of rapid increases in salinity).

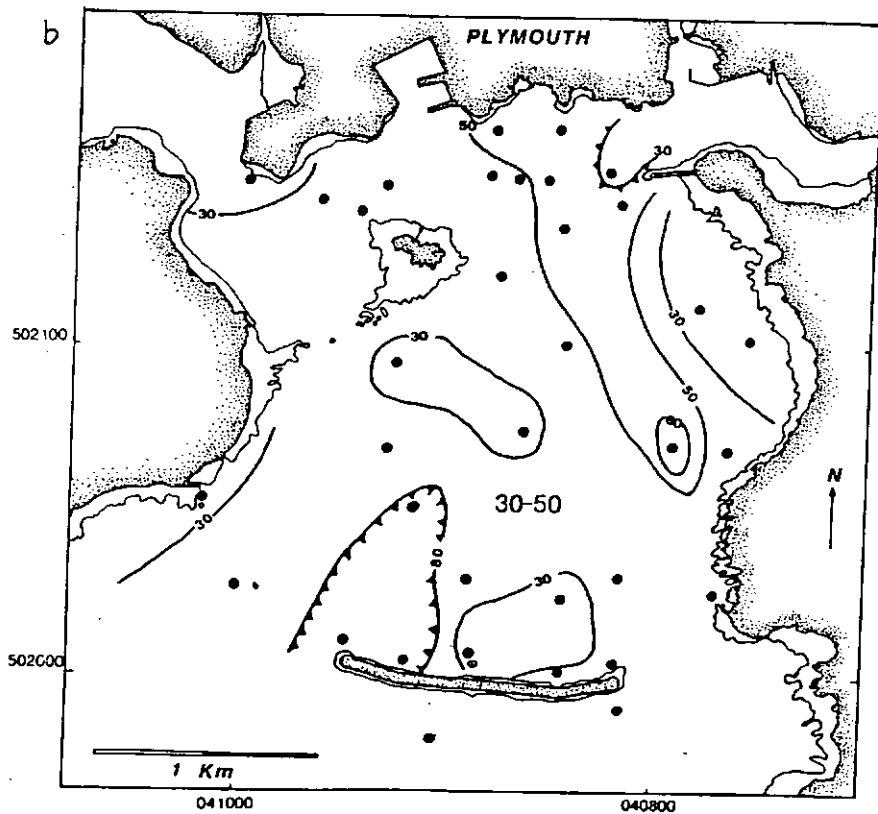
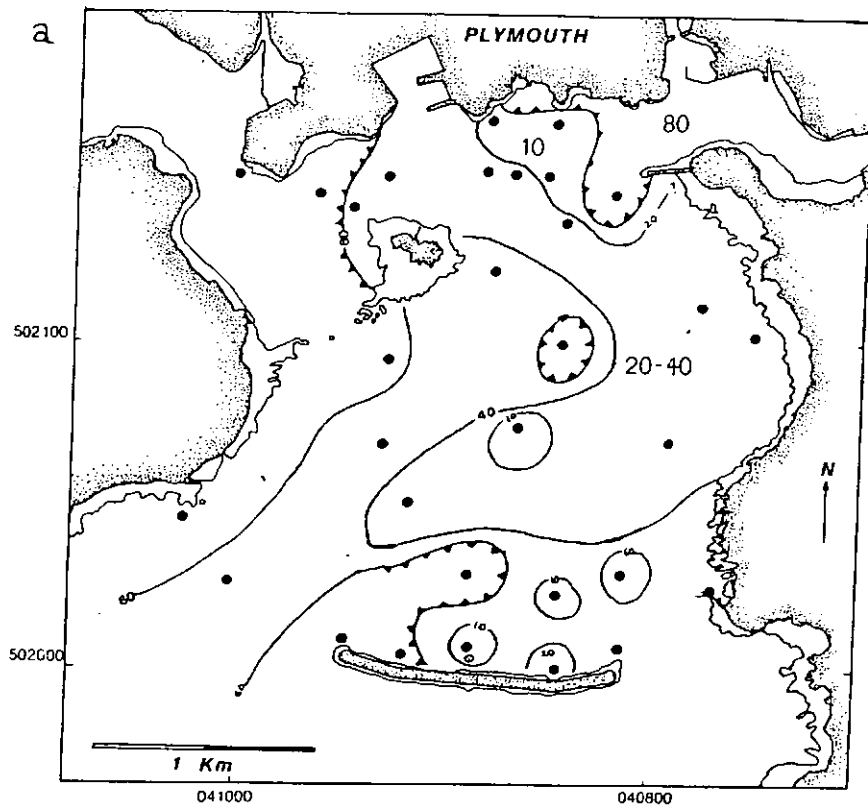


Figure 6.10 Spatial distributions of *in situ* Gravimetric concentrations, Low Water (a) 1989 ATM TSM (mg l⁻¹), (b) 1989 ATM TOM (%) (The chevrons indicate the direction of rapid increase in concentration).

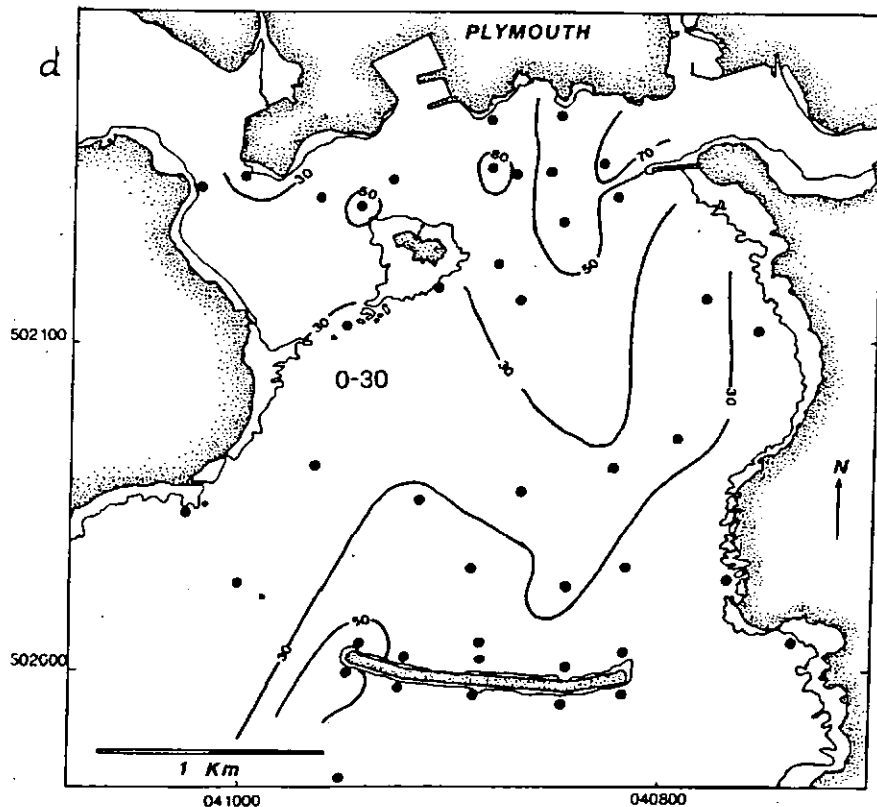
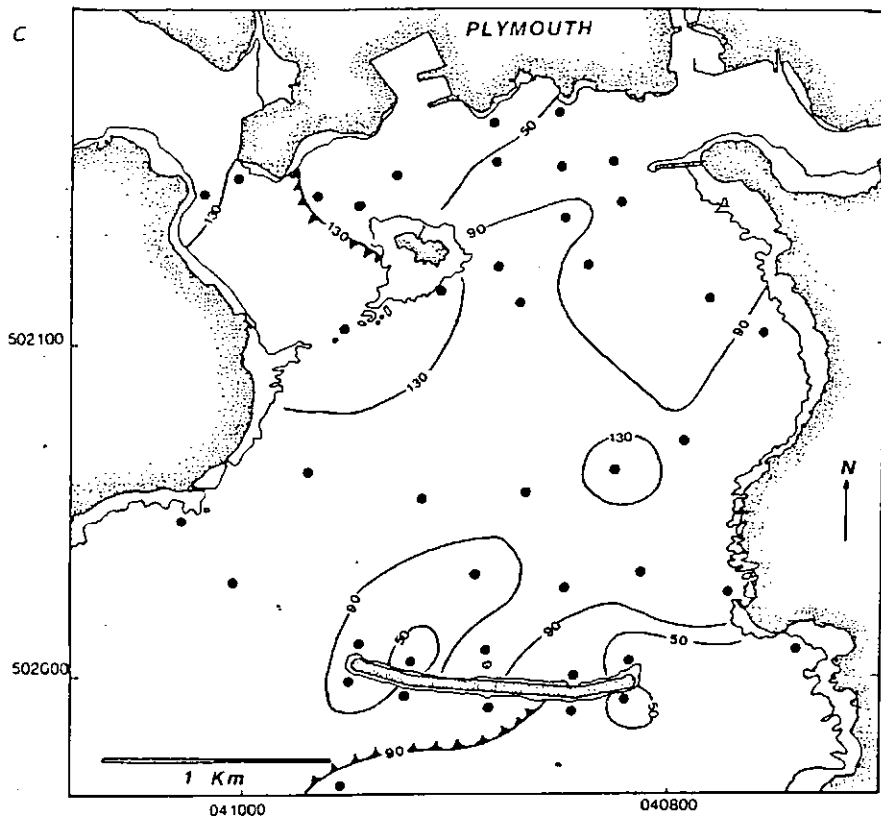


Figure 6.10 cont. Spatial distributions of *in situ* Gravimetric concentrations, Low Water(c) 1990 ATM TSM (mg l⁻¹) and (d) 1990 ATM TOM (%) (The chevrons indicate the direction of rapid increase in concentration).

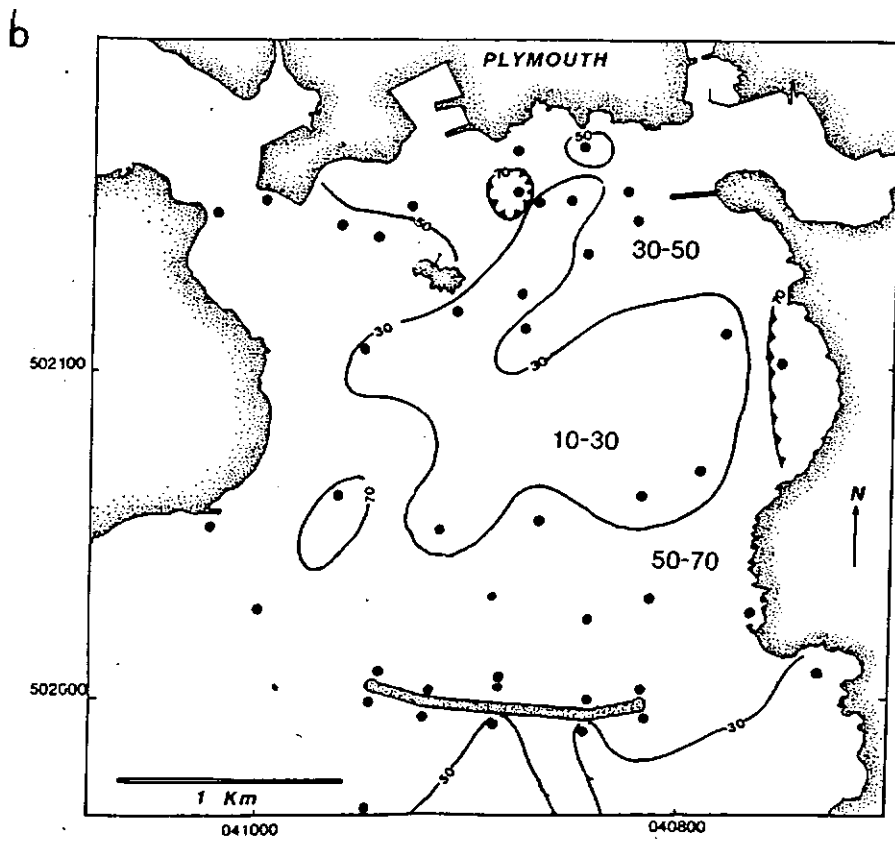
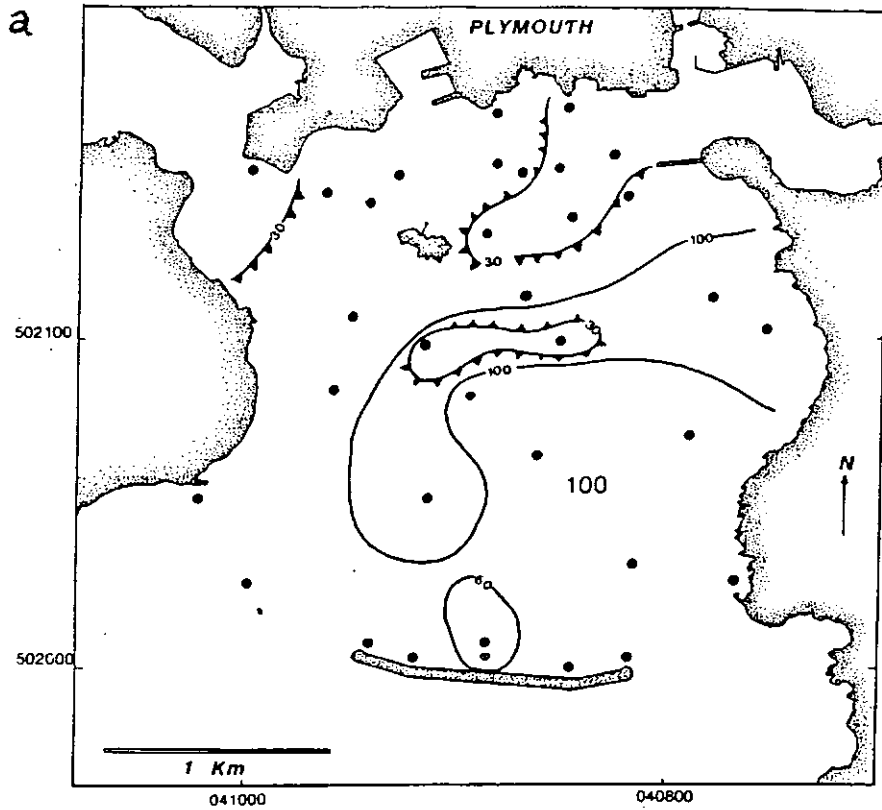


Figure 6.11 Spatial distributions of *in situ* Gravimetric concentrations, High Water (a) 1990 ATM TSM (mg l^{-1}), (b) 1990 ATM TOM (%) (The chevrons indicate the direction of rapid increase in concentration).

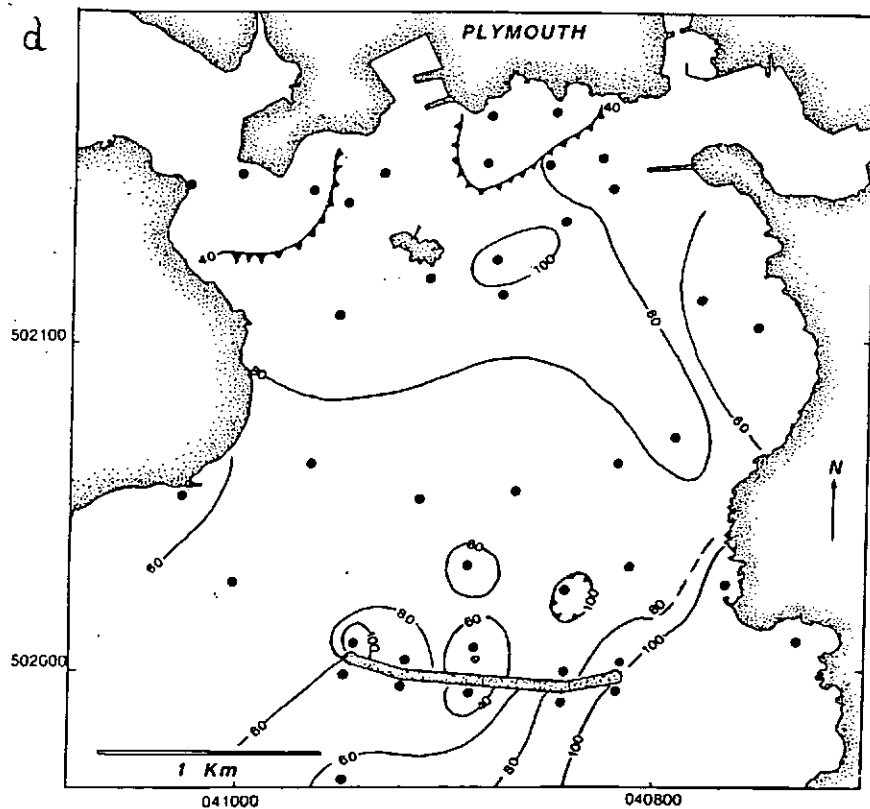
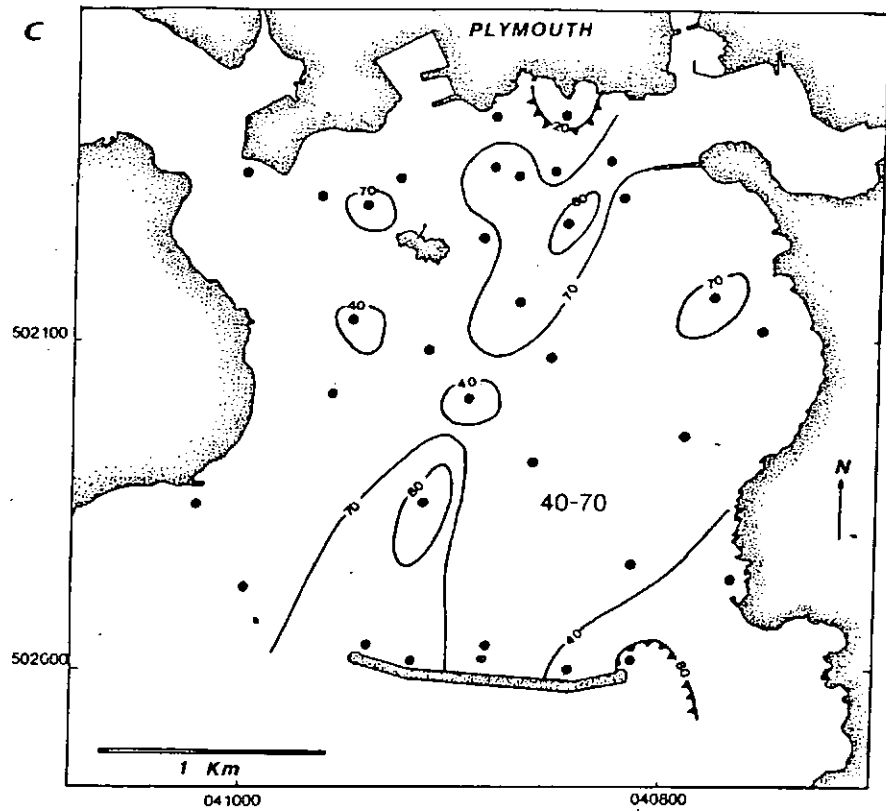


Figure 6.11 cont. Spatial distributions of *in situ* Gravimetric concentrations, High Water (c) 1990 CASI TSM (mg l^{-1}), and (d) 1990 CASI TOM (%) (The chevrons indicate the direction of rapid increase in concentration).

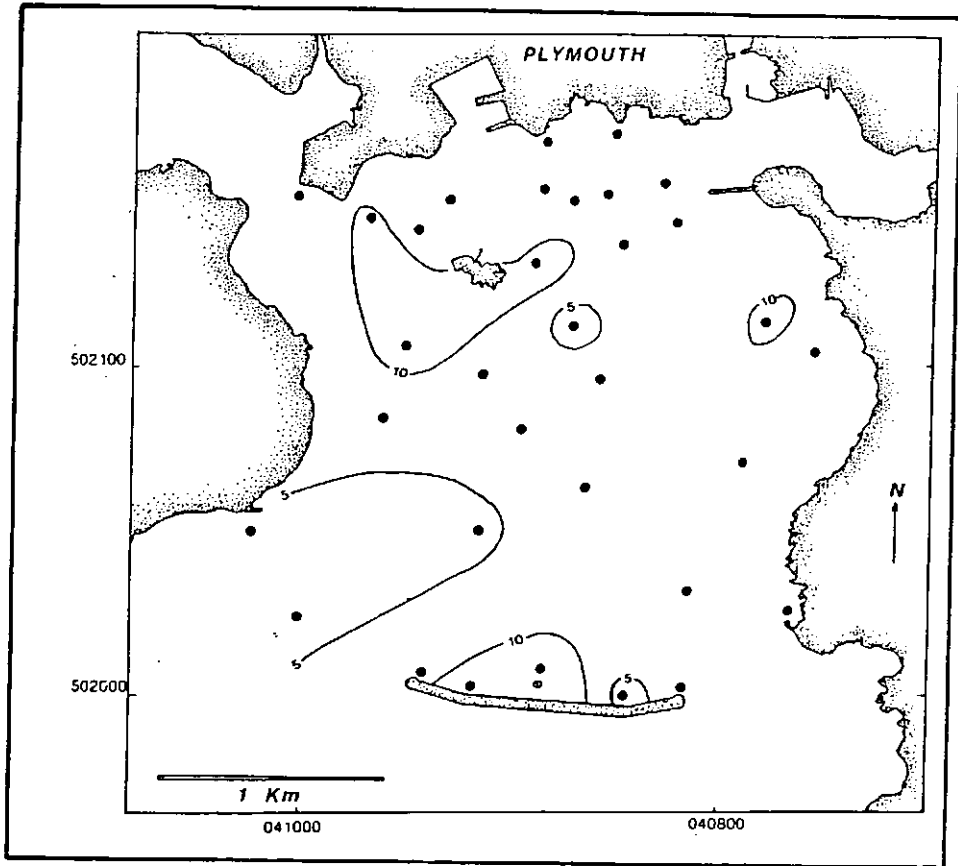


Figure 6.12 Spatial distribution of Chlorophyll- α concentrations at High Water (CASI) in mg l^{-1} .

The TSM concentrations in the water samples acquired during the CASI campaign are presented in Figure 6.11c. The distribution showed the West Hamoaze Channel to have had 40-70mg^l⁻¹ concentrations of TSM with a sharp increase to >80mg^l⁻¹ at the mouth of the Plym. The area around the Hoe showed an isolated concentration (20mg^l⁻¹). The body of the Sound was characterized by TSM concentrations of 40-70mg^l⁻¹, with higher values of TSM northeast of the Western Breakwater. Values of >80mg^l⁻¹ were present at the Eastern Entrance. The TSM concentrations in the Inner Breakwater showed a decrease from 70mg^l⁻¹ at the Centre Fort, to 102mg^l⁻¹ at West Breakwater and 85mg^l⁻¹ at East Breakwater. The TOM percentage distributions (Figure 6.11d) showed high percentages (100%) to occur throughout the Sound and the Hamoaze Channel. The Lower Tamar Estuary and the Plym outflow area were characterized by low TOM percentages (<30%). There were also slight decreases in TOM recorded in Jennycliff Bay (95%), New Ground Buoy (67%) and the Centre Fort (60%).

6.3.2 Chlorophyll- α

Measurements of Chlorophyll- α were made on samples acquired at each station during the CASI overflight. The Chlorophyll- α concentration was established using the method outlined in Section 5.5. The results are presented in Table 6.1 and in Figure 6.12. Values of 5-9 mg^l⁻³ were measured in the Hamoaze Channel and in the body of the Sound. There was a marked increase to >10mg^l⁻³ in the area around Drake's Island and at Dunstone Rock Buoy. The Western Entrance and Fort Picklecombe showed a southward decrease in chlorophyll- α to concentrations of 4mg^l⁻³. Measurements of water samples identified the Inner Breakwater to have had concentrations of 12.30mg^l⁻³ at the Centre Fort decreasing to c. 9.56mg^l⁻³ at the Western End, and to c. 9.06mg^l⁻³ at the Eastern Breakwater site.

6.4 The Imagery

The data available are (i) photographic images of the surface of the water of Plymouth Sound, (ii) re-processed imagery from previous overflights of the Plymouth Sound area, and (iii) the processed Plymouth Sound 1989 and 1990 airborne campaign images. These are all discussed separately, drawing attention to the location of any oceanographic features. The 1989 and 1990 images are considered under two sections: (i) single band thermal (ATM band 11) imagery, and, (ii) visible imagery, including both single band or composite images. The images have all been

geometrically corrected (Section 5.6) contrast stretched and the land signature removed. Both the visible and thermal band images have been calibrated against *in situ* measurements and, in many cases, pseudocoloured to enhance major features present in the imagery.

6.4.1 Aerial and Oblique Photographs

During the last 2 years, many photographs were taken of colour changes in the surface waters of Plymouth Sound. In the mid 1960's the Admiralty commissioned a reconnaissance survey of the South Devon coastline, including a complete set of stereographic aerial photographs of Plymouth Sound and environs. The photographs were kindly lent to the project by H.M. Port Surveyor of the Port of Plymouth. Analysis of both aerial and oblique photographs revealed a number of features, on the basis of changes in colour and visible to the naked eye (Section 5.2). These are discussed in two sections:

Foam lines

Foam lines, on a flooding tide, extend northeastward from either end of the Breakwater, marking the boundary of the dominant tidal streams. These foam lines are present in the aerial photographs, taken concurrently with the ATM and CASI overflights, and are plotted on Figure 6.13a (High Water) and Figure 6.13b (Low Water). Additional foam lines were present in the Admiralty aerial photographs (*Port Foam*) and were observed to have extended c. 500m northward from either end of the Breakwater. A third foam line extended 300m from Bovisand Pier with a $110^{\circ}/290^{\circ}$ orientation. The Low Water Scenario (Figure 6.13b) displayed a marked undulating foam line extending 2000m across the body of the Sound with a $090^{\circ}/270^{\circ}$ orientation approximately parallel to latitude $50^{\circ}20'40''$.

Colour and Hue Changes.

The aerial photographs, taken by the Wild RC-8 are monochrome, but hue changes were visible during the High Water overflights (Figure 6.13a). Well defined changes were observed south of the Breakwater, where the colour changed abruptly from darker hues in the centre to lighter surrounding tones. A similar tonal change was present southwest of Bovisand with a distinct c. 800m boundary with lighter tones to the north. The tonal changes observed on the two Low Water overflight photographs are marked on Figure 6.13b. The 1989 ATM photographs

exhibited two lighter tone water bodies (i) a small 250m diameter oblate body located immediately to the south of West Hoe, and, (ii) an elongate body which extended c. 1000m south of Mountbatten Breakwater. A marked tonal change was also present due west of the Breakwater, where, lighter tones were present to the west of a well defined boundary which extended c. 750m with a $045/225^\circ$ orientation. The 1990 ATM photographs showed three distinct tonal changes in the region of the Breakwater - (i) tones became lighter to the west of a prominent boundary which extended 750m southwest of the Western Breakwater, (ii) lighter tones were present north of a well defined boundary north of the Breakwater, and (iii) tones became lighter north of a boundary which extended northeast from New Ground Buoy. Oblique colour photographs taken on clear days from vantage points around Plymouth Sound showed colour changes. The most remarkable change was observed on an ebbing tide from Mount Edgecombe whilst looking across to Drake's Island (Figure 6.14). A marked change between light blue tones to the north and dark blue tones to the south, were observed, separated by a crenulated boundary which extended from the Island to Raveness Point.

6.4.2 Previous Images

No *in situ* calibrations could be performed on the imagery, as no concurrent groundtruth sets exist. The imagery has been processed so the the lighter tones indicate warmer temperatures and darker tones are cooler. The imagery is presented here and briefly discussed.

1983 Thermal Linescan - Hamoaze Channel.

These images were acquired using a thermal linescan AADS 1230 sensor, which obtains imagery in the thermal band (800-1,400nm) (state of the tide: 1 hour before L.W. neaps)(Roxburgh 1984). The re-processed image (Figure 6.15), shows a warm Tamar surface outflow water plume, which flowed southward along the Cornwall coast, through The Bridges into the body of the Sound. The comparatively cooler body of the Hamoaze Channel was dissected in the north by warm plumes discharging from the sewers along The Hoe. A circular-shaped body of cooler water was present at South Winter Buoy. The Hamoaze Channel system was dominated in the east by the warmer plume of the Plym estuary which can be traced towards the southwest, where it flowed into the body of the Sound and Jennycliff Bay.

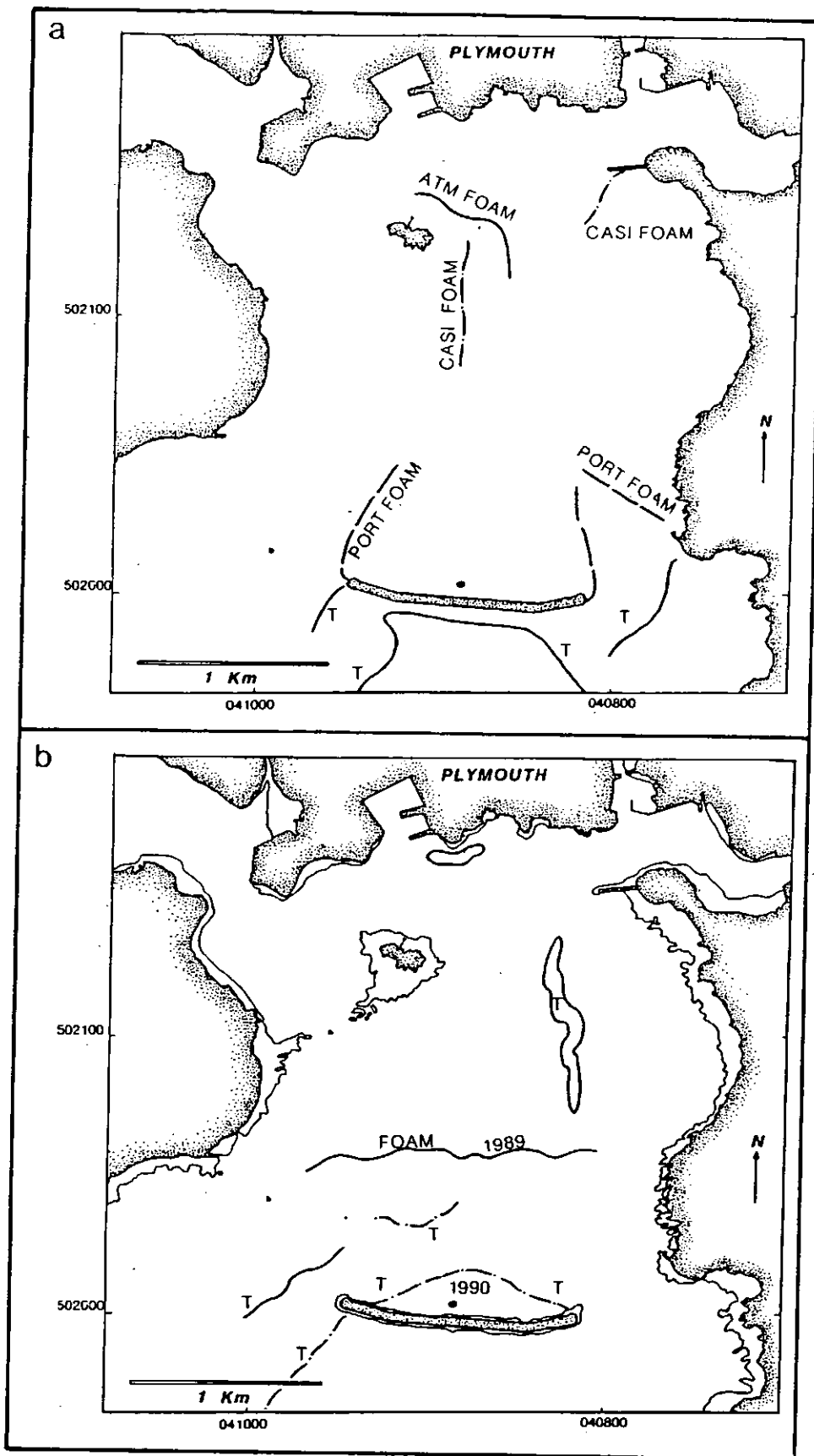


Figure 6.13 Foam lines and visible changes (a) High Water and (b) Low Water, T indicates the increase in hue.

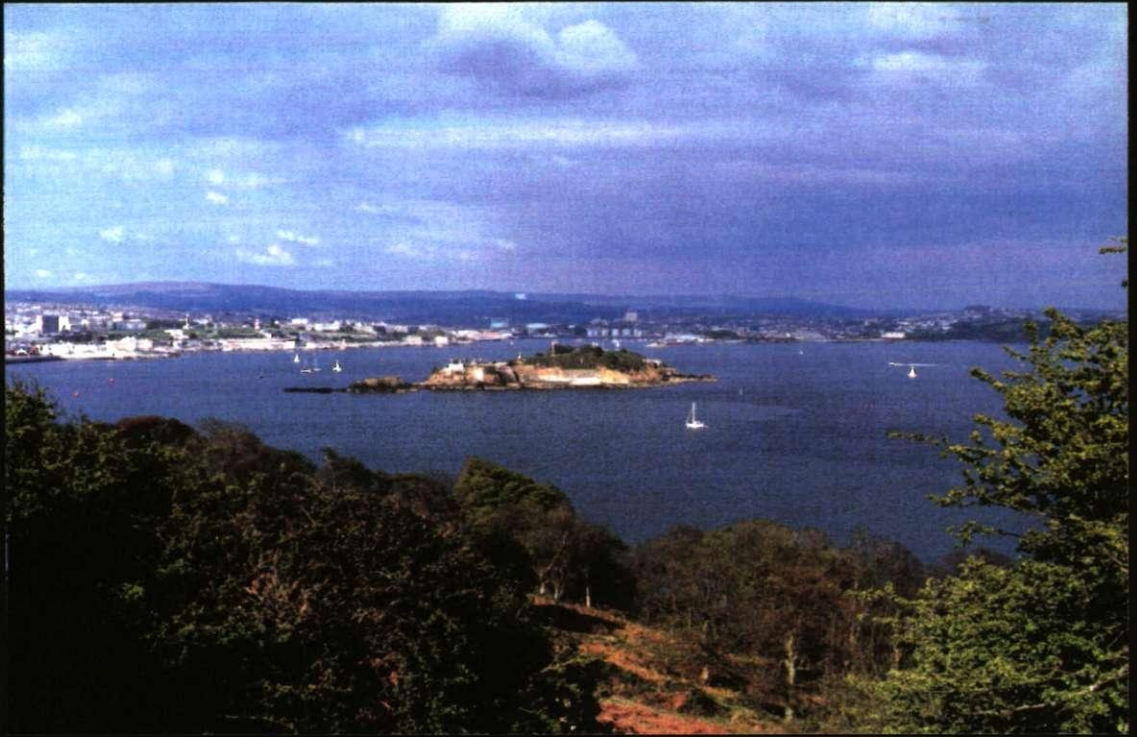


Figure 6.14 The Drake's Island upwelling.



Figure 6.15 Daedalus AADS 1230 a geometrically corrected and contrast stretched thermal image of the Hamoaze Channel.

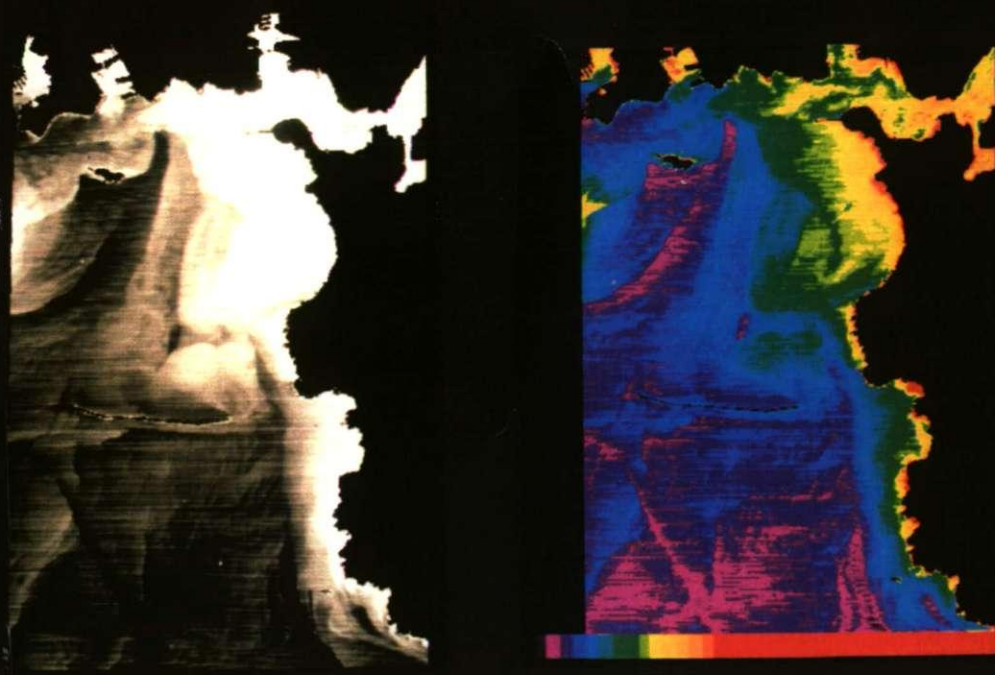


Figure 6.16 Daedalus AADS 1268 12.06.84 (a) a geometrically corrected band 11 contrast stretched image and (b) a pseudocoloured version of the same image (850-1300nm).



Figure 6.17 Daedalus AADS 1268 12.06.84 band 11 contrast stretched image of the gyre system (850-1300nm).



Figure 6.18 Daedalus AADS 1268 19.06.84 (a) band 11 contrast stretched image of the Rame head eddy and (b) a pseudocoloured version of the same image (850-1300m).

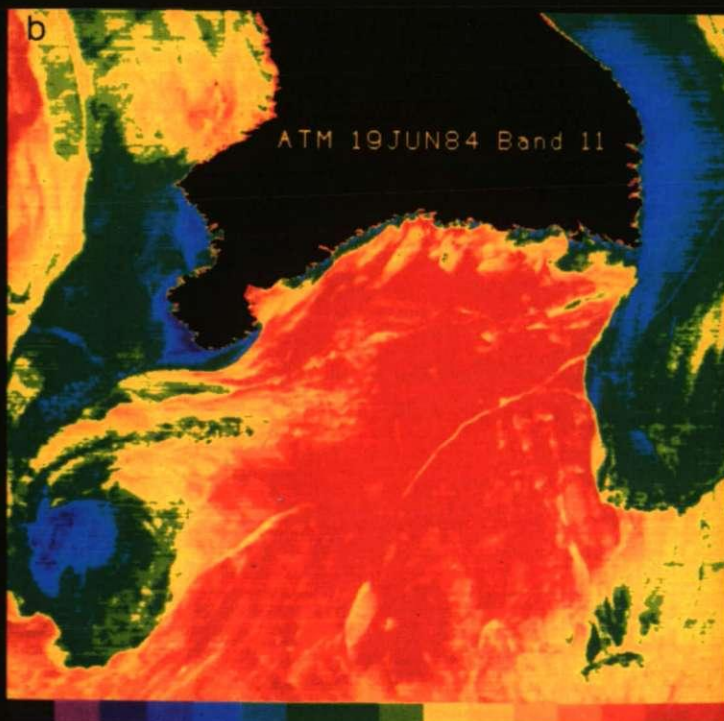




Figure 6.19 ATM 1989 Low Water band II contrast stretched mosaic of Plymouth Sound (850-1300nm).



Figure 6.20 ATM 1989 Low Water band II contrast stretched image of The Bridges (850-1300nm).

The 12.06.84 ATM transmanche image

This imagery was acquired using a Daedalus 1268 Airborne Thematic Mapper. The visible bands suffered severely from sunglint and are not shown here. Figure 6.16a shows a geometrically corrected Band 11 image (Thermal) in which the warm outflow of the Tamar is observed to have flowed along the Cornish coast and through The Bridges. The plume was separated in the east by the cooler waters of the East Hamoaze Channel. A pronounced warm plume was present issuing from the Plym, flowing in an eastward direction into Jennycliff Bay. The Hamoaze waters were separated from those of the Sound by a well defined temperature boundary which linked Drake's Island and Asia Knoll. The surface of the Sound was also observed to have been separated into two distinct temperature signatures by a north-south trending boundary. Figure 6.16b shows a pseudocoloured version of Figure 6.16a. This image illustrates temperature differentiation in the surface waters of the Plym, the Hamoaze Channel and Jennycliff Bay. In the area to the north of the Inner Breakwater, a distinct and spectacular gyre system is observed. This area is magnified in Figure 6.17, where the system is seen to have been composed of two gyres (i) the eastern gyre which had a diameter of c.250m and showed eddies spinning off the margins indicating an anticlockwise direction of gyration, and (ii) the western gyre which had a diameter of 500m, with undulating margins indicating a clockwise direction of gyration. A third anticlockwise gyre was present north of the Eastern Breakwater and separated from the Eastern stream by an eddy (see cartoon). The eastern part of the Western stream showed some turbulent mixing on the margins. The area of the Inner Breakwater showed relatively cool undifferentiated surface water.

The 19.06.84 ATM transmanche image

Although not strictly in the field area, Figure 6.18 shows a spectacular anticlockwise gyre system present to the south of Rame Head.

6.4.3 The ATM Band 11 Images

Analysis of the thermal band of the ATM imagery has been the most successful in the recognition of tidal water bodies. The images, especially those obtained during the 1990 overflights, suffered from "stripiness" caused by variable settings on the CCD array (Section 5.3.1). This does not affect interpretation but the images lose some aesthetic value. The mosaic images, which combine different flightlines and tapes, show distinct borders of the runs. This is due to the

thickness of the Earth's atmosphere and the sensor look-angle and could be avoided by merging the pixel hues, but this would affect a manipulation of the data set.

Low Water Scenario 1989:

A band 11 mosaic of the 1989 flightlines has been contrast stretched (Figure 6.19). Unfortunately, an Admiralty frigate steamed through the Hamoaze Channel minutes before the overflights, the path of which can be clearly seen as it disrupted the thermal stratification (see cartoon). Vessels underway and buoy wakes can also be seen as black striations on the image. The warm plume of the Plym Estuary is seen to have flowed into the Hamoaze Channel and extended westward to Asia Buoy, and southward to South Mallard. An area of cooler water occurs to the south of Drake's Island. The body of the Sound showed two distinct bodies; (i) a warmer western body which extended 2km east of the Cornish coast to a well defined boundary, which separates it from (ii) Jennicliff Bay waters. The path of the Frigate can be seen to pass through the eastern part of the western water body. The southern boundary of this water body was ill-defined and appears to extend parallel to a line from Fort Picklecombe to Ramscliff Point (latitude $50^{\circ}20'40''$). Figure 6.20 shows a magnified image of The Bridges. A cooler water body occurs between the warmer Hamoaze Channel and Western water body. The northern boundary of which was convex northward and the southern boundary was crenulated, showing striations created by water flowing between the cement blocks of the derelict Bridges Pier. Figure 6.21 shows a close up image of the East Hamoaze Channel where two indistinct ship's wakes are seen to cross the image diagonally (0-0). In the plume of the Plym and the warm western body of Plymouth Sound the wakes are relatively undisturbed by surface water motion and are well preserved. However, in the Central Channel the wakes showed disruption, indicating water movement towards the southwest. A zone of mixing can also be seen in the northern boundary of the plume of the Plym. Cool and warm water discharges can be seen issuing from the Plymouth Limestone along The Hoe; the colder discharges are the "Millbay Blue Holes", identified by Roxburgh (1983, 1984 and 1985), and the warm bodies are related to effluent derived from the sewer system. The surface water of Jennicliff Bay showed a series of longitudinal features extending c. 500m with a $020/200^{\circ}$ orientation and variable spacing. Parallel longitudinal features were also present in the area of the Inner Breakwater and extended 300-500m with a $135/325^{\circ}$

orientation. Two well defined warm eddies were present spinning southward off either side of the Breakwater. The Western eddy had an oblate shape with a circumference of 800m and a well defined northern boundary. The eastern eddy was much smaller, with a circumference of 250m, and extended southwestward where it developed into a frontal system separating warmer from cooler waters. The Western Entrance showed several elongate features with a spacing of *c.* 100m, discrete lengths of *c.* 1 km, and well defined turbulent mixing on their margins. A pseudocoloured calibrated version of the 1989 ATM Band 11 mosaic is shown in Figure 6.22. This illustrates an overall temperature variability of 1°C. Horizontal temperature variability occurred in the Tamar Estuary where the southward-deflected channels of St. John's Lake and West Mud showed temperatures 0.4°C warmer than the water flowing down the Estuary. The Hamoaze Channel had 0.2°-0.4°C differences between the cooler northern and southern waters. The outflow from Millbay Docks was relatively cool in comparison with the surrounding waters. This is the discharge from a distributary from the Mediaeval Mill Lake river, now an underground conduit. The river is marked on pre-1800 maps of the city of Plymouth. The image enhances horizontal differentiation in the area of the Inner Breakwater, where several distinct cooler "spots" of *c.* 40m diameter are present. Two circular features were present at Delta Buoy and west of Charlie Buoy (see cartoon), with diameters of 250-300m and temperatures 0.2°C cooler than the surrounding waters. A ship's wake dissects the centre of the Western water body and caused disruption of the thermal stratification, showing a difference of 0.4°C between the warmer sub-surface waters in the north and the cooler southern waters. Linear features are present in Cawsand Bay with a 045/225° orientation.

Low Water scenario 1990:

The 1990 Low Water Band 11 mosaic of flightlines 1, 2 and 3 is presented in Figure 6.23. The image shows the warm plume of Tamar to have flowed into the cooler waters of the Hamoaze Channel, from which it was separated by a distinct curved boundary extending from Devil's Point to Drake's Island. The warmer waters of the Tamar can also be discerned to have flowed southward through The Bridges and along the Cornish coast to Fort Picklecombe. The Hamoaze Channel showed three linear warmer bodies of water of variable length and trending east-west with widths of *c.* 40m. The plume of the Plym displayed a well defined eastern boundary against the cooler water of the Hamoaze Channel. The body of the Sound showed a

clearly defined front which extended southeastward from Drake's Island to 250m north of the Eastern Breakwater, where it abruptly deflected towards the west and terminated at the Western End of the Breakwater. This front separated warmer water in the west from cooler waters in the east. The area of the Inner Breakwater showed two spin-off eddies at either end. The eastern eddy extended 500m to the southwest and the western eddy extended c. 450m south-southwest. The Outer Breakwater area showed a continuation of the Sound frontal system, which extended 1000m east of Penlee Point to the edge of the image. The Outer Breakwater area also showed a distinct front separating warmer water adjacent to the Breakwater from cooler waters at Panther Rocks. Cawsand Bay exhibited a decrease in temperature from the south to the cooler temperatures to the north and Fort Picklecombe. The area immediately adjacent to Penlee Point showed cooler waters from the coast to a crenulated eastern boundary c. 50m offshore. Figure 6.24 shows a pseudocoloured magnified band 11 image of the Eastern Hamoaze Channel in which the green colours are cooler and the yellows are warmer. The southern margin of the Plym outflow can be seen to have flowed into Jennicliff Bay in an extended plume composed of a series of cusped turbulent mixing bodies. The margin of the front in the Sound showed a well defined boundary against the Hamoaze outflow, with very little turbulent mixing. Figure 6.25 shows a pseudocoloured calibrated image of the Figure 6.23, in which the Lower Tamar Estuary displayed horizontal temperature differentiation in which the western bank was c. 0.2°C warmer than the eastern bank. The outflow from Millbay Docks was warmer than the surrounding waters. The plume of the Plym and the area around The Hoe are separated by body of water which was c. 0.3°C cooler than that of the Hamoaze Channel. The combined waters of the Hamoaze Channel can be traced into Jennicliff Bay and towards the Inner Breakwater. The Inner Breakwater showed warm temperatures at the Western end and an eastward decrease in temperature. The waters around Bovisand Bay showed warm temperatures (>15.5°C).

High Water Scenario 1990:

The High Water band 11 uncalibrated image mosaic (Figure 6.26) shows the warm waters of the Lower Tamar to have flowed southward and abruptly terminate at Devonport where they met the cooler Hamoaze waters. The mud flats of St. Johns Lake and West Mud can be seen to have been dissected by cooler water channels. The discharges through Millbay Docks had distinctive warm signatures and illustrated some plume deflection

up-estuary. The waters immediately adjacent to the coast at Devil's Point and Eastern King showed small *c.* 20m diameter cooler outflows. The plume from the Plym estuary was well defined and appeared to be deflected westward into the Hamoaze Channel. The area of The Bridges showed a cooler body of water which retained its identity as far south as Fort Picklecombe. The body of the Sound was divided by a distinctive northeast-southwest frontal system extending from South Winter Buoy to 200m north of New Ground Buoy, where it was deflected towards the Eastern Breakwater. The southern margin of this front showed no mixing whereas the eastern margin showed turbulent mixing. The water body to the west of the front was characterized by cooler temperatures than those of the east. Two eddies were present and observed to spin southward off either end of the Breakwater (i) the western eddy was clearly defined and had a diameter of *c.* 500m, and (ii) the eastern eddy was heavily dissected by ship's wakes, it appears to have retained its identity 1000m south of the Breakwater. The waters of the Inner Breakwater area showed an increase in temperature towards the west. The Western Entrance and Cawsand Bay showed a well defined frontal system trending north-south separating a warm undifferentiated water body in the west from cooler eastern waters. The area to the south of the Breakwater displayed cooler waters adjacent to the centre of the Breakwater dissected by a stream of warmer water extending from the Western end south-eastward to the edge of the image. Figure 6.27 illustrates a pseudocoloured calibrated Band 11 mosaic showing a temperature variation of 2.0°C over the image. The intertidal water covering the mud flats in the Lower Tamar Estuary showed a +1°C difference when compared to the surrounding waters. The warm waters of the Lower Tamar Estuary showed a cooler stream to be present along the Cornish coast. The eastern and western bodies of water in the Sound showed a 1°C decrease westward. The area of the Inner Breakwater showed a cool "spot" 750m due north of the Centre Fort with a diameter of *c.* 250m.

6.4.4 ATM Visible Images

The visible bands (400-700nm), of the ATM imagery capture the spectral signatures of the total suspended and organic material, and all sunglint present in the surface waters. Several attempts were made to remove the sunglint by implementing algorithms developed for Coastal Zone Colour Scanner imagery. These algorithms either failed to improve the images or resulted in processing artifacts. Where possible, the images with least

sunlint have been calibrated against the *in situ* TSM mg l^{-1} concentrations.

Low Water Scenario 1989:

The 1989 ATM flightline 2, which covered the western part of Plymouth Sound, suffered severely from sunlint and has not been used. To evaluate the different components of the suspended sediment and the dominant contributor to the inlet, the visible bands were examined separately. The area to the northeast of the Breakwater (Flightline 1) had least sunlint, and was chosen as a test site. The images were uncalibrated, but, the lighter tones (i.e. Brighter pixel DN) correspond to higher concentrations of suspended material. Figure 6.28 shows an uncalibrated band 2 image displaying TSM with a spectral signature between 450-520nm. The highest concentrations of TSM were present in the western part of the image. The image also showed a marked crenulated linear feature which extended 900m and had a maximum width of *c.* 10m. The waters of the Inner Breakwater showed an increase in brightness northward to 200m offshore and westward to *c.* 350m offshore. The area immediately adjacent to the coast from Ramscliff Point to Bovisand Bay, and south of the Outer Breakwater, also demonstrated high TSM concentrations. Figure 6.29 is a band 3 uncalibrated image showing the concentration and distribution of TSM with a spectral signature of 520-600nm. High concentrations were in the area to the northwest of the Breakwater and west of the image. The lowest concentrations occurred southeast of the Eastern Breakwater in a large semi-circular water body with a diameter of *c.* 300m. Differentiation of TSM is seen in Bovisand Bay and the areas adjacent to the coast where the concentrations increased shoreward. Figure 6.30 is a band 4 image (605-625nm) showing high concentrations west of the Centre Fort and in the water adjacent to the coast. On the basis that the Band 3 image (Figure 6.29) showed the greatest differentiation of TSM, in comparison to the other bands, it was used to calibrate the imagery against the *in situ* TSM measurements. Figure 6.31 shows a Band 3 calibrated and pseudocoloured image of the eastern part of Plymouth Sound. The image illustrates high concentrations ($>100\text{mg l}^{-1}$) to be present in an east-west trending belt with a width of 50-200m in the centre of the Hamoaze Channel. This belt has well defined boundaries and the TSM values decreased to either side; to 60mg l^{-1} to the south and $<10\text{mg l}^{-1}$ to the north. The image shows TSM concentrations decreasing towards the centre and south towards the Outer

Eastern Breakwater area. A distinct boundary was present and extended northward in an arc from Charlie Buoy to Melampus Buoy, where it deflected southeastward into Jennycliff Bay and met the mainland at Ramscliff Point. This boundary showed some mixing on the margins and separated TSM concentrations of $>50\text{mg l}^{-1}$ to the north from values of 40mg l^{-1} .

Low Water Scenario 1990:

The 1990 ATM Low Water band 3 images showed the best spatial and concentration contrasts of TSM. Figure 6.32 shows a pseudocoloured band 3 image of flightline 1. The high concentrations of TSM are coloured red and low concentrations are blue. The image suffered too much sunglint to calibrate against the *in situ* measurements. The plume of the Plym extended *c.* 250m into the Hamoaze Channel, where it terminates at an abrupt boundary. The body of the Sound showed little overall differentiation of TSM, with the exception of the Inner Breakwater area in which a triangular shaped body of water is present. This body has low concentrations of TSM and its western margin is clearly defined, although, the eastern margin shows some mixing. High concentrations were present in Bovisand Bay and due south of the Eastern Breakwater. Figure 6.33 shows a pseudocoloured image of flightline 2. Again, red colours show the highest TSM concentrations and blues show low concentrations. The highest concentrations of TSM were present in the Lower Tamar Estuary, where they appear on the northeastern bank. The Bridges are shown to have been characterized as areas of low concentrations of TSM. The western side of the Sound, again, shows little differentiation of TSM. An area of low TSM was present to the west of the Western End of the Breakwater. This patch was kidney-shaped with a long diameter of 300m, and a short diameter of *c.* 200m. A well defined front was present extending from the Western End of the Breakwater, southwestward to the edge of the image, *c.* 500m offshore from Penlee Point. The image also shows sunglint (see cartoon).

High Water Scenario 1990:

The 1990 ATM visible bands were again processed separately, using the area of the Inner Breakwater, which suffered minimal sunglint, as a test site. Figure 6.34 illustrates a Band 2 (450-520nm) mosaic of flightlines 2 and 3. The image is dissected by several ship's wakes in which the ships themselves are clearly visible. The highest TSM concentrations

were located to the west of Ramscliff Point and the east of Fort Picklecombe. An area of low TSM concentrations occurred in an elongate body 500m west of the Western Breakwater. The water signature to the south of the Breakwater showed low concentrations of TSM separated from the surrounding waters by two fronts: (i) extending from the Outer Breakwater steps southeastward to the end of the image, and (ii) a circular eddy extends *c.* 450m south of the Breakwater where it meets a southern front. Figure 6.35 shows an uncalibrated Band 3 (520-600nm) image of the same area. The image shows greater differentiation of TSM in both the body of the Sound and the waters around the Breakwater. Two eddies are clearly defined spinning off either end of the Breakwater, their zones of influence can be seen to extend 600m south of the Breakwater. The eddies showed well defined boundaries between the turbid inlet waters and the less-turbid marine water located outside the Breakwater. Figure 6.36 shows band 4 (605-625nm) mosaic. The distribution and concentrations of TSM are less well defined in comparison to those observed in band 3. The image does, however, illustrate the same distribution patterns as the other two bands. On the basis that band 3 displayed the greatest differentiation, it was used to show TSM variability over the whole of the Sound (Figure 6.37). The image exhibits high concentrations of TSM to have been present in the estuaries of the Plym and Tamar. The Tamar plume retains its identity to a poorly defined line running due south from Devil's Point. The plume from the Plym Estuary is seen to terminate abruptly, 500m west of Mountbatten Breakwater, in a front extending from the Swimming Pool to South Winter Buoy. The waters adjacent to the coasts showed high concentrations of TSM.

6.3.5 The CASI Images

The CASI airborne campaign data tapes proved to be the largest disappointments of the project. The tapes did not arrive in Plymouth until 20.06.91. It was then found that the desired bands had not been selected and those selected by the operator "missed" the kaolinite and montmorillonite spectral peaks. Only preliminary processing has been applied to the data which includes geometric correction, removal of the land signature and contrast enhancement techniques. All the data suffer from extreme "Stripiness" where the the individual elements of the CCD array have various gain settings or ice crystals of the cooling fluid (liquid nitrogen) have build up on the sensor head during the flights.

In order to fly in the both spatial and spectral mode, the aircraft had to fly at 3000m, - this caused a reduction in resolution.

The Western Entrance was used as a test site to briefly show the differentiation of TSM. The brighter tones correspond with higher values of TSM in the individual spectral bands. Sunlint on the Ship's wakes are clearly discerned on all of the images. The Band 1 (436-473nm) image (Figure 6.38) displays high concentrations of TSM to have been present close to the shore at Fort Picklecombe and in the area around the Breakwater. The concentrations decreased towards the centre of the image. The Band 2 (540-551nm) image (Figure 6.39) showed less differentiation of TSM, with the highest concentrations occurring to the north of a line drawn from Fort Picklecombe to the southeast of the image. The Band 3 (586-595nm) image (Figure 6.40) showed high concentrations of TSM to the north of the Inner Breakwater, separated by a distinct curved boundary which extended northward from the Western End of the Breakwater. A second frontal system was evident in the centre of the Western Entrance with high values of TSM present in the west. The Band 4 (634-642nm) image (Figure 6.41) showed the same features that were present in Band 3, however, the differentiation was well defined. The Band 5 (661-670nm) image (Figure 6.42) displayed high concentrations of TSM in a belt which extended c. 500m off the Cornish mainland. The Band 6 (679-686nm) image (Figure 6.43) showed similar high concentrations of TSM adjacent to the coast, high concentrations in the waters of the Inner Breakwater. The Band 7 (709-715nm) image (Figure 6.44) displayed high concentrations of TSM to c. 300m offshore from Fort Picklecombe, and around the Breakwater. The concentrations decreased over a short distance and became almost negligible in the area to the south of the Western Entrance. The Band 8 (746-765nm) image (Figure 6.45) showed high concentrations of TSM in the areas adjacent to the shore and around the Breakwater, and a decrease towards the southwest. Figure 6.46 shows an uncalibrated Band 2 image of the Central Hamoaze Channel and Drake's Island. A distinct front was present extending 100m northwest of Drake's Island towards Asia Knoll, separating higher concentrations of TSM in the north from lower concentrations in the south. A second front was defined and extended from Melampus Buoy to Asia Knoll, with high TSM concentrations present to the east.

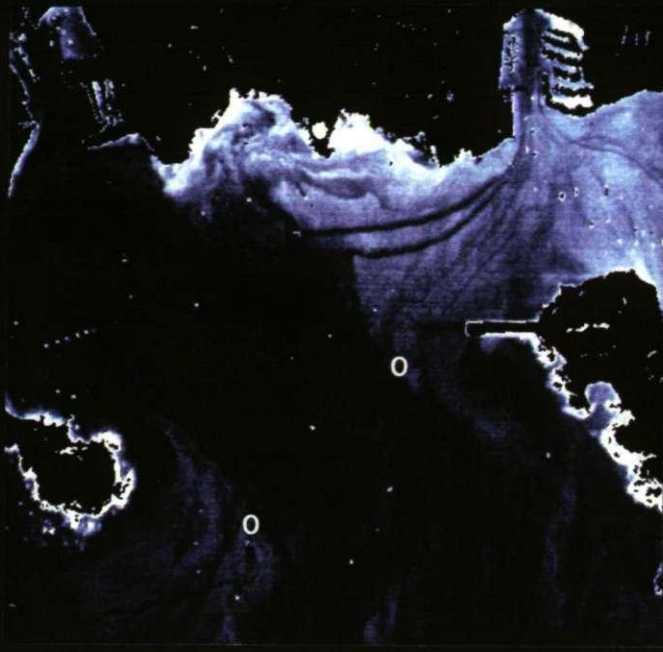


Figure 6.21 ATM 1989 Low Water band II contrast stretched image of the East Hamoaze Channel with the ship's wakes (marked 0-0) (850-1300nm).

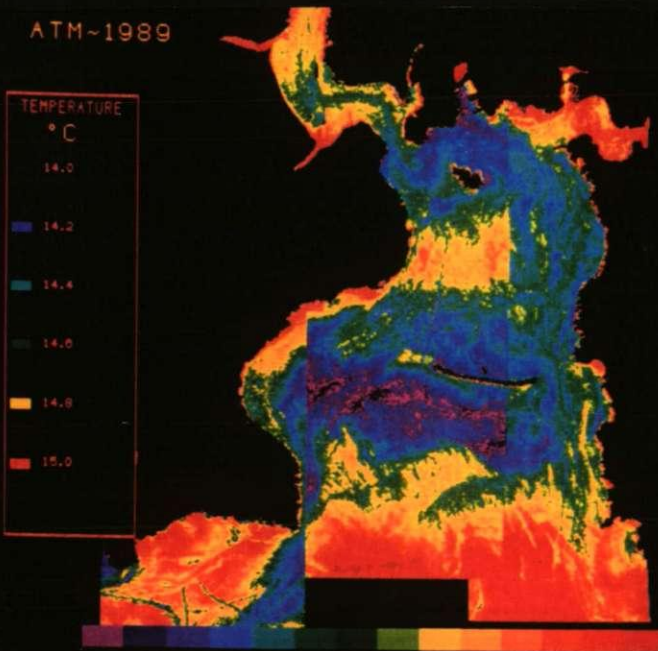


Figure 6.22 ATM 1989 Low Water band II pseudocoloured, calibrated mosaic image of Plymouth Sound (850-1300nm).

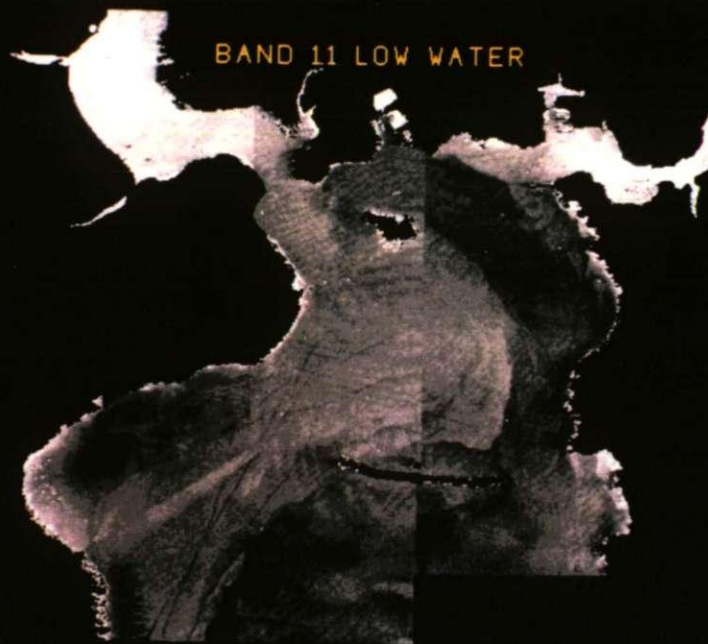


Figure 6.23 ATM 1990 Low Water band 11 contrast stretched mosaic of Plymouth Sound (850-1300nm).

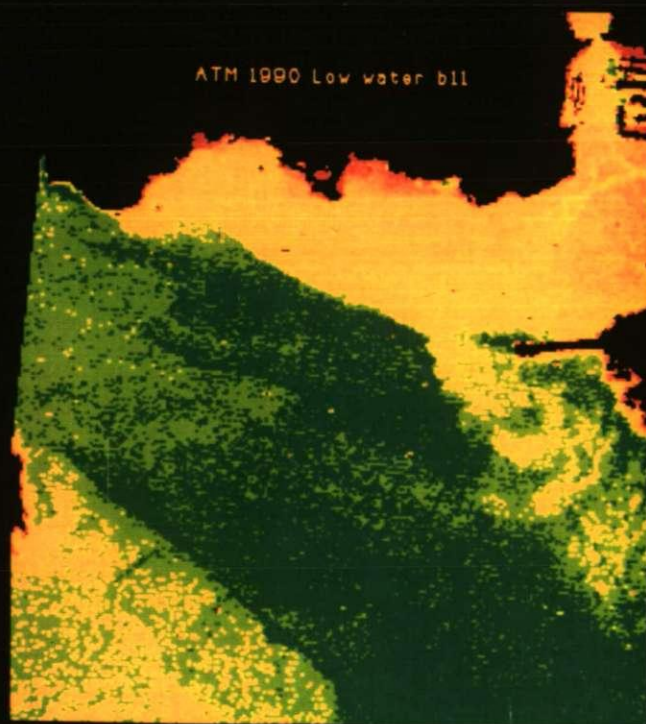


Figure 6.24 ATM 1990 Low Water band 11 pseudocoloured image of the East Hamoaze Channel where green = cool and yellow = warm temperatures (850-1300nm).

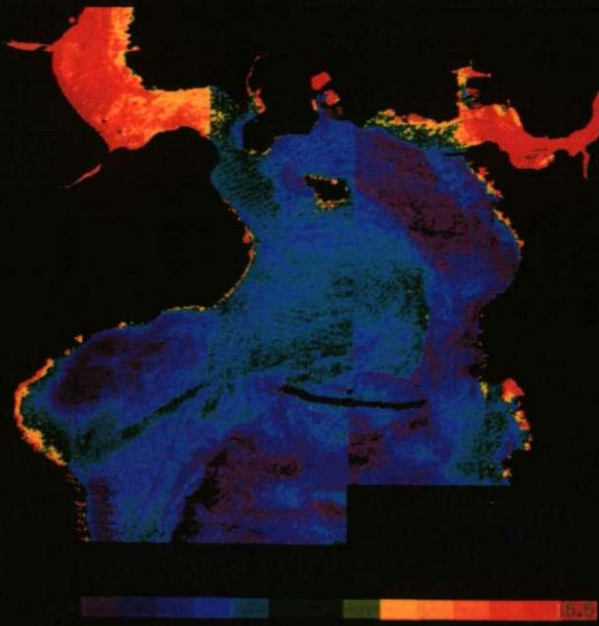


Figure 6.25 ATM 1990 Low Water band 11 pseudocoloured calibrated mosaic of Plymouth Sound (850-1300nm).



Figure 6.26 ATM 1990 High Water band 11 contrast stretched mosaic of Plymouth Sound (850-1300nm).

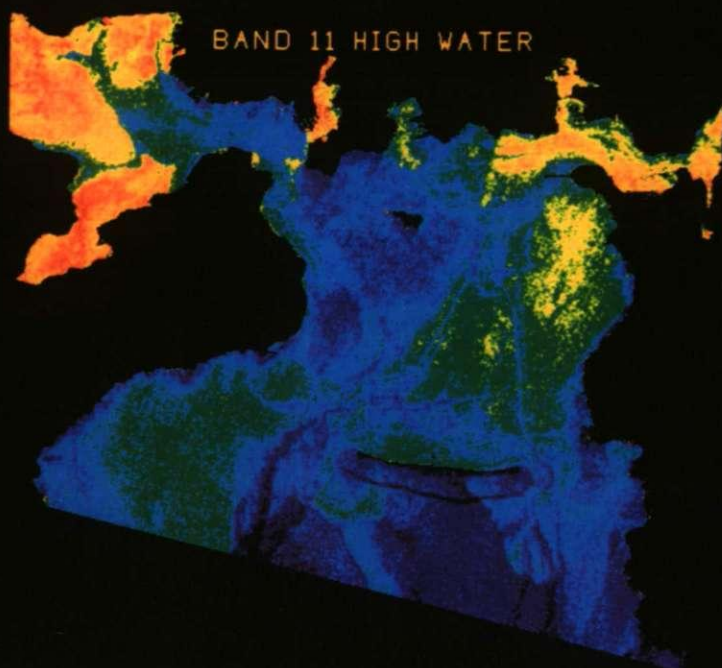


Figure 6.27 ATM 1990 High Water band 11 pseudocoloured mosaic Plymouth Sound (850-1300nm).



Figure 6.28 ATM 1989 Low Water contrast stretched band 2 image of the Eastern Entrance (450-520nm).



Figure 6.29 ATM 1989 Low Water contrast stretched band 3 image of the Eastern Entrance (520-600nm).



Figure 6.30 ATM 1989 Low Water contrast stretched band 4 image of the Eastern Entrance (605-625nm).

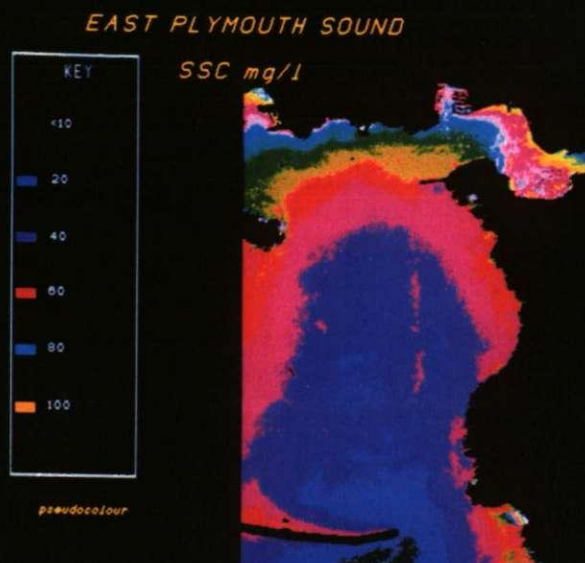


Figure 6.31 ATM 1989 Low Water band 3 pseudocoloured calibrated image of East Plymouth Sound (520-600nm).

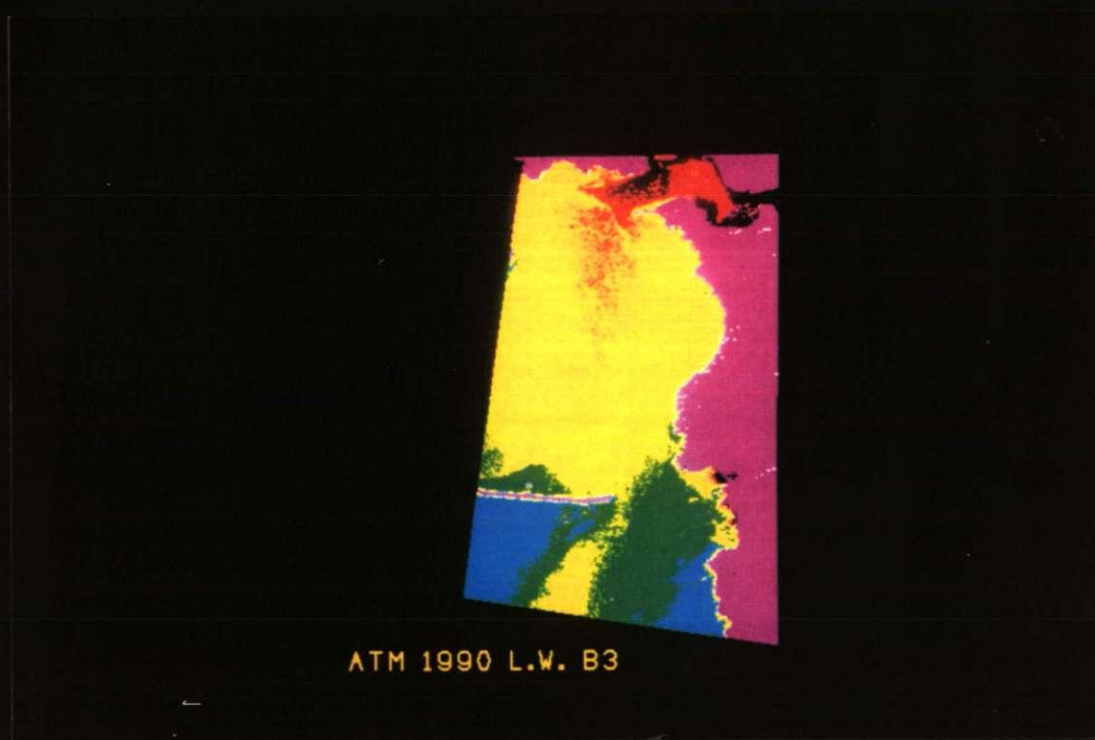


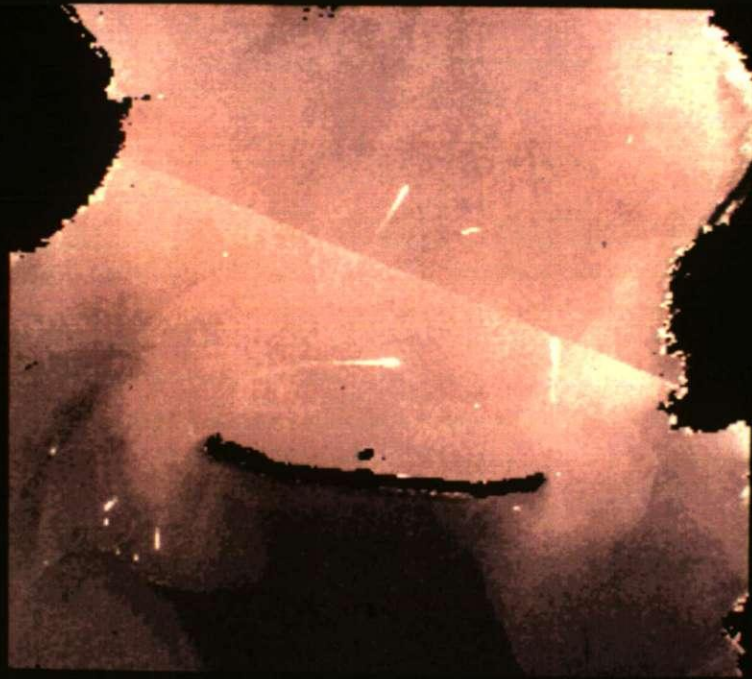
Figure 6.32 ATM 1990 Low Water band 3 pseudocoloured image of East Plymouth Sound (Flightline 1) (520-600nm).



Figure 6.33 ATM 1990 Low Water band 3 pseudocoloured image of East Plymouth Sound (Flightline 2)(520-600nm).

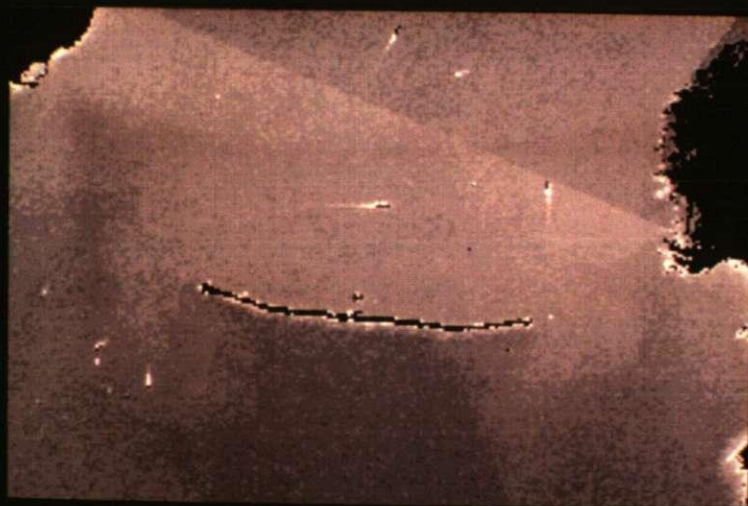


Figure 6.34 ATM 1990 High Water contrast stretched band 2 image of the Breakwater (450-520nm).



ATM 1990 H.W b.3

Figure 6.35 ATM 1990 High Water contrast stretched band 3 image of the Breakwater (520-600nm).



ATM 1990 H.W b.4

Figure 6.36 ATM 1990 High Water contrast stretched band 4 image of the Breakwater (605-625nm).



Figure 6.37 ATM 1990 High Water contrast stretched band 3 mosaic of Plymouth Sound (520-600nm).



Figure 6.38 CASI 1990 High Water band 1 contrast stretched image of the Western Entrance (436-473nm).

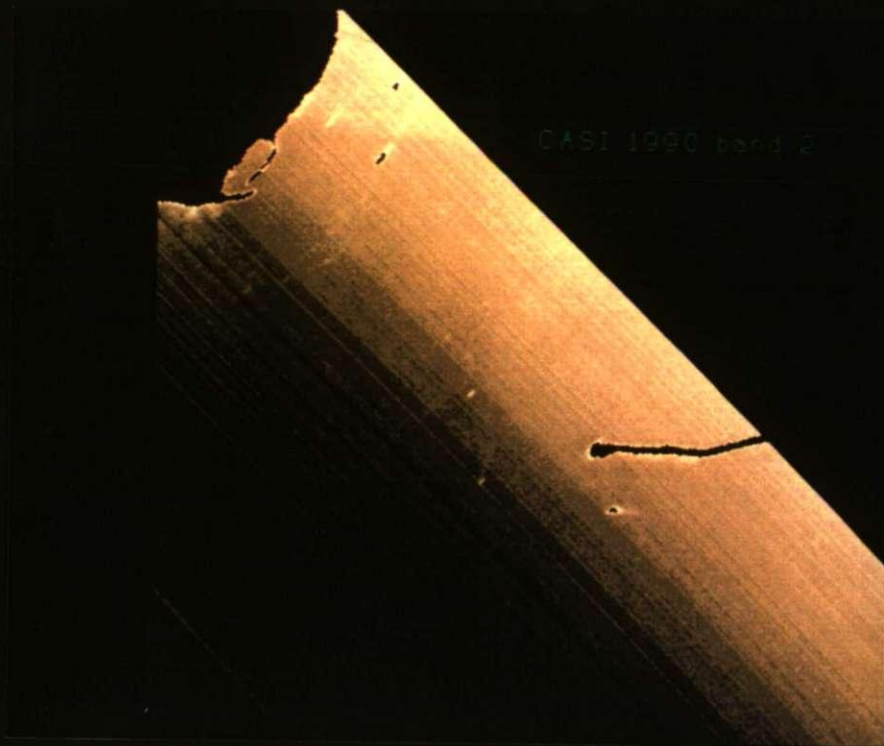


Figure 6.39 CASI 1990 High Water band 2 contrast stretched image of the Western Entrance (540-551nm).

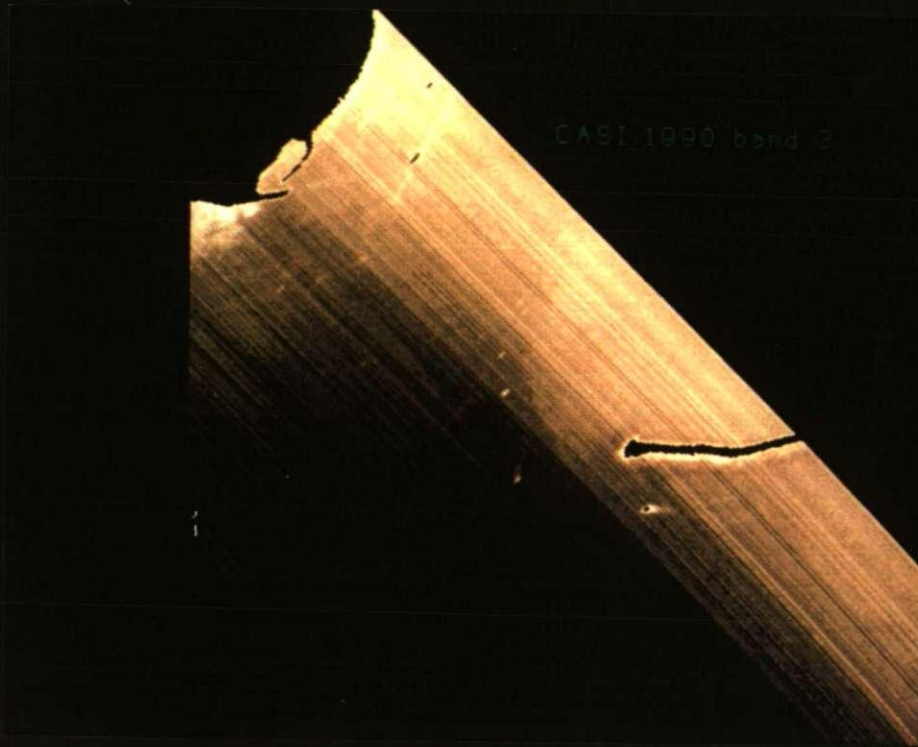


Figure 6.40 CASI 1990 High Water band 3 contrast stretched image of the Western Entrance (586-595nm).

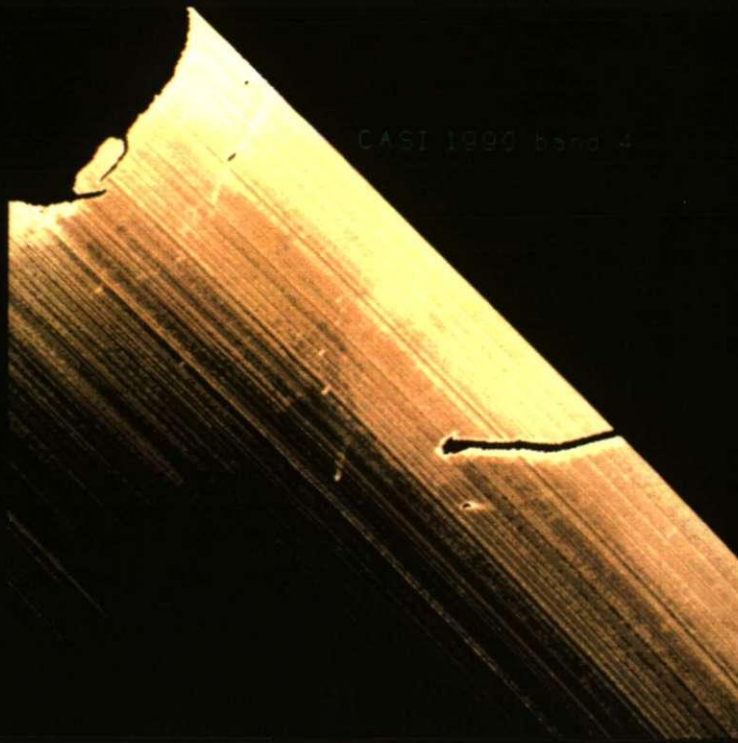


Figure 6.41 CASI 1990 High Water band 4 contrast stretched image of the Western Entrance (634-642nm).

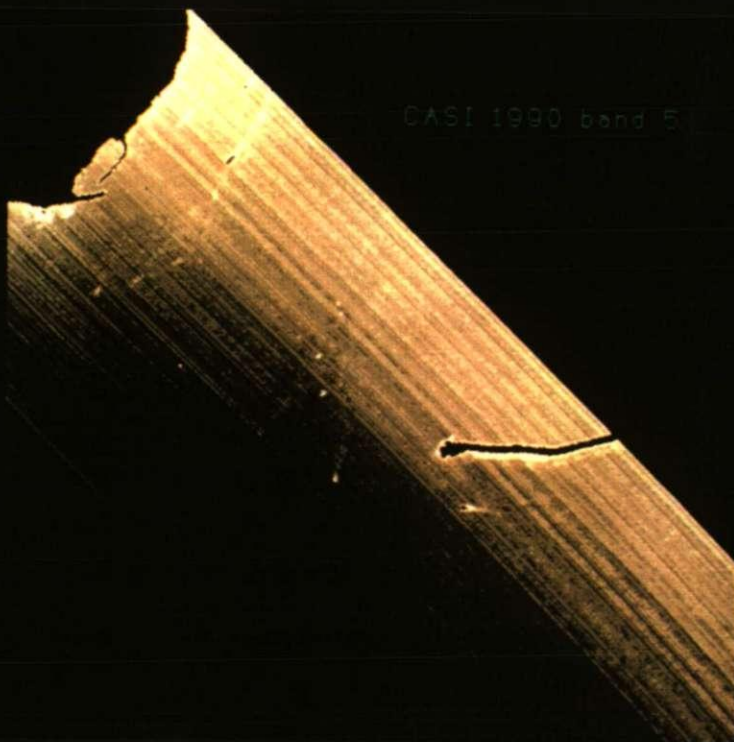


Figure 6.42 CASI 1990 High Water band 5 contrast stretched image of the Western Entrance (661-670nm).

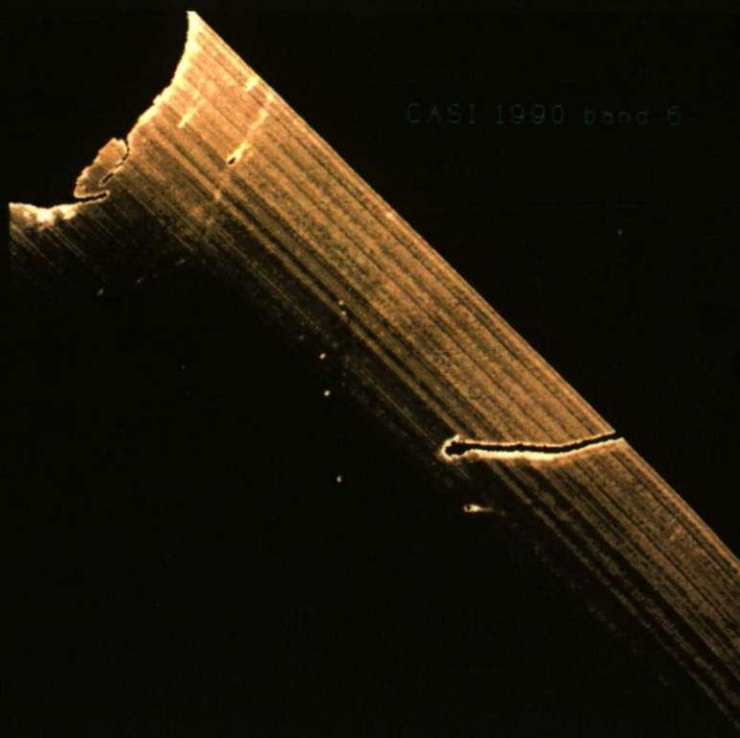


Figure 6.43 CASI 1990 High Water band 6 contrast stretched image of the Western Entrance (679-686nm).

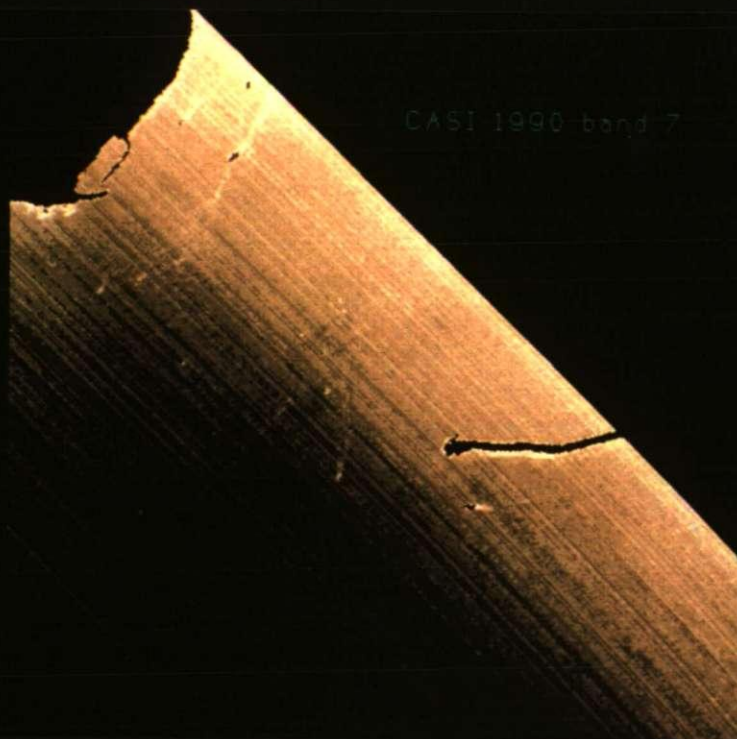


Figure 6.44 CASI 1990 High Water band 7 contrast stretched image of the Western Entrance (709-715nm).

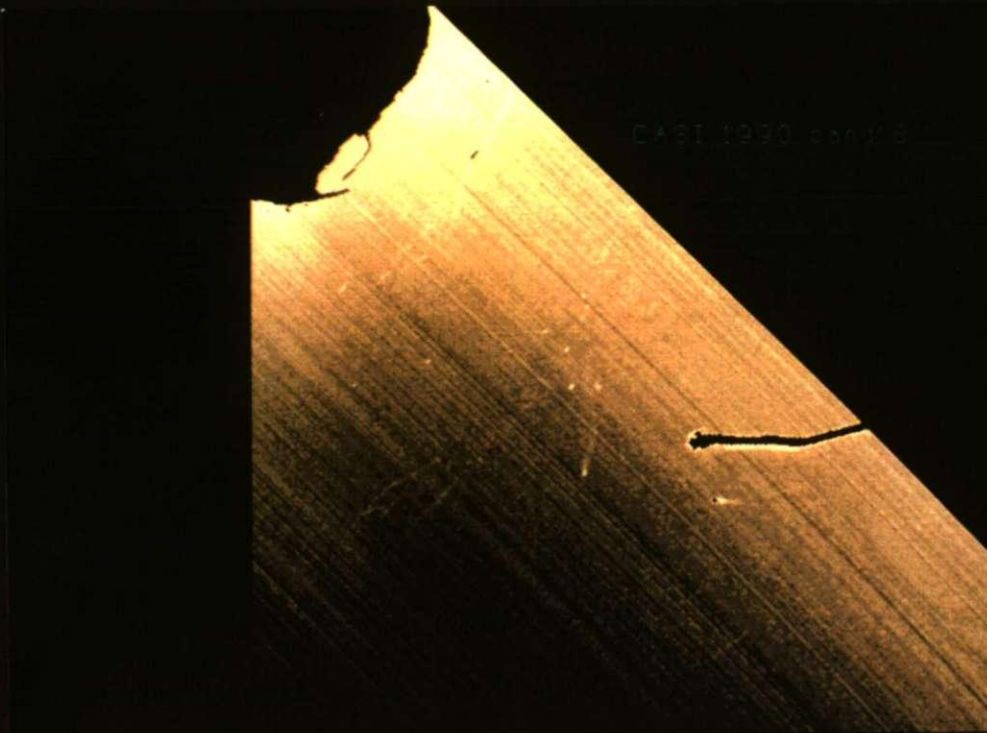


Figure 6.45 CASI 1990 High Water band 8 contrast stretched image of the Western Entrance (746-765nm).



Figure 6.46 CASI 1990 High Water band 2 contrast stretched image of the Central Hamoaze Channel (540-551nm).

- CHAPTER SEVEN -

- MAGNETIC MEASUREMENTS -

7.1 Introduction

Magnetic measurements can be divided into two disciplines - susceptibility and remanence (i) The quantity of magnetic carriers in sediments can generally be estimated from their susceptibility and their petrographic fabric can be evaluated from the anisotropy of magnetic susceptibility. Studies of the magnetic fabric of sediments were first published by Ising (1943) and advances in microprocessor technology have substantially shortened the measuring processes, making the measuring of magnetic fabric a quick and relatively cheap method (Hrouda 1982). (ii) The natural remanent magnetization (magnetic remanence) of sediments is conventionally divided into two components (Tarling 1983): primary remanence which is acquired during or soon after deposition of the sediments; and secondary remanence which is acquired later (e.g. post-depositional remanence). Under favourable conditions these can be separated by partial demagnetization procedures.

In this study there were several objectives:

- (i) to determine the intrinsic magnetic characters of different sedimentary environments, particularly those delineated using side-scan sonar (Section 3.6),
- (ii) to investigate whether the anisotropy of magnetic susceptibility could be used to establish the nature of the deposition and define the type-fabric of the sediments, and hence give an indication of the rate of sedimentation, and of the stability of the sediment in the presence of different disturbing forces,
- (iii) to see if anisotropy could be used to evaluate the prevailing hydrodynamic regimes and thus establish any residual current directions in the region of the gyres, tidal fronts etc., as identified on the ATM images (Section 6.4),

- (iv) to study the magnetic effect of the endobenthic biological community on primary sediments. The character of these communities (feeding, defecation, locomotive or dwelling) in a sediment gives a good indication of both the rates and types of depositional forces, which may be reflected in fabric and/or remanence measurements in both time and space,
- (v) to study the effects of overburden compaction on the inclination of remanence, and investigate the time/depth of acquisition of detrital remanence,
- (vi) to investigate authigenic changes in both the remanence and susceptibility measurements produced during methanogenesis and,
- (vii) to identify the optimum physical properties for future study in subtidal unconsolidated sediments.

7.2 Sampling

Previous studies of the susceptibility of unconsolidated sediments have tended to be on sub samples of large box cores or laboratory based experiments. The Inner Breakwater depocentre (Section 3.6.1) was chosen as the first magnetic sampling site. The Breakwater provided good protection from the elements, enabling accurate positioning of the vessel and, indeed, ensured the safe recovery of divers. The sea bed in this area is characterized by fine-grained cohesive sediment (Chapter 4.5.1). The nature of the sediment allowed 1m penetration by a 10cm diameter core barrel. The hydrodynamic conditions are known from analysis of the ATM and CASI data (Chapter 6.4), and the prevailing currents from the Admiralty Chart 1722 (<0.5 knots). The survey was later extended to include sites under Admiralty buoys and the Mountbatten mud depocentre. The samples were obtained in February 1990 and subsampled as described in Section 4.2. In any palaeomagnetic and sedimentary measurement, any form of dessication is detrimental to the analysis, so the cores were always subsampled and measured within 24 hours of sampling. On return to the laboratory, the cores were opened and split perpendicular to the north direction using a plastic cord. The boxes were then pressed in at measured intervals with the embossed arrow pointing up core (Figure 7.1). The boxes were then cut away from the core using a plastic knife, labelled and sealed using wax and scotch tape, and maintained at 4°C. The samples were transported to the laboratory in a cooled picnic box and measurements made of susceptibility, susceptibility anisotropy and natural remanence.

7.3 Susceptibility and the anisotropy of magnetic susceptibility

Bulk susceptibility is usually quoted in terms of susceptibility per unit volume in dimensionless SI units (Hrouda *et al.* 1983). The axial (bulk) susceptibility of the samples was measured using a Minisep low-field susceptibility meter which measures the change in inductance in a coil into which a specimen is inserted. Magnetic susceptibility is a symmetrical second-rank tensor (K) coefficient which relates an induced magnetic moment (J_i) to the induced magnetic field (H_j):

$$J_i = K_{ij} H_j \quad (I)$$

Hamilton & Rees (1970)

where i = direction of the axis and j = intensity of the magnetic field.

The anisotropy of magnetic susceptibility for any sample is expressed as a triaxial ellipsoid with the susceptibility defined by the directions and magnitude of three orthogonal principal axes of susceptibility ($K_{\max} \geq K_{\text{int}} \geq K_{\min}$). The principal axis, K_{\max} , is the direction of the maximum susceptibility and the direction of minimum susceptibility is at right angles to it. The mean susceptibility is calculated from the principal magnitudes as:

$$K = \frac{(K_{\max} + K_{\text{int}} + K_{\min})}{3} \quad (II)$$

(Nagata 1961)

where K = mean susceptibility.

In addition to the orientation of K_{\max} and K_{\min} , several other parameters have been developed to define the shape of the sedimentary fabric obtained using flume systems, of which q and V are the most commonly employed (Hamilton & Rees 1970). The q - factor, relates lineation to foliation and describes the relative importance of the two fabric elements of a triaxial ellipsoid:

$$q = \frac{K_{\max} - K_{\min}}{(K_{\max} + K_{\text{int}})^{1/2} K_{\min}} \quad (III)$$

The second statistical parameter, V , devised by Graham (1966), is derived from the axial magnitudes.

$$V = \sin^{-1} \left[\frac{K_{int} - K_{min}}{K_{max} - K_{min}} \right] \quad (IV)$$

(Graham 1966)

and is a measure of the shape of the ellipsoid.

7.3.1 Uses of anisotropy of magnetic susceptibility in unconsolidated sediments

Magnetic fabrics have been used to study a wide variety of sedimentary environments e.g. the intertidal (Ellwood & Hatten Howard 1981, Ellwood 1984), deep water (Rees *et al.* 1982) and lacustrine (Snowball & Thompson 1990) environments. These sediment samples were obtained by various long-coring mechanisms and box coring techniques, but were either unoriented or poorly orientated. The depth of water and diverse sedimentary environments within Plymouth Sound enabled a unique study to be made of orientated cores taken by SCUBA divers. Previous studies have shown that the fabric of unconsolidated sediments can give an indication of the prevailing environment at the time of deposition and have been used to determine four interrelated environments.

Still Water

In areas of still water, with low deposition rates, the depositional force is that of grain-by-grain gravity settling. The fabric of irregular grains would be expected to show a scatter in the horizontal (bedding) plane of the principal and intermediate axes with a clustering of the minimum axes around the vertical (Figure 7.2a).

Water Currents

Ising (1943) showed that the anisotropy of magnetic susceptibility can be used to infer the preferred grain orientation and hence the current direction in sediments (Granar 1958, Fuller 1963, Rees 1965, Rees *et al.* 1968, Hamilton & Rees 1970). Subsequent measurements of anisotropy in laboratory experiments for aeolian (Ellwood *et al.* 1986) and sub-aqueous deposits (Ellwood & Ledbetter 1977) showed fabrics to occur in two groups: K_{max} parallel to flow (Potter & Pettijohn 1963); and normal to flow (Granar 1958, Rees *et al.* 1968). The lineation of K_{max} has been found to

be dependant on the strength of the flow and the size of the particles. It has been demonstrated (King 1955) that in currents of 1cm s^{-1} the grains (diameter 4 to $20\mu\text{m}$) will become orientated parallel to the direction of flow. Slight imbrication also occurs which slightly tilts the vertical axes (0 to 20°) in the direction of flow. In strong prevailing currents ($>1\text{cm s}^{-1}$), the long axis will orientate perpendicular to flow. The definition of current direction and parallelism of the long axes is best demonstrated in sediments with current velocities slightly below the threshold of grain motion (Hamilton & Rees 1970). There are many anomalous examples of current directions: for example, in deep sea samples (Ellwood 1979), the sediments are found to be composed of floccules created by rolling of a "traction carpet" beneath the benthic boundary layer.

Post depositional effects

Mechanical deformation in soft sediment is common, and is caused by a number of factors. The most common is by dewatering and compaction due to overburden. Compaction will re-orientate and produce an even more pronounced "primary fabric" (Ellwood 1979). Graham (1966) showed that, with applied stress, the long and intermediate dimensions of the anisotropy ellipsoid rotate in a direction normal to the principal stress direction (Figure 7.2b) and that the degree of deformation is proportional to the degree of cluster of the principal anisotropy azimuth axes. Deformation of soft sediments in response to tectonic activity has been discussed by Lee *et al.* (1990), who showed that lineation develops perpendicular to compression.

Bioturbation effects.

Few papers examine the effect of bioturbation on sediment fabrics. Bioturbation would be expected to destroy both the remanence and the fabric but studies have shown that the primary fabric often persists after bioturbation and a more pronounced horizontal foliation may develop (Ellwood 1984, Chernow *et al.* 1986). It has been suggested (Rees *et al.* 1968) that the working of sediments by burrowing organisms is random, and therefore the effect on the magnetic particles is random so that there could be a reduction in the magnitude of susceptibility anisotropy, but the net azimuth directions and relative magnitudes are left intact. In addition the bioturbating process tends to fluidize the sediment enabling the gravitational forces to align the grains horizontally.

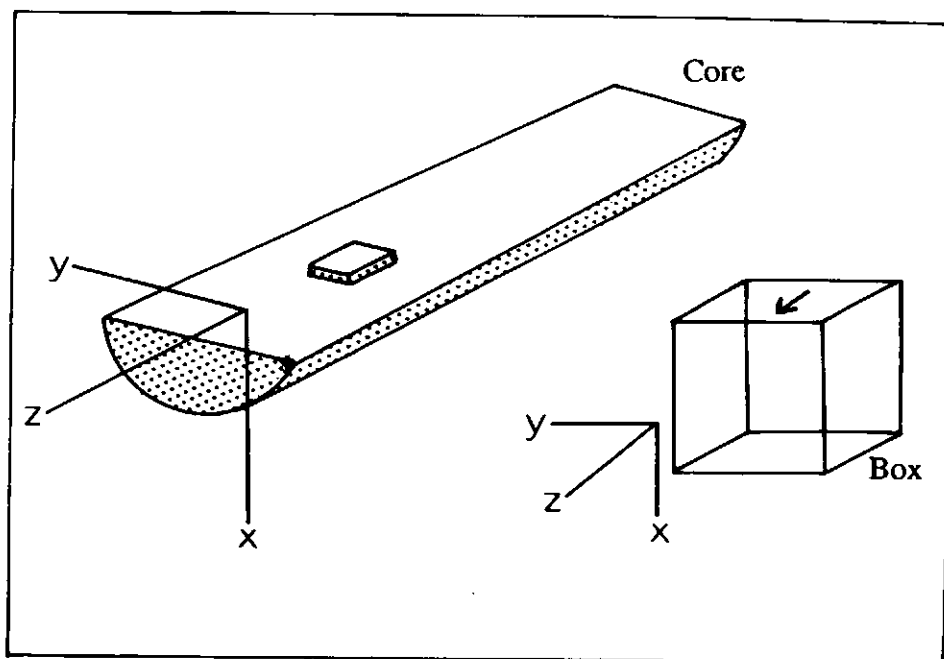


Figure 7.1 Orientation of the samples in the core and box.

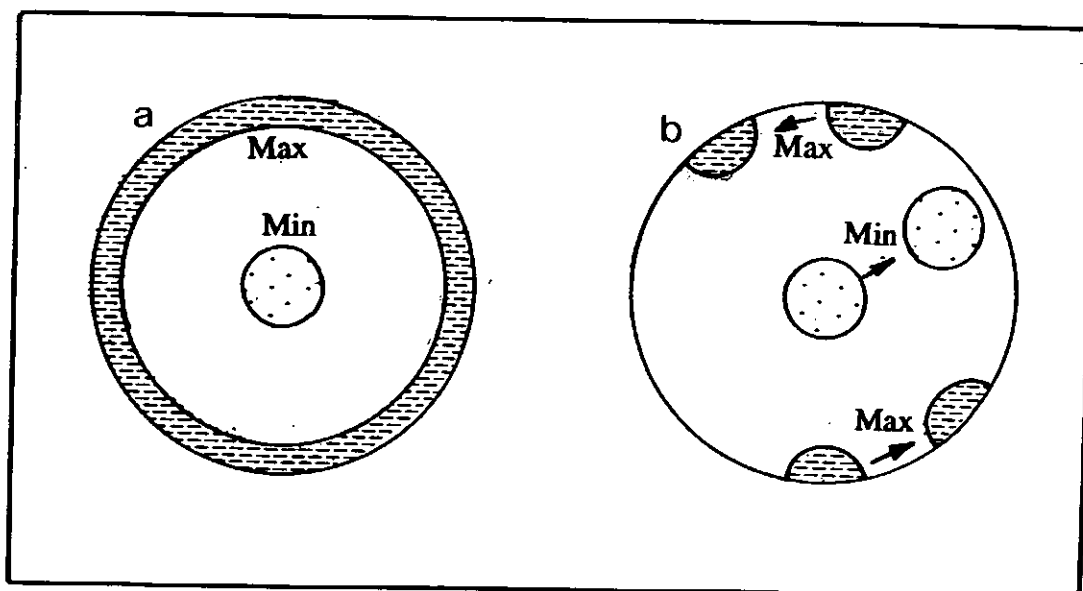


Figure 7.2 Anisotropy of magnetic susceptibility fabric types (a) still water grain-by-grain settling and (b) disrupted fabric.

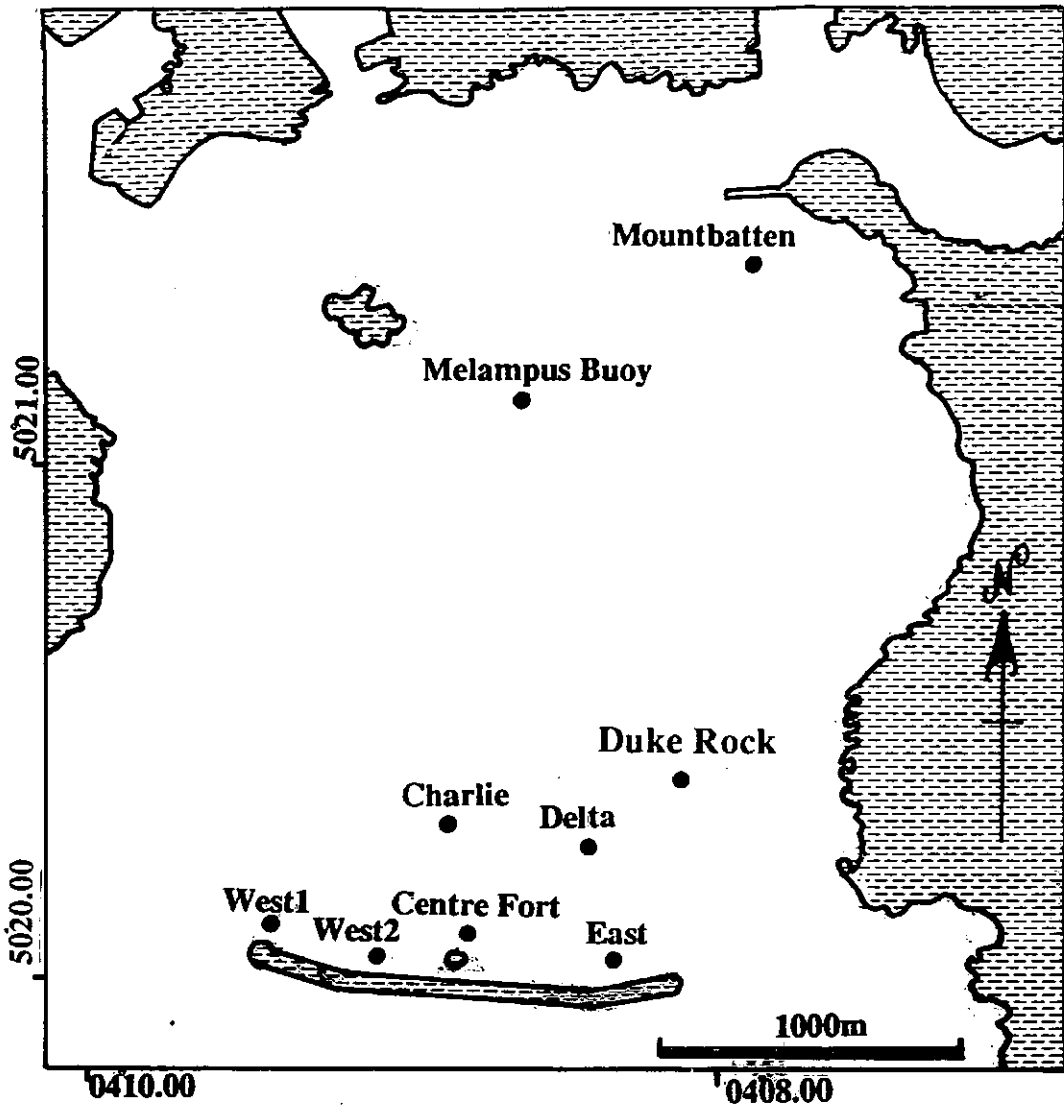


Figure 7.3 Magnetic measurement sampling stations.

Flume experiments, investigating the development of susceptibility anisotropy have shown that values of q range between 0.06 and 2.0 in most sediments, while $0.06 < q > 0.69$ has been used to distinguish undisturbed fabrics from disturbed, i.e. $q > 0.69$ (Hamilton & Rees 1970). Rees *et al.* (1968) found gravity settling to be characterized by $0.25 < q > 0.4$ and current lineation occurs for $0.4 < q > 1.3$, as evidenced by flume experiments (Rees & Woodall 1975). Oblate/undisturbed fabrics are characterized by $V > 45^\circ$, while the prolate/disturbed fabric by $V < 45^\circ$. Primary or undisturbed sedimentary fabric have also been defined as being characterized by a near-vertical minimum principal axis, and a near-horizontal maximum and intermediate axial orientation (Figure 7.2a) in addition to $0.06 < q > 0.69$ and $V > 45^\circ$.

7.3.2 Susceptibility and fabric results

The results (Table 7.1) are presented in site order (Appendix 3), with discussion of station signatures, and the depth of the cores is given in centimetres below sea floor (cmbsf). The sample stations are located on Figure 7.3.

Station East

The upper 5cm of the cores had low susceptibility values (c. $16.00 \cdot 10^{-6} 4\pi SI$), with a sharp 30% increase at -5cm. The fabric showed two equally well defined K_{max} orientations at $010/190^\circ$ and $170/350^\circ$. Samples C303, C311 and C312 show K_{min} near to vertical (Figure 7.4a.) while, in other samples they were close to the horizontal girdle. All K_{max} axes were in the horizontal plane.

Centre Fort

A high susceptibility surface value, c. $31.00 \cdot 10^{-6} 4\pi SI$, showed a sharp 40% decrease at -5cm, followed by increasing susceptibility down core with slight decreases at 15 and 30cm. The fabric showed two possible K_{max} orientations at $100/280^\circ$ and $160/340^\circ$. Sample C406 showed horizontal K_{min} and K_{max} axis (Figure 7.4b).

West2

Susceptibility ranged between 20.00 and $30.00 \cdot 10^{-6} 4\pi SI$ at the surface, and the -5cm samples range between 19.00 and $31.00 \cdot 10^{-6} 4\pi SI$, averaged c. $21.00 \cdot 10^{-6} 4\pi SI$. The -10 to -15cm susceptibility was between 24 and $30 \cdot 10^{-6} 4\pi SI$. Between -20 to -30 cm there was more variability with a minimum at

22.00 $10^{-6}4\pi\text{SI}$ and a maximum of 36.00 $10^{-6}4\pi\text{SI}$. The fabric showed two orientations of K_{\max} : a pronounced direction of 070/350° and a less well defined direction of 160/340°. The remaining samples formed two groups: C351, C372, C382, C391, and C397 plot with K_{\min} axes from >40°; C367, C366, C375, C393, C394 and C395, however, have K_{\min} and K_{\max} around the horizontal (Figure 7.4d).

West1

The Susceptibility had an average value of 21.00 $10^{-6}4\pi\text{SI}$, which ranged from 16.00 to 25.00 $10^{-6}4\pi\text{SI}$, which were 30% lower susceptibility values than the other three Inner Breakwater sites and closest to the intensities at station East. The samples had low surface susceptibility values with a 30% increase down core. The fabric had a single well developed K_{\max} orientation at 050/230°. Samples C322, C334 and C343 had near vertical K_{\min} axes, whereas C325 and C345 had horizontal K_{\min} and K_{\max} axes (Figure 7.4c).

Charlie and Delta Buoys

Samples from cores under Charlie and Delta Buoys showed low surface susceptibility values; 8.00 and 10.00 $10^{-6}4\pi\text{SI}$ at Charlie Buoy and averaged c. 14.00 $10^{-6}4\pi\text{SI}$ at Delta Buoy. The susceptibilities show a sharp increase of 35% at -5cm. Values of susceptibility fluctuate irregularly down core at both sites. Delta Buoy samples showed a 30% increase at -15cm and a further increase of 24% at -25cm in Core 63. The surface box samples BD1 and BD2 had high susceptibility values of 19.00 and 14.00 $10^{-6}4\pi\text{SI}$. Charlie Buoy samples showed a 27% increase between -15 and -20cm. Delta Buoy samples show a K_{\max} orientation of 160/340° and a second less well pronounced K_{\max} orientation at 050/230°. Other samples showed near horizontal values of K_{\min} and K_{\max} (Figure 7.4e). The fabric defined at Charlie Buoy showed a single well defined K_{\max} orientation at 140/320°. Samples C602, C604, C605 and C612 had K_{\max} near the horizontal and K_{\min} near the vertical, samples C606, C608, C617 and C618 have both K_{\max} and K_{\min} near the horizontal (Figure 7.4f).

Melampus Buoy

Box samples had susceptibility values between 7.00 and 10.00 $10^{-6}4\pi\text{SI}$. The fabric had a well defined K_{\max} orientation of 150/330°, and one sample in which K_{\min} and K_{\max} were horizontal (Figure 7.4h).

Location		Magnetic Results				Physical Results					
I.D	cmbsf	K	V ^o	q	F	Wet	Dry	M	O ₂	CaCO	τ _{ce}
East Breakwater											
C281	0	16.26	84	0.0	P						
C282	5	21.30	37	0.9	S						
C283	10	25.99	50	0.5	P						
C284	15	26.83	56	0.3	P						
C291	5	17.28	29	1.2	S						
C292	10	19.48	54	0.4	P						
C293	15	21.91	46	0.6	P						
C294	20	25.55	39	0.8	S						
C295	25	33.03	40	0.8	S						
C301	0	16.37	60	0.3	P	1.5	2.2	0.40	3	12	3.10
C302	5	24.72	60	0.2	P	1.8	2.4	0.34	4	10	3.55
C303	10	24.98	53	0.4	P	1.7	2.4	0.38	3	12	3.45
C304	15	26.22	70	0.1	P	1.7	2.3	0.37	4	10	3.26
C305	20	34.93	48	0.5	P	1.8	2.4	0.36	4	9	3.43
C306	25	25.95	39	0.8	S	1.7	2.3	0.37	4	11	3.40
C306	30	18.88	65	0.2	P	1.7	2.4	0.41	2	12	3.56
C311	5	19.03	54	0.4	P	1.4	2.1	0.47	5	10	3.02
C312	10	19.86	54	0.4	P	1.3	2.1	0.40	5	10	2.95
C313	15	22.01	35	1.0	S	1.8	2.4	0.35	4	11	3.51
C314	20	26.20	32	1.1	S	1.7	2.3	0.39	3	11	3.26
C315	25	30.65	26	1.3	S	1.8	2.4	0.37	4	10	3.56
West Breakwater 1											
C321	5	18.65	63	0.2	P	1.6	2.3	0.45	4	12	3.26
C322	10	20.21	35	1.0	S	1.6	2.3	0.38	3	12	3.32
C323	15	23.75	45	0.6	P	1.7	2.4	0.40	4	11	3.45
C324	20	23.50	54	0.4	P	1.8	2.4	0.30	4	11	3.59
C325	25	25.06	24	1.4	S	1.6	2.3	0.40	3	-	3.32
C331	5	16.36	45	0.6	P	1.6	2.3	0.46	5	11	3.34
C332	10	17.47	45	0.6	P	1.6	2.3	0.44	5	11	3.31
C333	15	22.90	45	0.6	P	1.6	2.3	0.41	5	10	3.36
C334	20	25.40	35	1.0	S	1.7	2.4	0.38	4	11	3.45
C341	5	18.85	50	0.5	P	1.6	2.4	0.42	3	13	3.43
C342	10	19.32	54	0.4	P	1.6	2.3	0.46	8	7	3.36
C343	15	22.27	28	1.2	S	1.7	2.4	0.38	4	11	3.43
C344	20	24.98	50	0.5	P	1.7	2.3	0.40	3	12	3.52
C345	25	22.08	42	0.7	S	1.6	2.0	0.27	3	12	2.70

Table 7.1a

where,

K = Mean susceptibility

V^o = Grahams parameter

q = Granar's parameter

F = Fabric type

Wet = Wet bulk density

Dry = Dry bulk density

M = Moisture content

O₂ = Percentage of total organic material

CaCO = Percentage of calcium Carbonate

τ_{ce} = Critical shear strength

Location		Magnetic Results				Physical Results					
I.D	cmbfsf	K	V ^o	q	F	Wet	Dry	M	O ₂	CaCO	τ _{ce}
West Breakwater 2											
C351	5	19.00	40	0.8	S	1.5	2.2	0.47	-	17	3.12
C352	10	26.47	47	0.6	P	1.6	2.2	0.37	1.6	15	3.15
C353	15	27.92	51	0.5	P	1.7	2.3	0.36	1.5	15	3.42
C354	20	27.46	63	0.2	P				1.5	15	
C361	0	19.88	61	0.2	P	1.5	2.2	0.48	2.3	14	3.12
C362	5	22.24	57	0.3	P	1.6	2.3	0.40	2.3	14	3.36
C363	11	32.71	48	0.5	P	1.7	2.3	0.37	2.3	14	3.26
C364	16	26.49	48	0.5	P	1.8	2.4	0.36	2.1	16	3.53
C365	22	34.39	68	0.1	P	1.8	2.4	0.34	2.1	16	3.48
C366	25	30.94	43	0.7	P/S	1.7	2.3	0.39	2.2	16	3.40
C367	29	25.41	46	0.6	P/S	1.7	2.4	0.37	2.0	16	3.42
C371	5	21.96	49	0.5	P						
C372	10	30.38	42	0.7	S						
C373	15	25.20	62	0.2	P						
C374	20	29.30	58	0.3	P						
C375	25	36.55	26	1.3	S						
C376	30	22.48	27	1.3	S						
C381	2	26.16	47	0.5	P	1.7	2.4	0.38	1.2	20	3.43
C382	4	20.02	35	1.0	S	1.5	2.5	0.48	1.6	16	3.22
C383	10	30.71	46	0.6	P/S	1.6	2.3	0.45	1.4	14	3.38
C384	14	26.33	63	0.2	P	1.5	2.4	0.45	1.4	16	3.18
C385	20	30.61	77	0.1	P	1.4	2.1	0.43	1.5	15	2.95
C391	0	30.10	39	0.8	S	2.8	2.5	0.36	0.8	23	3.60
C392	2	30.91	66	0.2	P	1.6	2.3	0.39	0.9	23	3.26
C393	5	21.98	40	0.8	S	1.5	2.2	0.45	1.7	15	3.12
C394	10	24.68	40	0.8	S	1.5	2.1	0.46	1.6	15	3.11
C395	15	30.51	37	0.9	S	1.6	2.3	0.40	1.2	16	3.31
C396	20	27.69	30	1.5	S	1.6	2.3	0.44	1.2	15	3.37
C397	25	30.52	40	0.8	S	1.6	2.3	0.40	0.3	16	3.26
Centre Fort											
C401	0	31.28	41	0.8	S	1.4	2.4	0.38	0.4	25	3.55
C402	5	18.50	90	0.0	P	1.4	2.2	0.51	1.2	16	3.55
C403	10	27.36	59	0.3	P	1.6	2.3	0.45	1.0	16	3.35
C404	15	26.74	52	0.4	P	1.6	2.4	0.42	1.0	18	3.09
C405	20	27.52	35	1.0	S	1.5	2.3	0.46	0.8	15	3.26
C406	25	27.14	60	0.2	P	1.5	2.3	0.44	1.0	17	3.24
C407	30	24.28	45	0.6	P	1.7	2.4	0.41	3.7	12	3.26
C411	0					1.3	2.1	0.57	3.0	13	2.99
C412	5					1.5	2.2	0.51	2.6	12	3.17
C413	10					1.6	2.3	0.44	2.3	13	3.29
C414	15					1.7	2.3	0.40	2.0	12	3.35
C415	25					1.6	2.3	0.44	2.4	13	3.25
C416	30					1.5	2.1	0.41	2.0	13	3.07

Table 7.1b

Location		Magnetic Results				Physical Results					
I.D	cmbf	K	V°	q	F	Wet	Dry	M	O ₂	CaCO	τ _{ce}
Charlie Buoy											
C601	0	8.55	53	0.4	P	1.5	2.5	0.60	5.0	12	3.60
C602	5	12.23	34	1.0	S	1.5	2.1	0.90	4.0	12	2.95
C603	10	13.91	59	0.3	P	1.4	2.1	0.51	6.4	16	3.05
C604	15	18.66	37	0.9	S	1.2	2.0	0.58	4.8	15	2.77
C605	20	18.00	31	1.1	S	1.5	2.1	0.42	4.3	16	3.07
C606	25	16.17	38	0.8	S	1.4	2.1	0.46	3.4	13	2.97
C607	30	28.78	54	0.4	P	1.3	2.1	0.52	3.0	13	2.96
C608	35	16.49	31	1.1	S	1.3	2.0	0.47	3.5	12	2.83
C611	0	9.59	49	0.5	P	1.0	1.9	0.82	7.3	12	2.69
C612	5	15.31	34	1.0	S	1.2	2.0	0.61	4.0	13	2.83
C613	10	14.80	56	0.3	P	1.2	1.9	0.59	3.8	14	2.59
C614	15	16.15	56	0.3	P	1.4	2.0	0.40	4.0	13	2.85
C615	20	20.86	66	0.1	P	1.6	2.2	0.36	10.0	12	3.24
C616	25	14.33	44	0.6	P/S	1.6	2.2	0.38	6.0	20	3.09
C617	30	16.80	27	1.0	S	1.4	2.1	0.49	4.0	12	3.05
C618	35	19.13	35	1.0	S	1.2	2.0	0.63	4.5	12	2.75
Delta Buoy											
C621	0	12.67	52	0.4	P	1.1	1.9	0.76	3.6	13	2.68
C622	5	16.79	41	0.8	S	1.1	1.8	0.58	3.3	15	2.42
C623	10	14.12	51	0.5	P	1.3	2.1	0.56	3.4	14	2.92
C624	15	21.91	46	0.6	P	1.2	1.9	0.53	3.4	13	2.60
C625	20	16.96	36	0.9	S	1.3	2.0	0.53	2.1	14	2.82
C626	25	17.90	68	0.1	P	1.2	1.9	0.51	2.0	14	2.60
C627	30	17.24	58	0.3	P	1.3	2.0	0.52	2.5	14	2.70
C628	35	19.53	75	0.1	P	1.3	2.0	0.52	2.6	14	2.77
C631	0	11.45	36	0.9	S	1.1	1.8	0.59	3.3	16	2.42
C632	5	17.98	43	0.7	S	1.3	2.0	0.59	2.2	17	2.75
C633	10	15.05	44	0.7	S/P	1.2	2.0	0.57	3.2	17	2.75
C634	15	19.06	63	0.2	P	1.3	2.1	0.54	2.0	14	2.92
C635	20	18.85	49	0.5	P	1.2	1.9	0.56	3.2	15	2.59
C636	25	25.06	59	0.3	P	1.3	2.0	0.51	2.4	14	2.75
C637	30	19.12	83	0.0	P	1.4	2.1	0.50	2.6	14	2.92
BD1	0	19.44	44	0.7	P/S	1.8	2.2	0.18			3.09
BD2	0	14.28	35	0.9	S	1.7	2.5	0.47			3.71

Table 7.1c

Location		Magnetic Results				Physical Results					
I.D	cmsf	K	V°	Q	F	Wet	Dry	M	O ₂	CaCO	T _{ce}
Duke Rock Buoy											
BDR1	0	45.84	26	1.3	S						
BDR2	0	47.68	45	0.6	P/S						
BDR3	0	48.10	50	0.5	P						
BDR4	0	53.09	42	0.7	P/S						
BDR5	0	52.35	50	0.5	P						
BDR6	0	34.19	26	1.3	S						
BDR7	0	31.15	45	0.6	P						
BDR8	0	37.63	39	0.8	S						
Mounbatten											
BMB1	0	22.19	56	0.3	P						
BMB2	0	12.38	61	0.2	P						
BMB3	0	13.72	30	1.2	S						
BMB4	0	14.30	26	1.3	S						
BMB5	0	12.15	45	0.6	P						
Melampus											
BM1	0	9.64	71	0.1	P	2.0	2.5	0.18	9.0	13	3.26
BM2	0	7.25	38	0.9	S	1.9	2.4	0.21	10.0	14	3.43
BM3	0	7.43	44	0.6	P/S	2.0	2.4	0.17	10.5	14.	3.34

Table 7.1d

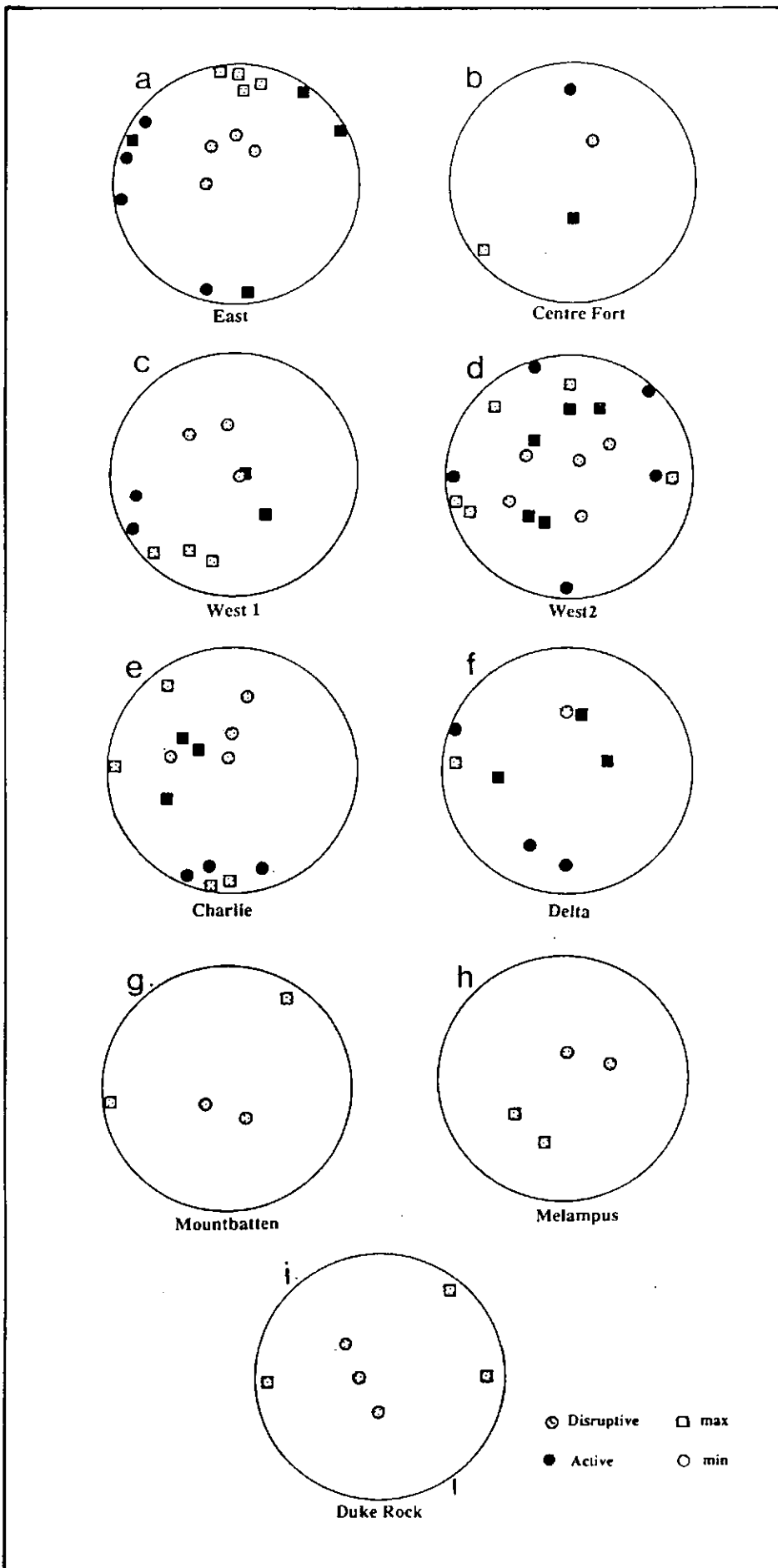


Figure 7.4 Fabric plots of all stations (a) East Breakwater, (b) Centre Fort, (c) West Breakwater 1, (d) WestBreakwater 2, (e) Charlie Buoy (f) Delta Buoy, (i) Mountbatten, (j) Melampus Buoy, and (k) Duke Rock Buoy (All plots are Upper Hemisphere).

Duke Rock Buoy

Box samples had relatively high susceptibility values which averaged *c.* $45.00 \cdot 10^{-6} 4\pi\text{SI}$ with a spread between 31.00 and $52.00 \cdot 10^{-6} 4\pi\text{SI}$. The fabric showed two K_{max} orientations at $160/340^\circ$ and $040/220^\circ$. The samples BDR1, BDR6 and BDR7 had fabrics with horizontal K_{max} axes and near vertical K_{min} axes (Figure 7.4i).

Mountbatten Breakwater

Samples taken from the south side of Mountbatten Breakwater had average susceptibility values of *c.* $15.0 \cdot 10^{-6} 4\pi\text{SI}$. Four of the box samples had values of about $13.00 \cdot 10^{-6} 4\pi\text{SI}$ and the fifth had a value of $22.00 \cdot 10^{-6} 4\pi\text{SI}$. The samples showed well grouped horizontal K_{max} orientation at $130/310^\circ$. Samples BMB3 and BMB4 have vertical K_{min} and near horizontal K_{max} (Figure 7.4g).

Storage and Drying Experiment

It was suspected, during initial experiments, that the length and type of storage modified the susceptibility and destroyed the fabric signature. To evaluate the change of both susceptibility and fabric with the duration of storage, several sediments samples were taken from two localities - Duke Rock Buoy and south of Mountbatten Breakwater. These were characterized by coarse silt and silt respectively, thereby eliminating grain size bias. The sediments were prepared following the method outlined in Section 4.3 and sealed. These samples were stored in the same orientation throughout the experiments (x axis - down). The samples were measured immediately after sampling and replaced in the refrigerator for 89 days. They were then removed from the refrigerator and allowed to warm to ambient temperature (11°C) for 15 days and then re-measured. The sediments were maintained at ambient temperature and re-measured after a further 17 days. The seals on the boxes were then broken and the sediment allowed to dry out for 52 days prior to measurement. The length of time between measurements was designed to be irregular and the sequence of the drying experiment is shown in Table 7.2.

The samples (Table 7.3) from Duke Rock Buoy all showed a decrease in susceptibility when removed from 4°C , except for BDR3 which had a small increase ($<1\%$). After initial drying susceptibility decreased by 4 to 11%. Three samples showed an increase in susceptibility in the 83 days between measuring in a sealed box and breaking the seals. The Mountbatten

muds showed an initial increase in susceptibility when the samples were removed from 4°C followed by a decrease between 2 to 0.2% of the original susceptibility value by the end of the experiment.

History	Dates
Core taken from sea bed	05.11.90
Sampled from core	06.11.90
Measured in sealed box	06.11.90
Removed from 4°C	24.01.91
Measured in sealed box	08.02.91
Measured in sealed box	25.02.91
Seal broken	01.03.91
Measured unsealed box	22.04.91

Table 7.2
History of the storage and drying experiment

Date Name	6.11.90			8.02.91			25.02.91	22.04.91		
	K	V	q	K	V	q	K	K	V	q
BDR1	45.84	26	1.3	44.05	83	0.1	44.11	43.98	54	0.4
BDR2	47.68	45	0.6	45.91	27	1.2	43.86	43.35	45	0.6
BDR3	48.10	50	0.5	48.33	50	0.5	43.17	43.52	55	0.3
BDR4	53.09	42	0.7	50.05	67	0.1	49.19	47.18	21	1.5
BDR5	52.35	50	0.5	51.53	22	1.4	50.88	49.06	44	0.6
BDR6	34.19	26	1.3	34.17	23	1.4	31.87	32.61	23	1.4
BDR7	31.15	45	0.6	30.20	47	0.6	29.38	29.77	53	0.4
BMB1	22.19	56	0.3	23.18	40	0.8	22.01	21.71	55	0.3
BMB2	12.38	61	0.2	13.12	41	0.8	12.63	12.23	52	0.4
BMB3	13.72	30	1.2	14.68	63	0.2	14.04	13.69	71	0.1
BMB4	14.30	26	1.3	14.39	21	1.5	13.50	13.84	46	0.6
BMB5	12.15	45	0.6	12.83	49	0.5	12.05	12.07	64	0.2

Table 7.3

Fabric parameters observed during the storage and drying experiment, where K = bulk susceptibility, V = Graham's parameter and q = Granar's parameter.

The fabric changes caused by storage and drying were more pronounced than the changes of susceptibility (Table 7.4 and Figure 7.5). Samples from Duke Rock showed K_{max} to migrate towards the horizontal, but with a high degree of scatter. K_{min} showed greater changes in direction, but with no clear pattern with either warming or drying. The mud samples from Mountbatten showed major changes in both inclination and declination of K_{min} and K_{max} with warming and drying, again, with no discernible pattern.

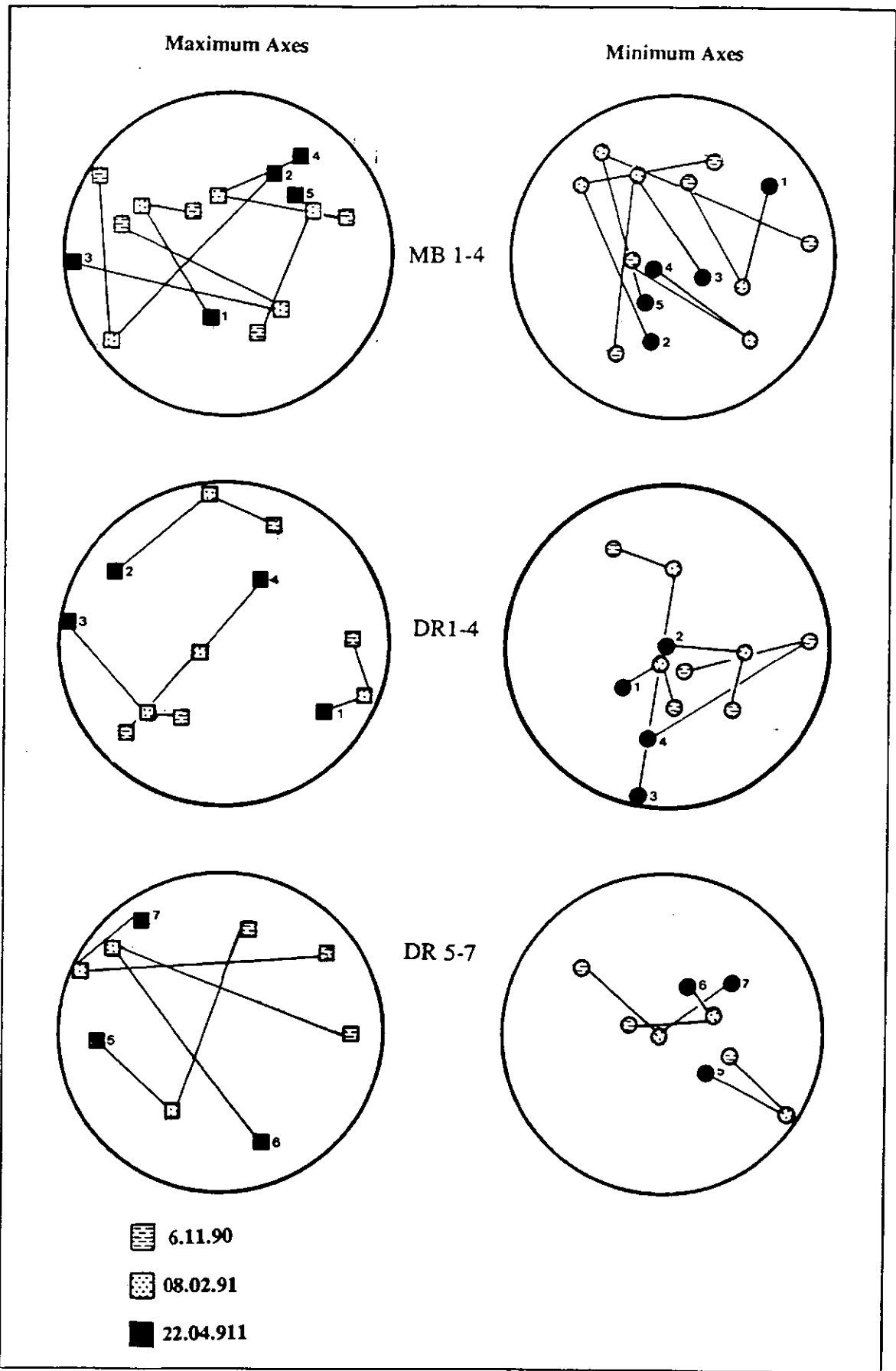


Figure 7.5 Fabric plots of the storage and drying experiment.

date	16.11.90				08.02.91				22.04.91			
	K _{max}		K _{min}		K _{max}		K _{min}		K _{max}		K _{min}	
samp	dec	inc	dec	inc	dec	inc	dec	inc	dec	inc	dec	inc
BDR1	272	6	172	56	125	20	225	60	115	1	216	82
BDR2	25	20	134	41	327	15	60	90	356	6	93	46
BDR3	210	44	330	26	279	.4	189	4	227	33	2	46
BDR4	226	18	109	53	27	51	191	38	247	78	86	11
BDR5	13	31	145	47	263	24	131	56	210	40	120	1
BDR6	91	19	282	70	159	21	26	60	311	15	69	59
BDR7	52	18	309	33	304	19	53	43	301	2	167	86
BMB1	191	52	59	27	300	42	116	47	288	37	14	46
BMB2	30	32	203	57	231	10	325	21	330	61	85	13
BMB3	265	7	154	72	138	46	336	41	304	8	210	30
BMB4	38	17	222	73	1	57	138	25	73	19	267	70
BMB5	48	35	193	48	63	37	309	28	153	43	24	34

Table 7.4

Fabric orientations, where K_{\max} and K_{\min} are the principle axes, and dec and inc are the declination and inclination in degrees.

7.3.3 Discussion

Discussion of the susceptibility results can be concluded under three aspects:

Primary and Secondary fabric development

Primary fabrics have previously been defined by (i) K_{\max} axes between 0 and 30° from the horizontal to accommodate for the development of imbrication, and (ii) K_{\min} axes between 0 to 20° deviation from the vertical to allow for mechanical or sampling errors. This classification, based mainly on flume experiments (Section 7.3.1) was found to be impractical. The inference of the term "primary fabric" is that it is the first developed fabric which may be later disrupted to form a "secondary fabric". However, in Plymouth Sound there are some sediments in which the only active depositional presence is disruptive so that their resultant depositional fabric would be classified as secondary, inferring the previous presence of an initial primary fabric, which is not the case. To eradicate this problem, whilst dealing with natural unconsolidated fabrics, it is proposed that the term secondary fabric is subdivided into two categories:

- (i) Secondary active - in which the depositional environment is dominated by an active disruptive process, e.g. bioturbation.
- (ii) Secondary disruptive - whereby the sediment has had a primary fabric which has since been reworked and disrupted.

Both fabrics can be defined initially using q and V , and then by the orientation of their principal axes. Secondary active fabrics were identified by $K_{\max} > 10^\circ$ from the horizontal, and K_{\min} axes with inclinations $> 30^\circ$. The orientation of K_{\max} was found to depend on the intensity of infaunal bioturbation. In areas of high organic content, with sediment communities dominated by *Capitella capitata*, which produce extensive vertical feeding traces, K_{\max} tended to plot near to vertical. However, in areas with low bioturbation and well defined current lineation, K_{\max} tended to be orientated around the horizontal. It was found that active secondary fabric in the Plymouth Sound silts are mostly confined to the oxic and sub-oxic zones of the sediment (Section 7.4.3), and therefore to areas with high deposition rates, high organic content and a large sub-oxic zone.

Secondary disruptive fabrics, tended to have both K_{\min} and K_{\max} within 30° of horizontal. This fabric type was confined to sub-samples from beneath the anoxic layer in the sediment. The development of this form of secondary fabric is tentatively attributed to either authigenic mineral production and possibly mechanical distortion created by compression during sampling. On the basis of the distributions of the azimuths of K_{\max} in the sediments characterized by primary fabric it was possible to create a series of current roses (Figure 7.6) using standard sedimentological techniques.

Problems were encountered during the Plymouth Sound investigation with the standard definitions of primary and secondary fabric based on q and V as well as the actual terminology. However, it is also apparent that Graham's V is related to susceptibility. High values of susceptibility ($> 20 \cdot 10^{-6} 4\pi\text{SI}$ units) are associated with V values of $> 45^\circ$, whereas lower susceptibility values ($< 20 \cdot 10^{-6} 4\pi\text{SI}$ units) give V values of $< 45^\circ$ for sediments with the same characteristics (Figure 7.7). Therefore values of V must be examined carefully prior to interpretation.

Relationship between Susceptibility and Physical parameters.

It was repeatedly found that the classification of the fabric type was related to grain size and the value of susceptibility. Grain diameter modal sizes of 63 to $45\mu\text{m}$ usually showed clear development of primary fabric. Sediments above and below that threshold were prone to mechanical disruption during sampling. Sediments with high susceptibility values

showed more distinction between primary and secondary fabrics. Susceptibility showed an increase down core at all sites by at least 30%, this is inversely related to the organic content which controls the state of the redox environment and thus the production of authigenic haematite within the anoxic zone. At the Centre Fort and West2, there is a sharp decrease in susceptibility between 0 and -5cm. This illustrates the effect of the prevailing redox conditions (Section 7.4.3). An inverse relationship was also found between susceptibility and grain size, related to the size of the magnetic carriers (<63 μ m) and the winnowing of the sediment. A decrease in susceptibility at 25cm was found in most cores, associated with an increase in grain size and carbonate deposited during the severe winter of 1962/63 (Section 1.7). There appeared to be no relationship between measurements of bulk density and susceptibility, except for the top 5cm - again related to the reduction and compaction of the oxic zone in which carbonate material is exsolved.

Geographical Controls

The distribution and concentration of magnetic minerals in Plymouth Sound is confined, by their modal sizes, to the silt depocentres (Section 3.6.1). On the basis of susceptibility, the sampling area can be divided into two zones. The higher susceptibility of the Inner Breakwater and the lower susceptibility of the Mooring Buoys (Charlie & Delta). This zonation is attributable to the source of the sediments. Inner Breakwater sites receive sediments from both marine and estuarine sources, whereas Charlie and Delta only capture estuarine sediments. This is also reflected in the decreased CaCO₃ and the increased O₂ percentages (Section 4.5.1). There is an increase in susceptibility in the top 5cm of each core, which is probably related to the amount of anthropogenic activity on the surface at each location. For example at the Centre Fort site, there is an underwater diving training centre which contributes to the metaliferrous content of the sediment, and metal ships moor onto Charlie and Delta Buoys.

Although no discernible patterns in fabric changes can be determined from the storage and drying experiment, the results show that the direct effect of drying and length of storage of a sample is to produce a net decrease in the susceptibility. This, and the observed changes, illustrate the necessity of making immediate measurements on the samples.

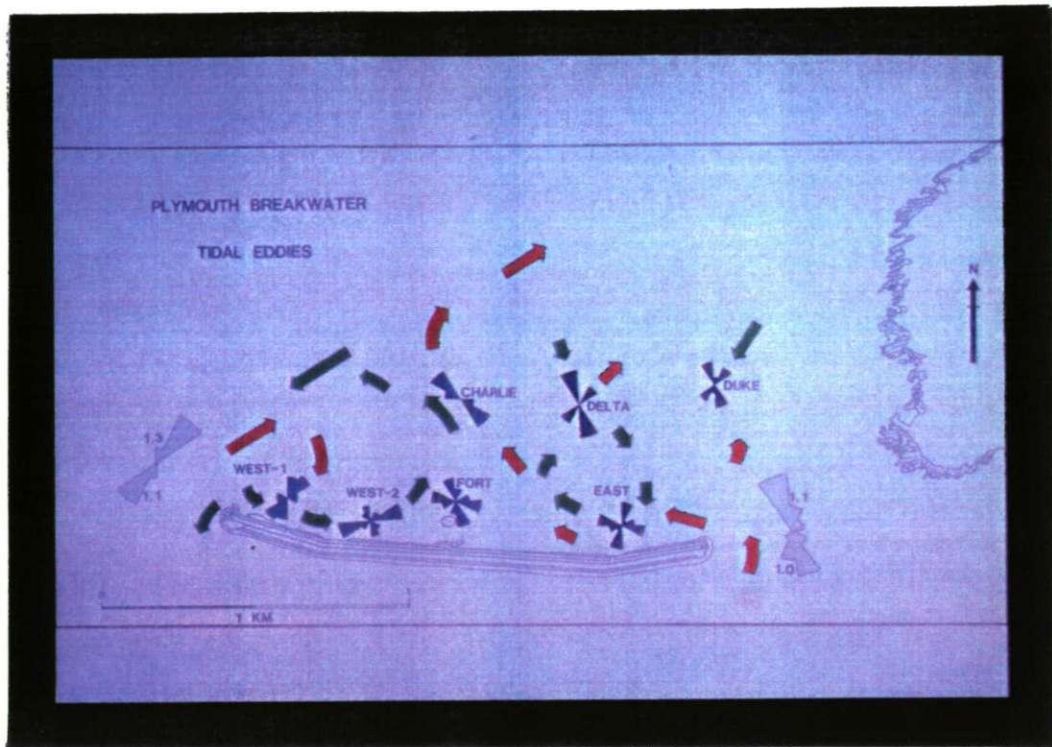


Figure 7.6 Current roses produced from the anisotropy measurements, where the green arrows indicate direction of water movement on an ebb tide and the red arrows indicate movement on a flood tide. The Current roses of water movement through the Entrances is also shown (figures in knots)

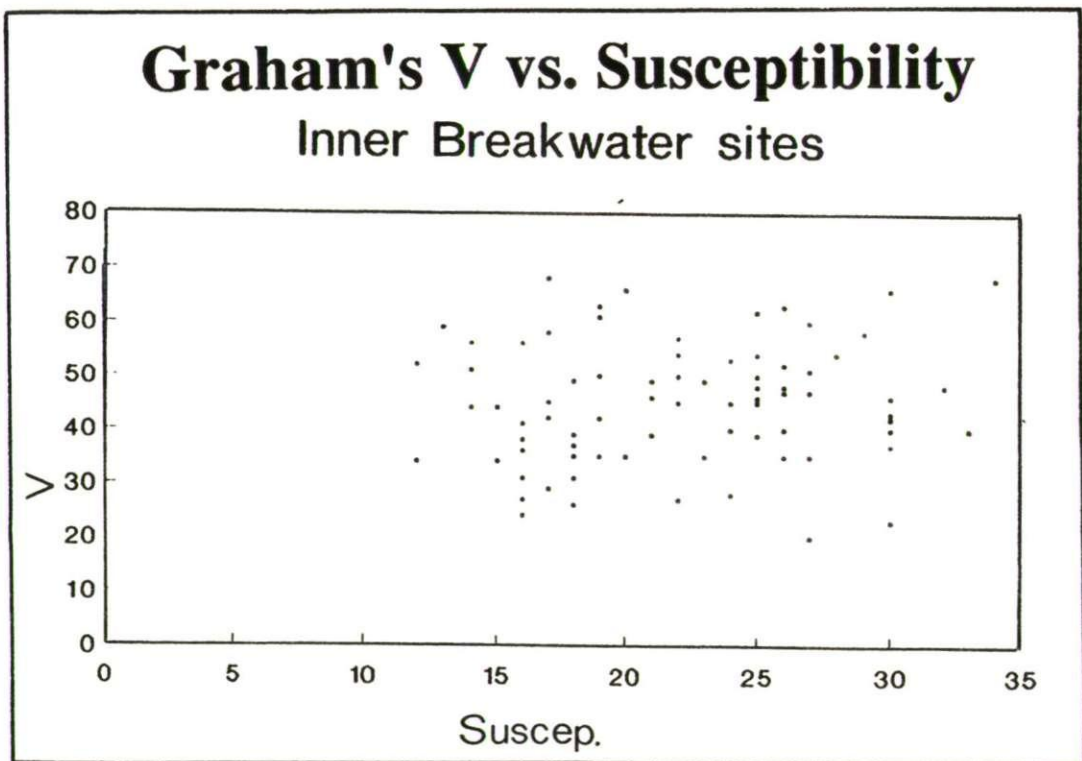


Figure 7.7 Grahams' V vs. Susceptibility.

7.4 Remanence Measurements

As detrital magnetic minerals sink in an aqueous environment, a torque is developed between their own magnetic moment and the prevailing geomagnetic force. The particles will then come to rest on the wet sea bed with their remanent magnetization in the prevailing field direction. This is termed depositional or detrital remanence. This remanence may then be modified by a number of processes resulting in further alignment within the field and in a post-depositional remanent magnetization (Irving 1957). The sediment also has a magnetic strength which is expressed as a vector with three components, x (north), y (east) and z (downwards). The magnetic directions are conventionally plotted as stereographic projections and cartesian (As-Zijderveld) plots (Tarling 1983).

The remanence of the boxed samples was measured on a Balanced Fluxgate Magnetometer, linked to a microprocessor, at the Plymouth Palaeomagnetic Laboratory. The sample is placed in a holder on a shaft and rotated inside a ring fluxgate. The rotating magnetization induces a voltage in the fluxgate, the amplitude of the voltage depends on the intensity of magnetization in the specimen in the plane perpendicular to the axis of rotation. A disc with slots is situated at the base of the spin shaft, each time a slot passes over a light source, the computer reads the output from the fluxgate. The direction within the plane is given by a phase angle between the fiducial mark and the peak positive amplitude. The sample is spun in three mutually perpendicular planes to define the remanence vector.

To establish and separate the different magnetic components of the sediments, it is necessary to "clean" the sample. This is executed by the use of demagnetization techniques in which the less stable components are selectively removed, leaving the more stable components. Demagnetization was achieved by applying an alternating field whilst tumbling the sample and so presenting all axes of the sample to the alternating field. The alternating field is produced by a coil, and reduced by a motor driven voltage regulator. The effect is to randomize that part of the remanence carried by magnetic grains with a coercive force less than the applied field. It is vital that the demagnetization is carried out in a zero field, in order to avoid the acquisition of an anhysteretic remanence.

7.4.1 Properties of remanence

The fidelity of the recorded remanence record in sediments has been examined in many experiments which investigated the actual mode of deposition and acquisition of remanence, using both synthetic and natural sediments. There is some uncertainty about the actual time of acquisition of remanence after deposition. Experiments show a time lag of 5 to 10 days (Løvlie 1974), 2 days (Barton & McElhinny 1979) and a few hours (Tucker 1980). The time of acquisition is strongly dependant on the physical properties of the sediment, including grain size, the shape of both the non-magnetic and magnetic carriers, the amount of clay minerals and the rate of sedimentation (Hamano 1980). Any change in the geomagnetic field is recorded in the magnetic carrier by post-depositional processes with a time lag up to several thousand years (Løvlie 1974, 1976). The laboratory results give mixed views and differences between the direction of the ambient field and that recorded in the sediment have been observed (Verosub 1977, Barton *et al.* 1980). The properties of detrital and post-depositional detrital remanence are summarized below:

Inclination

Early experiments designed to test the magnetic direction of sediments compared with that of the applied magnetic field in which they were deposited, gave a good reproduction of declination, but an error of about 20° was observed between the magnetic inclination and the ambient field (King 1955, Griffiths *et al.* 1960). This "error" comprises (i) bedding (King 1955), touchdown (Noel 1986), or rolling (Blow & Hamilton 1978) error, and is approximately equal to the slope of the bed (Hamilton & King 1964); and (ii) a current error (King 1966) whereby the shear stress applied by the prevailing current affects the resulting remanence direction. Several causes of inclination errors have been recognized including the effects of flocculation, Brownian motion (Collinson 1965), kinematic coagulation (Tucker 1983), clay mineralogy (below), the rates of deposition and compaction of the sediment, (Kent & Lowrie 1975, Barton *et al.* 1980), and the effects of partial drying (Barton & McElhinny 1979). In natural sediments, the observed inclination discrepancies are either small, or absent (Blow & Hamilton 1978, Tarling 1983) and assumed to diminish with compaction and post-depositional remanence processes. Recent experiments (Arason & Levi 1990a, 1990b) show that sediment fabric rearrangement with compaction is probably not a source of inclination shallowing.

Post-depositional realignment

Irving (1957) and Irving & Major (1964) showed that sedimentary grains could become realigned immediately after deposition or during compaction. Initially the secondary alignment of grains was attributed to grain rotation in pore spaces, but later analyses identified two main constraints on the occurrence of post-depositional remanence (i) the physical impedance and (ii) intensity of the field (Tucker 1980). The physical properties investigated in relation to these processes include the shape and size of pore spaces (Hamano 1980), grain size (Payne & Verosub 1982), uniformity of the matrix (King *et al.* 1983), and the development of *in situ* gas bubbles (Noel 1986). External influences have also been investigated, mainly, the rate of consolidation as a function of grain size, deposition rates and diagenetic properties (Løvlie 1974), the role of water (Verosub 1977), and sequential packing (Blow & Hamilton 1978). Drying experiments (Tucker 1980, Henshaw & Merrill 1979) have shown that only a slight grain rearrangement occurs. In clays, grain blocking occurs at 75% water, limiting movement of single-domain needles (Tucker 1980).

Clay minerals

It has been postulated that errors develop in response to the attractive force between opposite charges in clay minerals and the magnetic carriers (Anson & Kodama 1987). Lu *et al.* (1990) found the clay mineral species to be an important parameter in the acquisition of depositional detrital remanence. Montmorillonite, for example has a larger coagulation area than kaolinite, and is therefore more conductive and prone to sequestration of magnetic carriers. The clay content and type also reduces post-depositional remanence as all free magnetic carriers are captured by flocculation prior to deposition. The inclination shallowing increases with the clay content, as most clay particles tend to be deposited horizontally. It must be stressed, however, that these experiments were made in a laboratory, in the absence of natural perturbations, and using single species (un-mixed) clay minerals. The structure and method of deposition of the clay is important. It has been found that, near the surface, the clays are randomly orientated, but, with compaction, the flakes reorientate to the horizontal and physically align the clays (Meade 1966).

Disruptive events

Localised events can destroy both fabric, depositional detrital remanence and post-depositional detrital remanence - e.g. the movement of gas bubbles (Noel 1986) created during methanogenesis (Karlin & Levi 1985), dewatering, syneresis, subhorizontal stresses or deep sea slumping (Tucker 1983). Burrowing and bacterial activity can also mechanically re-arrange the sediment, the intensity of which is dependant on the rate of deposition, productivity and to a lesser extent, the grain size (Løvlie 1976). As the sediment is compacted mechanical disturbances require more energy; therefore, any realignment is attenuated with depth unless extra fluid is added (Tucker 1983).

Authigenesis and Diagenesis

Authigenic and diagenetic formation of magnetic minerals accounts for part of the magnetic signal carried by sediments. Most wet unconsolidated marine sediments are subjected to changing redox and pH environments (Karlin 1990a, 1990b) by a number of chemical and mechanical processes. If there is high organic input into a sedimentary system, the decomposition of the organic matter leads to the development of sulphur reducing bacteria which, in turn controls the metal sulphide authigenesis in a sequence of nitrate, manganese, iron and sulphate reduction in a process known as methanogenesis. Methanogenesis creates three distinct environments which are associated with the authigenic development of magnetic minerals:

- (i) Oxygenated environments (Henshaw & Merrill 1979) produce authigenic Fe and Mn oxyhydroxides (typified by haematite) although reactions are slow. The oxygenated sediment is characteristically a light colour.
- (ii) Suboxic zones are associated with Mn and Fe reduction with the production of authigenic magnetite. No sulphate reduction occurs. Bacteria tend to occur in a restricted zone between the nitrate and iron reduction boundary at the onset of suboxic conditions (i.e. ferric/ferrous transformation) (Karlin 1990a 1990b, McNeill 1990). Bacteria produce an authigenic magnetite both intra-cellularly (magnetotactic bacteria - Torres de Aravjo *et al.* 1986) or extra-cellularly (dissimilatory iron-reducing bacteria - Sparks *et al.* 1990). The presence of bacteria therefore affect the natural remanence of the sediment.
- (iii) Anoxic environment sediments are characteristically black in colour and characterized by Fe and sulphate reduction. This causes dissolution of magnetite (Cranfield & Berner 1987) and its transformation to pyrite,

haematite (Dunlop 1979), greigite (Snowball & Thompson 1990) and iron sulphides. If carbonate material is present, siderite may occur. The chemical processes and diagenesis are more fully discussed by Karlin & Levi (1985) and Leslie *et al.* (1990). Grain transformations are very much affected by grain size, and are more pervasive and rapid in finer sediments (Karlin 1990a, 1990b). Controls on the redox environment are imposed by the sedimentation rate, the rate of sulphate reduction and the intensity of biological activity. The diagenetic change may also produce a decrease or increase in pore space, dependant on the minerals involved (Tarling 1983). The inclination error has been found to shallow in response to decreasing oxidation in marine cores (Arason & Levi 1990a, 1990b). The minerals produced by authigenesis and diagenesis will affect the remanence of sediments as they may occur as pseudomorphs or grain coatings.

7.4.2 Remanence Measurements

The remanence measurements were made on sub-samples of the cores. Initially, the pilot samples in this study were demagnetized in steps of 3, 5, 7.5, 10, 15, 20, 25, 30, 40, 50, 60, 70, 80, 90, 100mT. It was repeatedly found that after subjecting the sample to demagnetization of 30 to 40mT, dependant on the initial intensity, the sample gained in intrinsic intensity. Continued AF-demagnetization stages showed the developed intensity then decreased sequentially, as expected for a normal sample. Demagnetization steps were then limited to a peak of 25 mT irrespective of the initial intensity of the sample. The developed intensity is attributed to anhysteretic magnetization but has not been adequately investigated..

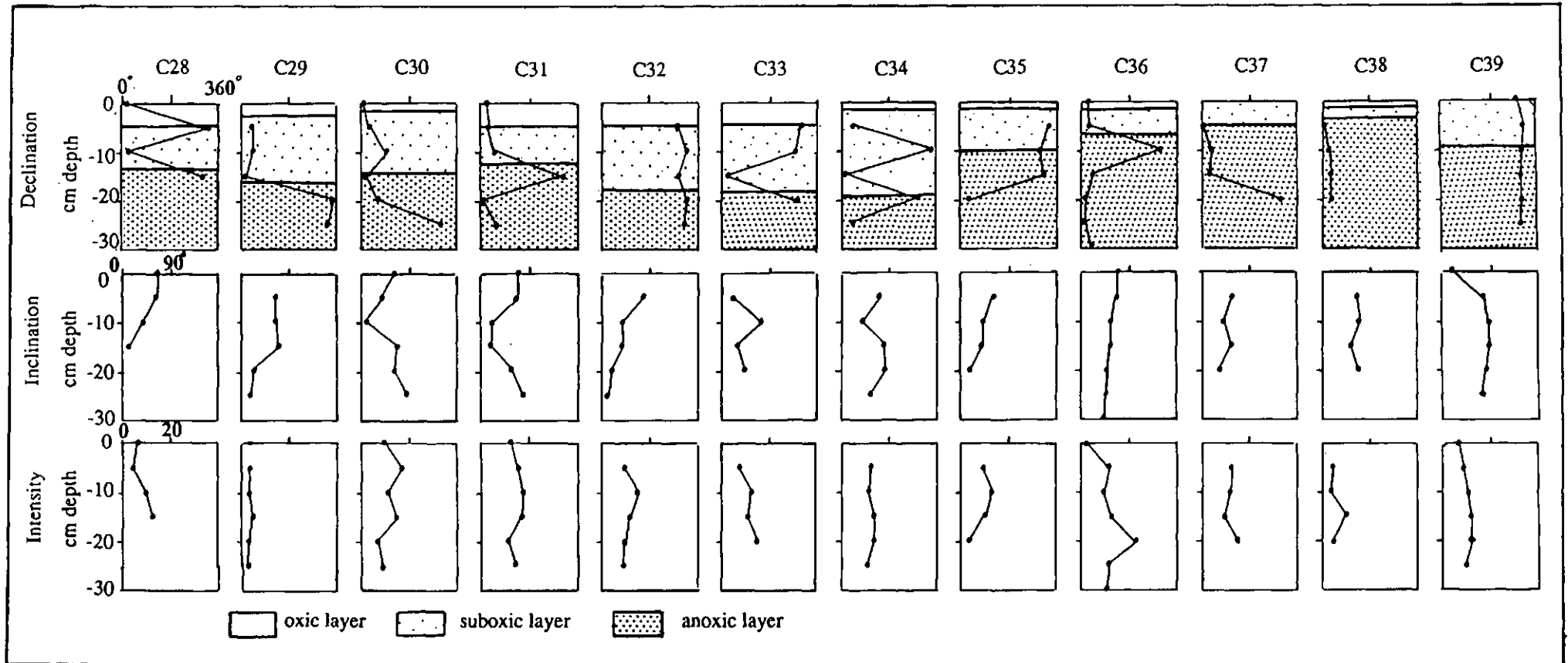


Figure 7.8 Declination, Inclination and Intensity of the cores (The position of the oxic, suboxic and anoxic zones are also marked).

The most stable inclination and declination directions of the sediment samples have been calculated using the Tarling & Symons (1967) stability index. The remanence results are presented in Table 7.5 and as a series of graphs (Figure 7.8). The data are discussed under site headings.

C28 (E)				C29 (E)			C30 (E)			C31 (E)		
cmbsf	Dec ^o	Inc ^o	Int mA/m	Dec ^o	Inc ^o	Int mA/m	Dec ^o	Inc ^o	Int mA/m	Dec ^o	Inc ^o	Int mA/m
0	7.8	15.0	7.4				1.9	23.6	10.6	29.9	16.5	13.8
5	348.2	15.2	5.1	42.6	44.5	4.5	27.0	55.3	18.8	26.0	17.3	16.0
10	33.7	42.8	11.0	45.9	42.8	4.5	100.0	80.6	12.4	71.4	68.0	18.0
15	334.5	64.2	12.3	24.8	24.3	6.0	23.0	15.0	14.8	345.9	61.9	18.8
20				359.5	61.0	4.7	79.9	15.0	9.2	7.2	34.1	13.3
25				349.9	61.5	5.8	341.8	0.7	15.2	77.2	1.4	16.8
30							32.6	44.7	12.3			

C32 (W1)				C33 (W1)			C34 (W1)			C35 (W2)		
cmbsf	Dec ^o	Inc ^o	Int mA/m	Dec ^o	Inc ^o	Int mA/m	Dec ^o	Inc ^o	Int mA/m	Dec ^o	Inc ^o	Int mA/m
0												
5	300.7	2.3	10.1	340.7	67.2	8.1	57.0	5.7	12.8	354.7	26.4	10.1
10	352.3	44.2	16.7	351.2	4.2	12.6	360.3	41.6	12.4	342.3	41.3	13.8
15	339.3	44.4	13.5	10.3	54.6	11.1	15.0	2.8	16.1	14.5	43.5	12.0
20	354.6	58.0	11.5	344.3	49.4	14.4	336.5	2.8	16.4	26.4	63.1	7.6
25	345.4	77.0	12.1				44.1	23.4	11.3			

C36 (W2)				C37 (W2)			C38 (W2)			C39 (W2)		
cmbsf	Dec ^o	Inc ^o	Int mA/m	Dec ^o	Inc ^o	Int mA/m	Dec ^o	Inc ^o	Int mA/m	Dec ^o	Inc ^o	Int mA/m
0	8.1	11.4	3.1							304.5	65.5	5.0
5	9.7	17.2	13.7	0.2	36.0	12.0	7.9	26.9	5.4	335.5	10.0	7.3
10	323.8	22.5	11.1	14.0	43.4	12.6	12.2	15.9	5.2	354.1	0.1	9.8
15	31.0	1.4	14.5	10.9	35.3	10.8	17.0	32.0	11.6	334.2	0.2	11.7
20	23.4	22.7	22.2	319.0	40.8	17.4	13.9	16.2	7.6	337.6	4.8	14.2
25	20.4	28.1	13.5							334.5	8.1	11.0
30	29.8	26.1	12.0									

Table 7.5

Remanence Results

where Dec^o = declination, Inc^o = inclination and Int = intensity in mA/m

East Breakwater

Core C28 showed an increase in both intensity and inclination down core. The declination varied irregularly down core by c. 68.0° between 334.0°

and 33.0° . Core C29 exhibited an *c.* 25% increase in the intensity curve to -15cm after which it decreased sharply by 21% at -20cm. The inclination initially decreased with depth from *c.* 44.0° with a 18.0° fall at -15cm to *c.* 24.0° . The declination varied between 349.0° and 24.0° . Cores C30 and C31 were characterized by a *c.* 15% increase in intensity from 0 to -15cm, with a *c.* 30% decrease at -20cm. The inclination increases down core to -15 and -20cm, after which depth it shallowed to 0.7° and 1.4° in core 30 and 31 respectively. The declination varied randomly by *c.* 118.0° between 341.0° and 100.0° in core 30 and between 345.0° and 77.0° in core C31.

West1

Core C32 exhibited two marked increases in intensity at -10 and -25cm by *c.* 37 and 10% respectively. The inclination increased regularly with depth from *c.* 2.0° to 77.0° and the declination fluctuated irregularly between 300.0° and 354.0° . Core C33 showed similar intensity curves, compared to C32, with a marked peak at -10cm. The inclination exhibited a sharp increase at -15cm, by 59° , and thereafter shallowed. The declination changed randomly down core between 340.0° and 10.0° . Core C34 demonstrated a 20% increase in intensity from 0 to -20cm, followed by a 31% decrease down core. The inclination showed two changes at -10 and -20cm, by $+35.0^\circ$ and $+20.0^\circ$ respectively. The declination varied by 80.5° . Core C35 exhibited a peak increase in intensity at -10cm from *c.* 10.1 to 13.8 mA/m. The inclination increased with depth and the declination varied irregularly between 342.0° and 26.0° .

West2

Core C36 exhibited two intensity peaks at -5 and -20cm with a 15% decrease at -10cm and a 40% decrease at -25cm. The inclination shallowed between 0 and -15cm and the declination varied randomly down core between 323.8° and 31.0° . Core C37 showed a decrease in intensity at -15cm from *c.* 12.0 to 11.0 mA/m, the inclination increased with depth by about 5° every 5cm. The declination showed an irregular down core variation between 319.0° and 0.2° . Core 38 had a peak of intensity at -15cm from *c.* 5.0 to *c.* 11.0 mA/m, and at the same point an increase in inclination was observed. The declination showed a variation between 7.9° and 17.0° . Core C39 displayed progressively increasing values of intensity from 0 to -25cm where they dropped by 23%. The inclination decreased between 0 and -10cm to *c.* 1° and thereafter augmented with depth. The declination varies irregularly between 304.5° and 354.1° .

7.4.3 Discussion

Discussion of the remanence results can be concluded under three aspects:

The relationship between Intensity and Redox environment

The intrinsic intensity of the sediment was found to be directly related to the redox conditions of the cores. The depth to each redox interface was measured from the sea floor during the subsampling stage (Table 7.6).

Redox environment	Colour	East	West1	West2	Delta	Charlie
Oxic	brown	0 to 2/5	0 to 5	0 to 2	0 to 15	0 to 8
Sub-oxic	grey	5 to 12/15	5 to 20	2 to 10	15 to 20	8 to 12
Anoxic	black	15+	20+	10+	20+	12+

Table 7.6
The oxidation state of the cores, depths in cm

The top of the all the cores were characterized by oxic conditions and exhibited intensities which were generally 30% lower than the deeper-buried sediments. This reflects a change in either the depositional patterns or authigenic formation of magnetic carriers, - the latter explanation is preferred. The suboxic zones were characterized by high intensities of *c.* 8 to >16mA/m. This is best exemplified in sampling sites East and West1 which continually receive nutrient-rich marine and organic-rich tidal waters, allowing a diverse and abundant infauna, which mechanically aerate the sediment (Section 4.5.1). A pronounced sub-oxic zone is developed in these sediments in response to the bioturbation. The position of the anoxic zone is marked by *c.* 25% increase in intensity. It is interesting to note that at -25cm (East and West1) and 20cm (West2) there is a decrease in the intensity. This is probably related to the decrease in the sulphur reducing bacteria associated with the cold winter of 1962/63. The intensities changed down core and were also site specific. The centre of the Breakwater was characterized by lower intensities than the outer locations. This is the direct opposite to the susceptibility results and is probably due to the presence of different magnetic minerals.

The relationship between Inclination and Redox Environment

The inclination of the geomagnetic field (February 1990) was 65.56° and the declination was -2.24° (357.76°) based on the IGRF system. Although the cores were collected over a two year period, neither the ambient

inclination nor declination has changed substantially ($<0.1^\circ$). The cores can be dated by a shelly layer at 25cm to January 1962 when the ambient inclination and declination was 65.76° and -5.52° respectively. The relative intensity of the ambient field has increased from 47199.0nT in 1963 to 47881.97nT at present. It would be expected that the declination recorded in the recently deposited sediments to be about 358° decreasing with depth to 354° above -25cm, and the inclination should be about 65° . This is clearly not the case. The inclination is generally anomalously shallow and becomes close to the ambient field direction in suboxic and anoxic zones of the sediment profile.

Recognized Errors

The declination and inclination varies from site to site and down core. The discrepancy between the prevailing field and that recorded by the sediments in the core is attributed to three main factors:

(i) Mechanical disturbance and Sampling Errors

During coring it was observed that after core penetration to *c.* >25cm, the sediment was prone to shearing and distortion. This problem was found to be directly related to the cohesivity, which is inversely proportional to the organic content of the sediment (Section 4.5.1). Although the cores were orientated on the sea floor using a calibrated diver compass, cores C36, 37 and 38 appear to have a consistent clockwise (positive) error of 10 to 30° in declination. Initially this error was thought to be caused during sampling when twisting the core barrels in order to free them from the sea bed. It is possible that during this action the sediment moved within the core. However, the cores were always twisted to the right, and the resulting error would have been negative. Apart from an actual error in positioning the core barrel, there is no solution to this problem at the moment.

(ii) Biological activity

To date, the most likely source of declination and inclination error is due to biological activity. This is evident when comparing the inclination and declination discrepancies of the organic-rich sites (East and West1) with site West2 (less infaunal activity), whereby it appears that anomalies increase with bioturbation.

(iii) Measurement errors

During the AF-demagnetization process, the sample cubes became warmed to the ambient air temperature, and although sealed, microbial generated gas bubbles were observed to develop in the cubes. The repeated spinning and

inverting of the sample resulted in the gas bubbles migrating through the sample, thereby creating disturbances.

Acquisition of Detrital Remanent Magnetization

The Physical bulk density and moisture content do not vary substantially down core (Section 4.5.1) indicating uniform sediment compaction. On this basis the down core change in inclination cannot be attributed to compaction. It is possible to give a very rough estimation of the time of acquisition of DRM in the cores. The nearest results to the present field occur below 20cm, assuming constant sedimentation rates and allowing for 10% compaction (see Bulk density measurements), therefore:

Depth of sediment (25cm + (10% of 25) = 28 years

Average rate of sedimentation = 1.018 cm^a

Acquisition of DRM at 20cm = 20 years and 4 months.

7.5 Sources of Magnetic Carriers

The sources of magnetic sediment in Plymouth Sound are four-fold:

(i) Anthropogenic, including industrial waste, sewage, particularly the intense metal activity from Devonport Docklands and, (ii) eroding cliffs and river drainage, are both sources for high concentrations of haematite and other magnetic minerals, (iii) marine bacteria, especially during thick algal blooms and, (iv) authigenic and re-working. Re-working of sands in the mobile areas creates suspension and deposition during favourable tides in the Breakwater zone.

- CHAPTER EIGHT -

- CONCLUSIONS -

8.1 Introduction

The initial aim of the investigation was to identify and quantify the vertical and horizontal constraints on the prevailing depositional environments in Plymouth Sound. These constraints were identified and found to be interrelated over a time scale from c. 20,000 B.P. to the present day. The conclusions of the project can be discussed under three headings - (i) the present hydrographic conditions, (ii) the present day sedimentary controls, and (iii) the history of Plymouth Sound. The future of Plymouth Sound with a continually rising sea level is also examined. During the course of this investigation many techniques and tools have been employed, several conclusions have been reached and these are briefly discussed. Inevitably, in such a multidisciplinary investigation, many avenues of future work are identified and these are briefly stated.

8.2 Present day Plymouth Sound

The present day hydrography and sedimentology of Plymouth Sound is described below:

8.2.1 Present day hydrography of Plymouth Sound

Several discrete water bodies, dominant tidal streams and tidal gyres have been identified, at High and Low Water, using airborne remote sensing, geophysical and sedimentological techniques. The water bodies have intrinsic physical properties, including temperature and salinity signatures, suspended sediment type and concentration, chlorophyll content and spectral signatures. The spatial and temporal occurrence of these water bodies is controlled by a complex interplay of factors. These controlling factors are primarily - the symmetry of tidally induced currents, the magnitude of residual currents and geostrophic forces. They are modified by the geology, bathymetry and anthropogenic influences

of Plymouth Sound. The effects of the present day tidal cycle in Plymouth Sound is discussed as a time series:

Two hours after Low Water slack (Figure 8.1a)

The flood tide initially enters Plymouth Sound from the southwest. It sweeps past Penlee Point into Cawsand Bay, towards Fort Picklecombe, where it is deflected northeast towards Melampus Buoy to establish the Western Stream. As the flood progresses, a second stream enters the Sound through the Eastern Entrance and flows towards the northwest, joining the Western Stream to the north of New Ground Buoy. The path of both streams is predominantly controlled by bathymetry. The Western Stream follows the path of the Western PalaeoChannel to New Ground Buoy and then continues northward in the main Central PalaeoChannel, while the Eastern Stream follows the Eastern PalaeoChannel. The eastward flow in the Hamoaze Channel begins to reverse, in response to the Western Stream in the centre of the Channel, but, water continues to flow through The Bridges along the Cornish coast. The water in Jennycliff Bay, the Inner Breakwater and the western part of the Sound is still.

Three hours after Low Water slack (Figure 8.1b)

The Western Stream is well established and flows northwest through the Sound, passing south of Melampus Buoy and loses its identity at Asia Knoll, where it meets the Hamoaze Channel waters. The Western Stream is bordered by two mixing zones. The eastern zone is c. 300m wide and separates the Western stream from Jennycliff Bay, where a gyre develops. A tributary of the Western Stream splits off the main flow south of Drake's Island and flows through The Bridges. The outflow from the Plym is deflected westward into the Hamoaze Channel and meets the Western stream at Asia Knoll. The Eastern Stream flows due north, and becomes separated on the surface, from the Western Stream, by the large clockwise gyre in Jennycliff Bay. Three large gyres occur c. 1km north of the Eastern Breakwater (6.4.2). The size and speed of the gyres are controlled by the Neap-Spring cycle. Two smaller gyres also occur immediately north of either end of the Breakwater. The position of the gyres is controlled by a local decrease in bathymetry which is related to the position of the Central PalaeoChannel. Two eddies develop at either end of the Outer Breakwater in response to the diffracting effect of the Breakwater. The Eastern Outer Eddy is the first to occur, and acts as a counter-current against the Western Stream, and flows to the southeast.

The Western Outer Eddy counter-current is smaller and flows towards the southwest. The currents in the Outer Breakwater zone show a general westwards drift from the Eastern Entrance and appear to be controlled by the bathymetry.

Four to Five hours after Low Water slack (Figure 8.1c)

The Eastern Stream splits into two at Duke Rock buoy; the dominant stream continues northwards, and the second smaller stream flows northeastward, close to shore, in Jennicliff Bay. The Western Stream continues to flow due north.

High Water (Figure 8.1d)

At High Water, the surface currents decrease to <0.2 knots. The Western Stream continues to flow northwestward to the east of Drake's Island into the Hamoaze Channel. Its path is clearly defined in the Z_{sd} depth distribution plot (Figure 6.4a) where a "more-transparent" stream can be seen to pass through the Western Entrance and flow towards the Hamoaze Channel. A ponding effect develops in the Lower Tamar Estuary as the surface waters are prevented from flowing southward by the rising Hamoaze Channel waters. The Hamoaze Channel develops stratification and four water bodies are identified (Figure 8.2a). Each have discrete temperature and salinity signatures and are separated by marked sloping thermoclines. The water bodies are named herein as: Lower, Middle, Upper and Plym.

(i) the Lower Body occurs in the eastern part of the Hamoaze Channel and had temperatures of 13.4-13.5°C and salinity of 34.90-35.10‰. This body was identified under all the Hamoaze Buoys, except West Vanguard, which showed an increase in temperature (+0.2°C) at -10m, attributed to warmer freshwater issuing from the Plymouth Limestone (Section 3.6.6). The Lower Body was also present at Melampus Buoy, and lost its identity southward of this point. It was separated from the Middle Body by a marked thermocline between 13.6° and 13.4°C, and showed some mixing in the Western Hamoaze Channel.

(ii) The Middle Water Body was characterized by temperatures of 13.6-13.8°C and salinities of 34.80-34.90‰. It was identified on the surface at West and East Vanguard Buoys, and was present at all stations in the Hamoaze Channel between -2 and -10m, extending to a maximum of -20m. The steep underwater cliff between South Winter Knoll and Mallard Shoal causes the Middle Body to flow upwards to the surface. The Middle

Body pinches out and loses its identity south of South Winter Buoy.

(iii) The Upper Water Body had temperatures of 13.7-14.0°C and salinities of 34.60-34.75‰ and was present at the surface in the centre of the Channel and at CASI 7 and CASI 8. It also occurred at -1 to -2m at CASI 5 and CASI 6. This water body, or one with similar characteristics, was present in Jennycliff Bay at -2 to -5m. The Upper Water body was separated from the surrounding waters by a sharp pycnocline.

(iv) The Plym Water Body was identified at the surface of the Eastern Hamoaze Channel and had a temperature of 14.1°C, a salinity between 34.30 and 34.54‰, and an inverse relationship between Z_{sd} and suspended sediment (Figure 6.2e). A continuation of this Water Body was also recognized in Jennycliff Bay, where the temperature and salinity signatures were more variable and showed some mixing.

The Body of the Sound can be divided into two, separated by a east-west line running from Fort Picklecombe to Ramscliff Point. The Northern Waters show well developed stratification. A parcel of water was located at The Bridges, which was characterized by low salinity (<19.80 to 28.00‰) and low temperatures (13.2 to 14.0°C). These waters occurred from a depth of -2m to the sea bed and are derived from the Tamar outflow which flows southward, below the surface, into Barn Pool and spills over The Bridges at High Water. The Southern part of the Sound is characterized by a well mixed water body of high salinity (36.50 to 36.80‰) and variable temperatures (12.80 to 15.4°C). Stations Golf Buoy and Fort Bovisand showed a temperature inversion of 0.3°C at -10m attributed to a local depression in bathymetry. The temperature/salinity profiles in the Inner Breakwater showed a high degree of stratification (Figure 8.2b), with the development of a sloping thermocline separating Upper Waters (>13°C) from the Lower Waters (<13°C). The thermocline was at -2m depth at the Centre Fort decreasing to -5m at either end of the Breakwater. This stratification is a remnant of the Inner Breakwater gyre systems. At High Water, three Z_{sd} populations are recognized (i) the Hamoaze Channel and Plym, (ii) the body of the Sound and the Western Stream and, (iii) the Channel Entrances. These can be correlated with the sediments on the sea bed and have been shown to be represented by (i) river-derived kaolinite (Section 4.5.4i), (ii) marine-derived mixed layer chlorites, illite, montmorillonite and kaolinite (Table 4.4). The third population has not been recognized.

Two hours after High Water slack (Figure 8.3a)

The ebb stream develops at the Western Entrance and flows southwestward, following the path of the Western PalaeoChannel, and initiating the Western Stream. Once the draw-down of the ebb reaches The Bridges, the ponding effect of High Water is destroyed and a rapid flow commences southeastward through The Bridges. The flood current between Drake's Island and Millbay continues running at 0.1 knots for an hour (Neaps) to an hour and a half (Springs) after High Water. This delay is caused by the mass and momentum of the water in the deep PalaeoTamar Channel. As the ebb progresses, the combined waters of The Hoe and Plym change direction rapidly and flow through Jennycliff Bay and the Eastern Entrance. A marked tidal front develops and extends southeastward from Drake's Island, separating the Western Stream from the water flowing through The Bridges. The area inside the Inner Breakwater is still.

Three hours after High Water slack (Figure 8.3b)

The Western Stream is well developed and flows into Jennycliff Bay, following the path of the Central PalaeoChannel, and then the Western PalaeoChannel. The Eastern Stream splits off 500m east of New Ground Buoy and follows the path of the Eastern PalaeoChannel. The position of the Drake's Island tidal front is maintained by the force of the water flowing through The Bridges, it migrates southeastward as the ebb intensifies. A complex three-gyre system develops inside the Breakwater, where (i) an anticlockwise gyre created as a counter-current to the Western Stream, (ii) a clockwise gyre which develops as a counter-current to the Eastern Stream and, (iii) the gyres are separated by a small anticlockwise gyre to the north of Centre Fort. Two spin-off eddies develop at either side of the Breakwater, the eastern eddy has an elliptical shape and is deflected westward.

Four to five hours after High Water Slack (Figure 8.3c)

During periods of high run-off, the southern edge of the tidal front will migrate southward and may meet the Western Entrance, the Western stream is then deflected eastward and flows through the Eastern Entrance. The gyre system in the Inner Breakwater decays.

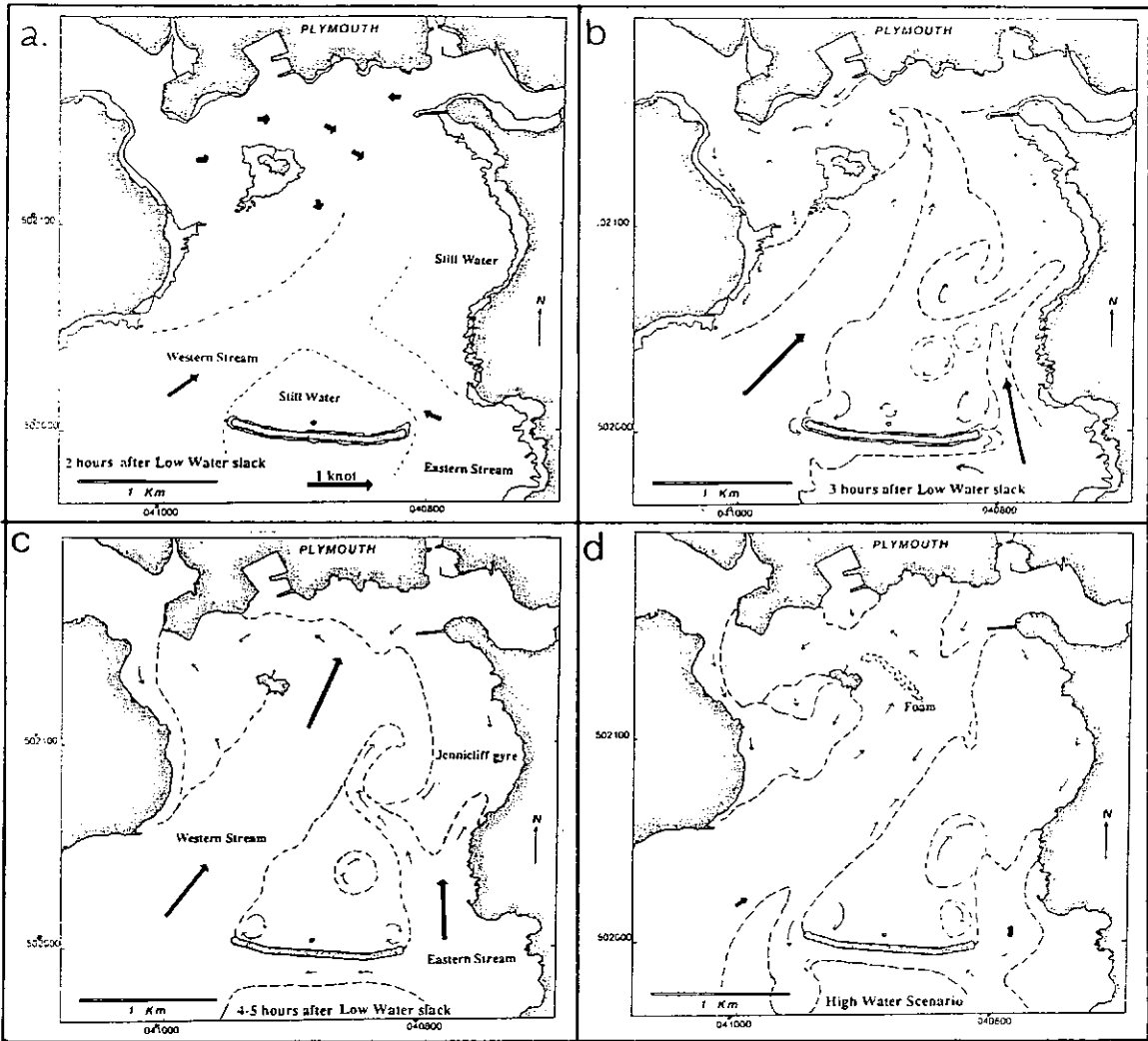


Figure 8.1 Development of High Water in Plymouth Sound, (a) two hours after Low Water slack, (b) Three hours after Low Water slack, (c) four-five hours after Low Water slack, and (d) High Water scenario. The bold arrows show current speed in knots. The fine arrows indicate direction of transport.

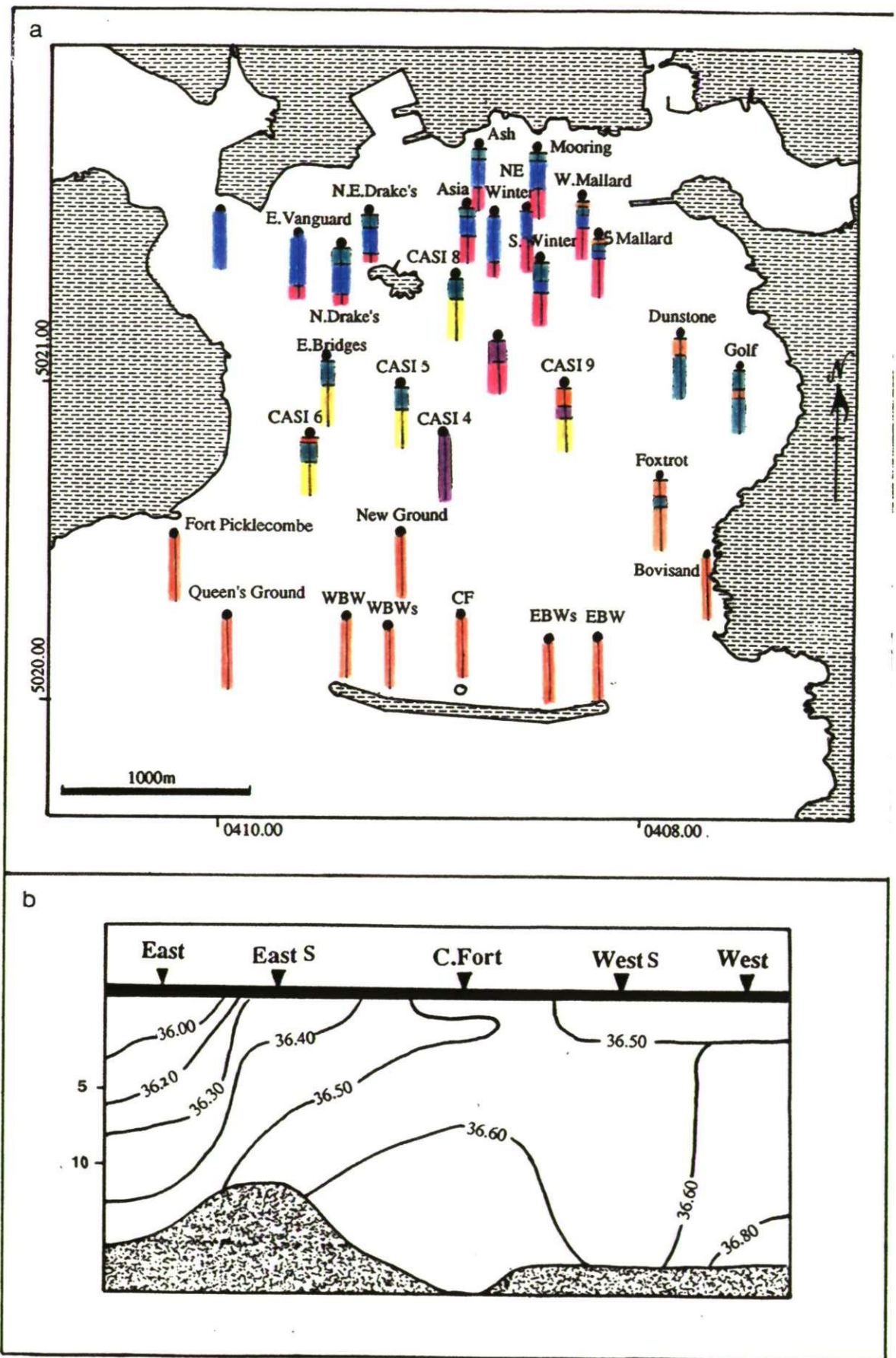


Figure 8.2 Stratification of Plymouth Sound, (a) the Temperature salinity probe results, green = Upper Body, blue = Middle Body, red = Lower Body, purple = mixing zones, brown = waters derived from the Plym, orange = saline waters and yellow = fluvial waters. (b) the Inner Breakwater stratification.

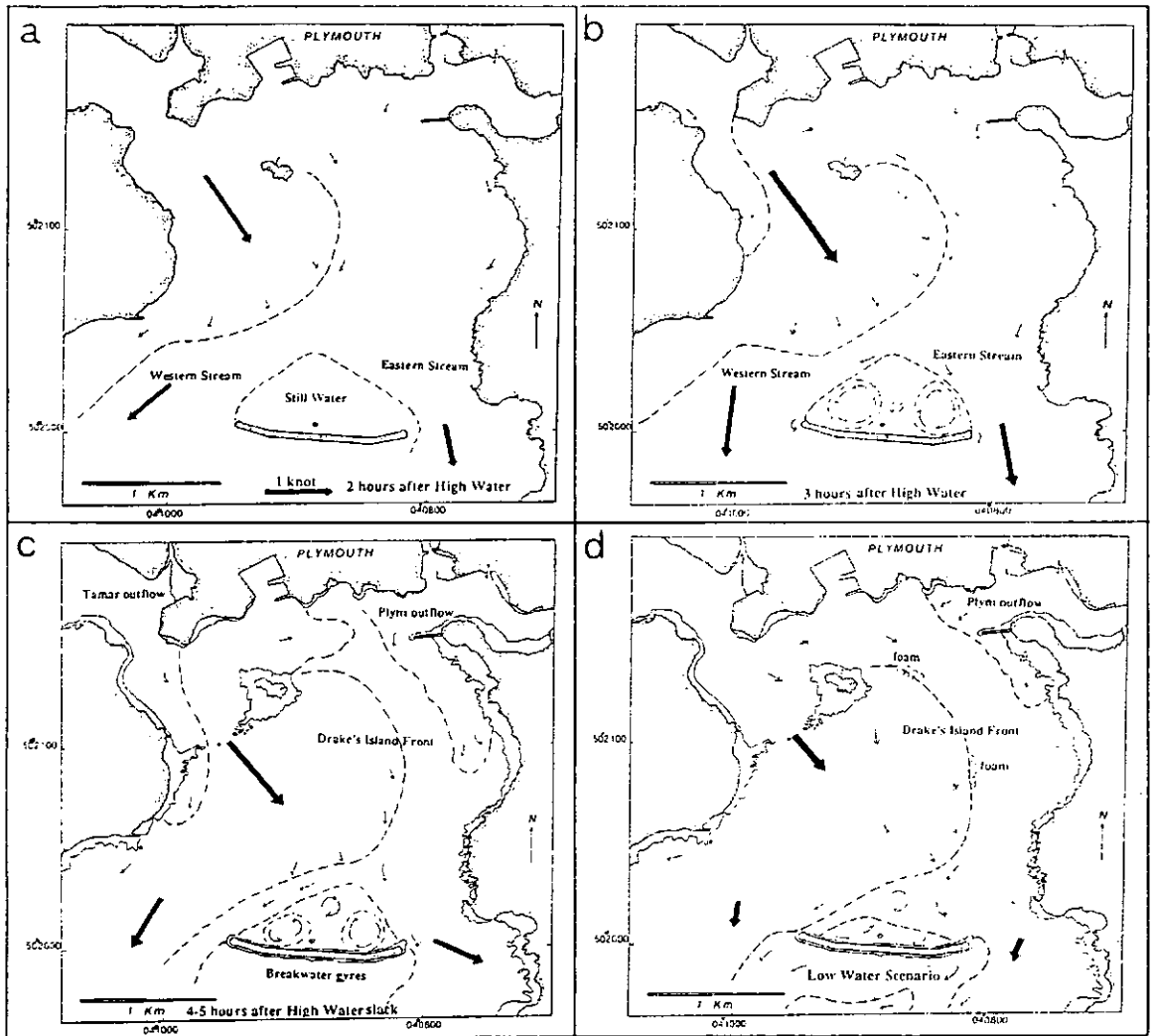


Figure 8.3 Development of Low Water in Plymouth Sound, (a) two hours after High Water slack, (b) Three hours after High Water slack, (c) four-five hours after High Water slack, and (d) Low Water scenario. The bold arrows show current speed in knots. The fine arrows indicate direction of transport.

Low Water (Figure 8.3d)

The turbid plume of the Lower Tamar estuary flows into the Hamoaze Channel and is deflected towards the Cornish coast at Devil's Point. This is caused by a velocity decrease on the outer edge of the meander and not related in any way to bathymetry. Both thermal ATM images show cooler areas in Barn Pool and at South Winter Buoy. These indicate the presence of a cooler water body at depth which is being deflected upwards at the steep sides of the PalaeoTamar Valley. The *in situ* measurements of these Lower Waters were characterized by low TOM contents. The plume of warmer turbid water from the Plym estuary flows along the northern coast of the Hamoaze Channel during times of high river run-off and southward into Jennicliff Bay at times of low run-off. The Secchi disc disappearance depths in the Hamoaze Channel are shallow due to the high concentration of kaolinite (as recognized on the sea bed) and the high percentage of organics. At maximum Low Water slack, the cooler surface and mid-water waters of the Lower Tamar continue to flow southeastward through The Bridges. The water in this area often shows a parallel streaking pattern caused by old pilings and shoal obstructions. The body of water between The Bridges and the tidal front becomes fairly stationary and the front decays. The final position of the tidal front can be seen, on calm days, as a foam line of organics/suspended sediment. The Western and Eastern Streams continue to flow southeastward, and both are deflected by the Coriolis Force. The Secchi disc disappearance depths recorded in the Entrances show an inverse relationship between Z_{sd} and suspended sediment concentration, and indicate a different population of suspended sediment to those of the Hamoaze Channel. The area of the Inner Breakwater is still and remnants of the gyres are present on the surface. The two spin-off eddies at either side of the Breakwater continue to move southward, and show turbulent mixing in their margins.

8.2.2 Sediments in Plymouth Sound

The sedimentary environments in Plymouth Sound have been identified. They can be divided into four main categories:

Relict sediments and bathymetric controls

The present day bathymetry of Plymouth Sound is predominantly controlled by the position and depth of the Devensian drainage channels of the ancestral inlet (Section 8.3). The maintenance of the Eastern and Western PalaeoChannels on the sea floor is controlled by the high tidal

currents which form the Western and Eastern Streams. Three types of relict gravels (Section 4.5.3) have been recognized in Plymouth Sound and are related to the rising sea levels of the Flandrian. These are (i) Fluvial (ii) Marine and, (iii) Beach Gravels. The source of the gravels was local and most of the clasts are derived from the Staddon Grit Formation (Section 2.2). The first gravels to form were fluvial. These floor the Central PalaeoChannel and show imbrication to the south. They were followed by the deposition of marine gravels, which included re-working of the fluvial clasts and a shoreward drift of clastic and carbonate material - as indicated by the high percentage of large shells. The beach gravels are thought to be contemporaneous with the marine gravels. A marked and indeed, unexpected continuity was established between the surface water bodies and the boundary of the gravels. The western boundary (Section 3.6.4) is maintained by the position of the Drake's Island ebb frontal system. The position of the sea bed boundary may not be exactly mimicked by the front, this is due to retardation by shearing on the sea bed which is exacerbated as the outflow from The Bridges moves over a lower water-body causing local surface lateral migration of the front. The western boundary is maintained clear of modern-day sediments by the high tidal currents present in Jennycliff Bay.

Current dominated environments and sediment transport

Many areas in Plymouth Sound are dominated by mobile sediments which are continually re-worked by the prevailing tidal currents. The strength of the tidal currents are modified by a number of factors, apart from those due to the intervention of man. The most important are geostrophic forcing and the river inflow into Plymouth Sound. Three areas in Plymouth Sound are affected by continual tidal reworking. They are delineated in Figures 4.1 and 8.4 and discussed separately.

(i) The Western Entrance

The bathymetry in this area is predominantly controlled by the incision of the ancestral Western PalaeoChannel. The deepest parts are in the centre of the channel. The sediments are predominantly fine grained in the northern part of the area and increase in grain size southward. They commonly form sheets and ribbons. In the northern limits of the area, the clastic content of the sediments is reworked on every tide. The dominant carbonate component is, however, only mobilized on a flooding tide. This, and the modal size, indicates that the source of the

sediment is from the south (marine) and derived from around Penlee Point. The dominant direction of transport is northeastward through the centre of the Channel with episodic deposition in the west.

(ii) The Anchorage

The sea bed is characterized by mobile coarse-medium sands. In the western part of the Anchorage, the sediments are continually reworked. The dominant direction of transport is to the northeast and was identified by the configuration of bedforms and the calcium carbonate content of the sediments. The northwestern parts of the Anchorage receive periodic inputs of shelly material from the Western Entrance. The eastern part is dominated by mobile sand waves. These are created during the intensification of the ebb during Spring tides which flows through The Bridges towards the east. The sediment in this area moves southeastward.

(iii) The Eastern Entrance

The sea bed is dominated by relict gravels with a covering of fine sands and silts. These are derived from a marine source, during flood currents (high carbonate content), and from the Sound during an ebb current (low carbonate content). The sands are commonly washed out of Plymouth Sound during the intensification of the Spring ebb, thus establishing an overall clockwise direction of sediment transport through Plymouth Sound.

Episodic deposition

There are two areas characterized by the episodic deposition of sediment:

(i) The Anchorage.

The northeastern boundary of the Anchorage shows a series of moribund cusped sand waves transgressing the relict gravels (Section 3.6.4). These were formed in response to episodes of high fluvial outflow through The Bridges, resulting in an eastward intensification of the ebb tidal front and a corresponding sea bed migration of sand waves.

(ii) Cawsand Bay and the Eastern Entrance

During north-northeasterly gales, sand is brought into Cawsand Bay and the Eastern Entrance, where it overlies the relict gravels.

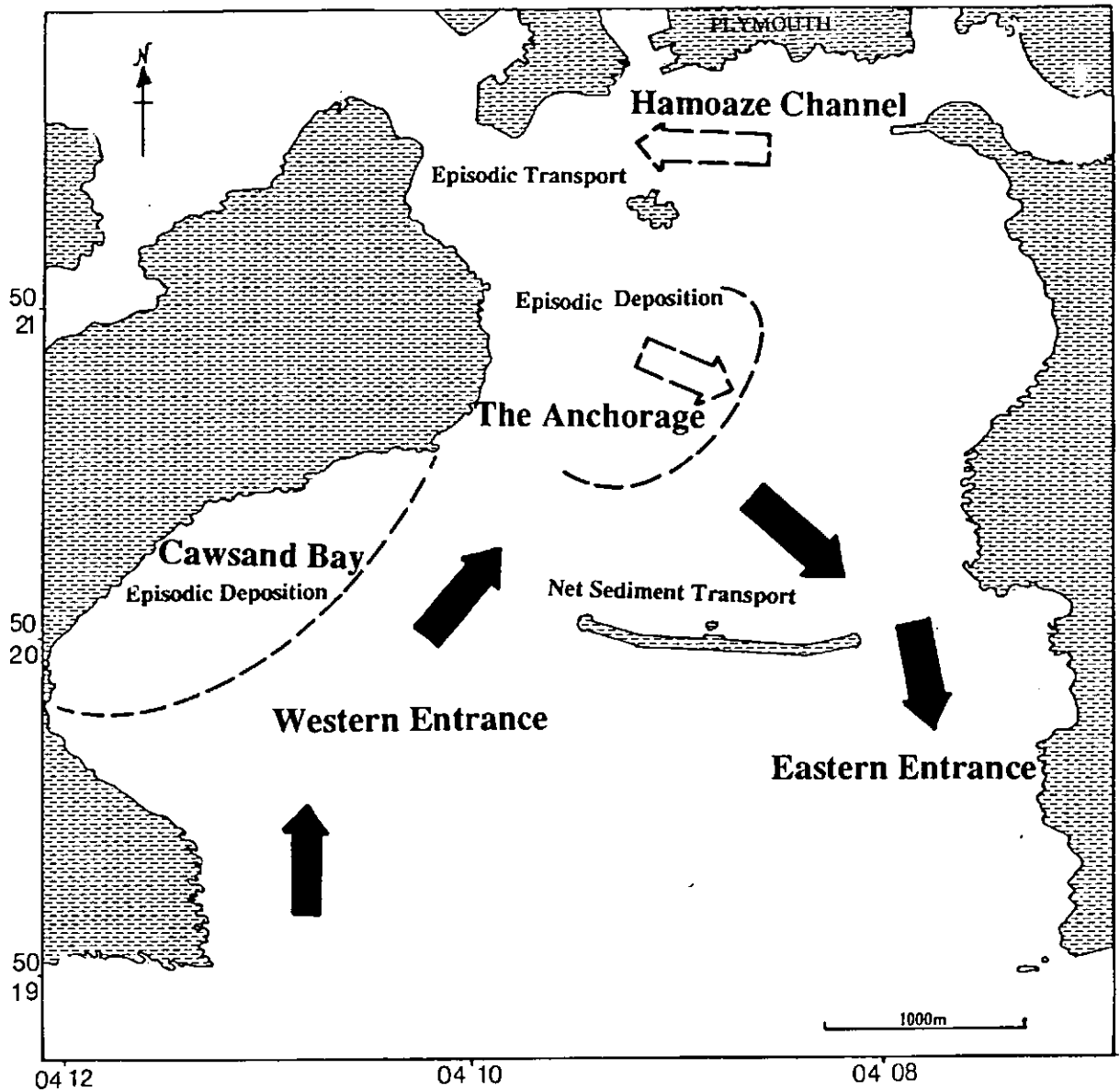


Figure 8.4 Locations and direction of net sediment transport in Plymouth Sound, where, the black arrows indicate the directions of continual movement and the white arrows indicate the directions of episodic movement.

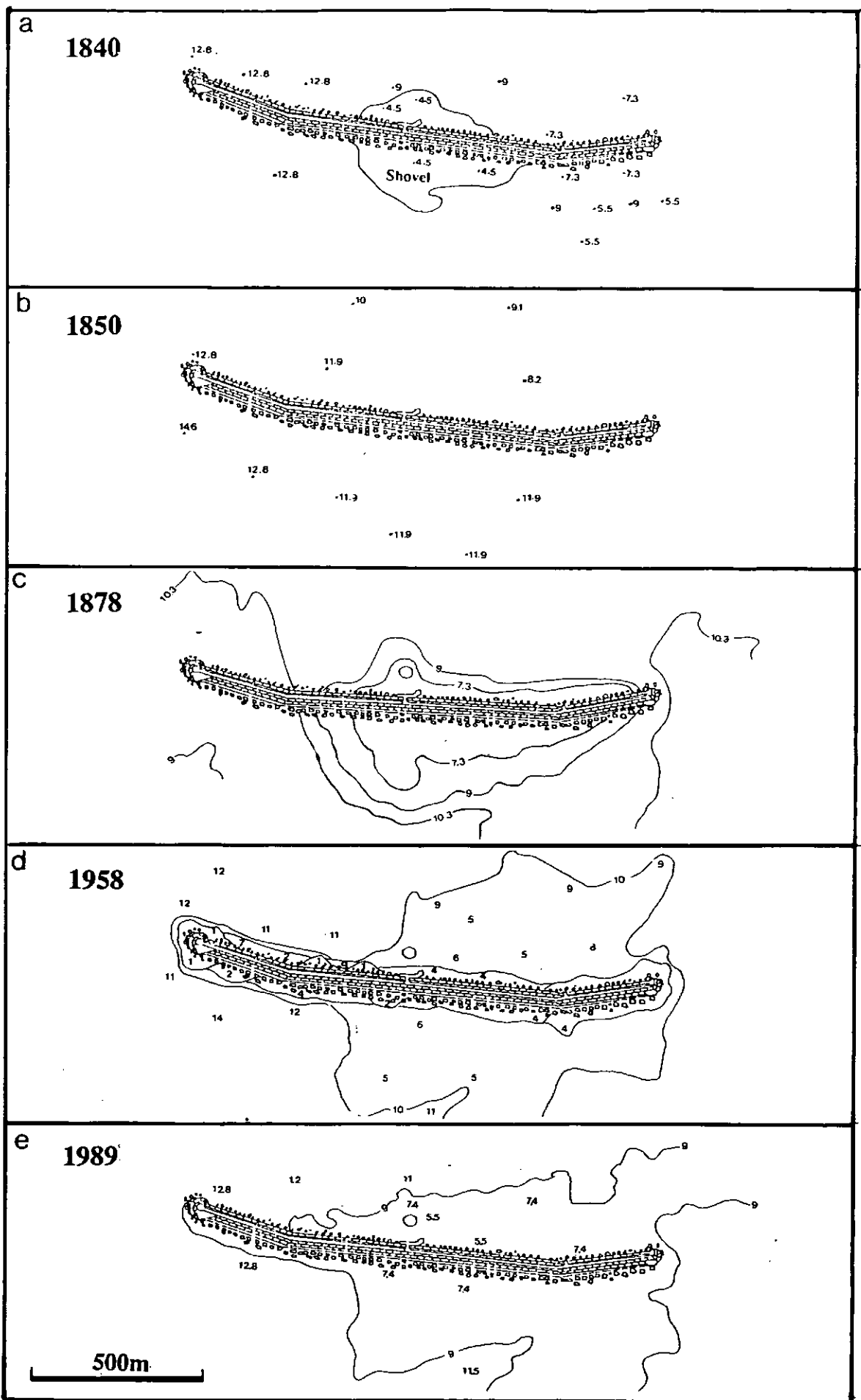


Figure 8.5 The History of sediment build-up in the Inner Breakwater extrapolated from historic Admiralty charts, all depths are converted to m O.D. (a) 1840, (b) 1850, (c) 1878, (d) 1958, and (e) 1989 (Plymouth Sound side-scan sonar survey)

Anthropogenic influences

The third control on sedimentation is that of anthropogenic modifications. These are discussed in five classes

(i) The Breakwater

The Breakwater was completed in 1848. The foundations were built on the St. Carlos and Shovel Rocks and the edifice itself straddles the Central PalaeoChannel (Section 3.6.5). The main effects of the Breakwater were to increase the shear stresses in the Western and Eastern Entrance, and to create a depocentre - the Inner Breakwater. The mineralogy of the sediments of the Inner Breakwater suggest the sources are the (i) fine grained kaolinite-rich river sediments, (ii) the high organic material released on an ebb tide, and (iii) marine waters which are entrained from the flooding Eastern and Western Streams by the gyre systems. The deposition is controlled by the position of the ebb and flood gyre systems and is uneven over the depocentre. The rate of deposition is identified by the depth to the anoxic layer and the direction of the depositional currents indicated by the magnetic measurements. The in- and epifaunal community is well established and highly diverse over the entire depocentre. The history of build-up in the Inner Breakwater can be extrapolated from historical soundings (Figure 8.5).

(ii) Mountbatten Breakwater

The Mountbatten Breakwater was built in 1882. The primary effect was to create an area of calm water in the northern part of Jennycliff Bay. The tidal current in this area has been identified as continually flowing southeastward, forming a counter-current on a flooding tide, and as part of the Western Stream on the ebb. The sediment is derived almost entirely from surface flow from the Plym and partly from the floating organic materials. The northern part of the depocentre supports no infauna, suggesting the deposit is primarily composed of nutrient-free kaolinite, whereas the southern part has a dense infaunal community.

(iii) Docks and artificial shores

The primary effect of the artificial shores and docks are to facilitate access to the sea shore. This causes maximum erosion of the intertidal area, which is exacerbated by the increased shear stresses as the uneven frictional forces are removed by paving and shoring.

(iv) Sewers and mining inputs

The influence of the sewers in Plymouth Sound are three-fold (i) to produce more particulate material which is available for entrainment into the sediment, (ii) to enhance flocculation of suspended material and

create a "snow" in areas of quiet waters and, (iii) to provide more food for infaunal activity which leads to increased re-working of the sediment, thereby reducing the critical shear stress.

(v) Dredging

The effects of dredging in Plymouth Sound are minimal. The primary reason for dredging is the acquisition of aggregate for the development of the Naval docklands. Trenches cut by a suction dredger in the Anchorage sands in 1988 are still present on the sea bed (June 1991).

8.3 The History of Plymouth Sound

The history of Plymouth Sound is complex and governed by the interplay of local geology, sea level rises and climatic variations. The sequence of events leading to the development of Plymouth Sound are presented as a series of stages. This description does not take into account the effects of the glacial forebulge, which are assumed to affect the Plymouth area as a whole (Section 2.3.6), and need only be applied when comparing with areas in other regions.

Stage One - Ipswichian.

The evidence concerning the raised beach on Plymouth Hoe has been re-examined (Section 2.4.4). It is possible to extrapolate the heights of these beaches to those dated in other parts of the European coastline.

(i) West (1988) recognized sea level heights of +7m on the eastern seaboard of Britain and ascribed them to Ipswichian age. Assuming that the downwarping of eastern Britain has been constant and at continual rate of -0.78 mm a^{-1} since 8,000 B.P. (Shennan 1989), then a vertical displacement of -15.6m has occurred and can be added to the present day height of +7m. If this is extrapolated to the South West, it approximates to the height of the +20m beach.

(ii) Guilcher (1969) recognized the Ipswichian interglacial and raised beaches on a global scale. The beaches can be divided into Lower Ipswichian at 0 to +4/5m O.D., and Upper Ipswichian at +12-18m O.D.

(iii) Caves and Raised Beaches on the Gower Peninsula have yielded Ipswichian ages (Ruddiman & McIntyre 1976). Relative warping of the Gower peninsula and the South West show the caves and beaches to be of similar height to those of Plymouth Sound. It is therefore postulated that the raised beaches on Plymouth Hoe are Ipswichian in age.

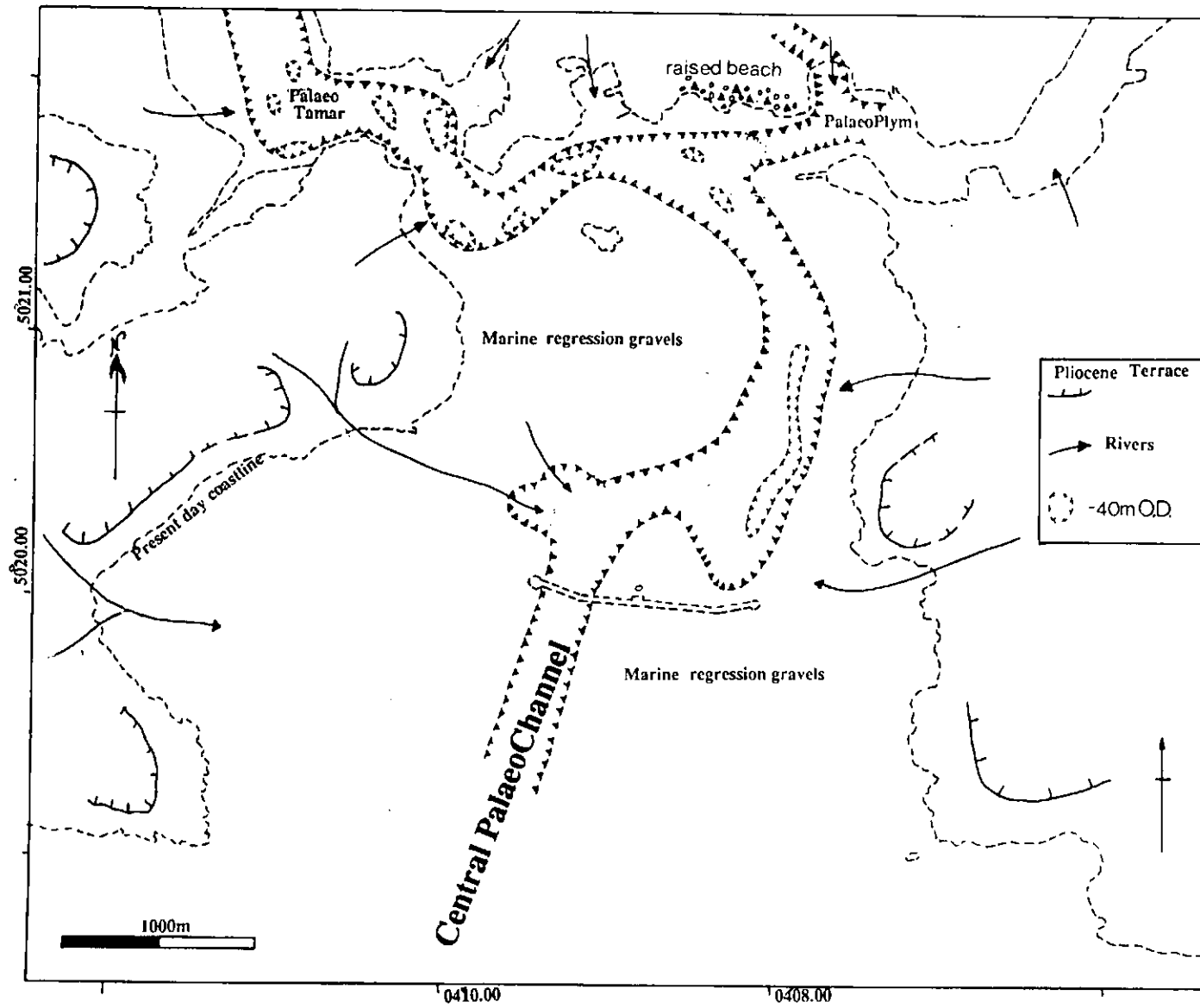


Figure 8.6 The configuration of Plymouth Sound in 20,000 B.P.

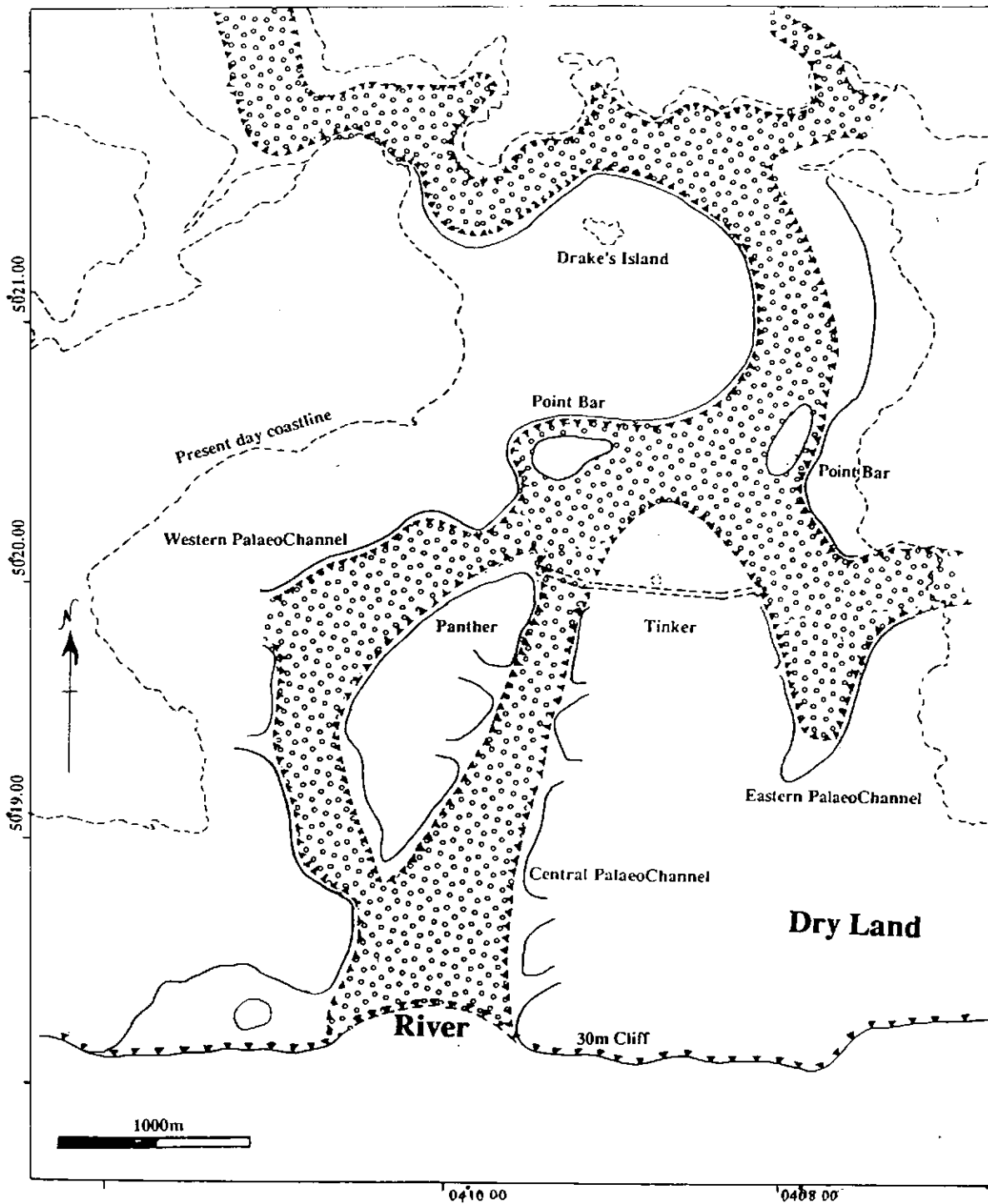


Figure 8.7 The configuration of Plymouth Sound between 9,000 - 7,000 B.P.

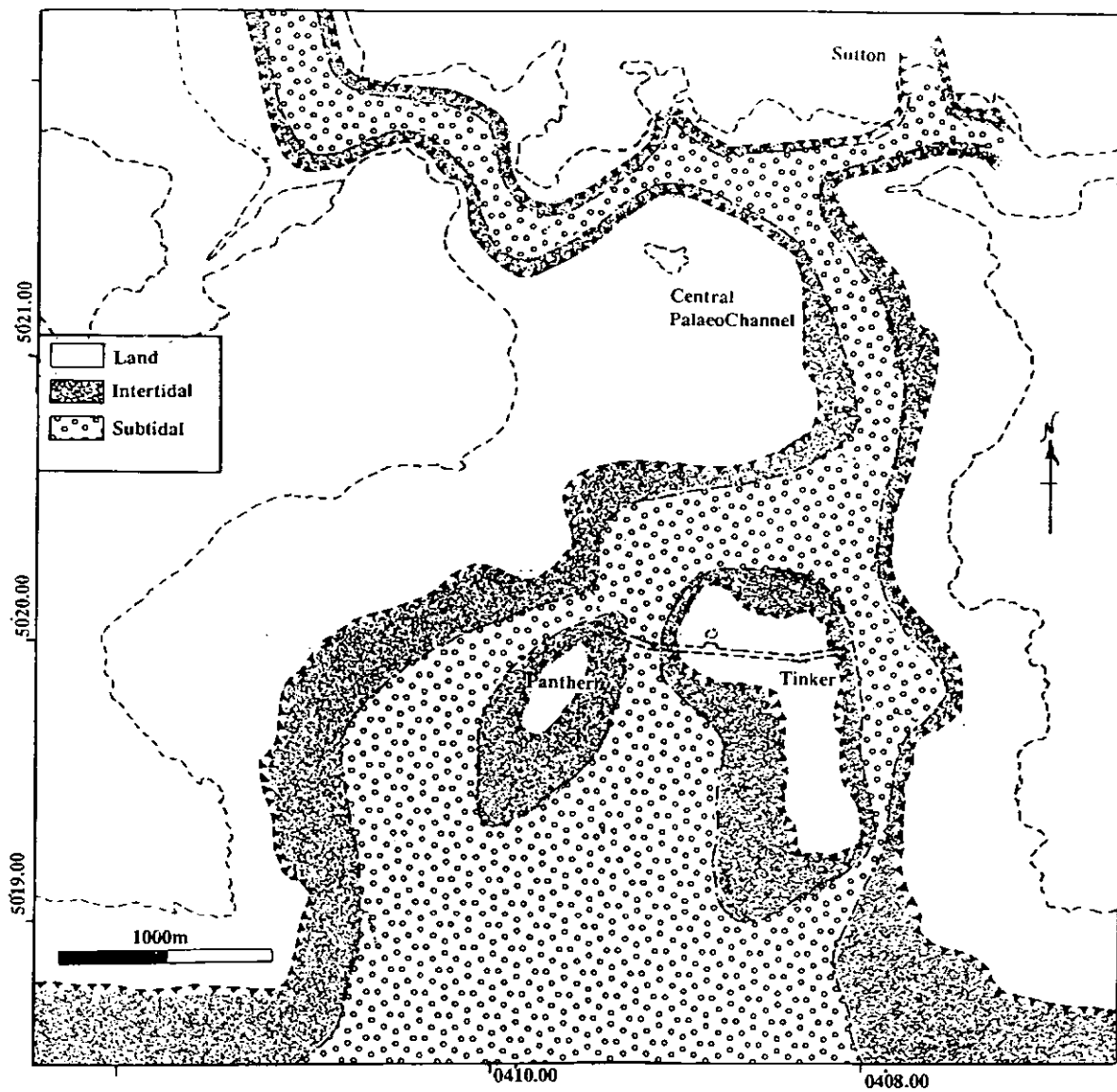


Figure 8.8 The configuration of Plymouth Sound between 7,000 - 6,000 B.P.

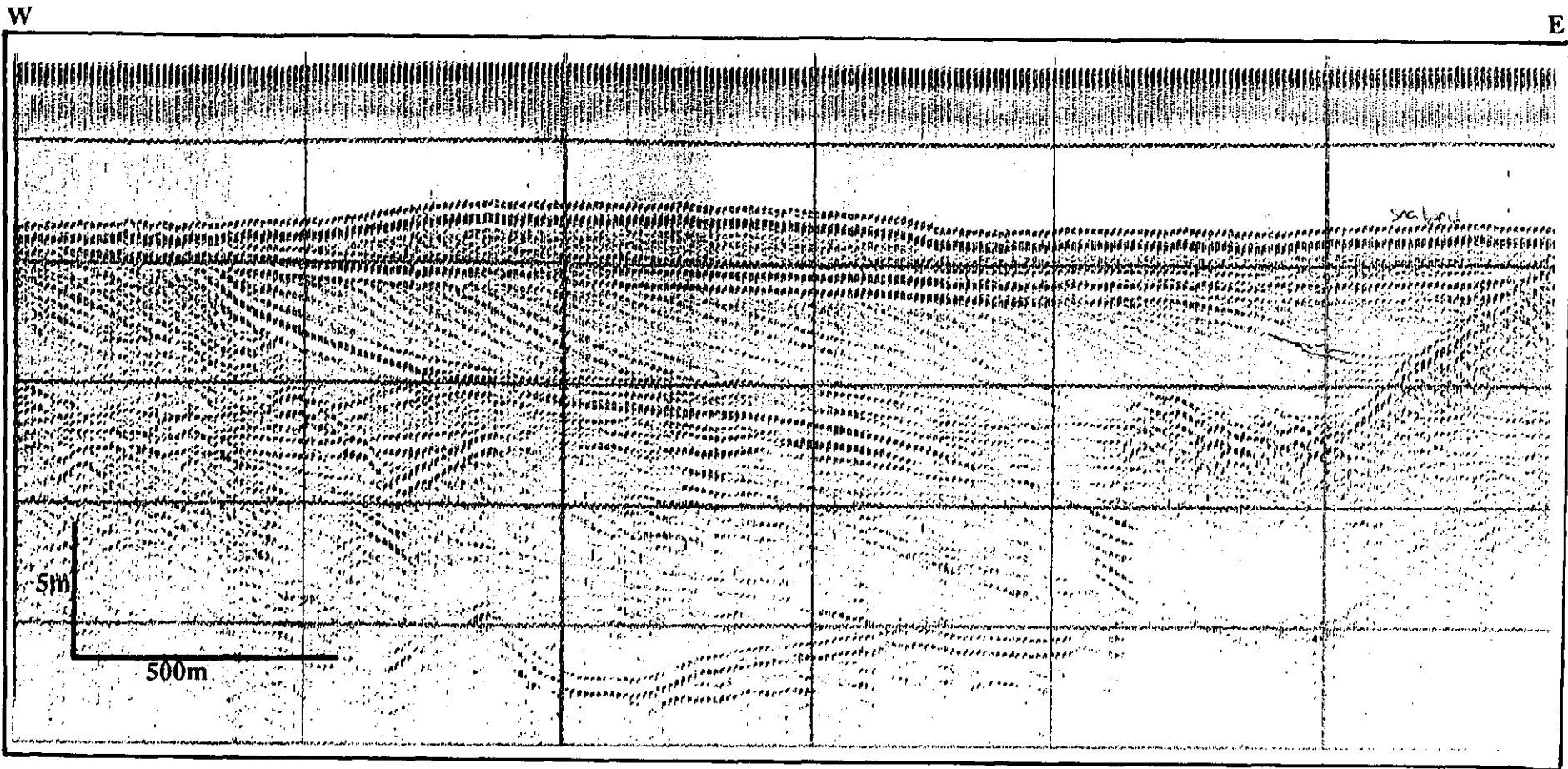


Figure 8.9 Sparker record (survey June 1991) showing planar sands in the buried PalaeoChannel.

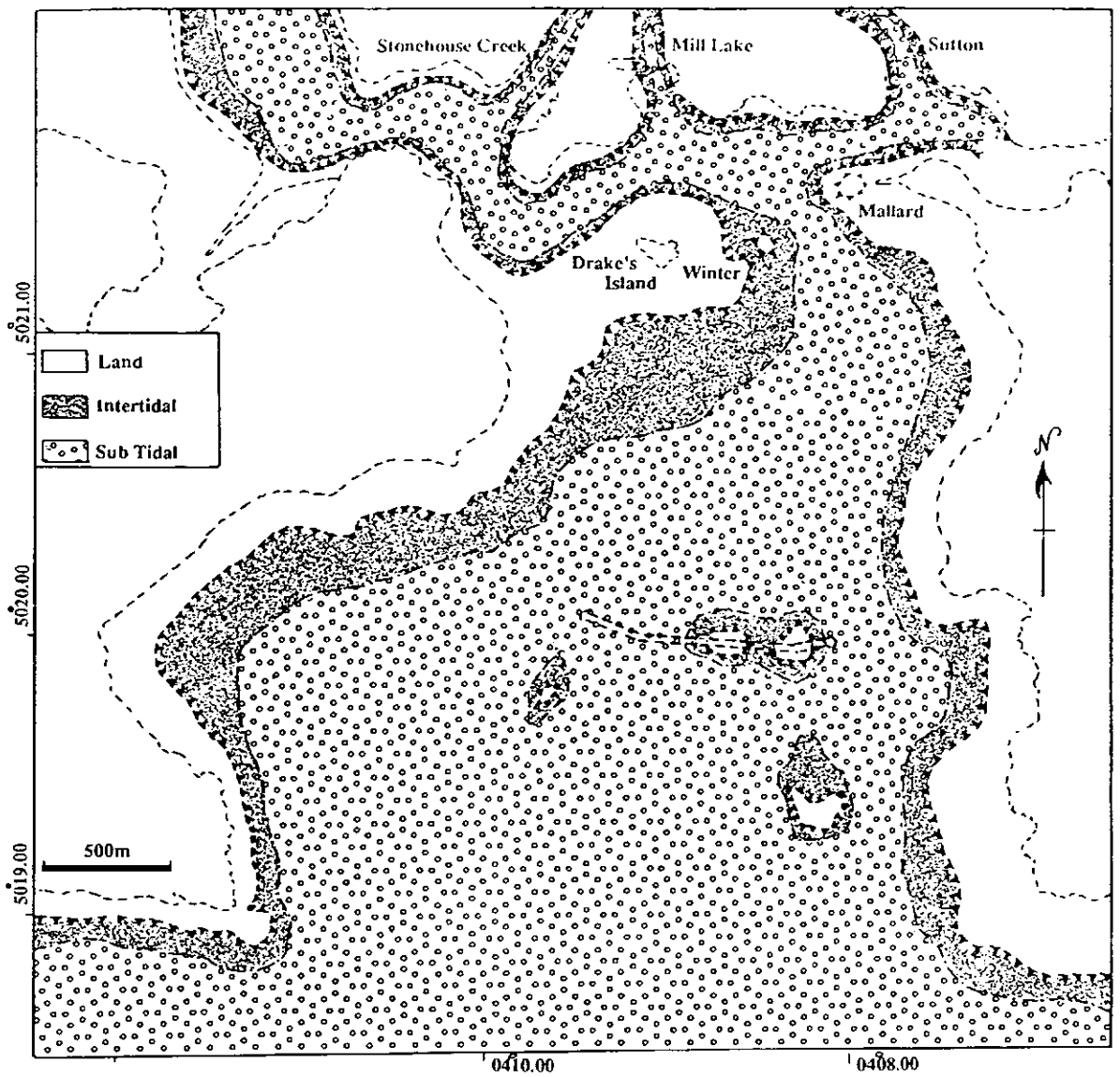


Figure 8.10 The configuration of Plymouth Sound between 6,000 - 4,000 B.P.

Stage Two 20,000 to 12,000 B.P. (Figure 8.6)

At the end of the Ipswichian Interglacial, sea level retreated to the -130m. O.D. isobath at 20,000 B.P. (Larsonneur *et al.* 1982). The maximum incision of the PalaeoTamar river channel to -42.0m O.D. corresponds to the maximum regression of the sea. At this time the PalaeoTamar flowed across Dartmoor and into the Hamoaze Channel, where it met the PalaeoPlym. The combined waters flowed into the Sound between Drake's Island and Mountbatten. The PalaeoTamar flowed to the east of the Sound, and incised the Central PalaeoChannel. The only apparent control for this appears to have been the Coriolis Force. The river was joined by several tributaries from around the present day Sound and then flowed southwestward towards the English Channel. The PalaeoTamar then joined the Channel River outflow at the Fosse de l'île Vierge, and flowed into the North Atlantic. Between 20,000 and 15,000 B.P. no trees or peats formed on Dartmoor and the summer rainfall was increasing in response to the position of the Polar Front in the North Atlantic. It would appear that, in response to the increasing runoff, the floor of the PalaeoTamar remained an environment of continual erosion and sediment reworking until the deposition of the basal fluvial gravels at 12,000 B.P. The arrival of the Gulf Stream on the British Shelf brought about a marked amelioration of the climate and a subsequent increase in vegetation. It is estimated here, to have arrived at the time of an unexplained climatic warming identified at 13,000 B.P by Ruddiman & McIntyre (1981).

Stage Three 12,000 to 9,000 B.P.

The fluvial gravels are deposited directly on bedrock and give foraminiferal ages of 12,000 B.P. relating to "very-fresh brackish water" conditions (Eddles & Hart 1989). At this time there appears to have been an episode of meandering and downcutting in the Central PalaeoChannel, possibly related to the fluctuations in sea levels recognized by Fairbridge (1961). At 12,000 B.P. the sea level in the English Channel was at the -50 to -60m isobath, which corresponds to the Lower Cliff sequence of Donovan & Stride (1975). The actual date of the cutting of the marine terraces and cliffs has led to much controversy. It is possible that the terraces were cut during a standstill at one of three events - (i) the Early Devensian transgression when sea levels reached +8.0m O.D. or, (ii) the Middle Devensian regression when sea level decreased to -130.0m O.D, or, (iii) the Flandrian transgression from c. 9,000 B.P.

If the terraces had been cut during either (i) or (ii), the cliff profiles would have experienced subaerial erosion, and the height continuity on either coast of the English Channel would be modified by forebulge movements. As the terraces show no evidence of erosion and have good height continuity, it is concluded that they were most probably cut at times of sea level standstill during the Flandrian transgression.

To estimate the age of the un-dated sediments in Plymouth Sound, deposited between 20,000 and 9,000 B.P., a simple extrapolation model can be developed using the foraminiferal evidence from the first fluvial deposits. On this basis sediments deposited at 35m correspond to a sea level height in the Channel of -60m (Larsonneur *et al.* 1982, Delibrias & Guillier 1971). The following change in sediment facies in Plymouth Sound occurred at -27.5m. Assuming the same gradient of 25m between the Sound and the Channel, the marine cliff levels (standlines) can be correlated with levels of the PalaeoTamar (Table 8.1). This is a very rough index and does not take into account any vertical movements or change in gradient with hydraulic head. (Ages are derived from the Delibrias & Guillier 1971 curve).

Channels m O.D.	Sea Level m O.D.	Age B.P.	Cliffs m O.D.
-22.0	-47.0	9,000	-38 to -49
-27.5	-52.0	11,000	-49 to -58
-35.0	-60.0	12,000	-58 to -69
-42.0	-130.0	20,000	

Table 8.1

Correlation between PalaeoTamar and the English Channel

Stage Four 9,000 to 7,000 B.P. (Figure 8.7)

At 9,000 B.P. the PalaeoPlym and PalaeoTamar were joined by three rivers in what is now the Hamoaze Channel. It was the incision of these rivers that lead Plymouth to be known as the Three Cities during the 13th century (Section 1.2). The rivers maintained their courses until they were channeled underground by the Victorian sewage system. The eastern part of Plymouth Sound was dominated by a meandering river with no tidal influence as anaerobic muds were deposited in areas of quiet water, and the channel was floored by gravels with sandy point bar sequences. The

Central river split into two between the Panther Shoal and Shovel Rock. These two channels are named herein as the Western and Central PalaeoChannels which re-converged eastward of Penlee Point (Section 3.6.5) where it is envisaged that estuarine conditions prevailed. A third tributary entered the river at a point to the south of the Eastern Breakwater and received waters from a smaller river which flowed off Staddon Heights and through Bovisand Bay. The third tributary is named the Eastern PalaeoChannel (Section 3.6.5). It is postulated that the -14.6m terrace on Rubble Bank (Section 2.4.1) corresponds to the average depth to exposed rock head in the Outer Sound area of -12 to -13m. O.D. The discrepancy in depth is ascribed to the difference in tidal height between the Outer Sound area and the Tamar, where the nature of the confluence increases the tidal height and thus the erosive potential of tidal currents. The terrace and planation surface were probably cut during the Boreal phase which experienced standstills. The top of the Upper Ledge corresponds to the height of terraces recognized by Durrance in the Teign and Exe (Durrance 1971, 1974).

Stage Five 7,000 to 6,000 B.P. (Figure 8.8)

By 7,000 B.P, Plymouth Sound was fully inundated by the sea (Sea Level = -10m.O.D) and was established as a tidal inlet. Two islands rose above sea level at Panther Rocks and St.Carlos/Shovel/Tinker Shoals. Sometime during the sea level rise between 9,000 and 7,000 B.P, the Eastern PalaeoChannel changed its identity from a tributary to a distributary. The 1988 borehole showed the -10m datum to be correlated with the upper surface of a series of planar sandstones infilling the Central PalaeoChannel, which migrate towards the east and are composed of medium sands (Figure 8.9) and related to a -10 to -11m planation surface. A change in sedimentation, occurring about 7,000 B.P. (-10m O.D. Delibrias & Gullier 1971), has been recognized throughout the literature on the Quaternary of the South West. Sediment changes included a massive development of peat bogs (Churchill 1965), the occurrence of stacked fluvial channels (Dyer 1975), the development of spits (Nicholls 1984), offshore sand banks and lagoons (Hails 1975, Fitzpatrick 1987), marine platforms (MacFarlane 1955, Kelland 1975), and an increase of marine siliclastics. The event has been recognized on both the Eastern Seaboard of North America and North West Europe. This 7,000 B.P. change has been ascribed to a standstill in sea level rise (Dyer 1975), followed by a rapid transgressive phase (Evans 1979). However, the sedimentation and

hydrographic conditions present in the Sound were also affected by changes in the English Channel. This had been changing since the Straits of Dover were breached *c.* 9,000 B.P (Section 2.3.5), and transformed from a quiet sea with low tidal ranges to a tidally dominated environment, with increased mixing and tidal scour. The main tidal component in the Sound and the English Channel is the M_2 semi-diurnal (Section 1.4), upon which most of the models of sea level rise during the Holocene are computed (Pingree 1980, Austin 1991). Joining of seas generally increases the number of amphidromic points which in turn affect the tidal range in an area. The co-tidal lines in the English Channel converge on the Isle of Wight towards a degenerate amphidromic point (i.e on land). It is suggested that, as sea level increased in the English Channel, the amphidromic point moved eastward. As the amphidrome migrated close to Plymouth, the tidal heights would have increased and then decreased as it passed. Migration of the amphidromic point is also associated with a migration of the sea bed sediment parting zone (Banner 1980). The English Channel sea bed parting of sediments is located beneath the amphidromic point on a line from the Isle of Wight to the Cotentin peninsula. As the amphidromic point migrated up the English Channel, the associated parting zone and bed shear stresses would have changed. The migrating bed shear stresses will have increased the input of mobile sediment into Plymouth Sound. It is postulated that the amphidromic point was located south of Plymouth at about 7,000 B.P. and that the consequential high tidal ranges and increased shear stresses resulted in the extensive planar bedding surfaces infilling the buried channels.

Stage Six 6,000 to 4,000 B.P. (Figure 8.10)

A -5m planation surface is present in Plymouth Sound (Section 2.4.4) and is interpreted as being cut during a standstill in sea level. However, no other planation surfaces at this depth have yet been recognized in the South West. However, Goodwin & Goodwin (1940) recognized a planation surface at -6m and the Fairbridge (1961) sea level curve identifies a planation surface at -5.5m, about 5,700 B.P. The -5m planation surface is therefore dated as *c.* 5,700 B.P. caused by erosion during a standstill, possibly exacerbated during a regressive event. At this time, the Sound had free connection to the English Channel, with several small rocky islands (Panther Rocks, Shovel Rock, Tinker Shoal, St. Carlos Rocks, South Winter Shoal and possibly a shoal at the Mallard). The tidal ranges were similar to those of the present day (Austin 1991).

Marine gravels began to transgress over the sands and fluvial gravels of the PalaeoTamar creating a series of furrows and gravel waves (Section 3.6.4).

Stage Seven 4,000-3,000 B.P.

The planation of the rock shoals at -3.0m O.D. and the overtopping of the Upper Ledge (Hamoaze Channel) is estimated to have occurred during a standstill at 3,700 B.P. (Fairbridge 1961).

Stage Eight 3,000 B.P to present

The depth to exposed rock head over The Bridge's is -2.0m O.D. Similar heights occur in Poole Bay (Fitzpatrick 1987). The time of breaching of the Drake's Island-Mount Edgecombe ridge is dated as c. 3,000 B.P., according to the curve proposed by Delibrias & Guillier (1971) for the English Channel. It was after the breaching of The Bridge's that the present day hydrographic conditions of Plymouth Sound began to develop fully.

8.4 The Future of Plymouth Sound

Sea levels are generally accepted to be rising at a rate of 1.0 to 2.0mm a⁻¹ (IPCC 1990). There is no firm evidence of acceleration this century, although sea level has risen faster than during the last two centuries (Table 8.2). The successor to Project 61 was IGCP Project 200 which was developed "To identify and quantify the processes of sea level change correlating for tectonic, climatic, tidal and oceanographic correlations" (1983-1987) and aimed at sea level correlations and applications. The ultimate purpose of Project 200 was to "provide a basis for predicting near-future changes for application to a variety of coastal problems, with reference to densely populated low-lying coastal areas" Many publications arose from Project 200, as summarized in Shennan (1989).

The main cause of the present sea level rise is generally accepted to be the so-called "Greenhouse effect" whereby emissions from human activities are causing an increase in the concentration of the greenhouse gases which include carbon dioxide, methane, CFC's and nitrous oxides. The IPCC (Intergovernmental Panel on Climate Change) "Business-as-usual" scenario has estimated a mean global temperature increase of 0.3°C per decade. By the year 2030, global sea level is estimated, on this basis, to rise 8 to 29cm higher than today (the best estimate is 18cm - Table

8.3) and by 2070 sea level will be 21 to 71cm higher than today (with a best estimate of 44cm). In order to maintain the greenhouse gases at their present level, emissions of CO₂ must decrease by 60%, and methane must be reduced by 15-20% (IPCC 1990). There are many uncertainties in the IPCC calculations. These include the potential development of sources and sinks, the effect of clouds, the response of the oceans and the behavior of the polar ice sheets. In addition to these uncertainties, recent studies have shown that, as temperature increases, oceanic phytoplankton and associated CO₂ emissions will increase proportionally (Williamson & Gribben 1991).

Estimated contributions to sea level rise in the last 100 years			
	Low	Best	High
	cm	cm	cm
Thermal expansion	2.0	4.0	6.0
Glaciers/small ice caps	1.5	4.0	7.0
Greenland ice sheet	1.0	2.5	4.0
Antarctic ice sheet	-5.0	0.0	5.0
Total	0.5	10.5	22.0
Observed	10.0	15.0	20.0

Table 8.2

Estimated contributions to sea level rise in the last 100 years

Four main contributors to sea level rises are identified in the IPCC report :

- (i) Thermal expansion of the oceans. In the period from 1885 to 1985 the oceans have had a 0.3° to 0.6°C increase in temperature resulting in a 2.6cm rise.
- (ii) Melting of the Greenland ice sheet. Contribution about 2.5cm.
- (iii) Melting of small ice caps and glaciers is estimated to be 1 to 2cm +/- 0.6mm^{-a} per 1°C warming.
- (iv) There will be an increase of snow cover on Antarctica, however the behavior of the West Antarctica ice sheet is unknown.

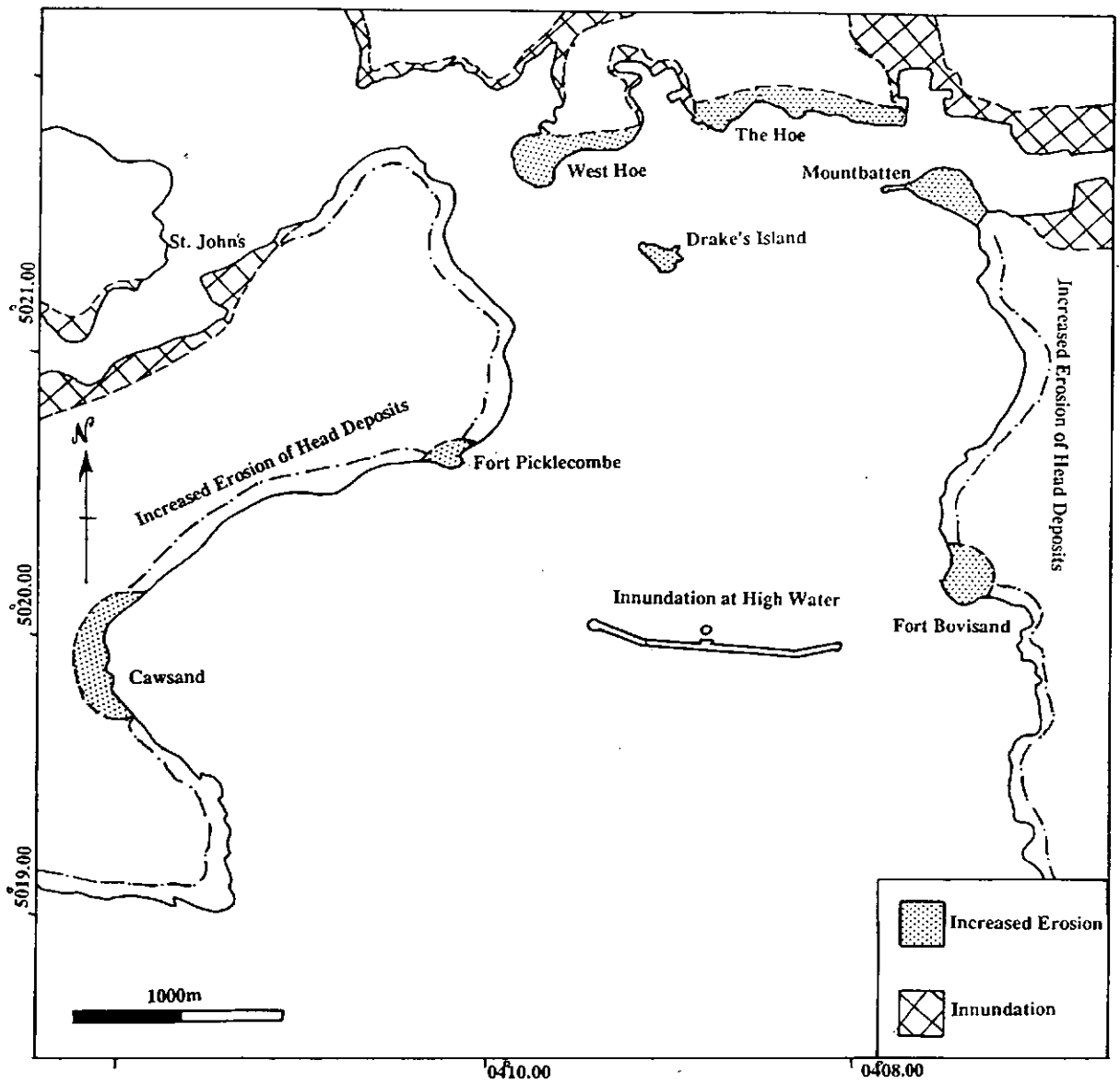


Figure 8.11 Effects of sea level rise in Plymouth Sound

Estimated contributions to sea level rise by 2030			
	Low	Best	High
	cm	cm	cm
Thermal expansion	6.8	10.1	14.9
Glaciers/small ice caps	2.3	7.0	10.3
Greenland ice sheet	0.5	1.8	3.7
Antarctic ice sheet	-0.8	-0.6	0.0
Total	8.7	18.3	28.9
Observed	10.0	15.0	20.0

Table 8.3
IPCC Business-as-Usual estimates for 2030

Four main models have been developed for predicting the effect of sea level rises: (i) an extrapolation of a trend (ii) the Bruun rule, (iii) the sediment budget, and (iv) the dynamic equilibrium model (Leatherman 1991).

The main effects of sea level rises are three-fold (i) increased erosion as waves will be closer to shore before they dissipate their energy, (ii) the deeper water will decrease wave refraction and increase the capacity for long shore drift and, (iii) the higher water level will increase the erosion potential further up the beach.

The effects of a sea level rise of 71cm have been estimated for Plymouth Sound using Leatherman's extrapolation of trend model. The primary effect of this sea level rise are:

- (i) inundation of the Breakwater during High Water, thus reducing its effectiveness and causing erosion of the mud depocentre.
- (ii) increased tidal currents will increase the shear stress on the bed and result in increased mobility of the sand sheets.
- (iii) greater erosive power of the sea will result in collapse of the head deposits surrounding Plymouth Sound and several areas will become the target for maximum erosion (Figure 8.11).
- (iv) the mobile material produced from (iii) will cause silting of the Sound in Mountbatten depocentre and The Anchorage.
- (v) several low-lying areas will be prone to flooding at High Water.

8.5 Methods and Techniques

In an investigation of this nature, involving many techniques, a critique of the method can be made at each stage and a list of required

modifications are identified. During this survey several conclusions on the methodology were made, these are outlined below.

Side-scan sonar

In this survey the side-scan sonar was used successfully; the only constraints were (i) some areas remained unsurveyed as they were either too shallow or supported heavy sea traffic and, (ii) it is absolutely essential to obtain groundtruth sea bed samples in order to calibrate the records.

Sampling

The use of SCUBA divers in any survey of this type is invaluable when compared to the "spot" sample of a grab; as they can make observations and measurements of features on the sea bed. Divers were limited in that permission was denied to dive in restricted areas, where grabs were allowed and diving was confined to Polytechnic term time.

Sedimentology

The collection and analysis of sediments from the sea bed formed an important role in the understanding of sediment transport and deposition. four areas of study proved invaluable in this investigation.

(i) the size and quantity of shelly material in the sediment gave an index of the actual relative age of the sediment, the source and the phase of mobility, i.e. whether continuous, limited to Spring tides or episodic.

(ii) the occurrence of relict gravels were recognized. Their modal sizes, sorting and clast shapes was used to identify the actual nature of deposition and gave a comprehensive insight into the history of development of the Sound.

(iii) Physical measurements made on the cores from the Inner Breakwater depocentre illustrated different prevailing tidal conditions over the depocentre. The depth of the anoxic/suboxic boundary was successfully used as an indicator of the presence and rate of deposition of organic detritus. The varying moisture content and critical shear stresses illustrated the areas of maximum instability to be at the periphery of the depocentre, which is controlled by the position of the Western and Eastern Streams.

(iv) The use of X-ray diffraction in the identification of the clay mineralogy of the sea bed samples was vital in the establishment of the position and source of the water bodies in Plymouth Sound. The clay

mineralogy, i.e. mixed-layer or pure, gave a comprehensive indication into the stability of the sea bed (Stephens *et al. in press*).

Oceanographic measurements

The *in situ* methods chosen for this survey were successful and gave a comprehensive overview of the surface characteristics of the water. The techniques allowed rapid, reproducible measurements to be made, and therefore many stations could be covered concurrent with the overflights. The techniques were also easy to master. This was important, as most of the ground crew were neither geologists nor oceanographers. It became apparent during laboratory work, that it is necessary to correct the weight of the filter papers for varying surface salinity.

Airborne remote sensing

The ATM proved an invaluable tool for the investigation of the inlet. The thermal bands provided accurate synoptic overviews of the water bodies present in Plymouth Sound. Once identified, these were tracked and their development and decay over the tidal cycle could be mapped. The thermal bands also allowed the temperature, and therefore stability and age of a body, to be evaluated in comparison with adjacent bodies and streams. The presence of ship's wakes was accurately used to indicate stratification, mobility of surface water and the relative position of the sampling vessels. The visible bands of the ATM are broad and could not be used to differentiate between the different suspended material in the water bodies. The Band 3 images, however, showed clear differentiation, and were used extensively in the mapping of the water bodies. The positions of the water bodies were supported by the results of the X-ray diffraction analysis. It is important to note that in a mixed-input inlet, such as Plymouth Sound, it is necessary to establish the suspended concentration type and spectral signature. It was hoped that the CASI data would counteract the wide bands of the ATM and allow differentiation of the suspended sediment by their spectral peaks. The presence of a concurrent groundtruth programme was found to be necessary in this study, primarily to calibrate the scanner data, and secondly to establish the continuity between the surface and the sea bed.

Magnetic measurements

The physical properties of the sediment must be taken into account when making magnetic measurements of unconsolidated sediments. Several

relationships have been established through this study including:

- (i) An inverse relationship between organic content and susceptibility.
- (ii) An increase in organic content is associated with the development of secondary active fabric (i.e 5-7% TOC = Active fabric)
- (iii) An increase in grain size of the silts and sand in association with a decrease in susceptibility which is directly related to the type of magnetic carrier - in this case haematite, as recognized in the samples.
- (iv) An increase in clay content causes an increase in the degree of primary fabric which seems to be related to the collapsing of clays from framework to horizontal laminated structures.
- (v) There is an increase of susceptibility with an increase in the definition of the magnetic fabric.
- (vi) It is apparent that natural sediments do not conform to the primary and secondary fabrics established in laboratory experiments. In order to describe the Plymouth Sound silts, three categories have been suggested (i) primary, (ii) secondary active and, (iii) secondary disruptive.
- (vii) Remanence results are generally unreliable due to the unconsolidated nature of the sediments involved. Remanence acquisition is tentatively suggested to occur after a lag of 20 years and to be associated with the development of anoxic conditions.
- (viii) Inclination shallowing decreases with depth and is related to the redox conditions. The inclination approaches the ambient field in suboxic and anoxic zones of the sediment profile. This is attributed to authigenic development of haematite under these conditions.
- (ix) The intrinsic intensity and susceptibility can be used to define the redox environment, at least in the areas studied here.

Sea Level rises

In addition to the general problems of identifying sea level changes, it is clear that each inlet or basin must be investigated individually. In addition to the global, or regional aspects, all of the local palaeoenvironmental constraints and effects must be identified. Ideally, to study sea level changes, the area is required to be stable and have a well developed river system, which is subaerially exposed between standstills (e.g. South Africa/Australia). Even then, it is also necessary to establish the nature and history of the surrounding/connecting sea and take any change of the tidal regime into account.

8.6 Future Work in Plymouth Sound

This work has successfully established the main features of the history and present day hydrodynamics, sedimentology and compiled a comprehensive data set for Plymouth Sound. Nonetheless, not all of this complex evolution has been investigated and many avenues of future work can be identified. The suggestions for future work can be divided into two categories; investigative and instrumental.

Investigative

This category includes work which can be carried out with existing techniques.

- (i) to process the CASI data.
- (ii) to establish the degree of seasonality and episodicity of the sediments in Plymouth Sound using fixed monitored stations.
- (iii) to establish the seasonality of re-suspension from the mud flats in the estuaries, i.e. is it dominated by the M_2 semi-diurnal, the Spring/Neap cycle or periods of bad weather?.
- (iv) to map the gyres and tidal fronts in the Sound using Lagrangian methods.
- (v) to map the distribution of water bodies from fixed stations at Low Water and throughout the tidal cycle.
- (vi) to investigate the effect of different salinities on the properties of remanence.
- (vii) to investigate the caves underneath The Hoe and possibly apply magnetic techniques in order to establish the exact date of inundation.

Instrumentation

This category includes modification of existing techniques

- (i) to develop a method for an underwater *in situ* relict gravel study.
- (ii) to develop a method of impregnating fine silts for magnetic measurements prior to agitation during sampling and measuring.
- (iii) to ensure the correct bands are selected on an airborne sensor that will maximize the difference between the water types.
- (iv) to develop reliable algorithms to extract the suspended sediment signature for waters characterized by mixed clays.

8.7 Final Comment

In this study, a time constraint of three years was imposed; therefore the methods and techniques used were chosen for their ability to provide

maximum data acquisition in a relatively short space of time. Particularly useful was the acquisition of instantaneous synoptic remotely sensed data (airborne remote sensing and side-scan sonar) in combination with SCUBA diver groundtruth. These results identified areas which required further and concentrated investigation. The use of magnetic measurements in the mud depocentres was invaluable in obtaining a rapid understanding of the depositional environment.

REFERENCES

- Admiralty Tide Tables 1988, The Port of Devonport, H.M.S.O.
- Admiralty Tide Tables 1989, The Port of Devonport, H.M.S.O.
- Admiralty Tide Tables 1990, The Port of Devonport, H.M.S.O.
- Admiralty Tide Tables 1991, The Port of Devonport, H.M.S.O.
- Albanakis, K.S. 1990. Testing of a model for the simulation of the volume reflectance of waste due to suspended sediment under controlled conditions for various sediment types. *Int. J. Remote Sensing*, **11**, 1533-1547.
- Al-Dabbas, M.A.M. and McManus, J. 1988. Shell fragments as indicators of bed sediment transport. *Proc. R. Soc. Edin.* **B92**, 335-344
- Amos, C.L. and Alfondi, T.T. 1979. The determination of suspended sediment concentration in a macrotidal system using LANDSAT data. *J. Sedi. Petrol.*, **49**, 159-174.
- Anderson, D.P. 1988. A seismic reflection survey of the River Tamar. *Unpublished B.Sc thesis, Plymouth Polytechnic Department of Geological Sciences.*
- Anderson, J. M. 1989. Remote sensing in the Tay Estuary using the Airborne Thematic Mapper. In: *Developments in Estuarine and Coastal study* (Ed: Elliott and J. McManus). 15-20.
- Anderson, J. and Callinson, R.D. 1987. The general applicability of airborne thematic surveys in the measurement of sea-surface temperatures. *Proc. R. Soc. Edin.*, **B92**, 237-255.
- Anderson, J.B. and Thomas, M.A. 1991. Marine ice-sheet decoupling as a mechanism for rapid, episodic sea-level change, The record of such events and their influence on sedimentation. *Sedimentary Geology*, **70**, 87-104.
- Andrews, J.T. 1973. The Wisconsin Laurentide Ice Sheet, dispersal centres, problems of rates of retreat and climatic implications. *Arctic and Alpine Research*, **5**, 185-199.
- Anson, G.L. and Kodama, K.P. 1987. Compaction-induced inclination shallowing a post depositional remanent magnetization in a synthetic sediment. *Geophys. J. R. astr. Soc.*, **88**, 673-692.
- Arason, P. and Levi, S. 1990a, Models of inclination shallowing during sediment compaction. *J. Geophys. Res.*, **95**, 4481-4490.
- Arason, P. and Levi, S. 1990b. Compaction and inclination shallowing in deep-sea sediments from the Pacific Ocean. *J. Geophys. Res.*, **95**, 4501-4510.
- Arthaud, F. and Matte, P. 1977. Late Palaeozoic strike-slip faulting in Southern Europe and Northern Africa, Result of a right lateral shear zone between the Appalachians and the Urals. *Geol Soc. Amer. Bull.*, **88**, 1305-1320.

- Austin, R.M. 1991. Modelling Holocene tides on the North West European Continental Shelf. *Terra Nova*, 3, 276-288.
- Babey, S.K. and Anger, C.D. 1989. Compact Airborne Spectrographic Imager CASI. *Itres Research Information*.
- Bale, A.J., Morris, A.W., and Howland R.J.M. 1984. Size distributions of suspended material in the surface waters of an estuary measured by laser Fraunhofer diffraction. In: *Transfer processes in cohesive sediment systems* (Ed. W.R. Parker and D.J.T. Kinsman), Plenum Press, 75-85.
- Banner, F.T. (with a contribution by Culver, S.J.) 1980. Sediments of the North-West European Shelf. In: *North West European Shelf Seas: Sea bed in motion Vol.I Sedimentology* (Ed, F.T. Banner, M.B. Collins and K.S. Massie) Elsevier Oceanography Series 24B, Amsterdam, 271-300.
- Barton, C.E. and McElhinny, M.W. 1979. Detrital remanent magnetization in five slowly redeposited long cores of sediment. *Geophys. Res. Letters.*, 6, 229-232.
- Barton, C.E., McElhinny, M.W. and Edwards, D.J. 1980. Laboratory studies of depositional depositional detrital remanent magnetization. *Geophys. J. R. astr. Soc.*, 61, 355-377.
- Barua, D.K. 1990. Suspended sediment movement in the estuary of the Ganges - Brahmaputra - Meghna River system. *Mar. Geol.*, 91, 243-253.
- Belderson, R.H. and Stride, A.H. 1966. Tidal current fashioning of a basal bed. *Mar. Geol.* 4, 237-257
- Belderson, R.H., Kenyon, N.H., Stride, A.H. and Stubbs, A.R. 1972, *Sonographs of the Sea floor*. Elsevier Amsterdam, p185.
- Belderson, R.H., Wilson, J.B., Holme, N.A. 1988. Direct observation of longitudinal furrows in gravel and their transition with sand ribbons in strongly tidal seas. In: *Tide-influenced Sedimentary Environments and Facies* (Ed P.L. de Boer) D.Reidel, 79-90.
- Bilham, R. and Barrientos, S. 1991. Sea level rise and Earthquakes. *Nature*, 350, 4th April 1991, 386.
- Blow, R.A. and Hamilton N. 1978. Effect of compaction on the acquisition of a detrital remanent magnetization in fine-grained sediments. *Geophys. J. R. astr. Soc.*, 52, 13-23.
- Bohme, E., Salusti, E. and Travaglioni, F. 1986. Satellite and field observations of shelf currents off Cape Santa Maria di Leuca, S. Italy. *Oceanologia Acta*, 9, 41-46.
- Boillot, G. 1964. Geologie de la manche occidentale fonds Roche, depots Quaternaires sediments actuels. *Annales de l'institute Oceanographie*, Tome XIII, 1-200.
- Bosence, D.W.J. 1979. Live and dead faunas from coralline algal gravels Co. Galway, Ireland. *Palaeontology*, 19, 365-395.
- Bowen, D.Q. and Skyes, G.A. 1988. Correlation of marine events and glaciation on the North East Atlantic margin. *Phil. Trans. R. Soc., Lond.*, B318, 619-635.

- Boxall, S. and Reilly, J. 1989. Results of the Fluorescent Line Imager Marine campaign in the West Solent. In: *Proc. of the N.E.R.C. workshop on Airborne Remote Sensing*, 93-108.
- Boxall, S. and Matthews, A. 1990. Results of the CASI campaign in the West Solent. In: *Proc. of the N.E.R.C. symposium on Airborne Remote Sensing 1990*. 225-258.
- Buller, A.T., Green, C.D. and McManus, J. 1975. Dynamics and sedimentation, the Tay is compared with other Estuaries. In: *Nearshore sediment dynamics and sedimentation* (Ed J. Hails and A. Carr) Wiley, 201-249.
- Buller, A.T. and McManus, J. 1979. Sediment sampling and analysis. In: *Estuarine hydrography and sedimentation - a handbook* (Ed. K R Dyer) C.U.P., 80-130.
- Catt, J.A. 1988. *Quaternary Geology for Scientists and Engineers*. Ellis Horwood Ltd. pp 339.
- Carthew, R. and Bosence, D.W.J. 1986. Community preservation in recent shell-gravels, English Channel. *Palaeontology*, **29**, 243-268.
- Chad, G.Y. 1969, 2θ (Cu) Table for common minerals. *Geological Paper 69A*, Carlton University, Ottawa.
- Chandler, P. and McCall, G.J.H. 1985. Stratigraphy and structure of the Plymouth - Plymstock area, a revision. *Proc. Ussher Soc.*, **6**, 253-257.
- Chapman, T.J. 1983. A guide to the structure of the Lower to Middle Devonian Staddon Grits and Jennicliff Slates on the east side of Plymouth Sound, Devon. *Proc. Ussher Soc.*, **5**, 460-464.
- Chapman, T.J., Fry, R.L. and Heavey, P.T. 1984. A structural cross-section through South West Devon. In: *Variscan Tectonics of the North Atlantic region* (Ed. D.H. Hutton and D.J. Sanderson) *Spec. Pub. Geol. Soc. Lond.*, **14**, 113-118.
- Chen, Z. Hansom, J.D. and Curran, P.J. 1990. The form of the relationship between suspended sediment concentration and spectral reflectance. *Int. J. Remote sensing*, **12**, 215-222.
- Chernow, R.M., Frey, R.W. and Ellwood, B.B. 1986. Biogenic effects on development of magnetic fabrics in coastal Georgia sediments. *J. Sedi. Petrol.*, **56**, 160-172.
- Chesterman, W.D., Clynick, P.R. and Stride, A.H. 1958. An acoustic aid to sea bed survey. *Acoustica*, **8**, 285-290.
- Christie-Blick, N., Mountain, G.S. and Miller, K.G. 1988. Sea level History - a technical comment. *Science*, **241**, 29th July 1988, 596.
- Churchill, D.M. 1965. The displacement of deposits formed at sea level 6,500 years ago in Southern Britain. *Quaternaria*, **7**, 239-249.
- Codrington, T. 1898. On some submerged rock valleys in South Wales, Devon and Cornwall. *Quart. J. Geol. Soc. Lond.*, **54**, 251-278.
- Colenso, J.W. 1832. A description of the Happy Union tin stream works at Pentuan. *Trans. R. Geol. Soc. Cornwall*, **4**, 29-39.

- Collins, M. and Pattiaratchi, C. 1984. Identification of suspended sediment in coastal waters using airborne thematic mapper data. *Int. J. Remote sensing*, **4**, 635-657.
- Collins, N. 1989. Doggies and Dolphins - Autosub community research projects. *N.E.R.C. News*, **11**, 16-17.
- Collinson, D.W. 1965. Depositional remanent magnetization in sediments. *J. Geophys. Res.*, **70**, 4663-4668.
- Congxian, L., Chen, G., Yao, M. and Wang, P. 1991. The influences of suspended load on the sedimentation in the coastal zones and continental shelves of China. *Mar. Geo.*, **96**, 341-352.
- Cook, F.J., Morrison, A.J., Rollin, E.M., Stockham, R.J. and White, S.R. 1989. Support operations, data archiving and radiometric calibration. In: *Proc. of the N.E.R.C. workshop on Airborne Remote Sensing 1989*, 7-18.
- Cooper, L.H.M, 1948, A submerged cliff-line near Plymouth. *Nature*, **161**, 280.
- Cope, J.C.W. 1987. The Pre-Devonian geology of South West England. *Proc. Ussher Soc.*, **7**, 473-486.
- Cracknell, A. 1989, Remote sensing in estuaries, an overview. In: *Developments in estuarine and coastal study techniques EBSA 17* (Ed. A.P. Elliott and J. McManus), 11-13.
- Cracknell, A.P., MacFarlane, N., McMillan, K., Charlton, J.A., McManus, J. and Ulbright, K.A. 1982. Remote sensing in Scotland using data received from satellite - a study of the Tay Estuary region using LANDSAT multispectral scanning imagery. *Int. J. Remote Sensing*, **3**, 112-137.
- Cranfield, D.E. and Berner, R.A. 1987. Dissolution and Pyritization of magnetite in anoxic marine sediments. *Geochim. Cosmochim. Acta*, **51**, 645-659.
- Crisp, D.J. 1964 (Ed.), The effects of the severe winter of 1962-63 on marine life in Britain. *J. Animal. Ecol.*, **33**, 165-210.
- Culver, S.J. 1979. Palaeolithic to Iron age archaeology and palaeoenvironment in the Swansea area. In: *Industrial embayments and their environmental problems a case study of Swansea Bay* (Ed. M.B. Collins, F.T. Banner, P.A. Tyler, S.J. Wakeheld and A.E. James), Pergamon Press, 59-69.
- Darbyshire, M. and Draper, L. 1962. Forecasting wind generated sea-waves. *Engineering (Lond.)*, **195**, 482-487
- Dart, P. 1985. Site Register Project, The dive sites in and around Plymouth Sound. *Marine Conservation Society*. (unnumbered).
- Delibrias, G. and Guillier, M.T. 1971. The Sea level on the Atlantic coast and the Channel for the last 10,000 years by the ¹⁴C Method. *Quaternaria*, **14**, 131-135.
- Delo, E.A. 1988. *Estuarine Mud Manual*. Hydraulics Research Report SR p164.

- Deveraux, B.J., Fuller, R.M., Carter, L. and Parsell, R.J. 1990. Geometric correction of airborne scanner imagery by matching Delaunay analysis. *Int. J. Remote Sensing*, **11**, 2237-2251.
- Devoy, R.J. 1982. Analysis of the geological evidence for Holocene sea-level movements in Southeast England. *Proc. Geol. Ass.*, **93**, 65-90.
- Dingwall, R.G. 1975. Sub-bottom infilled channels in an area of the Eastern English Channel. *Phil. Trans. R. Soc. Lond.*, **A279**, 233-241.
- D'Ollier, B. 1979. Side-scan sonar and reflection seismic profiling. In: *Estuarine hydrography and sedimentation - A handbook* (Ed. K.R. Dyer), C.U.P, 57-86.
- Donovan, D.T. and Stride, A.H. 1975. Three drowned coast lines of probable Late Tertiary age around Devon and Cornwall. *Mar. Geol.*, **19**, M35-M40.
- Duck, R.W. 1985. Traces made by the Amphipod *Gammarus* in subaerially-exposed marginal sediments of a freshwater lake. *Boreas*, **15**, 19-23
- Dunlop, D.J. 1979. On the use of Zijderveld vector diagrams in multicomponent palaeomagnetic studies. *Phys. Earth Planet. Int.*, **20**, 12-24
- Durrance, E.M. 1971. The buried channels of the Teign estuary. *Proc. Ussher Soc.*, **2**, 299-306.
- Durrance, E.M. 1974. Gradients of buried channels in Devon. *Proc. Ussher Soc.*, **3**, 111-119.
- Dyer, K.R. 1969. *Some aspects of coastal and marine sedimentation*. P.h.D. Thesis. The University of Southampton.
- Dyer, K.R. 1975. The buried channels of the "Solent River", Southern England. *Proc. Geol. Ass.*, **86**, 239-245.
- Eddies, R.D. and Reynolds, J.M. 1988. Seismic characteristics of buried rock-valleys in Plymouth Sound and the River Tamar. *Proc. Ussher Soc.*, **7**, 36-40.
- Eddles, A.P. and Hart M.B. 1989. Late Quaternary Foraminiferida from Plymouth Sound - preliminary investigation. *Proc. Ussher Soc.* **8**, 168-171
- Edmonds, E.A., McKeown, M.C. and Williams, M. 1969. *British Regional Geology, South West England*. Third Edition, H.M.S.O. London, p130.
- Ellwood, B.B. 1979. Particle flocculation, one possible control on the magnetization in deep-sea sediments. *Geophys. Res. Lett.*, **6**, 237-240.
- Ellwood, B.B. 1984. Bioturbation, minimal effects on the magnetic fabric of some natural and experimental sediments. *Earth Planet. Sci. Lett.*, **67**, 367-376.
- Ellwood, B.B. and Ledbetter, M.T. 1977. Antarctic bottom water fluctuations in the Vema Channel, effects of velocity changes on particle alignment and size. *Earth. Planet. Sci. Lett.*, **35**, 189-198.

- Ellwood, B.B. and Hatten Howard, J. 1981. Magnetic fabric development in an experimentally produced Barchan dune. *J. Sedi. Petrol.*, **51**, 97-100.
- Emery, K.O. and Aubrey, D.G. 1985. Glacial rebound and relative Sea levels in Europe from tide gauge records. *Tectonophysics*, **120**, 239-255.
- Emiliani, C. 1955. Pleistocene Temperatures. *J. Geol.*, **63**, 538-578.
- EOSAT/NASA. 1987. System concept for wide-field-of-view observations of ocean phenomena from space. *Report of the Joint EOSAT/NASA Sea-Wifs Working Group*.
- Evans, G. 1979. Quaternary transgressions and regressions. *Quart. J. Geol. Soc. Lond.*, **136**, 125-132.
- Evans, G. and Collins, M.B. 1975. The transportation and deposition of suspended sediment over the intertidal flats of the wash. In: *Nearshore sediment dynamics and sedimentation* (Ed. J. Hails and A. Carr), Wiley & Sons, p273-306.
- Evans, K.M. 1983. The marine Devonian of the Plymouth area. (Abst). *Proc Ussher Soc.*, **5**, 489.
- Everard, C.E. 1954. The Solent river, a geomorphological study. *Trans. Institute British Geographers*, **20**, 41-58.
- Fairbridge, R.W. 1961. Eustatic changes in Sea Level. In: *Physics and Chemistry of the Earth* (Ed. L.H. Ahrens, F. Press, K. Rankama and S.R. Runcorn), Pergammon Press, 99-185.
- Farnham, W.F and Bishop, G.M. 1975. Survey of the Fal Estuary, Cornwall. *Rep. Underwater Ass.*, **1**, 53-63.
- Ferrier, G. and Anderson J. 1990. Preliminary studies of frontal systems in the Middle and Outer sections of the Tay Estuary. In: *Proc. of the N.E.R.C. symposium on Airborne Remote Sensing 1990*, 221-234.
- Fitzpatrick, F. 1987. *A bathymetric and sedimentological study of Poole Bay, Dorset*. Unpublished M.Sc. Thesis, University of Southampton, Department of Oceanography.
- Fitzpatrick, F, 1990(a). Remotely sensed sedimentology of Plymouth Sound. *Proc. Ussher Soc.*, **7**, 289-294.
- Fitzpatrick, F. 1990(b). The use of Airborne Thematic Mapper data in the correlation of surface waters and sedimentary environments; Plymouth Sound. In: *Proc. of the N.E.R.C. symposium on Airborne Remote Sensing 1990*, 235-248.
- Fisher, J. and Schlüssel, P. 1990. Sun-simulated chlorophyll fluorescence 2, Impact of atmospheric properties. *Int. J. Remote Sensing*, **11**, 2149-2162.
- Flemming, B.W. 1976. Side-scan sonar - a practical guide. *Int. Hydrographic Rev.*, **53**, 65-92.
- Flemming, N.C. 1982. Multiple regression analysis of Earth movements and eustatic sea level change in the United Kingdom in the past 9000 years. *Proc. Geol. Ass.*, **93**, 113-125.

- Flood, R.D., Kent, D.V., Shor, A.N. and Hall, F.R. 1985. The magnetic fabric of surficial deep-sea sediments in the HEBBLE area (Nova Scotian continental rise). *Mar. Geol.*, **66**, 149-167.
- Folk, R.L. 1966. Review of grain size parameters. *Sedimentology*, **6**, 73-93.
- Folk, R.L. and Ward, W.C. 1957. Brazos river bar, a study in the significance of grain size parameters. *J. Sedi. Petrol.*, **27**, 3-26.
- Frankel, S.L. and Pearce, B.R. 1973. *Determination of water quality parameters in the Massachusetts Bay (1970-73)*. M.I.T., Cambridge Report No MITSG 74-8.
- Friedman, G.M. and Sanders, J.E. 1978, *Principles of Sedimentology*, Wiley & Sons, New York, p792.
- Friedman, G.M. and Johnson, K.G. 1982. *Exercises in Sedimentology*, Wiley & Sons, p208.
- Fuller, M.D. 1963. Magnetic Anisotropy and Palaeomagnetism. *J. Geophys. Res.*, **68**, 293-309.
- Gayer, R. and Jones, J. 1989. The Variscan Foreland in South Wales. *Proc. Ussher Soc.*, **7**, 177-189.
- George, D.G. 1990. The results of the 1989 imaging spectroscopy surveys of Windermere and Esthwaite Water. In: *Proc. of the N.E.R.C. symposium on Airborne Remote Sensing 1990*, 297-302.
- George, D.G. and Hewitt D.P. 1989. The trophic classification of lakes in the Windermere area. In: *Proc. of the N.E.R.C. workshop on Airborne Remote Sensing 1989*, 109-120.
- George, K.J. 1982. Tides and tidal streams. *Est. Brack. Water. Sci. Ass. Bull.*, **44**, 6-7.
- Gibbard, P.L. 1988. The history of the great North European rivers during the past three million years. *Phil. Trans. R. Soc. Lond.*, **B318**, 559-602.
- Gill, C. 1966. *Plymouth: A new history*. David & Charles, Newton Abbot.
- Graham, J.W. 1966. Significance of magnetic anisotropy in Appalachian sedimentary rocks. In: *The Earth beneath the continents* (Ed. J.S. Steinhart and T.J. Smith) *Geophys. Monog. Amer. Geophys. Union.*, **10**, 27-648.
- Granar, L. 1958. Magnetic measurements on Swedish varved sediments. *Arkiv. f. Geofysic*, **3**, 1-40.
- Greensmith, J.T. and Tooley, M.J. (Eds) 1982. IGCP Project 61, Sea level movements during the last deglacial hemicycle (about 15,000 years), final report of the UK working group. *Proc. Geol. Ass.*, **93**: 53-63.
- Griffiths, D.H., King, R.F., Rees, A.I. and Wright, A.E. 1960. The remanent magnetism of some recently varved sediments. *Proc. R. Soc. Lond.*, **A256**, 359-383.

- Griffin, S. 1989. *Plymouth Sound: A seismic survey*. Unpublished B.Sc. Thesis. Plymouth Polytechnic. Department of Geological Sciences.
- Goodwin, H. and Goodwin, M.E. 1940. Submerged peat at Southampton. Data for the study of postglacial history. *J. New Phytologist*, **39**, 303-307.
- Gower, J.F.R. and Borstad, G.A. 1990. Mapping of phytoplankton by solar-simulated fluorescence using an image spectrometer. *Int. J. Remote Sensing*, **11**, 313-320
- Groom, S.B. 1991. Ph.D thesis, in prep.
- Guilcher, A. 1969. Pleistocene and Holocene Sea levels. *Earth Sci. Rev.*, **5**, 69-97.
- Hails, J.R. 1975. Offshore morphology and sediment distribution, Start Bay, Devon. *Phil. Trans. R. Soc. Lond.*, **A279**, 221-228.
- Hamilton, N. and King, A.I. 1964. Comparison of the bedding error of artificially and naturally deposited sediments with those predicted from a simple model. *Geophys. J. R. astr. Soc.*, **8**, 370-374.
- Hamilton, N. and Rees, A.I. 1970. The use of magnetic fabric in palaeocurrent estimation. In: *Palaeogeophysics* (Ed. S.K. Runcorn), Academic Press, London, New York, 445-464.
- Hamilton, D. and Smith, A.J. 1972. The origin and sedimentary history of the Hurd Deep, English Channel, with additional notes on other deeps in the Western English Channel. *Mem. Bur. Rech. Geol. Min.*, **79**, 59-78.
- Hamano, Y. 1980. An experiment on post-depositional remanent magnetization in artificial and natural sediments. *Earth Planet. Sci. Lett.*, **51**, 221-232.
- Haq, B. U., Hardenbol, J. and Vail, P. R. 1987, Chronology of fluctuating Sea Levels since the Triassic. *Science*, **232**, 1156-1165.
- Haq, B.U., Vail, P.R., Hardenbol, J. and Van Wagoner, J.C. 1988. Reply to Sea level fall. *Science*, July 29 1988, 224.
- Hardy, R. and Tucker, M. 1989. X-ray powder diffraction of sediments. In: *Methods in sedimentology* (Ed. M. Tucker) Wiley & Sons, 191-228.
- Hawkins, A.B. 1971. The Late Weichselian and Flandrian Transgression. *Quaternaria*, **14**, 115-130.
- Hawkins, A.B. 1979. Sea level changes around South West England. *Colston papers*, **10**, 67-87.
- Henshaw, P.C. and Merrill, R.T. 1979. Characteristics of drying remanent magnetization in sediments. *Earth Planet. Sci. Lett.*, **43**, 315-320.
- Heyworth, A. and Kidson, C. 1982. Sea level changes in South West England and Wales. *Proc. Geol. Ass.*, **93**, 93-111.
- Hiscock, K. and Moore J. 1986. *Survey of Harbours, rias and estuaries in Southern Britain: Plymouth Area including the Yealm Vol I*. Rep, Peterborough Nature Conservancy Council. (FSC OPRU 136/186), p143.

Hojerslev, N.K. 1982. Bio-optical properties of the Fladden Ground, "Meteor" -FLEX-75 and FLEX-76. *Journal du Conseil International pour l'exploration de la mer*, **40**,272-290.

Holligan, P.M., Aarup, T. and Groom, S.B. 1989. The North Sea Satellite Colour Atlas. *Continental Shelf Research*, **9**, p765.

House, M.R., Richardson, J.B., Chalconer, W.G., Allen, J.R.L, Holland, G.M. and Westoll, T.S. 1977. A correlation of the Devonian rocks of the British Isles. *Geol. Soc. Spec. Report 7*. London.

Hrouda, F. 1982. Magnetic anisotropy of rocks and its applications in geology and geophysics. *Geophys. surveys*, **5**, 37-82.

Hrouda, F., Stephenson, A. and Woltar L. 1983. On the standardization of measurements of the anisotropy of magnetic susceptibility. *Phys. Earth. Planet. Int.*, **32**, 203-208.

Hughes, T.J. 1987. Deluge II and the continent of Doom, rising Sea level and collapsing Antarctic ice. *Boreas*, **16**, 89-100.

Hunt, G.R. and Salisbury, J.W. 1970. Visible and near-infrared spectra of minerals and rocks Vol 1, Silicate Minerals. *Modern Geology*, **1**, 283-300.

The Hydrographer of the Navy. Admiralty Chart No.1722 *Plymouth Sound and Approaches*, scale 1,12,500.

The Hydrographer of the Navy Admiralty Chart No.1967 *Plymouth Sound*, scale 1,75,000.

Hydrographic Professional Paper 24. 1987. The use of side-scan sonar for hydrographic surveying and gathering of bottom texture information. *Professional Paper 24*, 1 & 2.

I²S User Manual, 1990. Compiled by I²S software services.

Inglis, J C, 1878, Plymouth Sound - Its tidal currents. *Trans. Plymouth Institute and Devon and Cornwall Natural history Soc.*, **6**, 275-289.

IPCC, 1990, *Scientific assessment of climate change*. Report prepared for the Intergovernmental Panel on Climate Change (IPCC) by Working group 1.

Irving, E. 1957. The origin of palaeomagnetism of the Torridonian sandstone of north west Scotland. *Phil. Trans. R. Soc. Lond.*, **A250**, 110.

Irving, E. and Major, A. 1964. Post-depositional detrital remanent magnetization in a synthetic sediment. *Sedimentology*, **3**, 135-143.

Ising, G. 1943. On the magnetic properties of varved clay. *Arxiv. f. Matematik, Ast. Fysik.*, **29A**, 1-37.

Jenkins, D.G., Whittaker, J.E. and Carlton, R. 1986. On the age and correlation of the St. Earth beds, South West England. *J. Micropalaeont.*, **5**, 93-105.

Jones, S.R. 1974. Some results from Woodhead sea bed drifter releases in the Western English Channel and Celtic sea. *Fisheries Laboratory Technical Report Series*, **10**, 1-22.

- Jonsson, L. 1986. Remote sensing of the flow characteristics of the strait of Oresund. In: *Symposium on Remote Sensing for Resources Development and Environmental Management*, Enshede, 725-726.
- Kanazawa, K. 1990. Early Pleistocene glacio-eustatic sea level fluctuations as deduced from periodic changes in cold- and warm-water molluscan associations in the Shimokita Peninsula, N. E. Japan. *Palaeogeog. Palaeoclim. Palaeoecol.*, **79**, 263-273
- Karlin, R. 1990a. Magnetite mineral diagenesis in suboxic sediment at Bettis Site W-N, North East Pacific Ocean. *J.Geophys. Res.*, **95**, 4421-4436.
- Karlin, R. 1990b. Magnetite diagenesis in marine sediments from the Oregon continental margin. *J.Geophys. Res.*, **95**, 4405-4491.
- Karlin, R. and Levi, S. 1985. Geochemical and sedimentological control of the magnetic properties of hemipelagic sediments. *J. Geophys. Res.*, **90**, 10,373-10,392.
- Keen, D.H. 1990. Significance of the record provided by Pleistocene fluvial deposits and their included molluscan faunas for palaeoenvironmental reconstruction and stratigraphy, a case study from the English Midlands. *Palaeogeog. Palaeoclim. Palaeoecol.*, **80**, 25-34.
- Kelland, N.C. 1975. Submarine Geology of Start Bay determined by continuous seismic profiling and core sampling. *Quart. J. Geol. Soc. Lond.*, **131**, 7-17.
- Kelland, N.C. and Bailey, A.B. 1975. An underwater study of sandwave mobility in Start Bay. *Rep. Underwater Ass.*, **1**, 74-80.
- Kellaway, G.A., Redding J.H., Shephard-Thorn, E.R. and Destombes, J.B. 1975. The Quaternary History of the English Channel. *Phil. Trans. R. Soc. Lond.* **A279**, 189-218.
- Kent, D.K. and Lowrie, W. 1975. On the magnetic susceptibility of deep sea sediments. *Earth. Planet. Sci. Lett.*, **28**, 1-12.
- Kenyon, N.H. 1970. Sand ribbons of the European Tidal seas. *Mar. Geol.* **9**, 25-39
- Kenyon, N.H. and Stride, A.H. 1970. The tide-swept continental shelf sediments between the Shetland Isles and France. *Sedimentology*, **14**, 159-173.
- Kidson, C. 1977. The coast of South West England. In: *The Quaternary History of the Irish Sea*. (Ed. C. Kidson and M.J. Tooley). *Geological Journal Special Issue*, 257-297.
- Kidson, C. and Heyworth, A. 1976. Quaternary deposits of the Somerset Levels. *Quart. J. Engineering Geol.*, **9**, 217-235.
- King, R.F. 1955. Remanent magnetism of artificially deposited sediments. *Mon. Not. Roy. Astron. Soc. Geophys. Supp.*, **7**, 115-134.

- King, J.W., Banerjee S.K. and Marvin J. 1983. A new rock magnetic approach to selecting sediments for geomagnetic palaeointensity studies - applications to palaeointensity for the last 4,000 years. *J. Geophys. Res.*, **88**, 5911-5921
- Krumbein W.C. 1934. Measurements and geological significance of shape and roundness of particles. *J. Sedi. Petrol.* **11**, 64-72.
- Lambeck, F. and Nakada, M. 1991. Sea level constraints. *Nature*, **350**, 6314.
- Larsonneur, C., Bouysse, P. and Auffret, J. P. 1982. The superficial sediments of the English Channel and its Western Approaches. *Sedimentology*, **29**, 851-864.
- Lattimore, M. 1961. The deep channel of the Tamar Estuary. *Trans. Devonshire Ass.*, **XCIII**, 304-309.
- Leatherman, S.P. 1991. Modelling shore response to sea level rise on sedimentary coasts. *Prog. in Phys. Geog.* **14**, 447-464.
- Lee, A.J. and Ramster J.W. 1976. Atlas of the seas around the British Isles. *Fish. Res. Tech. Rep. MAFF. Direct Fish. Res. Lowestoft.*, **20**, p4.
- Lee, T-Q., Kissel, C., Laj, C., Horng, C-S. and Lue, Y-T. 1990. Magnetic fabric analysis of the Plio-Pleistocene sedimentary formations of the coastal range of Taiwan. *Earth Planet. Sci. Lett.*, **98**, 23-32.
- Leslie, B.W., Lund, S.P. and Hammond, D.E. 1990. Rock magnetic evidence for the dissolution and authigenic growth of magnetite minerals within anoxic of the California Borderland. *J. Geophys. Res.*, **95**, 4437-4452.
- Lopez-Garcia, M.J. and Caselles, V. 1990. A multi-temporal study of chlorophyll- α concentration in the Albufera lagoon of Valencia, Spain using Thematic Mapper data. *Int. J. Remote Sensing*, **11**,301-311.
- Lorenzen, M.W., Boyer, H.A., Megard, R.O., Combs, W.S., Settles, J.C., Edmonson, W.T. and Carlson, R.E. 1980. Comments on Secchi discs. *Limnology and Oceanography*, **25**, 371-372.
- Løvlie, R. 1974. Post-depositional remanent magnetization in a redeposited deep-sea sediment. *Earth. Planet. Sci. Lett.*, **21**, 315-320.
- Løvlie, R. 1976. The intensity pattern of post-depositional remanence acquired in some marine sediments during a reversal of the external magnetic field. *Earth. Planet. Sci. Lett.*, **30**, 209-214.
- Løvlie, R., Lowrie, W. and Jacobs, M. 1971. Magnetic properties and mineralogy of four deep-sea cores. *Earth Planet Sci. Lett.*, **21**, 315-320.
- Lu, R., Banerjee, S.K. and Marvin, J. 1990. Effects of clay mineralogy and the electrical conductivity of water on the acquisition of depositional remanent magnetization in sediments. *J. Geophys. Res.*, **95**, 4531-4538.
- MacFarlane, P.B. 1955. Survey of two drowned river valleys in Devon. *Geol. Mag.*, **92**, 419-429.

- Maddock, L. and Swann, C.L. 1977. A statistical analysis of some trends in sea temperature and climate in the Plymouth Area in the last 70 years. *J. Mar. Bio. Ass. U.K.*, **57**, 317-338.
- Matthews, S.C. 1977. The Variscan Fold Belt in South West England. *N. Jb Geol. Palaont. Abh.*, **154**, 94-127.
- Mantz, P.A. 1977. Incipient transport of fine grains and flakes by fluids - Extended Shields diagram. *J. Hydraulics Division Amer. Soc.*, **103**, 601-615.
- Manheim, F.T., Hathaway, J.C. and Uchupi, E. 1972. Suspended matter in surface waters of the Northern Gulf of Mexico. *Limnology and Oceanography*, **17**, 17-27.
- McCallum, K.D. and Reynolds, J.M. 1987. High resolution seismic profiling in Plymouth Sound and the River Tamar. *Proc. Ussher Soc.*, **6**, 562.
- McCave, I.N. 1971. Sandwaves in the North Sea off the coast of Holland. *Mar. Geol.* **10**, 199-255.
- McCullagh, M.J. and Ross C.G. 1980. Delaunay Triangulation of a Random Data Set for Isarithmic Mapping. *The Cartographic Journal*, **17**, 93-99.
- McLaren, P. and Bowles, D. 1985. The effects of sediment transport on grain-size distributions. *J. Sedi. Petrol.*, **55**, 457-470.
- McManus J. 1965. A study of maximum load for small diameter sieves. *J. Sedi. Petrol.* **35**, 792-796.
- McManus, J. 1975. Quartile derivation - median diameter analysis of surface and core sediments from Start Bay. *Quart. J. Geol. Soc. Lond.*, **131**, 51-56.
- McManus, J. 1989. Grainsize determinations and interpretations. In: *Methods in Sedimentology* (Ed, M. Tucker), Wiley & Sons, 63-85.
- McNeill, D.F. 1990. Biogenic magnetite from surface Holocene Carbonate sediments, Great Bahama Bank. *J. Geophys. Res.*, **95** 4363-4371.
- Meade, R.H. 1966. Factors influencing the early stages of the compaction of clays and sands - a review. *J. Sedi. Petrol.*, **36**, 1085-1101.
- Mead, R.H., Sachs, P.L., Manheim, F.T., Hathaway, J.C. and Spencer D.W. 1975. Sources of suspended matter in the water of the Middle Atlantic Bight. *J. Sedi. Petrol.*, **45**, 171-188.
- Megard, R.O. and Berman, T. 1989. Effects of Algae on the Secchi disc transparency of the southeastern Mediterranean Sea. *Limnology and Oceanography*, **34**, 1640-1655.
- Merratt, L.H. 1980. Smeaton's Tower and the Plymouth Breakwater. Reprint *Maritime History*, **5**, (unnumbered). Devon.
- Miller, M.C. McCave, I.N. and Komar, P.D. 1977. Threshold of sediment movement under unidirectional currents. *Sedimentology*, **24**, 507-527.
- Millman, J.D. and Emery K.O. 1968. Sea levels during the past 35,000 years. *Science*, **126**, 1121-1123.

- Mook, D.H. and Hoskin, C.M. 1982. Organic determination by ignition, Caution advised. *Est. Coast. Shelf. Sci.*, **15**, 697-699.
- Moore, G.F. and Dyer, K.R. ATM data of Plymouth Sound, atmospheric corrections and suspended sediment retrieval. *In press*.
- Morel, A. 1980. In-water and remote measurement of ocean colour. *Boundary-layer Meteorology*, **18**,177-201.
- Morner, N-A. 1976. Eustasy and geoid changes. *J. Geol.*, **84**, 123-151.
- Morner, N-A. 1980. Eustasy and geoid changes as a factor of core/mantle changes. In: *Earth, rheology, isostasy and eustasy* (Ed. N-A Morner) Wiley & Sons, Chichester, 535-553.
- Mottershead, D.N. 1977. The Quaternary Evolution of the South Coast of England. In: *The Quaternary history of the Irish Sea* (Ed. C Kidson), 299-320.
- Murray, J.W. 1965. The significance of benthic foraminiferids in plankton samples. *J. Palaeont.*, **39**, 156-157.
- Nagata, T. 1961. *Rock Magnetism*, 2nd ed. Maruzan, Tokyo. p. 350.
- Newman, W.S. and Bateman, C. 1987. Holocene excursions of the North West European Geoid. *Progress in Oceanography*, **18**, 287-322.
- Nicholls, R.J. 1984. The formation and stability of Shingle Spits. *Quaternary Newsletter*, **44**,14-21.
- Noel, M. 1986. The palaeomagnetism and magnetic fabric in sediments from Peak Cavern, Derbyshire. *Geophys. J. R. astr. Soc.*, **84**, 445-454.
- Novo, E.M.M., Hansom, J.D. and Curran, P.J. 1989. The effect of sediment type on the relationship between reflectance and suspended sediment concentration. *Int. J. Remote Sensing*, **10**, 1283-1289.
- Oakley, C.P. 1943. A note on the post-glacial submergence of the Solent margins. *Proc. of the Prehistory Soc.*, **9**, 56-59.
- Painter, P.J. 1986, *A seismic reflection study of buried channels in Plymouth Sound*. Unpublished B.Sc thesis, Plymouth Polytechnic, Department of Geological Sciences.
- Payne, M.A. and Verosub, K.L. 1982. The acquisition of post-depositional detrital remanent magnetization in a variety of natural sediments. *J. Geophys. R. astr. Soc.*, **68**, 625-642.
- Peltier, W.R. 1987. Mechanisms of relative sea-level change and the geophysical responses to ice-water loading. In: *Sea surface studies: a global view* (Ed. R.J.N. Devoy) Croom Helm, London, 57-94.
- Peltzer, R.D. and Griffin, O.M. 1988. Stability of a three-dimensional foam layer in seawater. *J. Geophys. Res.*, **93** C9, 10,804-10,812.
- Perkins, J.W. 1972. *Geology explained: Dartmoor and the Tamar Valley*. Land and Charles, Newton Abbot. p196.

- Pettersson, L.H. 1990. *Project Report and Recommendations*. Technical Report 28, Norsmap 89.
- Pilgrim, D.A. 1988. *Optical attenuation in Oceanic and Estuarine Waters*. Unpublished P.hD Thesis, Plymouth Polytechnic, Institute of Marine Studies.
- Pingree, R.D. 1980. Physical oceanography of the Celtic Sea and English Channel. In: *North West European shelf seas: the sea bed in motion Vol II Physical and Chemical Oceanography and Physical Resources* (Ed; F.T. Banner, M.B. Collins and K.S. Massie) Elsevier Oceanography series 24B, Amsterdam, 415-465.
- Pinot, J.P. 1968. Littoraux Wurmien submerges a l'oves de Belle-Ile. *Bull Assoc. Francais pour l'etude du Quaternaire*, 3, 197-216.
- Poole, H.H. and Aitkins W.R.G. 1929. Photoelectric measurements of submarine illumination throughout the year. *J. Mar. Bio. Ass. U.K.*, 16, 297-324.
- Potter, P.E. and Pettijohn, F.J. 1963. *Palaeocurrent and basin analysis*. Springer-Verlag, p296
- Pound, C.J. 1983. The sedimentology of the Lower - Middle Devonian Staddon Grits and Jennycliff Slates on the east side of Plymouth Sound, Devon. *Proc. Ussher Soc.*, 5, 465-472.
- Purdie, D.A. and Garcia, C.A.E. 1988. The use of Airborne Thematic Mapper data in studying the effects of the tidal state on the distribution of phytoplankton blooms in Southampton water. *Proc. of the N.E.R.C 1987 Airborne Campaign Workshop*, 195-204.
- Rees, A.I. 1965. The use of anisotropy of magnetic susceptibility in the estimation of sedimentary fabrics. *Sedimentology*, 7, 257-271.
- Rees, A.I., Von Rad, U. and Shephard, F.P. 1968. Magnetic fabric of sediments from the La Jolla submarine canyon and fan, California. *Mar. Geol.*, 6, 145-178.
- Rees, A. I., Brown, C.M., Hailwood, E.A. and Riddy, P.J. 1982. Magnetic fabric of bioturbated sediment from the Northern Rockall Trough: comparison with modern currents. *Mar. Geol.*, 46, 161-173.
- Rees, A.I. and Woodall, W.A. 1975. The magnetic fabric of some laboratory-deposited sediments. *Earth Planet. Sci. Lett.*, 25, 121-130.
- Reid, C. 1913. *Submerged Forests*. Cambridge University Press. p124.
- Reynolds, J.M. 1987. Geophysical detection of buried channels in Plymouth Sound, Devon. *Geophys. J. R. astr. Soc.*, 89, 457.
- Rimmer, J.C., Collins, M.B. and Pattiaratchi, C.B. 1987, Mapping of water quality in coastal waters using Airborne Thematic Mapper data. *Int. J. Remote Sensing*, 8, 85-102.
- Robinson, I.S. 1985. *Satellite oceanography - an introduction for oceanographers and remote-sensing scientists*. Wiley & Son, London, p455.

- Rollin, E. 1990. Global spectral irradiance measurements at aircraft altitude during CASI test flight programme. *Proc. of the N.E.R.C. symposium on Airborne Remote sensing 1990*, 339-342.
- Roxburgh, I.S. 1983. Notes on the hydrogeology of the Plymouth Limestone. *Proc. Ussher Society*, 5, 479-481.
- Roxburgh, I.S. 1984. *The hydrogeology of the Plymouth Limestone with special reference its coastal location*. Unpublished P.hD Thesis. University of Exeter. p409.
- Roxburgh, I.S. 1985. Thermal infra-red detection of submarine springs associated with the Plymouth Limestone. *Hydrological Sciences Journal*, 30, 185-196.
- Ruddiman, W.F. and Duplessy J.C. 1985. Conference on the last Glaciation, Timing and Mechanism. *Quaternary Research*, 23, 1-17.
- Ruddiman, W.F. and McIntyre, A. 1976. North East Atlantic palaeoclimate change over the past 600,000 years. *Mem. Geol. Soc. Amer.* 145, 120-132.
- Ruddiman, W.F. and McIntyre, A. 1981. The North Atlantic Ocean during the last glaciation. *Palaeogeog, Palaeoclim, Palaeoecol.*, 35, 145-214.
- Salomons, W. and Mook, W.G. 1987. Natural tracers for sediment transport studies. *Cont. Shelf Res.*, 7, 1333-1343.
- Sathyendranath, S. and Morel, A. 1983. Light emerging from the sea - interpretation and uses in remote sensing. In: *Remote sensing Applications in Marine Science and Technology* (Ed. A.P. Cracknell), Durdrecht D. Reidel, 323-358.
- Seago, R.D. and Chapman, T.J. 1988. The confrontation of the structural styles and the evolution of a foreland basin in Central Southwest England. *Quart. J. Geol. Soc. Lond.*, 145, 789-800.
- Selwood, E.B. 1990. A review of the basin development in Central South West England. *Proc. Ussher Soc.*, 7, 199-205.
- Shennan, I. 1983. Flandrian and Late Devensian Sea level changes and crustal movements in England and Wales. In: *Shorelines and Isostasy* (Ed. D.E. Smith and A.G. Dawson), Academic Press, London, 225-283.
- Shennan, I. 1987. Holocene sea level changes in the North Sea. In *Sea Level Changes* (Ed: M. J. Tooley & I. Shennan), Blackwell, Oxford, 109-151.
- Shennan, I. 1989. Holocene crustal movements and sea level changes in Great Britain. *J. Quaternary Science* 4, 77-89.
- Simpson, J.H. and Brown, J. 1987. The interpretation of visible band imagery of turbid shallow seas in terms of the distribution of suspended particulates. *Continental Shelf Research*, 7, 1307-1313.
- Singer, J.K. and Anderson, J.B. 1984. Use of total grain-size distributions to defined bed erosion and transport for poorly sorted sediment undergoing simulated bioturbation. *Mar. Geol.*, 57, 335-359.

Singer, J.K., Anderson, J.B., Ledbetter, M.T., McCave, I.N., Jones, K.P.N. and Wright, R. 1987. An assesment of analytical techniques for the size analysis of fine-grained sediments. *J. Sed. Petrol.*, **58**, 534-543.

Smith, A.J. 1989. The English Channel - by geological design or catastrophic accident?. *Proc. Geol. Ass.*, **100**, 325-337.

Smith, A.J. and Curry, D. 1975. The Structure and Geological Evolution of the English Channel. *Phil. Trans. R. Soc. Lond.*, **A279**, 3-20.

Snowball, I. and Thompson, R. 1990. A mineral magnetic study of Holocene sedimentation in Lough Catherine, Northern Ireland. *Boreas*, **19**, 127-146.

Southward, A.J. and Butler, E.I. 1972. A note on further changes of sea temperature in the Plymouth Area. *J. Mar. Biol. Ass. U.K.*, **52**, 931-937.

Sparks, N.H.C., Mann, S., Bazylinski, D.A., Lovley, D.R., Jannasch, H.W. and Frankel R.B. 1990. Structure and morphology of magnetite anaerobically-produced by a marine magnetotactic bacterium and a dissimilatory iron-reducing bacterium. *Earth Planet. Sci. Lett.*, **98**, 14-22.

Spitzer, D. and Dirks, R.W.J. 1986. Classification of bottom composition and bathymetry of shallow waters by passive Remote Sensing. *Symp. on Remote Sensing for sources Development and Environmental Management*. Enshede, 775-777.

Stephens, J.A., Uncles, R.J., Barton, M.E. and Fitzpatrick, F. Cohesive sediment shear stresses in the intertidal zone of a macrotidal estuary. *In press (Mar. Geol)*.

Strickland, J.D.H. and Parsons, T.P. 1968. A practical handbook of sea water analysis. *Bulletin of the Fisheries Research Board of Canada*, **167**, Ottawa, Fisheries Research Board.

Stride, A.H. 1959. A linear pattern on the sea floor and its interpretation. *J. Mar. Bio. Ass. U.K.*, **38**, 313-318.

Stride, A.H. 1963. Current-swept sea floors near the Southern half of Great Britain. *Quart. Geol. Soc. Lond*, **119**, 175-199.

Stride, A.H. 1990. Growth and burial of the English Channel Unconformity. *Proc. Geol. Ass.*, **101**, 335-340.

Tarling, D.H. 1983. *Palaeomagnetism - principles and applications in geology, geophysics and archaeology*. Chapman & Hall, London, New York, p 379.

Tarling, D.H. and Symons, D.T.A. 1967. A stability Index of remanence in palaeomagnetism. *Geophys. J. R. astr. Soc.*, **12**, 443-448.

Tebble, N. 1976. *British bivalve sea shells*. H.M.S.O. publications

Terasme, J. 1984. Radiocarbon dating: some problems In: *Developments in Palaeontology and Stratigraphy 7: Quaternary dating methods* (Edit: W.C. Mahoney) Elsevier Scientific Publications, 1-17.

Tooley, M.J. 1985. Sea levels. *Prog. Phys. Geog.*, **9**, 113-120.

- Tooley, M.J. 1986, Sea levels. *Prog. Phys. Geog.*, **10**, 120-129.
- Topliss, B.J. Almos, C.L. and Hill, P.R. 1990. Algorithms for remote sensing of high concentration, inorganic suspended sediment. *Int. J. Remote Sensing*, **11**, 945-966.
- Torres de Aravjo, F.F. Pires, M.A. Frankel, R.B. and Bicudo, C.E.M. 1986. Magnetite and magnetotaxis in algae. *Biophysical J.*, **50**, 375-378.
- Tucker, P. 1980. Grain mobility model of post-depositional realignment. *Geophys. J. Roy. astr. Soc.*, **63**, 149-163.
- Tucker, P. 1983. Magnetization of unconsolidated sediments and theories of DRM. In: *Geomagnetism of Baked Clays and Recent Sediments* (Ed. K.M. Creer, P. Tucholka and C.E. Barton), Elsevier, 9-19.
- Turner, C. and Hannon, G.E. 1988. Vegetational evidence for late Quaternary climate changes in South West Europe in relation to the influence of the North Atlantic. *Phil. Trans. R. Lond.*, **B318**, 451-486.
- Tyler, J.E. 1968, The Secchi Disc. *Limnology and Oceanography*, **13**, 1-6.
- Uncles, R.J., Bale, A.J., Howland, R.J.M., Morris, A.W. and Elliott, R. C.A. 1983. Salinity of surface water in a partially-mixed estuary and its dispersion at low run-off. *Oceanologia Acta*, **6**, 289-296.
- Ussher, W.A.E. 1907. The Geology of the country around Plymouth and Liskeard. *Mem. Geol. Surv. G.B.*
- Verosub, K.L. 1977. Depositional and post-depositional process in the magnetization of sediments. *Rev. Geophys. Space Physics*, **15**, 129-143.
- Voulgaris, G. and Collins, M.B. 1991. Linear features on side-scan sonar images, an algorithm for the correction of angular distortion. *Mar. Geol.*, **96**, 187-190.
- Wentworth, C. 1922. A scale of grade and class terms for clastic sediments. *J. Geology*, **30**, 377-392.
- West, R.G. 1988. The record of the cold stages. *Phil. Trans. R. Soc. Lond.*, **B318**, 505-519.
- Williamson, P. and Gribben, J. 1991. How plankton change the climate. *New Scientist*, 16th March, 48-52.
- Wood, A. 1976. Successive regressions and transgressions in the Neogene. *Mar. Geol.*, **22**, M23-M29.
- Woodworth, P.L. 1987. Trends in UK mean Sea level. *Marine Geodesy*, **11**, 57-87.
- Worth, R. H. 1989. *Evidence of Glaciation in Devonshire.*

Personnel R.V. Catfish 17.11.89

Captain	Trevor Parrott (<i>P.S.W Institute Marine Studies</i>)
Party Chief	Fiona Fitzpatrick
Equipment	Paul Riddy (<i>Dept. Oceanography Southampton</i>)
Surveyors	Bob Foster (<i>Marine Biological Association</i>)
	Gareth Osborne (<i>P.S.W Undergrad. Geology</i>)
	Adam Wooler (<i>P.S.W Postgrad. Geology</i>)

Appendix 1b The Divers

Affiliation

John Vaudin	<i>Student Services (Dive Officer)</i>
Andy Revill	<i>Postgraduate Environmental Sciences</i>
Rod Jones	<i>Institute of Marine Studies</i>
Derek Pilgirm	<i>Lecturer Marine Studies</i>
John Douglas	<i>Lecturer Marine Studies</i>
Paul Witherton	<i>Lecturer Marine Studies</i>
and many many students	

Appendix 1c Crew Listings Plymouth Sound Overflights

Operation Imaging Plymouth Sound 1989

Inflatable 1

Affiliation

Mark Burdass	<i>Postgraduate Biological Sciences</i>
Richard Gibb	<i>Lecturer Geographical Sciences</i>
Alex Cunliff	<i>Lecturer Economics</i>
Grant Pollock	<i>Image Analysis Unit</i>

Inflatable 2

Peter Campbell	<i>Postgraduate Biological Sciences</i>
Meriel Fitzpatrick	<i>Postgraduate Geological Sciences</i>
Ailbhe Duane	<i>Postgraduate Geological Sciences</i>
Sandy Beecham	<i>Free-lance Television Producer</i>

D.V. Aquatay

Frank Knott	<i>Coxside Boat Handler</i>
Rod Eddies	<i>Postgraduate Geological Sciences</i>
Tim O'Clarigh	<i>3rd year Marine Science</i>
Fiona Fitzpatrick	

R.V. Squilla

Paul Riddy and Southampton University 2nd year Oceanography students.

Appendix 1c cont...

Operation CASI

Breakwater Inflatable

John Moore	<i>Image Analysis Unit</i>
Andy Revill	<i>Postgraduate Environmental Sciences</i>
Alex Kim	<i>Postgraduate Environmental Sciences</i>
Frank Cross	<i>Postgraduate Biological Sciences</i>

Hamoaze Inflatable

John Vaudin	<i>Student Services</i>
Steve Caswell	<i>Lecturer Geological Sciences</i>
Ken Vines	<i>Lecturer Geological Sciences</i>
Nick Johnston	<i>Free-lance Geophysicist</i>

Sound Dory

Bob Hopgood	<i>Boathandler Coxside Centre</i>
Aziz Abdeldayem	<i>Postgraduate Geological Sciences</i>
John Abraham	<i>Draughtsman Geological Sciences</i>
Fiona Fitzpatrick	

D.V.Aquatay

Frank Knott	<i>Boathandler Coxside Centre</i>
Derek Pilgrim	<i>Lecturer Marine Sciences</i>
Gerald Moore	<i>Lecturer Marine Sciences</i>
Jerry McCave	<i>Postgraduate Marine Sciences</i>

Operation **ATM Overflight 1990**

Hamoaze Dory

John Vaudin	<i>Student Services</i>
Laura Smithurst	<i>Postgraduate Geological Sciences</i>
Sheelagh Matear	<i>Postgraduate Marine Sciences</i>
Frank Cross	<i>Postgraduate Biological Sciences</i>

Sound Inflatable

Lorne Roberts	<i>Postgraduate Biological Sciences</i>
Andy Revill	<i>Postgraduate Environmental Sciences</i>
Meriel Fitzpatrick	<i>Postgraduate Geological Sciences</i>
Sue Warr	<i>Postgraduate Geographical Sciences</i>

Breakwater Bass

Peter Brown	<i>Boathandler Coxside Centre</i>
Adam Wooler	<i>Postgraduate Geological Sciences</i>
Aziz Abdeldayem	<i>Postgraduate Geological Sciences</i>
Steve Judd	<i>3rd year Computing Fiona's Flate-mate</i>

Panther Dory

Bob Hopgood	<i>Boathandler Coxside Centre</i>
John Abraham	<i>Draughtsman Geological Sciences</i>
David Smith	<i>Postgraduate Geographical Sciences</i>
Metten Calim	<i>Technician Geological Sciences</i>

D.V.Aquatay

Frank Knott	<i>Boathandler Coxside Centre</i>
Derek Pilgrim	<i>Lecturer Marine Studies</i>
Gerald Moore	<i>Lecturer Marine Studies</i>
Rob Jones	<i>Technician Marine Studies</i>
Jerry McCave	<i>Postgraduate Marine Studies</i>
+ BBC Camera Crew	<i>(Morning)</i>

PLYMOUTH SOUND SEDIMENT ANALYSIS PROGRAMME

Name CB3

No	φ	mm	weight		Pre	Post	%	%	Went.	c.%
1	-2.50	5600	1.5	A	1.5	1.5	0	0.82	-	0.82
2	-2.00	4000	1.6	B	1.6	1.1	31	0.90	-	1.72
3		3350	2.4				pg	1.3		3.02
4		2800	3.4					1.9		4.82
5		2360	4.6					2.6		7.42
6	-1.00	2000	4.8	C	3.5	1.2	65	2.6	8.3	10.02
7		1700	6.9				vcs	4.0		14.02
8		1400	12.2					6.7		20.72
9		1180	13.7					7.6		28.32
10	0.00	1000	21.2	D	6.3	0.6	90	11.7	30	40.02
11		850	26.6				cs	14.8		54.82
12		710	27.7					13.8		68.62
13		600	22.5					12.5		81.12
14	+1.00	500	23.5	E	12.0	7.1	40	13.0	54	94.12
15		425	10.2				ms	5.7		99.82
16		355	0.3					0.1		99.92
17		300	0.1					0.05		99.97
18	+2.00	250	0.1	F	0.5	0.3	40	0.05	59	99.98
19		212	0.1				fs	0.05		99.98
20		180	0.2					0.10		99.99
21		150	0.1					0.05		99.99
22	+3.00	125	0.2	G	0.6	0.4	33	0.1	0.4	99.99
23		106	0.1				vfs	0.05		100
24		90	0.1					0.05		100
25		75	-							→
26	+4.00	63	-	H	0.2	0.1	50		-	
P.			-							

PLYMOUTH SOUND SEDIMENT ANALYSIS PROGRAMME

Name C54

No	φ	μm	weight		Pre	Post	%	%	Went.	c.%
1	-2.50	5600	37.84	A	-	-	-	21.2	21.2	21.2
2	-2.00	4000	16.44	B	-	-	-	9.2	9.2	30.4
3		3350	15.49				pg	8.7		39.1
4		2800	18.24					10.9		49.3
5		2360	17.70					9.9		59.8
6	-1.00	2000	16.31	C	0.08	7.35	8	9.1	30	67.9
7		1700	15.82				vcs	8.8		76.7
8		1400	15.56					8.7		85.4
9		1180	8.53					4.7		87.1
10	0.00	1000	8.30	D	8.45	6.60	20	4.6	30	90.7
11		850	4.35				cs	2.4		93.1
12		710	2.19					1.2		94.3
13		600	0.91					0.5		95.0
14	+1.00	500	0.54	E	4.43	2.60	40	0.4	4	100.00
15		425					ms			
16		355								
17		300								
18	+2.00	250		F						
19		212					fs			
20		180								
21		150								
22	+3.00	125		G						
23		106					vfs			
24		90								
25		75								
26	+4.00	63		H						
P.										

PLYMOUTH SOUND SEDIMENT ANALYSIS PROGRAMME

Name *PP1*

3-05-59

No	φ	μm	weight		Pre	Post	%	%	Went.	c. %
1	-2.50	5600	175.9	A	-	-	-	45.3	45.3	45.3
2	-2.00	4000	110.0	B	-	-	-	28.	28.8	73.3
3		3350	28.4	C			pg	7.3		80.6
4		2800	12.7					3.2		83.8
5		2360	17.3					2.0		85.8
6	-1.00	2000				13.0	10.5		19	
7		1700	7.3	D			vcs	1.8		89.6
8		1400	10.1					2.6		92.2
9		1180	6.3					1.6		93.8
10	0.00	1000	8.9		8.5	4.4	48	2.2	8.2	96.0
11		850	5.4	E			cs	1.4		97.4
12		710	2.6					0.6		98.0
13		600	1.4					0.3		98.3
14	+1.00	500	0.8		4.1	1.9	53		2.3	99
15		425	0.5	F			ms			100
16		355	0.3							
17		300	0.2							
18	+2.00	250	0.1		1.1	0.3	72			
19		212		G			fs			
20		180								
21		150								
22	+3.00	125			-	-	-			
23		106		H			vfs			
24		90								
25		75								
26	+4.00	63								
P.										

PLYMOUTH SOUND SEDIMENT ANALYSIS PROGRAMME

Name RHA

No	φ	μm	weight		Pre	Post	%	%	Went.	c.%
1	-2.50	5600		A						
2	-2.00	4000		B						
3		3350					pg			
4		2800								
5		2360								
6	-1.00	2000	.1	C						
7		1700	.1				vcs			
8		1400	.4							
9		1180	.8					0.7		0.7
10	0.00	1000	2.3	D	2.1	0.1	95	2.2	2	2.9
11		850	2.3				cs	2.2		5.1
12		710	3.9					3.8		8.9
13		600	5.7					5.5		14.4
14	+1.00	500	7.8	E	3.9	0.5	87	7.6	15.8	22.0
15		425	11.7				ms	11.4		33.4
16		355	11.9					11.6		45.0
17		300	13.7					13.4		58.4
18	+2.00	250	8.8	F	4.1	2.2	76	8.6	45	67.0
19		212	11.9				fs	11.6		75.6
20		180	8.9					8.6		87.2
21		150	6.2					11.3		98.0
22	+3.00	125	2.8	G	3.6	2.6	27	2.1	33.6	100
23		106	2.2				vfs	2.0		
24		90	0.4							
25		75	0.2							
26	+4.00	63	-	H	1.0	0.8	20			
P.			-							

PLYMOUTH SOUND SEDIMENT ANALYSIS PROGRAMME

Name 116

No	φ	μm	weight		Pre	Post	%	%	Went.	c.%
1	-2.50	5600		A						
2	-2.00	4000		B						
3		3350		C			pg			
4		2800								
5		2360								
6	-1.00	2000								
7		1700		D			vcs			
8		1400	0.52							
9		1180	0.13							
10	0.00	1000	0.21							
11		850	0.34	E			cs			
12		710	0.39							
13		600	0.80							
14	+1.00	500	1.15							
15		425	1.38	F			ms			
16		355	2.23							
17		300	2.20							
18	+2.00	250	2.63							
19		212	2.60	G			fs			
20		180	2.60							
21		150	10.23							
22	+3.00	125	7.82							
23		106	26.16	H			vfs			
24		90	4.25							
25		75	4.75							
26	+4.00	63	2.50							
P.			1.15							

PLYMOUTH SOUND SEDIMENT ANALYSIS PROGRAMME

Name PP2

No	φ	μm	weight		Pre	Post	%	%	Went.	c.%
1	-2.50	5600	0.5	A	-	-				
2	-2.00	4000	-	B						
3		3350	-				pg			
4		2800	0.11							
5		2360	0.2							
6	-1.00	2000	-	C	0.3	0.0	100	0.2	0.2	0.2
7		1700	0.2				vcs	0.2		0.4
8		1400	0.4					0.3		0.7
9		1180	0.3					0.3		1.0
10	0.00	1000	0.5	D	1.0	0.1	90	0.4	1.2	1.4
11		850	0.5				cs	0.4		1.8
12		710	0.7					1.3		2.6
13		600	0.8					0.9		3.5
14	+1.00	500	1.7	E	1.8	0.2	90	2.0	4	5.5
15		425	1.8				ms	2.1		7.6
16		355	2.1					2.5		10.1
17		300	3.0					3.5		13.6
18	+2.00	250	2.4	F	1.3	0.4	70	3.0	11	16.6
19		212	5.2				fs	6.1		22.7
20		180	11.6					13.6		36.2
21		150	11.5					13.6		49.8
22	+3.00	125	11.5	G	2.9	1.9	34	13.6	47	63.4
23		106	17.8				vfs	21.1		84.5
24		90	4.7					5.4		90
25		75	4.6					5.6		96
26	+4.00	63	1.5	H	2.8	2.3	17	1.7	33	98
P.			0.6							100

PLYMOUTH SOUND SEDIMENT ANALYSIS PROGRAMME

Name CB4

No	ϕ	μm	weight		Pre	Post	%	%	Went.	c.%
1	-2.50	5600	32.3	A	32.3	24.2	25	13.8		13.5
2	-2.00	4000	6.6	B	6.6	4.2	36	2.8		16.6
3		3350	3.7				pg	1.6		18.2
4		2800	4.8					2.0		20.2
5		2360	5.1					2.2		22.4
6	-1.00	2000	5.2	C	4.1	2.4	41	2.2	8	24.6
7		1700	6.2				vcs	2.6		27.2
8		1400	10.3					4.4		31.6
9		1180	11.5					5.0		36.6
10	0.00	1000	19.9	D	6.6	2.6	60	8.4	20.4	45.0
11		850	22.2				cs	9.5		54.5
12		710	28.6					12.2		66.7
13		600	21.5					9.2		75.9
14	+1.00	500	24.4	E	4.1	1.9	53	10.3	4.1	86.2
15		425	17.2				ms	7.3		93.5
16		355	6.3					2.7		96.2
17		300	3.3					1.4		97.6
18	+2.00	250	1.1	F	3.0	1.6	46	.4	11.5	98.0
19		212	0.9				fs	.4		98.4
20		180	0.5					.4		98.7
21		150	0.4					.3		98.9
22	+3.00	125	0.4	G	2.2	1.1	50	.2	1.1	99.1
23		106	1.1				vfs	.2		99.5
24		90	0.5					.4		99.3
25		75	0.2					.3		100
26	+4.00	63	0.4	H	2.7	2.1	22	.2	1.3	100.
P.			0.1					.1		

PLYMOUTH SOUND SEDIMENT ANALYSIS PROGRAMME Name BW1

No	φ	μm	weight		Pre	Post	%	%	Went.	c.%
1	-2.50	5600	81.5	A	39		100	39.1	39.1	39.1
2	-2.00	4000	15.6	B	36.0	8.0	78	7.5	5.5	46.6
3		3350	5.8				pg	2.8		49.4
4		2800	6.0					2.8		52.2
5		2360	4.3					2.1		54.3
6	-1.00	2000	4.3	C	-	-		2.1	9.8	56.4
7		1700	5.3				vcs	2.5		58.9
8		1400	4.5					2.1		61.0
9		1180	3.2					1.5		62.5
10	0.00	1000	4.0	D	1.5	0.7	54	1.9	8	64.4
11		850	4.1				cs	1.9		66.3
12		710	4.3					2.0		68.3
13		600	5.2					2.5		70.5
14	+1.00	500	7.1	E	3.5	4	89	3.4	10	74.2
15		425	9.8				ms	4.7		78.9
16		355	7.9					3.8		82.7
17		300	7.7					3.5		86.5
18	+2.00	250	4.3	F	3.6	0.7	51	2.0	14.3	88.8
19		212	5.6				fs	2.7		91.2
20		180	4.9					2.3		93.5
21		150	3.9					1.8		95.3
22	+3.00	125	2.4	G	3.4	2.0	49	1.1	8	96.4
23		106	3.2				vfs	1.5		97.9
24		90	1.3					0.6		98.5
25		75	1.5					0.7		99.2
26	+4.00	63	0.6	H	2.0	-	-	0.2	3	100
P.			0.3							

PLYMOUTH SOUND SEDIMENT ANALYSIS PROGRAMME Name CB1

No	φ	μm	weight		Pre	Post	%	%	Went.	c.%
1	-2.50	5600	1.4	A	1.4	0.4	72	0.67		0.67
2	-2.00	4000	3.8	B	—	—	—	1.8		2.47
3		3350	1.8				pg	0.86		3.33
4		2800	3.1					1.00		4.43
5		2360	5.1					2.4		6.83
6	-1.00	2000	5.1	C	1.1	0.3	73	2.4		9.23
7		1700	10.4				vcs	5.0		14.23
8		1400	16.9					8.1		22.33
9		1180	20.2					9.7		32.03
10	0.00	1000	31.1	D	2.5	0.6	76	15.0		47.03
11		850	27.5				cs	13.2		60.23
12		710	25.3					12.2		72.43
13		600	20.1					9.6		82.03
14	+1.00	500	16.8	E	2.0	0.6	70	8.0		90.03
15		425	10.9				ms	5.2		95.23
16		355	4.0					1.9		97.13
17		300	1.5					0.72		97.55
18	+2.00	250	0.4	F	1.4	0.7	50	0.2		98.05
19		212	0.3				fs	0.1		98.15
20		180	0.1					0.04		98.19
21		150	0.1					0.04		98.23
22	+3.00	125	0.1	G	0.6	0.2	77	0.04		98.27
23		106	0.5				vfs	0.2		98.47
24		90	0.4					0.2		98.67
25		75	0.5					0.2		98.97
26	+4.00	63	0.3	H	1.6	1.6	100	0.1		100.00
P.			0.2							

PLYMOUTH SOUND SEDIMENT ANALYSIS PROGRAMME

Name F. BOOY. PS 11

No	φ	μm	weight		Pre	Post	%	%	Went.	c.%
1	-2.50	5600	—	A						
2	-2.00	4000	0.1	B			100	0.09		0.09
3		3350	—				pg	0		"
4		2800	—					0		"
5		2360	—					0		"
6	-1.00	2000	—	C				0.09	12	0.18
7		1700	0.1				vcs	0.09		0.27
8		1400	0.2					0.18		0.45
9		1180	0.4					0.36		0.81
10	0.00	1000	1.0	D	1.7	0.2	88	0.91	1.7	1.72
11		850	1.6				cs	1.46		3.14
12		710	2.3					2.10		5.24
13		600	3.1					2.83		5.07
14	+1.00	500	4.9	E	22	0.3	86	4.47	12	12.54
15		425	7.5				ms	6.84		19.38
16		355	5.9					5.33		24.76
17		300	6.0					5.47		30.23
18	+2.00	250	3.9	F	3.0	0.8	73	3.56	23	33.79
19		212	7.5				fs	6.84		40.63
20		180	10.7					9.77		50.40
21		150	12.1					11.05		61.45
22	+3.00	125	9.2	G	2.9	1.3	37	5.40	3.9	69.55
23		106	19.2				vfs	17.53		87.38
24		90	5.8					5.29		92.67
25		75	4.0					3.65		96.32
26	+4.00	63	2.0	H	2.4	1.9	20	1.52	3.1	45.14
P.			0.9					0.82		100

PLYMOUTH SOUND SEDIMENT ANALYSIS PROGRAMME Name *NC1*

No	φ	μm	weight		Pre	Post	%	%	Went.	c.%
1	-2.50	5600	0.2	A	0.2	0	100	.14	.14	.14
2	-2.00	4000	0.9	B	0.9	.1	90	.60	.80	.74
3		3350	0.6				pg	.40		1.14
4		2800	0.8					.54		1.68
5		2360	0.8					.54		2.22
6	-1.00	2000	3.6	C	0.8	0.1	90	2.4	372	4.62
7		1700	6.7				vcs	4.8		9.42
8		1400	11.4					7.6		17.02
9		1180	14.2					9.5		26.52
10	0.00	1000	23.4	D	2.2	0.2	90	15.6	37.8	42.12
11		850	20.0				cs	13.4		55.52
12		710	16.2					10.9		66.46
13		600	12.3					9.2		74.62
14	+1.00	500	8.1	E	2.3	0.5	80	5.4	379	80.00
15		425	4.8				ms	3.2		83.22
16		355	2.5					1.8		85.02
17		300	1.6					1.7		86.72
18	+2.00	250	1.0	F	1.7	0.2	89	0.7	74	87.42
19		212	1.5				fs	1.0		88.42
20		180	2.4					1.6		90.02
21		150	2.6					1.7		91.72
22	+3.00	125	2.7	G	1.6	1.1	30	1.8	6.0	93.52
23		106	6.6				vfs	1.6		95.12
24		90	2.4					1.6		96.72
25		75	1.5					1.0		97.72
26	+4.00	63	0.6	H	3.4	2.8	1.5	0.4	4	98.12
P.			0.6					0.1		100

PLYMOUTH SOUND SEDIMENT ANALYSIS PROGRAMME

Name BW2 COARSE

No	φ	μm	weight		Pre	Post	%	%	Went.	c. %
1	-2.50	5600		A						
2	-2.00	4000		B						
3		3350					pg			
4		2800								
5		2360								
6	-1.00	2000								
7		1700					vcs			
8		1400								
9		1180								
10	0.00	1000								
11		850					cs			
12		710								
13		600								
14	+1.00	500								
15		425					ms			
16		355								
17		300								
18	+2.00	250	1.4							
19		212	0.2				fs	0.53		4.3
20		180	0.4							
21		150	1.2							
22	+3.00	125	1.1							
23		106	3.8				vfs	10		21.6
24		90	3.1							
25		75	6.1							
26	+4.00	63	7.6							
P.			12.7		3.4	2.5	23	37.6		100

PLYMOUTH SOUND SEDIMENT ANALYSIS PROGRAMME

Name BW1 COARSE

No	φ	μm	weight		Pre	Post	%	%	Went.	c.%
1	-2.50	5600		A						
2	-2.00	4000		B						
3		3350		C			pg			
4		2800								
5		2360								
6	-1.00	2000								
7		1700		D			vcs			
8		1400								
9		1180								
10	0.00	1000								
11		850		E			cs			
12		710								
13		600								
14	+1.00	500								
15		425		F			ms			
16		355								
17		300								
18	+2.00	250	0.2							
19		212	0.7	G			fs			
20		180	1.2							
21		150	1.5							
22	+3.00	125	1.4							
23		106	3.6	H			vfs			
24		90	2.0							
25		75	3.1							
26	+4.00	63	3.0							
P.			4.8		1.9	1.5	22	14.6		95

PLYMOUTH SOUND SEDIMENT ANALYSIS PROGRAMME

Name C11

No	φ	mm	weight		Pre	Post	%	%	Went.	c.%
1	-2.50	5600	515.33	A			-	90		95.6
2	-2.00	4000	32.17	B				5.6		97.6
3		3350	10.93				pg	2.0		98.5
4		2800	5.35					0.9		99.2
5		2360	3.92					0.7		99.6
6	-1.00	2000	2.28					C		
7		1700	1.24				vcs	0.2		99.9
8		1400	0.81					0.1		100
9		1180	0.31					0.1		100
10	0.00	1000	0.17					D		
11		850					cs			
12		710								
13		600								
14	+1.00	500						E		
15		425					ms			
16		355								
17		300								
18	+2.00	250						F		
19		212					fs			
20		180								
21		150								
22	+3.00	125						G		
23		106					vfs			
24		90								
25		75								
26	+4.00	63						H		
P.										

No	φ	μm	weight		Pre	Post	%	%	Went.	c.%
1	-2.50	5600	181.81	A	181.81	179	.5	92	92.0	92.0
2	-2.00	4000	5.84	B	5.84	5.61	.5	2.8	2.8	94.8
3		3350	1.43				pg	0.7		95.5
4		2800	1.26					0.6		96.1
5		2360	0.88					0.4		96.5
6	-1.00	2000	0.89	C	1.35	0.80	40	0.4	2	96.9
7		1700	0.92				vcs	0.4		97.3
8		1400	0.58					0.2		97.5
9		1180	0.38					0.1		97.6
10	0.00	1000	0.35	D	0.94	0.21	77	0.1	1	97.7
11		850	0.27				cs	0.1		97.8
12		710	0.18					0.1		97.9
13		600	0.09					0.1		98.0
14	+1.00	500	0.20	E	0.74	0.16	80	0.1	1	98.1
15		425	0.12				ms	0.1		98.2
16		355	0.11					0.1		98.3
17		300	0.09					0.1		98.4
18	+2.00	250	0.08	F	0.40	0.03	80	0.1	<1	98.5
19		212	0.08				fs	0.1		98.6
20		180	0.086					0.1		98.7
21		150	0.15					0.1		98.8
22	+3.00	125	0.11	G	0.40	0.13	60	0.1	<1	98.9
23		106	0.30				vfs	0.1		99.0
24		90	0.14					0.1		100.
25		75	0.20					0.1		7
26	+4.00	63	0.12	H	0.70	0.54	30	0.1		
P.										

PLYMOUTH SOUND SEDIMENT ANALYSIS PROGRAMME Name S4

No	φ	μm	weight		Pre	Post	%	%	Went.	c.%
1	-2.50	5600	80.05	A	80.05	42.45	50	40	40	40
2	-2.00	4000	8.12	B	8.17	4.42	50	4	4	44
3		3350	5.18				pg	2		46
4		2800	5.22					2		48
5		2360	4.82					2		50
6	-1.00	2000	5.44	C	2.65	1.09	60	2	8	52
7		1700	7.78				vcs	4		56
8		1400	9.88					4		60
9		1180	9.31					4		64
10	0.00	1000	15.24	D	5.68	1.39	75	7	19	71
11		850	13.98				cs	8		79
12		710	12.47					8		87
13		600	8.86					5		92
14	+1.00	500	5.80	E	6.17	1.94	70	4	21	96
15		425	1.76				ms	2		98
16		355	0.56					1		99.9
17		300	0.15							100
18	+2.00	250		F	2.59	1.03	60		2	
19		212					fs			
20		180								
21		150								
22	+3.00	125		G						
23		106					vfs			
24		90								
25		75								
26	+4.00	63		H						
P.										

PLYMOUTH SOUND SEDIMENT ANALYSIS PROGRAMME

Name BSW4

No	φ	μm	weight		Pre	Post	%	%	Went.	c.%		
1	-2.50	5600	324.9	A	324.9	329.4	0	69.72	69	69.72		
2	-2.00	4000	19.2	B	-	-	-	4.1	4.1	73.82		
3		3350	7.6	C			pg	1.6		75.42		
4		2800	5.5								1.2	76.62
5		2360	4.7									
6	-1.00	2000	5								2.2	0.8
7		1700	5.2	D			vcs	1.1		79.62		
8		1400	8.0								1.7	81.42
9		1180	7.8									
10	0.00	1000	11.6	1.9	0.4	80	2.4	6.9	85.52			
11		850	12.2	E			cs	2.6		88.12		
12		710	13.9								3.0	91.12
13		600	10.5									
14	+1.00	500	10.7								2.6	0.6
15		425	9.3	F			ms	2.0		97.52		
16		355	4.4								1.0	98.32
17		300	4.1									
18	+2.00	250	2.2								2.0	0.7
19		212	2.7	G			fs	0.4		99.92		
20		180	2.2								0.4	99.95
21		150	1.8									
22	+3.00	125	1.0								2.0	1.1
23		106	1.3	H			vfs	0.3				
24		90	.4								0.1	
25		75	.5									
26	+4.00	63	.3								1.2	0.8
P.												

PLYMOUTH SOUND SEDIMENT ANALYSIS PROGRAMME

Name AB1

No	φ	μm	weight		Pre	Post	%	%	Went.	c.%
1	-2.50	5600	17.5	A	17.5	17.3	1	22.8	22.8	22.8
2	-2.00	4000	8.0	B	8.0	0.2	97	10.4	70.4	33.2
3		3350	4.7				pg	6.1		39.3
4		2800	5.9					7.7		49.0
5		2360	4.4					6.1		53.1
6	-1.00	2000	5.0	C	4.1	0.1	97	6.1	26.0	59.2
7		1700	3.8				vcs	5.0		64.2
8		1400	3.9					5.1		69.3
9		1180	2.7					3.5		72.8
10	0.00	1000	3.0	D	1.3	0.2	84	4.0	17.6	76.8
11		850	2.3				cs	3.0		79.8
12		710	1.9					2.5		82.3
13		600	1.9					2.5		84.8
14	+1.00	500	2.1	E	1.2	0.4	66	2.7	10.7	87.5
15		425	2.4				ms	3.1		90.6
16		355	1.8					2.4		93.0
17		300	1.7					2.3		92.9
18	+2.00	250	0.9	F	1.3	0.8	38	1.2	9	94.1
19		212	1.1				fs	1.4		95.5
20		180	0.8					1.1		96.6
21		150	0.6					.8		97.4
22	+3.00	125	0.3	G	1.7	1.0	41	.3	3	97.7
23		106	0.6				vfs	.8		98.5
24		90	0.2					.1		98.6
25		75	0.4					.4		99.0
26	+4.00	63	0.2	H	1.4	0.9	35	.1	1.5	99.1
P.			0.1					.1		100

PLYMOUTH SOUND SEDIMENT ANALYSIS PROGRAMME

Name C132

No	φ	μm	weight		Pre	Post	%	%	Went.	c.%
1	-2.50	5600	188	A	18.8	14.6	23	8.0	8.0	8.0
2	-2.00	4000	13.1	B	-	-	-	5.5	5.5	13.5
3		3350	11.6				pg	5.0		18.5
4		2800	15.2					6.5		25.0
5		2360	15.3					7.8		32.8
6	-1.00	2000	15.4	C	2.1	0.7	67	7.8	27	40.6
7		1700	27.9				vcs	11.9		52.5
8		1400	31.6					13.4		65.9
9		1180	25.1					10.7		76.6
10	0.00	1000	24.4	D	1.3	0.3	77	10.4	46	87.0
11		850	14.5				cs	6.2		93.2
12		710	8.3					3.5		96.7
13		600	4.6					1.9		98.6
14	+1.00	500	2.3	E	2.0	0.3	85	1.1	12.7	97.6
15		425	.9				ms	0.3		99.9
16		355	.3					0.01		99.9
17		300	.1					0.01		99.9
18	+2.00	250	.1	F	1.3	0.4	70	0.01	0.3	100.
19		212					fs			
20		180								
21		150								
22	+3.00	125		G						
23		106					vfs			
24		90								
25		75								
26	+4.00	63		H						
P.										

PLYMOUTH SOUND SEDIMENT ANALYSIS PROGRAMME

Name BLW24

No	φ	mm	weight		Pre	Post	%	%	Went.	c.%
1	-2.50	5600	38.0	A	-	-	-	14	14	14
2	-2.00	4000	18.3	B	-	-	-	6.8	6.8	20.8
3		3350	13.6	C			pg	5.0		25.8
4		2800	13.6					4.8		30
5		2360	13					4.8		35
6	-1.00	2000	13					12.1		8.8
7		1700	12.8	D			vcs	4.7		48
8		1400	19.6					7.3		55
9		1180	18.8					7.0		62
10	0.00	1000	25.5					6.5		2.2
11		850	24.3	E			cs	9.0		80
12		710	17.1					6.3		56
13		600	13.1					5.0		71
14	+1.00	500	11.3					6.8		2.4
15		425	8.3	F			ms	3.0		98
16		355	4.4					1.6		99
17		300	2.7					1.0		100
18	+2.00	250	0.9					2.5		1.0
19		212	0.6	G			fs	0.2		
20		180	0.8					0.3		
21		150								
22	+3.00	125						1.4		0.8
23		106		H			vfs			
24		90								
25		75								
26	+4.00	63								
P.										

No	φ	μm	weight		Pre	Post	%	%	Went.	c.%
1	-2.50	5600	5.4	A			-	4.6	4.6	4.6
2	-2.00	4000	6.6	B			-	5.6	5.6	11
3		3350	3.4				pg	3.0		14
4		2800	3.9					3.3		17.3
5		2360	2.3					2.2		19.5
6	-1.00	2000	3.0	C	5.7	1.6	75	2.2	10.7	21.7
7		1700	3.6				vcs	3.0		24.7
8		1400	4.8					4.1		28.8
9		1180	4.4					3.7		32.5
10	0.00	1000	6.4	D	5.2	1.0	80	5.4	16.27	37.9
11		850	6.4				cs	5.4		43.3
12		710	6.4					5.4		48.4
13		600	6.8					5.8		54.5
14	+1.00	500	7.5	E	6.0	5.0	70	6.3	22.9	60.8
15		425	8.6				ms	7.3		68.1
16		355	6.6					5.6		73.7
17		300	6.3					5.3		79.0
18	+2.00	250	3.8	F	2.5	0.7	72	3.2	21.4	82.2
19		212	5.4				fs	4.6		86.8
20		180	4.9					4.1		90.5
21		150	3.7					3.1		93.6
22	+3.00	125	2.5	G	1.4	0.8	42	2.1	13.5	95.7
23		106	4.7				vfs	4.0		99.7
24		90	2.4					2.0		99.8
25		75	2.4					2.0		100
26	+4.00	63	1.6	H	1.8	1.5	16	1.3	9.3	
P.			1.0		1.0	0.8	20			

PLYMOUTH SOUND SEDIMENT ANALYSIS PROGRAMME

Name B31

No	φ	μm	weight		Pre	Post	%	%	Went.	c.%
1	-2.50	5600	-	A	-	-	-		0	
2	-2.00	4000	0.21	B	-	-	0	.1	.1	.1
3		3350	-	C	1		pg	0		.1
4		2800	.20				.1	.2		
5		2360	.26				.1	.3		
6	-1.00	2000	.14				-	.1		.3
7		1700	.15	D			vcs	.1		.5
8		1400	.27				.1	.6		
9		1180	.32				.1	.7		
10	0.00	1000	.75				1.58	1.04		34
11		850	1.37	E			cs	.7		1.7
12		710	2.49				1.3	2.0		
13		600	4.61				2.4	4.4		
14	+1.00	500	34.17				5.51	2.38		56
15		425	43.74	F			ms	23.33		45.94
16		355	18.88				10.06	56.0		
17		300	35.57				18.96	74.96		
18	+2.00	250	20.75				6.81	4.57		32
19		212	14.68	G			fs	7.8		93.82
20		180	5.01				2.6	96.42		
21		150	3.45				1.8	98.22		
22	+3.00	125	0.31				3.34	1.94		41
23		106	0.22	H			vfs	0.1		98.99
24		90								
25		75								
26	+4.00	63								
P.										

PLYMOUTH SOUND SEDIMENT ANALYSIS PROGRAMME

Name S1

No	φ	μm	weight		Pre	Post	%	%	Went.	c.%		
1	-2.50	5600	107.85	A			-	32.4	32.4	32.4		
2	-2.00	4000	48.95	B			-	14.7	14.7	47.1		
3		3350	33.23	C			pg	10.0		57.1		
4		2800	31.50								7.4	66.5
5		2360	22.53									
6	-1.00	2000	20.98								12.48	10.72
7		1700	20.48	D			vcs	6.1		85.6		
8		1400	16.74								5.0	90.6
9		1180	9.22									
10	0.00	1000	8.89								13.00	10.88
11		850	4.84	E			cs	1.4		96.6		
12		710	2.84								0.8	97.4
13		600	1.80									
14	+1.00	500	1.39								2.48	1.46
15		425	0.64	F			ms	0.1		99.7		
16		355	0.35								0.1	99.8
17		300	0.20									
18	+2.00	250	0.11								1.28	0.45
19		212		G			fs					
20		180										
21		150										
22	+3.00	125										
23		106		H			vfs					
24		90										
25		75										
26	+4.00	63										
P.												

PLYMOUTH SOUND SEDIMENT ANALYSIS PROGRAMME

Name M1

No	φ	μm	weight		Pre	Post	%	%	Went.	c.%
1	-2.50	5600	2.8	A			-	2.23	2.23	2.23
2	-2.00	4000	1.4	B			-	1.11	1.11	3.34
3		3350	1.2	C	4.3	2.4	45	.68	3	6.7
4		2800	1.4							
5		2360	0.85							
6	-1.00	2000	0.85							
7		1700	1.5	D	3.4	0.7	80	2.8	9.4	16.1
8		1400	3.9							
9		1180	2.9							
10	0.00	1000	3.5							
11		850	4.6	E	5.0	1.8	64	5.9	19	34.5
12		710	5.2							
13		600	6.1							
14	+1.00	500	7.4							
15		425	8.2	F	9.0	6.8	25	3.3	18	83.1
16		355	5.6							
17		300	5.5							
18	+2.00	250	4.2							
19		212	7.9	G	61	4.0	35	7.4	34	87.1
20		180	11.7							
21		150	13.9							
22	+3.00	125	9.3							
23		106	9.4	H	6.7	5.4	20	0.95	11	98.9
24		90	2.3							
25		75	1.9							
26	+4.00	63	1.2							
P.			1.1					.87		99.8

PLYMOUTH SOUND SEDIMENT ANALYSIS PROGRAMME

Name *CPI*

No	φ	μm	weight		Pre	Post	%	%	Went.	c.%
1	-2.50	5600	3.0	A	3.00	1.78	40	2.2	2.2	2.2
2	-2.00	4000	2.38	B	2.38	2.10	11	1.7	1.7	3.9
3		3350	1.11				pg	0.8		4.7
4		2800	1.56					1.1		5.8
5		2360	1.43					1.0		6.8
6	-1.00	2000	2.04	C	2.03	0.31	80	1.5	4.4	8.3
7		1700	2.71				vcs	2.0		10.3
8		1400	2.94					2.2		12.5
9		1180	2.97					2.2		14.7
10	0.00	1000	4.78	D	3.23	0.64	80	3.5	9.7	18.2
11		850	5.30				cs	4.0		22.2
12		710	6.01					4.4		26.6
13		600	7.10					5.3		31.9
14	+1.00	500	13.12	E	3.03	0.51	83	9.7	19.2	41.6
15		425	6.59				ms	4.9		46.5
16		355	8.70					6.5		53.0
17		300	9.69					7.2		60.2
18	+2.00	250	9.41	F	2.00	0.59	70	7.0	25.6	67.2
19		212	9.87				fs	7.3		72.5
20		180	8.87					6.0		81.0
21		150	10.69					8.0		90.0
22	+3.00	125	3.40	G	3.50	2.10	40	2.5	23.8	93.0
23		106	6.40				vfs	4.7		98.0
24		90	1.37					1.0		99
25		75	1.50					1.1		99.9
26	+4.00	63	0.60	H	4.60	3.51	23	0.4	7.1	100
P.			0.51					0.4	0.4	

PLYMOUTH SOUND SEDIMENT ANALYSIS PROGRAMME

Name PS10

No	φ	μm	weight		Pre	Post	%	%	Went.	c.%
1	-2.50	5600	15.7	A			-	13.9	13.9	13.9
2	-2.00	4000	5.4	B	20.4	130	37	4.7	4.7	19.3
3		3350	3.4				pg	3.0		22.7
4		2800	3.6					3.1	1	25.8
5		2360	3.9					3.5		29.3
6	-1.00	2000	3.9	C			-	3.5	13	32.7
7		1700	5.8				vcs	4.8		37.5
8		1400	6.0					5.3		42.8
9		1180	5.2					4.6		47.4
10	0.00	1000	6.3	D	21	0.6	72	5.5	21	52.9
11		850	6.1				cs	5.3		58.2
12		710	5.2					4.6		62.8
13		600	4.7					4.1		66.9
14	+1.00	500	4.5	E	3.0	0.6	80	4.0	21	70.9
15		425	3.9				ms	3.4		74.3
16		355	2.4					2.1		76.4
17		300	2.2					1.9		78.3
18	+2.00	250	1.7	F	2.3	.5	79	1.5	7	79.8
19		212	3.0				fs	2.6		82.7
20		180	4.6					4.0		86.4
21		150	4.5					4.0		90.4
22	+3.00	125	2.8	G				2.4	12	92.8
23		106	4.6				vfs	4.0		96.8
24		90	1.7					1.5		98.3
25		75	1.7					1.5		99.8
26	+4.00	63	0.4	H	1.3	.8	39	.3	7	100
P.			0.1					0.08		

PLYMOUTH SOUND SEDIMENT ANALYSIS PROGRAMME Name **S9**

No	φ	μm	weight		Pre	Post	%	%	Went.	c.%
1	-2.50	5600	68.27	A	68.27	68.27	0	40	40	40
2	-2.00	4000	11.67	B	11.67	11.29	3	6.6	6.6	46.6
3		3350	7.15				pg	4.0		50.0
4		2800	5.40					3.1		53.1
5		2360	2.94					1.6		54.3
6	-1.00	2000	2.73	C	303	2.58	14	1.5	11	57.9
7		1700	2.90				vcs	1.6		59.2
8		1400	2.89					1.6		60.3
9		1180	2.21					1.2		61.9
10	0.00	1000	2.29	D	3.68	2.75	24	1.6	7	63.4
11		850	2.66				cs	1.5		64.6
12		710	2.19					1.2		65.6
13		600	1.72					1.0		66.7
14	+1.00	500	1.89	E	2.72	2.02	25	1.1	5	67.7
15		425	1.60				ms	1.0		68.4
16		355	1.27					0.7		69.2
17		300	1.43					0.8		69.9
18	+2.00	250	1.22	F	1.73	1.04	40	0.7	3	70.0
19		212	1.43				fs	0.8		71.1
20		180	2.06					0.9		74.7
21		150	5.28					3.1		74.7
22	+3.00	125	4.32	G	2.50	1.58	44	2.2	7	76.9
23		106	15.58				vfs	16.3		93.0
24		90	4.00					2.2		95.2
25		75	3.86					1.8		97.4
26	+4.00	63	1.60	H	2.21	1.73	21	0.9	20	99.2
P.			1.32					0.8		100

PLYMOUTH SOUND SEDIMENT ANALYSIS PROGRAMME

Name PSG

No	φ	mm	weight		Pre	Post	%	%	Went.	c.%
1	-2.50	5600	47.3	A			-	33.6	33.6	33.6
2	-2.00	4000	2.1	B			-	1.5	1.5	35.1
3		3350	2.7				pg	1.9		37
4		2800	2.9					2.0		39
5		2360	3.9					2.8		41.8
6	-1.00	2000	3.9	C	1.9	0.1	95	2.8	9.5	44.6
7		1700	5.6				vcs	4.0		48.6
8		1400	5.5					4.0		52.6
9		1180	4.0					2.8		55.4
10	0.00	1000	4.6	D	3.3	0.3	91	3.2	12	58.6
11		850	4.0				cs	2.8		61.4
12		710	3.3					2.3		63.7
13		600	3.0					2.1		65.8
14	+1.00	500	3.6	E	3.1	.9	70	2.5	10	68.3
15		425	3.7				ms	2.6		70.9
16		355	3.1					2.2		73.1
17		300	3.2					2.2		75.3
18	+2.00	250	2.3	F	4.3	1.0	77	1.6	9	76.9
19		212	4.2				fs	3.0		79.9
20		180	6.0					4.2		84.1
21		150	5.7					4.0		88.1
22	+3.00	125	3.5	G	1.3	.5	62	2.5	14	90.6
23		106	4.9				vfs	3.5		94.1
24		90	1.9					1.3		95.4
25		75	2.2					1.5		96.9
26	+4.00	63	1.2	H	3.6	2.1	42	0.8	7	98
P.			0.4					0.4		100

Appendix 3

ANISOTROPY OF MAGNETIC SUSCEPTIBILITY

Sample	Ams axes								
	Max			Int			Min		
	Dec	Inc	Int	Dec	Inc	Int	Dec	Inc	Int
C281	23.3	31.0	16.3	36.3	5.0	16.2	104.5	58.4	1.2
C282	50.2	3.5	21.4	143.8	46.4	21.3	316.9	43.3	21.2
C283	67.0	22.0	26.0	320.2	35.7	26.0	181.8	46.1	25.8
C284	95.8	10.1	27.0	300.8	78.8	26.8	186.6	4.6	26.3
C291	285.4	10.7	17.4	64.7	76.0	17.2	193.7	8.9	17.2
C292	266.9	7.7	19.5	8.7	56.3	19.5	171.9	32.5	19.4
C293	273.2	22.8	22.0	163.8	38.5	21.9	26.0	42.9	21.8
C294	292.2	8.1	25.7	121.3	81.7	25.5	22.3	1.2	25.4
C295	281.0	15.6	33.2	180.4	33.3	33.1	32.1	52.3	32.9
C301	266.5	36.9	16.5	16.8	24.7	16.4	132.1	42.9	16.1
C302	106.3	46.8	24.9	358.7	15.8	24.8	255.6	38.8	24.5
C303	12.9	25.7	25.4	108.8	11.9	24.9	221.4	61.4	24.0
C304	129.0	57.2	26.4	18.0	12.8	26.3	280.6	29.5	26.5
C305	15.0	3.8	35.2	128.0	80.4	34.9	284.4	8.8	34.5
C306	168.1	39.9	26.5	261.9	4.5	25.9	357.4	49.7	25.5
C307	199.9	18.4	19.0	64.1	65.1	18.9	295.5	16.1	18.4
C311	187.0	18.8	19.2	284.0	18.2	19.1	54.9	63.2	18.9
C312	342.0	7.2	20.1	250.0	11.2	20.0	103.8	76.6	19.8
C313	180.0	8.1	22.2	84.4	35.3	22.0	281.4	53.5	21.9
C314	8.8	10.6	26.6	152.1	76.9	26.1	277.3	7.6	25.9
C315	356.9	16.6	31.0	150.6	17.7	30.6	263.9	7.4	30.5
C321	80.5	20.9	19.1	180.1	25.1	19.0	315.9	56.5	18.6
C322	188.7	27.9	20.4	79.6	31.5	20.2	311.2	45.4	20.1
C323	356.3	14.2	23.9	255.4	31.5	23.8	107.2	54.9	23.7
C324	30.0	9.7	23.6	156.7	74.0	23.5	297.8	12.6	23.3
C325	7.0	31.8	25.5	140.8	48.1	25.0	260.8	24.2	24.9
C331	328.6	26.8	16.5	112.5	58.1	16.4	230.2	16.2	16.3
C332	167.6	17.1	17.6	74.1	11.2	17.5	312.4	69.1	17.4
C333	207.2	8.4	23.1	300.1	20.5	23.0	96.0	67.7	22.9
C334	209.6	28.5	25.6	108.5	19.5	25.4	348.9	54.4	25.3
C341	295.0	0.1	19.1	204.7	73.1	18.9	25.3	16.8	18.6
C342	95.7	9.6	19.8	199.9	55.3	19.5	359.4	32.9	18.9
C343	238.6	4.3	23.1	328.8	2.8	22.4	91.7	84.9	22.2
C343	11.3	5.2	25.3	107.9	51.9	25.1	227.7	37.6	24.8
C345	151.4	52.2	22.4	353.8	35.6	21.7	225.8	10.9	21.1
C351	1.5	37.9	19.2	124.4	34.8	18.9	241.0	33.1	18.7
C352	52.3	32.9	26.8	252.6	55.5	26.3	148.5	9.5	25.6
C353	82.4	20.9	29.4	350.4	5.1	28.7	247.3	68.4	27.6
C354	354.1	24.5	27.7	147.9	63.1	27.4	259.2	10.5	26.2
C361	223.1	18.9	20.1	69.5	69.8	19.8	316.2	8.6	18.9
C362	109.4	49.7	22.6	0.8	15.1	22.3	259.3	36.2	21.5
C363	64.1	75.2	32.8	199.3	10.6	31.9	291.2	10.0	30.7
C364	64.1	78.0	30.0	210.0	12.6	29.1	280.0	15.3	28.5
C365	90.6	12.7	28.0	356.2	18.6	27.7	213.1	67.2	26.2
C366	175.4	16.9	31.1	41.9	66.1	30.4	270.5	16.3	29.7
C367	206.2	48.8	25.8	340.7	31.4	25.1	86.2	23.7	24.3
C371	70.5	1.8	23.4	338.9	40.6	22.6	162.7	49.3	21.5
C372	262.0	15.5	31.2	168.6	12.1	30.7	42.2	70.2	30.3
C373	143.0	35.5	25.6	25.1	33.3	25.4	265.5	36.9	24.6
C374	201.3	56.8	30.0	107.2	2.7	29.3	15.2	33.0	27.5
C375	87.6	21.5	38.1	292.2	66.5	36.3	181.1	8.8	35.8
C378	105.2	3.3	23.5	3.4	74.1	22.5	196.1	15.5	22.2

Appendix 3 cont..

Sample	Ams axes								
	Max			Int			Min		
	Dec	Inc	Int	Dec	Inc	Int	Dec	Inc	Int
C381	349.7	1.0	26.9	258.5	49.5	26.4	80.6	40.5	25.8
C382	31.9	0.5	20.3	122.3	36.5	20.1	301.1	53.5	20.0
C383	31.2	34.2	31.2	24.1	48.9	30.6	269.1	20.3	29.9
C384	353.4	3.8	26.6	255.2	64.4	26.5	85.2	25.2	26.1
C385	326.1	9.9	30.9	331.4	27.9	30.8	128.3	60.0	30.5
C391	310.2	26.3	31.1	195.8	39.9	30.2	63.6	38.8	29.6
C392	258.2	57.1	30.9	62.3	31.8	30.7	156.8	7.2	29.7
C393	75.6	2.0	22.1	189.7	85.1	21.9	345.5	4.5	21.9
C394	265.8	8.1	24.9	161.5	59.8	24.7	1.0	28.9	24.5
C395	216.4	44.6	30.9	60.9	42.6	30.2	319.1	12.4	29.8
C397	160.4	29.0	31.0	261.0	19.7	30.6	21.8	53.7	30.3
C401	274.5	15.4	32.4	172.3	36.9	31.6	22.7	48.9	31.0
C402	164.4	19.2	18.5	259.7	14.8	18.5	24.9	65.4	18.4
C403	71.0	49.1	27.6	180.3	20.3	27.5	289.4	41.3	27.2
C404	21.7	41.1	27.2	160.4	40.7	26.6	270.8	22.1	25.6
C405	171.5	21.5	27.8	269.2	18.7	27.6	36.6	60.7	27.5
C406	183.0	59.1	27.2	90.0	1.7	27.1	358.8	30.8	26.8
C407	297.2	36.6	24.3	87.0	49.1	24.2	195.4	15.5	21.1
C601	141.8	29.6	9.8	263.4	42.7	9.8	263.4	42.7	7.3
C602	139.1	14.1	14.3	232.5	13.4	12.7	4.3	70.3	12.0
C603	140.1	12.3	14.7	230.9	3.4	14.5	336.3	77.2	13.9
C604	243.1	35.4	20.8	136.7	21.8	18.6	21.7	46.6	17.3
C605	355.3	36.0	16.8	110.0	30.0	16.0	288.3	39.5	15.7
C606	315.2	50.7	17.1	90.3	30.0	15.2	194.3	22.8	14.0
C607	23.2	48.5	30.4	176.9	38.4	27.3	277.7	13.3	21.4
C608	296.5	10.7	18.0	92.8	78.8	16.4	205.8	4.5	15.8
C611	304.6	10.3	10.2	55.2	62.5	9.7	209.7	25.5	9.0
C612	183.5	8.3	17.6	92.4	7.4	16.2	321.2	78.8	15.3
C613	133.3	33.0	15.4	242.3	26.6	15.1	2.5	45.1	14.3
C614	267.7	2.5	19.1	177.6	3.5	18.2	33.0	85.6	16.2
C615	21.7	41.9	21.5	290.5	1.4	21.1	199.0	48.1	20.5
C616	347.9	42.0	16.8	85.6	8.5	14.5	184.7	46.8	12.2
C617	278.4	0.3	18.3	22.7	88.7	16.8	188.4	1.3	16.4
C618	312.5	20.5	20.9	46.6	10.9	19.5	162.9	66.6	18.8
C621	218.2	19.0	12.9	124.2	11.2	12.8	5.1	67.7	12.6
C622	80.8	53.2	16.9	309.2	26.3	16.6	206.7	23.6	16.3
C623	305.8	36.9	14.4	81.7	43.7	14.1	196.5	23.6	13.6
C624	84.5	67.1	21.9	266.3	22.9	21.7	176.1	0.6	21.4
C625	266.9	40.2	17.3	131.2	40.0	16.8	19.2	24.0	16.5
C626	281.3	21.0	17.9	96.2	68.9	17.8	190.6	1.7	17.2
C627	290.1	70.8	17.2	100.4	18.9	16.9	191.4	3.0	16.4
C628	294.3	17.7	20.4	187.8	41.6	19.7	41.7	43.0	10.1
C631	273.2	17.9	11.6	40.1	61.7	11.4	176.0	21.1	11.3
C632	24.9	22.4	18.5	273.8	41.0	18.0	135.7	40.6	17.7
C633	108.8	24.2	15.3	351.8	45.3	15.0	217.0	34.8	14.8
C634	264.0	0.8	19.1	356.1	67.9	19.0	173.6	22.0	18.5
C635	106.6	23.4	19.1	301.7	65.8	18.8	199.1	5.6	18.4
C636	143.7	33.3	26.7	15.5	43.2	25.4	254.7	28.6	21.9
C637	94.8	62.4	19.1	269.3	27.4	19.1	0.5	2.2	18.2
BM1	191.1	52.3	22.4	316.0	23.8	22.1	59.2	26.7	21.4
BM2	30.5	32.0	13.0	298.5	3.2	12.8	203.3	57.7	12.1
BM3	267.8	7.1	14.0	359.8	15.8	13.7	154.2	72.5	13.6
BMB5	48.9	35.5	12.6	305.4	18.1	12.2	193.6	48.7	11.8

Appendix 3 cont.

Sample	Ams axes								
	Max			Int			Min		
	Dec	Inc	Int	Dec	Inc	Int	Dec	Inc	Int
BDR1	272.4	6.6	46.8	6.6	32.8	46.0	172.3	56.3	45.8
BDR2	25.5	20.2	48.7	276.3	41.8	47.9	134.4	41.3	47.1
BDR3	210.6	44.5	49.0	79.5	33.7	47.8	330.0	26.5	46.1
BDR4	226.9	18.4	54.5	328.0	30.0	53.5	109.9	53.8	52.7
BDR5	13.6	31.5	53.7	266.4	25.7	52.8	145.1	47.2	51.5
BDR6	91.4	19.1	35.1	182.6	3.4	34.3	282.4	70.6	34.1
BDR7	52.2	18.5	32.1	166.3	50.5	31.3	309.4	33.3	30.5
BDR8	284.6	10.8	39.1	15.0	1.7	38.2	114.2	78.9	37.6
BME1	128.5	9.9	10.5	222.2	20.0	10.4	13.5	67.4	9.5
BME2	219.8	54.5	8.9	125.9	2.8	5.7	33.9	35.3	3.8
BME3	248.4	39.1	9.1	155.6	3.5	7.5	61.3	50.7	6.2
BD1	272.7	32.8	20.4	157.9	32.9	19.5	35.3	39.8	18.6
BD2	293.8	21.9	15.8	160.1	59.7	14.4	32.2	19.7	13.3

Appendix 4 Location of samples and stations

Name	Location	Latitude 50°	Longitude 04°
BW1	E. Breakwater	20.05	08.00
PS12	F Buoy	20.70	07.88
PS6	N. Duke Rock	20.30	08.06
PS5	Dunstone Rock	21.12	07.80
PS10	Duke Rock	20.29	08.17
M1	Melampus Buoy	21.12	08.65
BW2	W. Breakwater	20.05	09.13
CB1	Cawsand Bay	20.31	10.47
CB2	Cawsand Bay	20.45	09.90
NG1	New Ground	20.50	09.17
CB3	Nr. Picklecombe	20.65	09.59
CB4	W. Channel	20.22	09.73
BW4	E. Channel	19.98	08.00
AB1	Ash Buoy	21.65	08.80
RH1	Rame Head	18.76	12.80
PS23	W. Breakwater	20.10	09.48
PP1	Penlee Point	18.82	11.35
RH4	Penlee Point	18.65	11.08
PP2	Penlee Point	19.15	11.03
BW24	E. Breakwater	20.15	09.45
CS4	W. Channel	20.00	10.00
OP1	nr. Duke Rock	20.45	07.55
S1	Panther Knoll	19.85	09.38
BG1	S. Breakwater	19.18	09.24
C11	Cawsand Bay	19.52	11.28
BB1	Bovisand Bay	20.08	07.45
116	S. Breakwater	19.57	08.93
S9	S. Breakwater	19.38	09.23
S4	Penlee Point	19.12	10.58
S3	Cawsand Bay	20.10	10.70

Appendix 4 cont.

Location	Latitude 50°	Longitude 04°
Battery Buoy	21.50	10.15
West Vanguard Buoy	21.46	09.90
East Vanguard Buoy	21.45	09.65
North West Drake.s Buoy	21.42	09.32
North Drake.s Buoy	21.50	09.45
Asia Buoy	21.55	08.83
Ash Buoy	21.65	08.80
Mooring	21.68	08.50
West Mallard Buoy	21.56	08.28
South Mallard Buoy	21.49	08.24
North East Winter Buoy	21.50	08.46
Foxtrot Buoy	20.70	07.88
Golf Buoy	21.04	07.55
ATM1	20.58	08.21
ATM2	20.77	08.88
ATM3	20.75	09.36
Picklecombe	20.52	10.12
East Bridges Buoy/CASI7	21.03	09.50
ATM4	20.97	09.08
ATM5	21.10	08.85
South Winter Buoy	21.38	08.50
North West Winter Buoy	21.52	08.63
Bovisand Harbour	20.23	07.77
Duke Rock Buoy	20.29	08.17
Delta Buoy	20.24	08.43
Charlie Buoy	20.30	08.85
New Ground Buoy	20.50	09.17
West Breakwater	20.10	09.48
West Breakwater steps	20.00	09.22
Centre Fort	20.05	08.85
East Breakwater steps	19.95	08.42
Bovisand Bay	20.08	07.45
Outer E.Breakwater	19.95	07.45
Outer E.Breakwater step	19.90	08.42
Outer Centre Fort	19.90	08.85
Outer W.Breakwater step	19.90	09.22
Outer W.Breakwater	20.00	09.28
Panther Buoy	19.87	09.48
Dunstone Rock Buoy	21.12	07.80
Melampus Buoy	21.10	08.65
A	20.36	08.16
B	20.53	08.72
C	20.71	09.21
D	20.87	09.00
E	20.80	08.26
Squilla 1	18.82	08.11
Squilla 2	19.79	09.13
Squilla 3	19.36	07.80
CASI 3	20.78	08.60
CASI 4	20.88	08.60
CASI 5	20.94	09.16
CASI 6	20.85	09.46
CASI 8	21.18	08.88
CASI 9	20.88	08.46
Ramscliff Point	20.55	07.62